AD-A081 184 SOLAR TURBINES INTERNATIONAL SAN DIEGO CA F/G 21/5
APPLICATION OF CERAMIC NOZZLES TO 10 KW ENGINE.(U)
DEC 78 J C NAPIER, A G METCALFE, T E DUFFY DAAK02-75-C-0138
UNCLASSIFIED SR80-R-4375-43 NL

1 OF 3
AD-
A081184

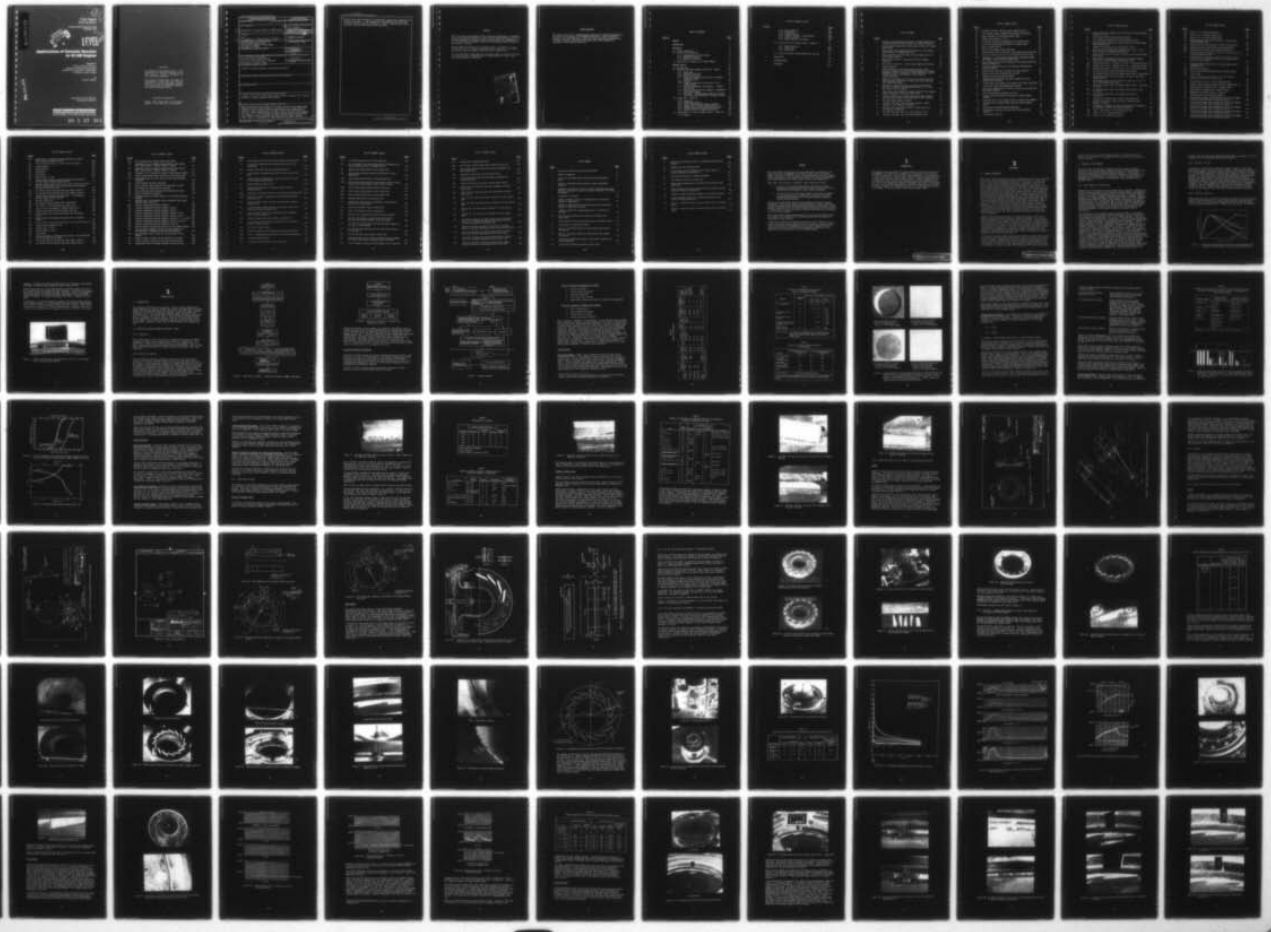

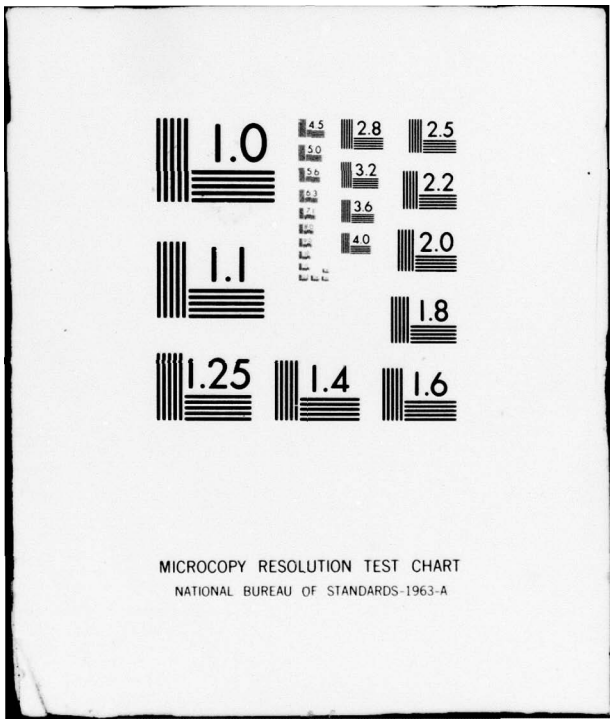
1.0
1.1
1.25
1.4
1.6
1.8
2.0
2.2
2.5
2.8
3.2
3.6
4.0
4.5
5.0
5.6
6.3
7.1
8.0
9.0
MICROCOPY RESOLUTION TEST CHART
NATIONAL BUREAU OF STANDARDS-1963-A

12

Final Report
S.O. 6-4375-7

Contract Number DAAK02-C-0138
December 1979

LEVEL II

Application of Ceramic Nozzles to 10 kW Engine

Prepared for
U.S. Army Mobility Equipment
Research and Development Command
Electrical Power Laboratory - DRDME-EMA
Fort Belvoir, Virginia 22060

by
James C. Napier

Approved for Public Release;
Distribution Unlimited

SOLAR TURBINES INTERNATIONAL
An Operating Group of International Harvester
2200 Pacific Highway, P.O. Box 80966, San Diego, California 92138

Disclaimer

The findings in this report are not to be construed as an official Department of the Army position, unless so designated by other authorized documents.

The citation of trade names and names of manufacturers in this report are not to be construed as official Government indorsement or approval of commercial producers or services referenced herein.

Disposition Instructions

Destroy this report when it is no longer needed. Do not return to the originator.

SECURITY CLASSIFICATION OF THIS PAGE *(When Data Entered)*

REPORT DOCUMENTATION PAGE

READ INSTRUCTIONS BEFORE COMPLETING FORM

1. REPORT NUMBER	2. GOVT ACCESSION NO.
3. RECIPIENT'S CATALOG NUMBER	
4. TITLE *(and Subtitle)*	5. TYPE OF REPORT & PERIOD COVERED
(6) Application of Ceramic Nozzles to 10kW Engine	(9) Final Report,
6. PERFORMING ORG. REPORT NUMBER	(14) SR80-R-4375-43, SR-4375-7
7. AUTHOR(s)	8. CONTRACT OR GRANT NUMBER(s)
(10) James C. Napier, A. G. Metcalfe & T. E. Duffy	(15) DAAK02-75-C-0138
9. PERFORMING ORGANIZATION NAME AND ADDRESS Solar Turbines International 2200 Pacific Highway, P.O. Box 80966 San Diego, CA 92138	10. PROGRAM ELEMENT, PROJECT, TASK AREA & WORK UNIT NUMBERS (12) 265
11. CONTROLLING OFFICE NAME AND ADDRESS	(11) 12. REPORT DATE December 1978
	13. NUMBER OF PAGES 246
14. MONITORING AGENCY NAME & ADDRESS *(if different from Controlling Office)* U.S. Army Mobility Equipment Research and Development Command Electrical Power Laboratory - DRDME-EMA Fort Belvoir, Virginia 22060	15. SECURITY CLASS. *(of this report)* Unclassified
	15a. DECLASSIFICATION/DOWNGRADING SCHEDULE

16. DISTRIBUTION STATEMENT *(of this Report)*

Approved for Public Release; Distribution Unlimited

17. DISTRIBUTION STATEMENT *(of the abstract entered in Block 20, if different from Report)*

18. SUPPLEMENTARY NOTES

19. KEY WORDS *(Continue on reverse side if necessary and identify by block number)*

Ceramics, Gas Turbine, Nozzle Vanes, Nozzle Shrouds, Thermal Shock, Erosion, Corrosion, Joining, Relaxing Glass Adhesive

20. ABSTRACT *(Continue on reverse side if necessary and identify by block number)*

Work on application of ceramics to the nozzle section of the small radial MERADCOM 10 kW gas turbine engine for meeting the two separate goals of improved erosion resistance and increased turbine inlet temperature is reported. Engine demonstrations of each of the two ceramic nozzle designs were completed. Efforts leading to engine demonstrations are documented and included; ceramic materials properties studies; design studies; engine simulator experiments for high temperature erosion, corrosion and →over

DD FORM 1 JAN 73 1473 EDITION OF 1 NOV 65 IS OBSOLETE

326550

UNCLASSIFIED

SECURITY CLASSIFICATION OF THIS PAGE *(When Data Entered)*

thermal shock; and development of specialized relaxing glass adhesives for joining of ceramics. It was demonstrated that ceramics can offer from 10 to 100 times the erosion resistance at 1700°F to superalloys and have excellent corrision and thermal shock properties.

PREFACE

This final report was prepared by Solar Turbines International, an Operating Group of International Harvester, under Contract Number DAAK02-75-C-0138 for the Electromechanical Division, Electrical Power Laboratory, DRDME-EMA, of the U.S Army Mobility Equipment Research and Development Command (MERADCOM), Fort Belvoir, Virginia.

The Principal Investigator for the program is Mr. J. C. Napier. Dr. A. G. Metcalfe and Mr. T. E. Duffy are Project Technical Advisors. This report covers work conducted between 7 March 1975 and 17 August 1979.

The work described in this report was conducted under the technical direction of Mr. Frank Jordan of MERADCOM until his death when Mr. J. Paul Arnold continued monitorship of the work.

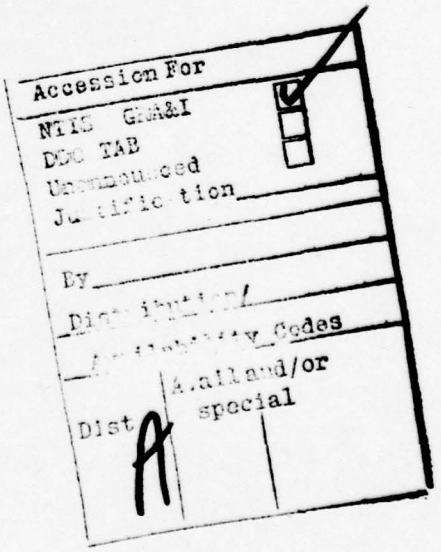

ACKNOWLEDGEMENTS

The author would like to acknowledge the conception and continuing support of this project by personnel at both MERADCOM and Solar. Credit is given to Gregory M. East and Frank Ritz of Solar for their technical contributions in the areas of design, fabrication and testing which were essential in achieving critical project milestones.

TABLE OF CONTENTS

Section		Page
	SUMMARY	1
1	INTRODUCTION	3
2	BACKGROUND	5
	2.1 Service Experience	5
	2.2 Erosion in Gas Turbines	6
	2.1.1 Requirements for Nozzle Vanes	6
	2.1.2 Erosion in Service	7
	2.1.3 Materials Evaluation	7
	2.3 Application of Ceramics to a Radial Engine	9
3	PROGRAM RESULTS	11
	3.1 Program Plan	11
	3.2 Material and Nozzle Segment Evaluation - Phase I	11
	3.2.1 Objectives	11
	3.2.2 Material Evaluation	11
	3.2.3 Fabrication Studies	26
	3.2.4 Design and Analysis for Rig Test of Ceramic/Superalloy Nozzle	32
	3.2.5 Analysis	35
	3.2.6 Design and Analysis for Rig Test of All-Ceramic Nozzle	35
	3.2.7 Rig Test Fabrication and Assembly - Ceramic/Metal Nozzle	44
	3.2.8 Rig Test Fabrication and Assembly - Simplified All-Ceramic Nozzle	44
	3.2.9 Rig Tests - Standard Nozzle Baseline, Ceramic Vane Nozzle and Preliminary All-Ceramic Nozzle	47
	3.3 Engine Test - Phase II	80
	3.3.1 Objective	80
	3.3.2 Design and Analysis	84
	3.3.3 Nozzle Fabrication and Engine Assembly	93
	3.3.4 Engine Test of Ceramic Vane Section Nozzle	96
	3.3.5 Ceramic Vane Nozzle Design Modifications	99
	3.3.6 Engine Re-Test of Ceramic Vane Nozzle	107
	3.4 Development of 10 kW All-Ceramic Nozzle - Phase III	119
	3.4.1 Design	119

TABLE OF CONTENTS (Contd)

Section			Page
	3.4.2	Design Analysis	136
	3.4.3	Procurement	140
	3.4.4	Assembly Mock-Up	144
	3.4.5	Assembly Analysis - Design Update	146
	3.4.6	Static Rig Tests	166
	3.4.7	Engine Simulator Rig Tests	191
	3.5	Engine Test of All-Ceramic Nozzle - Phase IV	195
	3.5.1	Design Selection	200
	3.5.2	Fabrication	201
	3.5.3	Engine Test	206
	3.6	Second All-Ceramic Nozzle Engine Test (Run #4)	210
4	CONCLUSIONS		241
5	RECOMMENDATIONS		243
	REFERENCES		245

LIST OF FIGURES

Figure		Page
1	Predicted and Experimental Variation of Volume Removal With Incidence Angle for Various Ductile and Brittle Materials	7
2	Typical Titan Turbine Nozzle Vanes After 68 Hours of Vietnam Dust Erosion	8
3	Titan Nozzle Vane Assembly After 10 Hours of Test Showing Severe Erosion of Conventional Vanes	8
4	Silicon Nitride and N-155 Vanes in Titan Engine After 10 Hours Erosion Testing	10
5	Work Plan for Phase I - Materials and Nozzle Segment Evaluation	12
6	Work Plan for Phase II - Nozzle Ring Assembly and Testing	13
7	Program Sequence	14
8	Eroded Surfaces of 713LC Nickel-Base HPSi_3N_4, HPSiC Superalloy and NC-430; 3/8 Inch Nozzle Diameter; 90 Degree Impingement Angle; 15 Minutes at Room Temperature; 840 fps Particle Velocity; and 80 mg/ft^3 of 43-74 Micron Arizona Road Dust	18
9	Summary of Test Results for SiC and Si_3N_4 Simulated Vane Shape Specimens Evaluated at 1200°C in a Mach 1 Simulated Gas Turbine Environment	21
10	Corrosion of Various Materials in Turbine Test Passage Exposed to Combustor Gas Contaminated With 0.5% S, 5 ppm Na, 2 ppm V, and 0.6 ppm Mg	22
11	Three Point Bend Strength of Ceramic Materials and Ultimate Tensile Strength of 713C Nickle Base Alloy	23
12	Failure Probability for Norton Hot Pressed Si_3N_4 HS-130, and Norton Hot Pressed Silicon Carbide at 982°C (1800°F)	24
13	Unnotched Charpy Impact Strength	24
14	40% GN19, 20% B402, 40% Cr_2O_3 After 60 Hours, 2000°F Exposure in Air (RBSi_3N_4 to HPSi_3N_4)	27
15	60% GN19, 40% Cr_2O_3 After 60 Hours, 2000°F Exposure in Air (RBSi_3N_4 to HPSi_3N_4)	29
16	30% B402, 30% GN19, 40% Cr_2O_3 After Exposure Cycle	31
17	35% B402, 35% GN19, 30% Cr_2O_3 After Exposure Cycle	31

LIST OF FIGURES (Contd)

Figure		Page
18	20% GN19, 40% B402, 40% Cr_2O_3 After Exposure Cycle	32
19	10 kW Turbine Nozzle Assembly With Ceramic Vane Inserts	33
20	Layout Drawing of Vane Trailing Edge Insert	34
21	Ceramic Vane Section - 10 kW	36
22	10 kW Front Turbine Shroud Modified for Ceramic Vanes	37
23	10 kW Aft Turbine Shroud Modified for Ceramic Vanes	38
24	Rivet, Turbine Nozzle	39
25	Vane for All-Ceramic Nozzle Rig Tests	40
26	Forward Shroud Ring to be Used in All-Ceramic Nozzle Rig Test	40
27	Aft Shroud Rings to be Used in All-Ceramic Nozzle Rig Test	41
28	Comparison of Present Nozzle Design With Preliminary Design for Ceramic Vanes, Shroud and Seal Plate	42
29	Shroud Recess and Vanes for Simplified All-Ceramic Nozzle For Rig Test Evaluation	43
30	10 kW Rear Nozzle Shroud With Two HPSi_3N_4 Trailing Vane Sections Inserted	45
31	Tooling Set-Up for EDM of Recesses in Nozzle Shrouds	46
32	HPSi_3N_4 Nozzle Vane Trailing Edge Sections	46
33	Standard 10 kW Forward Nozzle Shroud	47
34	Ceramic/Superalloy Nozzle Partially Assembled Prior to Firing Glass Interface	48
35	Cooled Nozzle Test Chamber With Ceramic Vane Nozzle Installed	50
36	10 kW Nozzle Test Rig Thermocouple Location	50
37	Location of Thermocouple #1 and #2 in Rig Tests and Sketch of Dust Erosion Device	51
38	Plate With Refrasil Insulation in Place	52
39	HPSi_3N_4 Vanes Installed With Hastelloy X Spacer Washers and Pins	53
40	Downstream View of All-Ceramic Nozzle in Cooled Test Chamber	54
41	Upstream View of Spring Loaded Hastelloy Nozzle Support Pin 'A'	55
42	Thermocouple Inserted Through Insulation	56
43	Thermocouple Location and Glass Joint Filler Material Location	57
44	10 kW Nozzle Test Rig	58

LIST OF FIGURES (Contd)

Figure		Page
45	Cooled Nozzle Test Chamber With Lid Inverted to Show Upstream Section of Nozzle	58
46	10 kW Nozzle Test Rig Thermocouple Location	59
47	10 kW Soakback Temperatures; Run Down Under No Load	60
48	Time Temperature Profiles of Various Shroud Locations During Thermal Shock Cycle	61
49	Standard 10 kW Nozzle After 500 Rig Test Cycles	63
50	Close-up View of Nozzle Vane Locations (A) 7 and 8, (B) 14, After 500 Rig Test Thermal Shock Cycles	65
51	Close-up View of Vane Location #15 After 500 Rig Test Thermal Shock Cycles	66
52	Rear Shroud of Bi-Material Nozzle After 500 Test Thermal Shock Cycles Showing Thermal Cracking at Holes	67
53a	Thermal Shock Cycle - 15°F/Sec at T/C #2 - All-Ceramic Nozzle	68
53b	Thermal Shock Cycle - 15°F/Sec at T/C #2 - All-Ceramic Nozzle	69
54	Thermal Shock Cycle - 60°F/Sec at T/C #1 - All-Ceramic Nozzle	70
55	All-Ceramic Nozzle After 500 Thermal Shock Cycles	72
56	All-Ceramic Nozzle After 500 Thermal Shock Cycles - Downstream	73
57	All-Ceramic Nozzle at Pin Locations 'A' and 'B' After 500 Thermal Cycles	74
58	All-Ceramic Nozzle at Pin Location 'C' and Pins 'A' and 'C' After 500 Thermal Shock Cycles	75
59	All-Ceramic Nozzle After 500 Thermal Shock Cycles - Locations #1 and #2	76
60a	All-Ceramic Nozzle After 500 Thermal Shock Cycles - Vane Location #3	77
60b	All-Ceramic Nozzle After 500 Thermal Shock Cycles - Location #4	77
61	Standard 10 kW Nozzle After 10-Hour Rig Erosion Test	78
62	HPSi_3N_4 Vane Section After 10 Hours of Rig Test Dust Erosion at 1700°F	79
63	Comparison of Erosion of Nozzle Vanes from 713LC Superalloy and HPSi_3N_4 at 1700°F in an Engine Simulator	80
64a	Vanes 5 and 6 After 5 Hour Dust Erosion Test	81
64b	Vanes 1, 2 and 3 After Erosion Test	81
65a	Vanes 4, 5 & 6 After Erosion Test	82

LIST OF FIGURES (Contd)

Figure		Page
65b	Vanes 7, 8 & 9 After Erosion Test	82
66a	Vanes 10, 11 & 12 After Erosion Test	83
66b	Vanes 13, 14 & 15 After Erosion Test	83
67a	Vane Locations 8 and 7 After 60 Hours, 3 ppm Sea Salt, 1700°F Corrosion Test	85
67b	Close-up View of Vane Location 7, After Corrosion Test	85
68a	Downstream Side of Nozzle After Rig Corrosion Test	86
68b	Upstream Side of Nozzle After Rig Corrosion Test	86
69	Sea Salt Corrosion; 60 Hours at 927°C in Turbine Simulator, 3 ppm Artificial Sea Salt	87
70	Upstream View of Simplifed Ceramic Nozzle After 70 Hour, 3 ppm Sea Salt Corrosion Test (Pin 'A' at Bottom Right, Pin 'B' at Left Center)	88
71a	Simplified Ceramic Nozzle After 70 Hours 3ppm Sea Salt Corrosion Test	89
71b	Second View of Nozzle	89
72a	View of Crack From Downstream Side of Ceramic Nozzle	90
72b	Crack Origin	90
73	Crack Originating at Holding Pin 'B' (Dye Penetrant Applied for Visibility in this View)	91
74	Pin Locations 'A' and 'C' After Corrosion Test	92
75	Thermal Crack in Bottom Ceramic Shroud at Holding Pin 'B'	93
76	Forward Shroud for Engine Test of Ceramic Vanes	94
77	Rear Shroud for Engine Test of Ceramic Vanes	95
78	MERADCOM 10 kW Engine Set-up in Test Cell	96
79	Clearance Chart 10 kW Turbine Assembly	97
80	10 kW Nozzle Ceramic Vane Sections #1 and #2 After Engine Test #1 25 Hour Run Plus 50 Start/Stop Cycles	100
81	10 kW Nozzle Ceramic Vane Sections #3 and #4 After Engine Test #1 25 Hour Run Plus 50 Start/Stop Cycles	101
82	10 kW Nozzle Ceramic Vane Sections #5 and #6 After Engine Test #1 25 Hour Run Plus 50 Start/Stop Cycles	102
83	10 kW Nozzle Ceramic Vane Sections #7 and #8 After Engine Test #1 25 Hour Run Plus 50 Start/Stop Cycles	103
84	10 kW Nozzle Ceramic Vane Sections #9 and #10 After Engine Test #1 25 Hour Run Plus 50 Start/Stop Cycles	104

LIST OF FIGURES (Contd)

Figure		Page
85	10 kW Nozzle Ceramic Vane Sections #11 and #12 After engine Test #1 25 Hour Run Plus 50 Start/Stop Cycles	105
86	10 kW Nozzle Ceramic Vane Sections #13 and #14 After Engine Test #1 25 Hour Run Plus 50 Start/Stop Cycles	106
87	10 kW Nozzle Ceramic Vane Sections #15 and #16 After Engine Test #1 - 25 Hour Run Plus 50 Start/Stop Cycles	107
88	10 kW Nozzle With Hot Pressed Si_3N_4 Vane Sections After Engine Test #1 - 25 Hour Run Plus 50 Start/Stop Cycles	108
89	Design Changes to Ceramic Vane Nozzle Prior to Engine Test #2	109
90	Nozzle Spacer Ring	110
91	Nozzle Spacer Ring Shims	111
92	Diffuser Housing Modification	112
93	Seal Plate Modification	113
94a	Belleville Washer and Locknut Method of Fastening Nozzle D-Bolts to Compressor Housing	114
94b	Belleville Washer and Locknut Method of Fastening Nozzle D-Bolts to Compressor Housing	114
95	Modification to Ceramic Vane Nozzle Assembly	116
96	Modification to Ceramic Vane Nozzle Assembly	117
97a	Redesigned All-Ceramic Nozzle After Engine Test #2	120
97b	Hot Pressed Silicon Nitride Vane Sections 1, 2 and 3 After Engine Test #2	120
97c	Hot Pressed Silicon Nitride Vane Section 4 After Engine Test #2	121
97d	Hot Pressed Silicon Nitride Vane Section 5 After Engine Test #2	121
97e	Hot Pressed Silicon Nitride Vane Section 6 After Engine Test #2	122
97f	Hot Pressed Silicon Nitride Vane Section 7 After Engine Test #2	122
97g	Hot Pressed Silicon Nitride Vane Section 8 After Engine Test #2	123
97h	Hot Pressed Silicon Nitride Vane Section 9 After Engine Test #2	123
97i	Hot Pressed Silicon Nitride Vane Section 10 After Engine Test #2	124

LIST OF FIGURES (Contd)

Figure		Page
97j	Hot Pressed Silicon Nitride Vane Section 11 After Engine Test #2	124
97k	Hot Pressed Silicon Nitride Vane Section 12 After Engine Test #2	125
97l	Hot Pressed Silicon Nitride Vane Section 13 After Engine Test #2	125
97m	Hot Pressed Silicon Nitride Vane Section 14 After Engine Test #2	126
97n	Hot Pressed Silicon Nitride Vane Section 15 After Engine Test #2	126
98	Ceramic Nozzle Assembly - Concept #1	127
99	Ceramic Nozzle Assembly - Concept #2	128
100	Ceramic Nozzle Assembly - Concept #3	129
101	Seal Plate for Use With Si_3N_4 and SiC All-Ceramic 10 kW Nozzles	132
102	Seal Plate Diaphram for Use With Si_3N_4 and SiC Ceramic 10 kW Nozzles	133
103	Retaining Rivet for Diaphram Inner Diameter	134
104	Retaining Rivet for Diaphram Outer Diameter	135
105	Seal Diaphram and Seal Plate With Spares	136
106	Diaphram Attached to Seal Plate With Retaining Rivets	136
107	Outer Shroud Retaining Can for Use With Si_3N_4 and SiC Ceramic Nozzles	137
108	Bolt for Attachment of Nozzle Retaining Can	138
109	Retaining Cap Pins for Attachment of Nozzle Retaining Can to Nozzle Retaining Ring	139
110	Retaining Can From René 41 Superalloy	140
111	Retaining Ring for Attachment of Ceramic Outer Nozzle Shroud	141
112	Nozzle Retainer Ring Installed With Retaining Cap Pins	142
113	Rear Shroud to Exhaust Scroll Seal for Use With Si_3N_4 and SiC Ceramic Nozzles	143
114	Exhaust Scroll Face Seal	144
115	Exhaust Scroll for Use With Si_3N_4 and SiC Ceramic Nozzles	145
116	Scroll and Bellows Positioned	146
117	Modification of Air Inlet Housing for Ceramic Nozzle Design Concept #1	147

LIST OF FIGURES (Contd)

Figure		Page
118	Modification to Standard Diffuser Housing for Ceramic Nozzle Design Concepts #1 and #2	148
119	Cooled Superalloy Bolt for Ceramic Nozzle Assembly	149
120	Forward Shroud	150
121	Forward Shroud	151
122	Rear Shroud	152
123	Rear Shroud	153
124	Ceramic Vane - 10 kW	154
125	Reaction Bonded Silicon Nitride Forward Shroud With Hot Pressed Silicon Nitride Vanes in Place	155
126	Reaction Bonded Silicon Nitride Rear Shroud With Hot Pressed Silicon Nitride Vanes, Hot Pressed Silicon Nitride Bolts and Inco 718 Bolts in Place	155
127	Hot Pressed Silicon Nitride Vanes RSK 230630, Detail 1	156
128	Hot Pressed Silicon Nitride Vanes RSK 230630, Detail 2	156
129	Ceramic Nozzle Shrouds and Bolts From: 718 Superalloy and Hot Pressed Silicon Nitride	157
130	$HPSi_3N_4$ Ceramic Bolt	158
131	Hot Pressed Silicon Nitride Bolts, RSK 230635	159
132	RSK 230786 - Collet Fastener for Ceramic Bolt	159
133	View of Collet Attachment of $HPSi_3N_4$ Ceramic Bolt	160
134	Ceramic Bolts After 100 Cycle Furnace Rig Test	160
135	First Ceramic Vane Design Alternative for All-Ceramic Nozzle	163
136	Second Ceramic Vane Design Alternative for All-Ceramic Nozzle	164
137	Third Ceramic Vane Design Alternative for All-Ceramic Nozzle	165
138	Ceramic Nozzle Assembly 10 kW	168
139	Ceramic Vane - 10 kW	169
140	Forward Shroud - 10 kW	170
141	Rear Shroud	171
142	Ceramic Components As-Received From Norton. Five Additional NC 350 Rear Shrouds Not shown	172
143	Hot Pressed Silicon Nitride Vanes RSK 230630, Detail 1	172
144	Hot Pressed Silicon Nitride Vanes RSK 230630, Detail 2	173

LIST OF FIGURES (Contd)

Figure		Page
145	Hot Pressed Silicon Nitride Bolts, RSK 230635	173
146	Aluminum Mock-up of Ceramic Forward Shroud, Rear Shroud, Bolt, Vane, Detail 2 (Short), Detail 1 (Long)	174
147	Aluminum Mock-up of Ceramic Forward Shroud, Rear Shroud, Bolt, Vane, Detail 2 (Short), Detail 1 (Long)	174
148	Components to be Included in Ceramic Nozzle Engine Assembly	174
149	Fixture Simulating Diffuser Housing for Rig Furnace Test	175
150	Spring Retaining Can, Seal Plate and Seal Plate Diaphram Installed	175
151	Forward Shroud and Vanes Installed	175
152	Nozzle Retainer Ring Installed With Retaining Cap Pins	176
153	Rear Shroud and Through Bolts Installed	176
154	Nozzle Retainer Ring Installed With Retaining Cap Pins	176
155	Scroll and Bellows Positioned	177
156	Aluminum Mock-up of Ceramic Nozzle in 10 kW Inlet-Diffuser Housing	177
157	Exploded View of All-Ceramic Nozzle Components With Si_3N_4 Shrouds, Vanes and Bolts	177
158	Pressure Compensated Bellows Assembly	178
159	Pressure Compensated Bellows Assembly, Detail 1	179
160	Pressure Compensated Bellows Assembly, Detail 2	180
161	Pressure Compensated Bellows Assembly, Details 3 and 4	181
162	Pressure Compensated Bellows Assembly, Details 4 and 5	182
163	Pressure Compensated Bellows Assembly, Details 6, 7, 8, and 9	183
164	Pressure Compensated Bellows Assembly, Details 11 and 13	184
165	Pressure Compensated Bellows Assembly, Detail 12	185
166	Furnace Thermal Cycling Test Fixture for All-Ceramic Nozzle	186
167	View of Furnace Thermal Cycling Test Rig Showing Case Corresponding to Combustion Can Downstream Section	187
168	Heat Exchanger Coils to Heat Air Flow Upstream to Test Chamber	187
169	Furnace Thermal Cycling Test Rig Installed in Furnace	188
170	Furnace Thermal Cycling Test Rig Removed From Furnace	188
171	Thermocouple Code for Furnace Thermal Cycling Test Rig	189

LIST OF FIGURES (Contd)

Figure		Page
172	Time Temperature Trace for Furnace Thermal Cycle Rig Test	190
173	Ceramic Bolt Assembled into Furnace With Collet and Pt Interlayer	192
174	Ceramic Bolts After 100 Cycle Furnace Rig Test	192
175	Close-up View of Ceramic Bolt After 100 Cycle Furnace Tet Rig	193
176	Thermal Rig Test Apparatus for Engine Simulation Testing of All-Ceramic Nozzle Design	194
177	Modified Engine Simulator Rig	195
178	Thermocouple Locations for Engine Simulator Test of Cermaic Nozzles	197
180a	Components From Design Concept #1 After Engine Simulator Test	202
180b	Subcritical Crack in $RBSi_3N_4$ Forward Shroud After Engine Simulator Test	202
181	Design Concept #3 RBSiC Shroud, After Successful Engine Simulator Run	203
182	Design Concept #3 RBSiC Shroud, NC 203 HPSiC Vanes After Succcessful Engine Simulator Run	203
183	Typical $HPSi_3N_4$ Vanes After Successful Engine Simulator Run in Design Concept #1	204
184	Typical $HPSi_3N_4$ Bolts After Engine Simulator Run	204
185	Clearance Chart 10 kW Turbine Assembly With All-Ceramic Nozzle - Engine Test #3	205
186	Bolt Seal, Ceramic Nozzle	207
187	Hybrid All-Ceramic Nozzle After 33 Hours Engine Running	210
188	Crack in $RBSi_3N_4$ Rear Shroud After 33 Hours Engine Running	211
189	Collapsed Exhaust Scroll	212
190	All-Ceramic Nozzle After 50 Hour Engine Run	212

LIST OF FIGURES (Contd)

Figure		Page
191	All-Ceramic Nozzle After 50 Hour Engine Run	213
192	Gap in Exhaust Scroll Heat Shield Below Cam Combustor for an Above Exhaust Scroll Collapsed Section	215
193	$RBSi_3N_4$ Rear Shroud After 50 Hour Engine Test	216
194	$HPSi_3N_4$ Vanes and RCSiC Forward Shroud After 50 Hours Engine Test	216
195a	RCSiC Forward Shroud After 50 Hours Engine Test	217
195b	RCSiC Forward Shroud After 50 Hour Engine Test With Spring Retainer Can, Heat Shield and Bolt Seals in Place	217
195c	RCSiC Forward Shroud After 50 Hour Engine Test	218
195d	RCSiC Forward Shroud After 50 Hour Engine Test	218
195e	RCSiC Forward Shroud After 50 Hour Engine Test	219
196	$HPSi_3N_4$ Vanes After 50 Hour Engine Test	219
197	Centering of Rear Shroud From $RBSi_3N_4$ to Turbine Wheel After 50 Hour Engine Test	220
198	Scroll and Combustor Seals, Modification	221
199	Scroll and Combustor Seals, Modification	222
200	Bellows, Seal, Exhaust All-Ceramic Turbine, Modified	223
201	SiC (NC 430) Forward and Rear Shrouds With Rene 41 Mounting Bolts Before Assembly into Test Engine	224
202	SiC (NC 430) Forward Shroud With Through Holes Added and Pt Layer in Vane Recesses	224
203	SiC (NC 430) Rear Shroud With Slots Added and Pt Layer in Vane Recesses	225
204	SiC (NC 430) Rear Shroud Before Engine Test	225
205	Combustor Housing With Pressure Activated Bellows Assembly for Loading Rear Shroud to Exhaust Scroll Face Seal	226
206	View of Combustor Housing Showing Exhaust Scroll Face Seal	226

LIST OF FIGURES (Contd)

Figure		Page
207	Components of Combustor Housing	227
208	SiC (NC 430) Ceramic Nozzle Before Engine Test Run #4	227
209	Gemini Raial Ceramic Turbine Nozle After Successful 200 Hour Engine Test	229
210	Combustor housing aFter 200 Hour Engine Test	229
211	Ceramic Forward Shroud and Vanes After Successful 200 Hour Engine Test	231
212	Ceramic Rear Shroud and Radial Turbine Wheel Exducer	231
213	RBSiC (NC 430) Forward Shroud After Successful 200 Hour Engine Test	232
214	RBSiC (NC 430) Forward Shroud After Successful 200 Hour Engine Test	232
215	RBSiC (NC 430) Rear Shroud After Succesful 200 Hour Engine Test	233
216	RBSiC (NC 430) Rear Shroud After Successful 200 Hour Engine Test	233
217	$HPSi_3N_4$ (NC 132) Vanes After Successful 200 Hour Engine Test	234
218	$HPSi_3N_4$ (NC 132) Vanes After Successful 200 Hour Engine Test	234
219	Cold Start Transient for Gemini Engine With All-Ceramic Nozzle TIT and EGT Thermocouple Traces Versus Time and Pressure at Compressor Discharge (PCD)	236
220	Shutdown Transient for Gemini Engine With All-Ceramic Nozzle TIT and EGT Thermocouple Traces Versus Time and PCD	237
221	Hot Start Transient for Gemini Engine With All-Ceramic Nozzle TIT and EGT Thermocouple Traces Versus Time	238
222	Cold Start Transient for Gemini Engine With All-Ceramic Nozzle TIT and EGT Thermocouple Traces Versus Time	239
223	Shutdown Transient for Gemini Engine With All-Ceramic Nozzle TIT and EGT Thermocouple Traces Versus Time	240

LIST OF TABLES

Table		Page
1	Erosion Test Results Using Arizona Road Dust	9
2	Material Properties	16
3	Erosion of Candidate Nozzle Materials Versus Impingement Angle	17
4	Erosion of Candidate Nozzle Materials Versus Impingement Velocity	17
5	Summary of Test Results for SiC and Si_3N_3 Simulated Vane Shape Specimens Evaluated at 1200°C on a Mach 1 Simulated Gas Turbine Environment	21
6	Preparation of Glasses	28
7	Summary of $RBSi_3N_4$ Shroud to $HPSi_34N_4$ Vane Fill Materials Exposed to Temperature	28
8	Summary of Metal Shroud to $HPSi_3N_4$ Relaxing Joint Materials Exposed to Temperature Cycling	30
9	Assembly Schedule for Ceramic/Superalloy 10 kW Nozzle for Rig Test	49
10	Test Rig Flow Conditions for Standard and Ceramic Vane Nozzle Tests	59
11	Engine Simulator Rig Flow Conditions With All-Ceramic Nozzle	71
12	Constituents of Simulated Sea Salt	84
13	Test #1 - Calibration Data for Gemini Engine With Ceramic Vane Nozzle	98
14	Test #2 - Calibration Data for Gemini Engine With Ceramic Vane Nozzle	118
15	Steady State Diametrical Growth at Seal Plate Interface for Various Materials	161
16	Steady State Diametrical Growth at Bolt Circle	161

LIST OF TABLES (Contd)

Table		Page
17	Steady State Diametrical Growth a Downstream Turbine Wheel Diameter	162
18	Emergency Shutdown Thermal Sizes	162
19	Cost Estimate for Hot Pressed Silicon Ceramic Vanes of Variable Complexity and Quantity	166
20	Procurement Schedule for Ceramic Components	167
21	Seal Leakage in Furnace Cycling Test	191
22	Steady State Temperatures for Nominal 1700°F Turbine Inlet Temperature	199
23	Engine Simulator Rig Flow Conditions With All-Ceramic Nozzle Designed for Engine Installation	199
24	Summary of Engine Simulatory Testing of All-Ceramic Nozzles	200
25	Axial and Radial Turbine Tip Clearances Measured During *1700°F TIT Steady State Run*	201
26	Test #3 - Calibration Data for Gemini Engine With All-Ceramic Nozzle	209
27	Test #4 - Calibraiton Data for Gemini Engine With All-Ceramic Nozzle	235

SUMMARY

This final report covers project work for application of ceramics to the nozzle section of the MERADCM 10 kW (Gemini) radial inflow gas turbine engine. The goals of the work were to introduce ceramics for better engine life through higher erosion resistance of the nozzle vanes and subsequently better performance by facilitating higher turbine inlet temperature.

These goals were realized in successful engine runs which include:

1. A 25 hour run of hybrid-ceramic/metal radial turbine nozzle assembly with $HPSi_3N_4$ ceramic vane inserts which yields a ten to one-hundred fold increase in nozzle erosion resistance.

2. A 200 hour run of an all-ceramic radial turbine nozzle assembly for up-rated turbine inlet temperature incorporating erosion resistant $HPSi_3N_4$ vanes, with siliconized reaction bonded SiC forward and rear shrouds.

Program work leading these results included materials selection studies, development of specialized relaxing glass adhesives for stress reduction at ceramic interfaces, design studies and engine simulator experiments. Engine simulator experiments were for proving design feasibility and providing data on thermal shock, erosion and sea salt corrosion characteristics of ceramics in the turbine environment.

The program results demonstrated feasibility of operating the Gemni engine with ceramic vane inserts and an all-ceramic nozzle and highlighted the advantages of using ceramics.

A Manufacturing Methods and Technology project for cost reduction of the ceramic vane insert nozzle concept has been initiated in a separate project under the sponsorship of MERADCOM at Solar (Contract #DAAK70-78-C-0156). Continued work on durability testing and temperature uprating of other elements of the Gemini engine is in the planning stages.

1

INTRODUCTION

The objective of this program is to apply ceramics to the nozzle section of the MERADCOM 10 kW engine for increased erosion resistance and to provide the means of achieving a higher turbine inlet temperature. The program work to date, reported here, includes engine simulator tests and engine tests of a ceramic vane nozzle and an all-ceramic nozzle. Further program work will be necessary to meet the objective of higher turbine inlet tmeperature and will include high temperature combustor development and ceramic scroll demonstration. The successful development of the above components will establish the primary elements for technical feasibility of a high temperature version of the Gemini (10 kW) gas turbine engine with increased output.

2

BACKGROUND

2.1 SERVICE EXPERIENCE

Small radial flow gas turbines have found widespread use by the U.S. Army and Air Force in ground generator sets and as APU's for service in essentially all U.S. Army and Navy transport helicopters. Experience in service has shown that the nozzle guide vanes are the most vulnerable portion of the radial turbine engine and suffer the most degradation. There appears to be two principal sources of this degradation. The first results from the ingestion of dust because service conditions do not allow use of highly effective filters or other devices to remove particulate materials. This problem was particularly acute in the Vietnam war where the dust generated at take-off by helicopters seriously affected APU life. The dust caused erosion throughout the engine but coatings were readily found to give signficiant improvement in the cooler sections as described by Shoemaker and Shutmate (Ref. 1). No really effective coating was found for the nozzle guide vanes. However, even in the absence of dust, the nozzle suffers from a second source of degadation. It is more difficult to design a small combustor to have as high efficiency as a large one particularly when the engine must be capable of operations by unskilled personnel and must keep operating under adverse conditions such as the dust ingestion described earlier. Hot spots and carbon particles result from loss of combustor performance and accelerate nozzle degradation.

Extensive effort has been devoted to developing solutions to the nozzle erosion problem in small gas turbines. Larger gas turbines, such as those used for propulsion do not present quite the same problem. The exposure to ingested dust and other erodants is limited to quite short periods, primarily during landing and take-off. In contrast, small radial gas turbine generators used by the U.S. Army for APU's and ground generator sets may be exposed continuously to ingested dust. Further, the power output-to-weight ratio would be affected adversely in these small engines by addition of a dust separator. Some types of solutions to dust erosion in propulsion engines are described by Connors and Murphy (Ref. 2).

Consideration for small radial engines caused attention to be directed to use of erosion resistant materials that would be used in monolithic form rather than as coatings. Ceramics were an obvious candidate. Work began on Solar internal programs and showed that cermics offered a potential solution to the problem. In addition, it was recognized that ceramics offered a longer term advantage in terms of higher inlet temperatures and hence higher power

outputs from the engine without weight increase. The background work at Solar and its application to the MERADCOM 10 kW gas turbine are described in the next section.

2.2 EROSION IN GAS TURBINES

The initial work was directed to tests of selected ceramic materials, selection of hot pressed silicon nitride and tests in an engine where three cast N-155 vanes had been replaced with this material. This work was sufficiently promising so that the difficult problems of replacement of all the vanes and of replacement of the metallic shrouds could be proposed to MERADCOM and become the basis of this program. The preliminary work is described here.

2.2.1 Requirements for Nozzle Vanes

Materials for nozzle guide vanes must possess many properties. Resistance to thermal cycling, resistance to hot spots and thermal flashes, and resistance to erosion by carbon and particulate matter are a few of the requirements. These, in turn, lead to specific property requirements including: high hot strength, low thermal expansion, good oxidation and hot corrosion resistance, minimum dynamic oxidation effects, high thermal conductivity, good impact resistance, and so on. Good design must be used to minimize the demands on the material and, in this regard, it has been found that a mechanical joint between shroud and vane reduces the thermal stress problem in these small radial gas turbines. However, once the design has been optimized, the intrinsic properties of the materials impose the ultimate limit on performance.

The high pattern factor associated with small gas turbines, particularly those operated under unfavorable service conditions, had led to adoption of low turbine inlet temperatures, e.g., 927°C (1700°F) maximum. This has an adverse effect on efficiency but is warranted to permit the high reliability required. Materials capable of withstanding higher temperature flashes would permit increase of TIT with a beneficial effect on efficiency. Silicon nitride appeared to have the combination of strength at temperature and low expansion required for this application. However, the greatest problem in field service results from erosion. Erosion opens up the critical nozzle openings with a decrease of efficiency revealed by a rise in the exhaust gas temperature until it exceeds a specified value [e.g., 727°C (1340°F)]. Because of its importance on performance, several studies have been made at Solar to understand the mechanism of erosion and to evaluate materials (Refs. 1, and 3 through 5). These studies have permitted the basic mechanisms to be identified for metallic materials (Ref. 4). Strength, hardness and heat treatment had little effect on erosion resistance. Indeed, the erosion weight loss was found to deviate less than ±10 percent for many common metallic materials, although the differences in density between metals result in greater differences on a volume basis. However, non-metallic, elastic materials showed a markedly different rate of erosion that varied in a

different way than metals when measured against angle of incidence. Data due to Finnie (Ref. 6) illustrates this point in Figure 1.

2.2.2 Erosion in Service

The erosion of nozzle vanes in service is shown in Figure 2 for a Titan turbine nozzle after 68 hours service in Vietnam. Note the severe erosion at the trailing edges of the vanes. Similar wear has been induced in the test cell by controlled ingestion of -140 mesh silica dust for 10 hours as shown in Figure 3. Such wear results from low angle impingements and reference to Figure 1 shows that metals are at their worst under such conditions. Shoemaker and Shumate (Ref. 1) had investigated hard, brittle coatings for nozzle guide vanes but had found little success because of porosity in some coatings (e.g., plasma sprayed), spalling of dense coatings, or inadequacy of thickness. The work suggested that a monolithic ceramic material might provide the answer. Published data attested to the adequacy of silicon nitride in most respects but no data were available on erosion resistance.

2.2.3 Materials Evaluation

Measurements were made to compare the erosion resistance of the two principal forms of silicon nitride with a typical metal (type 410 stainless steel). Arizona road dust was used in the standard Solar erosion test rig (Refs. 1, 4 and 5) and was accelerated by air to 600-700 feet per second. The loading

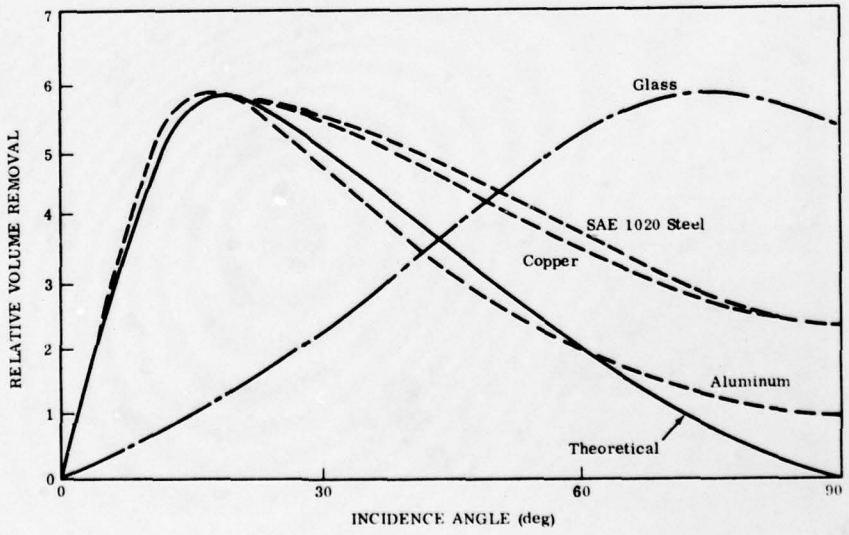

Figure 1. Predicted and Experimental Variation of Volume Removal With Incidence Angle for Various Ductile and Brittle Materials

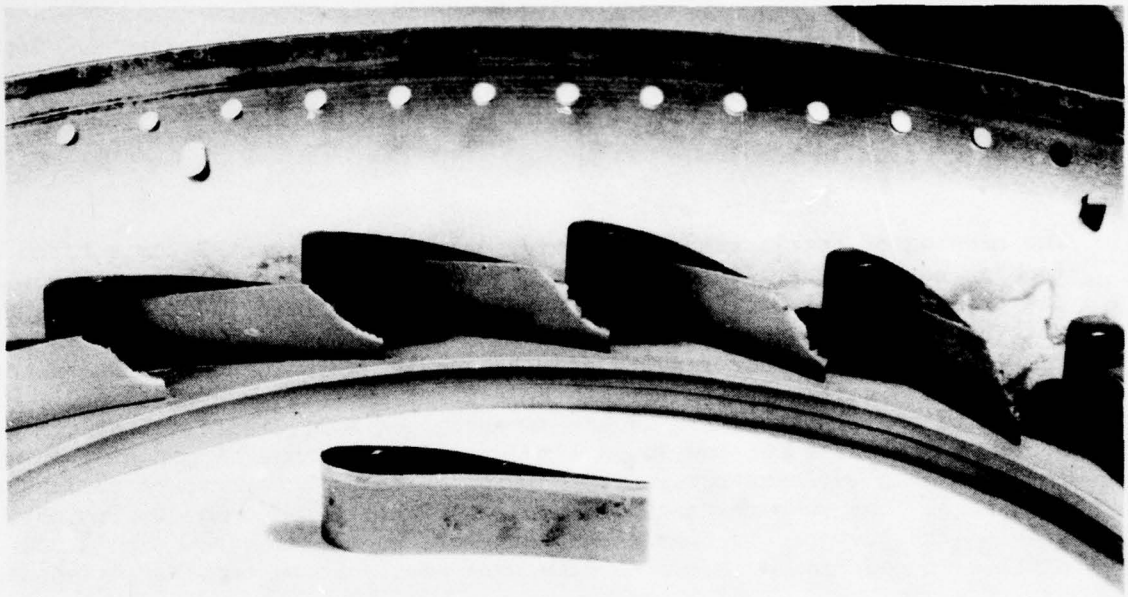

Figure 2. Typical Titan Turbine Nozzle Vanes After 68 Hours of Vietnam Dust Erosion (Note eroded, curled edge as compared to uneroded vane in foreground)

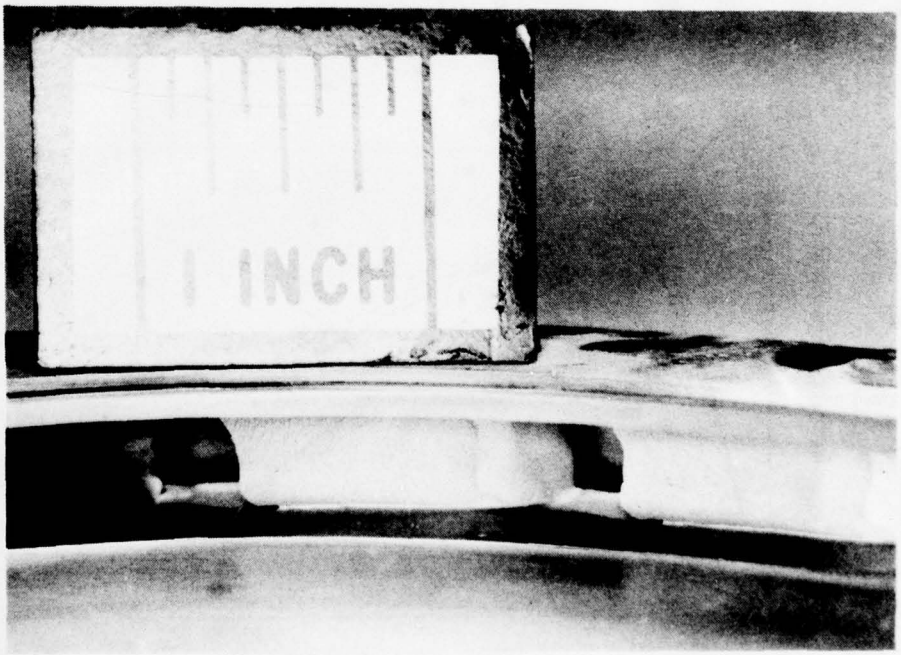

Figure 3. Titan Nozzle Vane Assembly After 10 Hours of Test Showing Severe Erosion of Conventional Vanes

was 80 mg dust per ft^3. Results for the two impingement angles of 30 and 90 degrees are compared in Table 1.

The porous, reaction sintered silicon nitride shows a small improvement over the 410 steel at the critical 30-degree impingement angle, but not enough to warrant consideration. However, the hot pressed silicon nitride shows almost unmeasurable loss of weight and should increase the life nearly a hundred-fold.

Table 1

Erosion Test Results Using Arizona Road Dust
(Average Velocity 600-700 fps, 80 mg Dust/ft^3)

Material	Particle Size	30-Degree Impingement Angle Average Volume Loss x 10^3 cc For Time in Minutes			90-Degree Impingement Angle Average Volume Loss x 10^3 cc For Time in Minutes		
		5	10	45	5	10	45
410 SS	43-74	0.46	0.92	3.7	0.28	0.47	1.9
Reaction Sintered Si_3N_4	43-74	--	0.47	2.2	1.1	2.1	5.6
Reaction Sintered Si_3N_4	-43	--	--	2.3	--	--	4.5
Hot Pressed Si_3N_4	43-74	--	--	0.06	0.10	0.10	0.13
Hot Pressed Si_3N_4	-43	--	--	0.00	--	--	0.03

2.3 APPLICATION OF CERAMICS TO A RADIAL ENGINE

Solar supplies eight separate Titan engine models for use on various versions of four military helicopters, i.e., the CH46 Navy Sea King, CH47 Army Chinook, CH53 Navy Sea Stallion and the CH54 Army Flying Crane. Ceramic vanes were evaluated on the T62T-27 engine used on various versions of the CH53. This work was performed as part of a product support program for the U.S. Navy (Ref. 7).

The nozzle guide vane in the Titan engine is shown in the foreground in Figure 2. The hole allows mechanical attachment of the outer and inner shrouds. Such a design would not be suitable for ceramics, so that in the first engine tests, only three vanes were replaced by hot pressed silicon nitride with reliance placed on the mechanical fasteners at the other metallic vanes to hold the silicon nitride in place in recesses. The method of mechanical attachment used in the Titan is to upset or rivet each

fastener. Although the silicon nitride vane was not fastened in this manner, attachment of adjacent vanes caused some small cracks to form.

The T62 engine was run in the normal manner at 61,300 rpm except that 4.4×10^{-5} pounds of dust per pound of air was introduced. The dust was -140 mesh silica and required 172.5 grams per hour. The first erosion test extended 10 hours during which time nearly four pounds (1800 gms) of dust was passed through the engine. No special precautions were taken at light-off in this test.

A comparison of an N-155 vane with the adjacent hot pressed silicon nitride vane is shown in Figure 4. Preservation of the sharp fracture edges reflects the remarkable erosion resistance of $HPSi_3N_4$ at 927°C (1700°F). (Fractures were due to an improper fit of vane in the recesses. Subsequent work in the current project demonstrated the capability to avoid fractures of this type.)

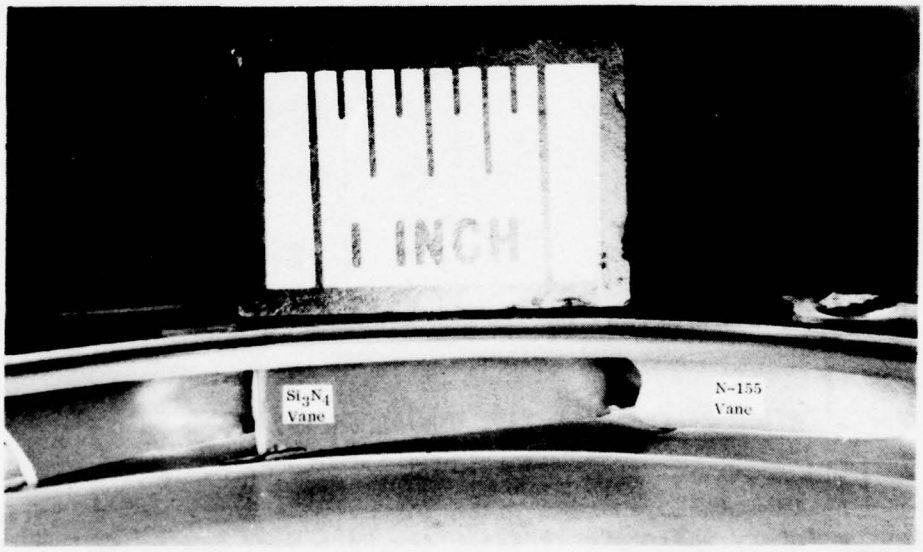

Figure 4. Silicon Nitride (left) and N-155 Vanes (right) in Titan Engine After 10 Hours Erosion Testing

3

PROGRAM RESULTS

3.1 PROGRAM PLAN

This program is divided into four phases. The first phase culminated in engine simulator rig tests of ceramic vane section and simplified all-ceramic nozzles and included background steps required to reach this goal: material evaluation and selection; analysis and design; fabrication studies and preliminary tests. The second phase included design, fabrication and engine test of a ceramic vane section nozzle. The third phase involved analysis, design, fabrication and engine simulator testing of an all-ceramic nozzle. An all-ceramic nozzle design concept was selected and engine tested in the fourth phase. Figures 5, 6 and 7 show a block diagram of the program work plan.

3.2 MATERIAL AND NOZZLE SEGMENT EVALUATION - PHASE I

3.2.1 Objectives

This program phase was for the purpose of generating background information necessary to design a part-ceramic nozzle suitable for engine test. The feasibility of using silicon nitride parts for an all-ceramic nozzle in a small radial engine hot end environment was also investigated. Both of these nozzle concepts were subjected to engine simulator rig tests to meet these objectives.

3.2.2 Material Evaluation

Silicon nitride and silicon carbide are recognized as the best ceramic materials commercially available today for use in the gas turbine hot end environment. A paper study was conducted at program initiation to select the best materials and fabrication processes for nozzle vanes and nozzle shrouds. In addition, experimental erosion studies were conducted at Solar since this information was unavailable in the literature. The four primary material forms considered were hot pressed silicon nitride ($HPSi_3N_4$), reaction bonded silicon nitride ($RBSi_3N_4$), hot pressed silicon carbide (HPSiC) and recrystallized silicon carbide (RCSiC). Another variation on silicon carbide considered was silicon filled recrystallized silicon carbide.

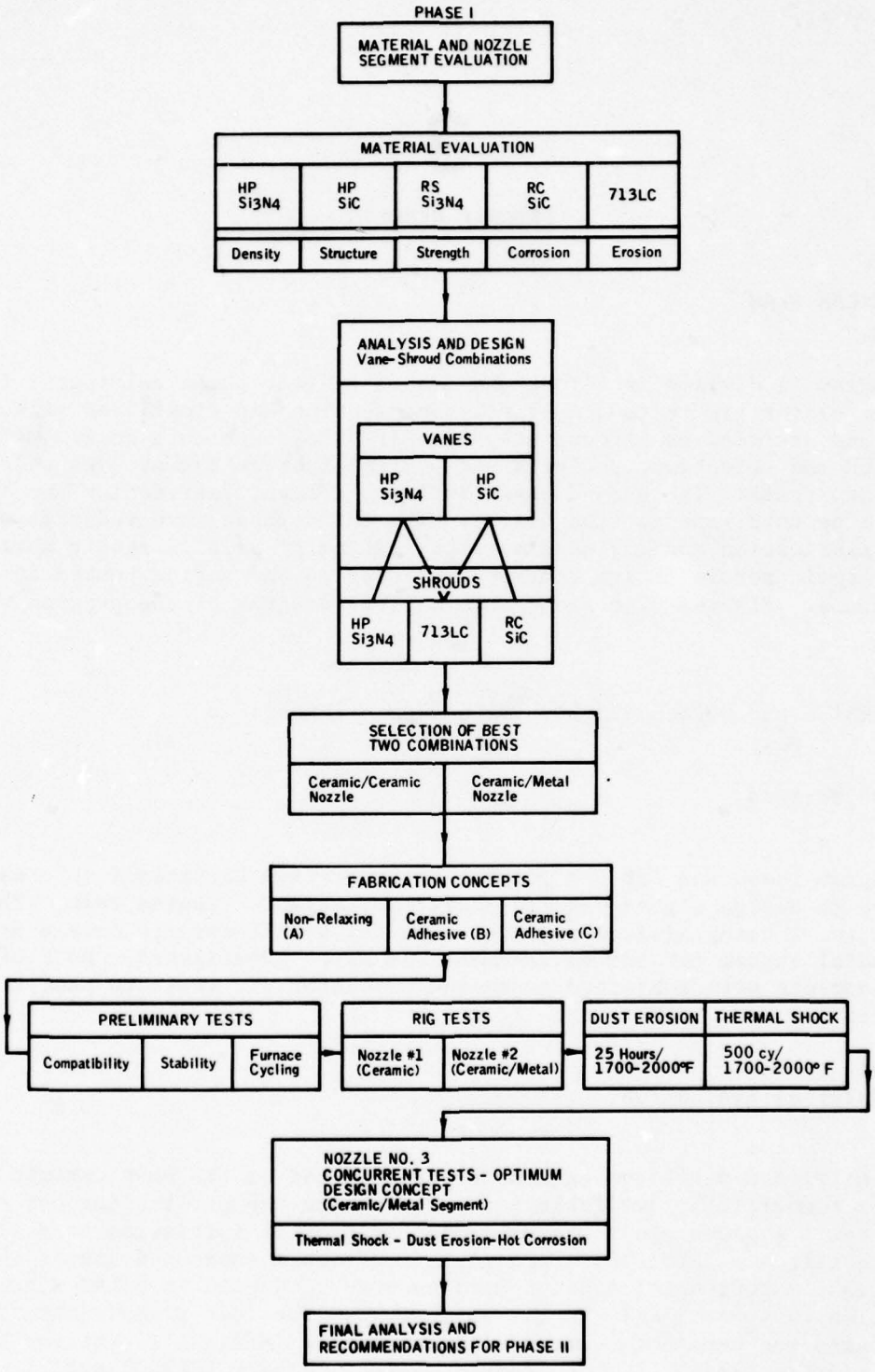

Figure 5. Work Plan for Phase I - Materials and Nozzle Segment Evaluation

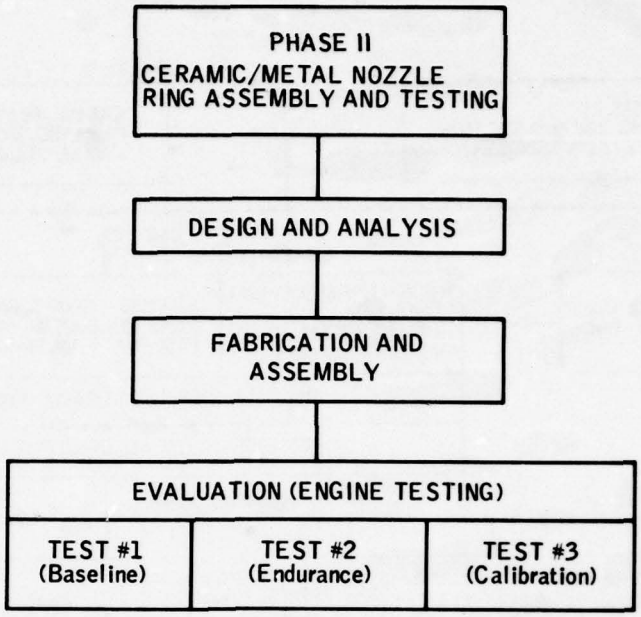

Figure 6. Work Plan for Phase II - Nozzle Ring Assembly and Testing

Through the duration of this program, up to material procurement, no new ceramic materials which warranted consideration for turbines were developed to the point where they are commercially available for application. For example, Sialon (Ref. 8) shows the potential of good strength and fabrication characteristics, but is not fully characterized and is unavailable in finished form. Sinterable silicon carbide and silicon nitride have also shown promise as excellent materials, but had not been developed or characterized to the point where it was practical to make gas turbine parts (Ref. 9). Therefore the above candidate ceramic materials were still considered the best available for this application study.

Criteria for Material Selection

Selection of silicon nitride and silicon carbide materials for Phase I vane and shroud rig tests was accomplished by considering fundamental materials property data available in the literature and experience of numerous researchers who have tested ceramics for turbine application. Data in the literature was inadequate in the case of dust erosion properties and was supplemented by experimental studies.

In order to allow a logical scheme for materials selection, relevant properties and their priority were defined as follows:

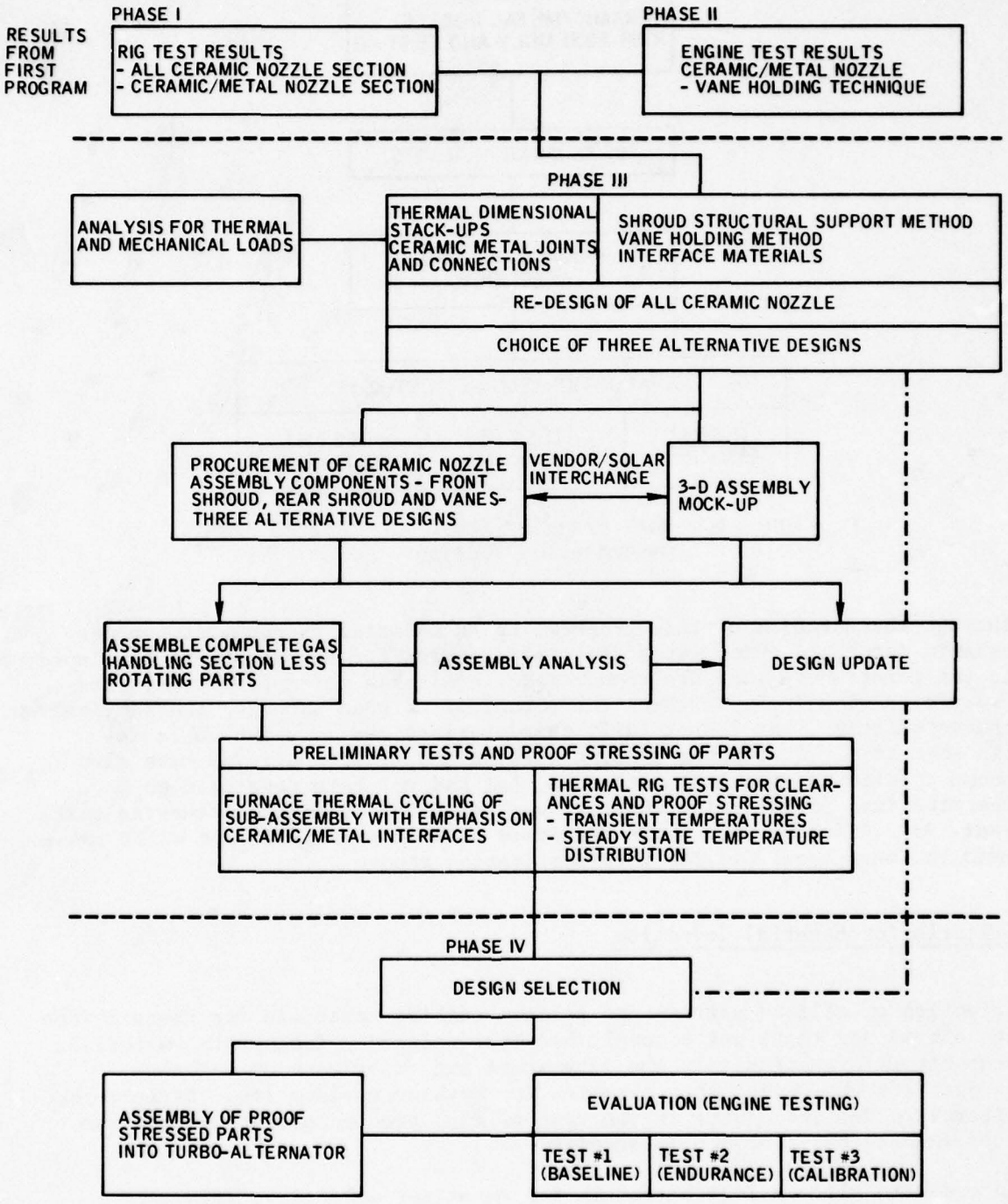

Figure 7. Program Sequence

Priority of Material Properties for Vanes

1. Erosion resistance
2. Thermal shock resistance*
3. Corrosion resistance
4. High temperature strength
5. High impact strength and energy of fracture at temperature

Priority of Material Properties for Shrouds

1. Ease of fabrication
2. High temperature strength
3. Thermal shock resistance
4. Erosion/corrosion resistance

Table 2 presents a summary of the properties for hot pressed silicon nitride, hot pressed silicon carbide, reaction bonded silicon nitride, recrystallized silicon carbide and 713LC nickel base superalloy. The data on ceramics refer to Norton Company materials, NC-132, NC-203, NC-350 and NC-400 except where indicated. The more recent materials are the result of process refinement rather than composition variation of the materials reported in many of the references given here. For example, NC-132 silicon nitride is nearly identical in composition and structure to HS-130 silicon nitride except that the NC-132 has higher strength due to better control of maximum internal void size (Ref. 10). Properties, other than strength, such as thermal conductivity or corrosion resistance would be expected to be nearly identical between these two materials. In the case of thermal shock resistance or Charpy impact strength, data available on the former materials are at least qualitatively comparable to the most recent materials.

Vane Materials

Erosion Resistance. Tables 3 and 4 summarize results of erosion tests conducted at Solar on 713LC superalloy, reaction sintered Si_3N_4 and hot pressed Si_3N_4. The hot pressed Si_3N_4 shows at least one order of magnitude superior erosion resistance to 713LC in both 90 and 30 degree impingement tests. Figure 8 pictures test samples after erosion experiments. Further evidence of good erosion properties of hot pressed silicon nitride can be seen in Figure 4 which shows both $HPSi_3N_4$ and N-155 vanes run in a Solar T62 Titan engine exposed to severe dust injection. (Each pound of inlet air was injected with 4.4×10^{-5} pounds of -140 mesh silica.)

*Thermal shock resistance relates primarily to strength, elastic modulus, thermal conductivity, thermal expansivity and plasticity.

Table 2

Material Properties

Material	Flexural Strength kPa (psi) 3 Pt. Bend at 982°C (1800°F)	Tensile Strength kPa (psi) at 982°C (1800°F)	Modulus of Elasticity kPa (psi) at 25°C (77°F)	Density gm/cc	Thermal Expansion Coefficient $°C^{-1}$ (20-1000°C (1832°F)	Thermal Conductivity W/m°C (Btu/hr ft °F) at 25°C	Specific Heat Cal/gm °C at 25°C	Thermal Stress Resistance Parameter R_1 Rapid Temperature Variation $°C^{-1}$	Thermal Stress Resistance Parameter R_2 Slow Temperature Variation $°C^{-1}$	1000 Hour Stress Rupture at Temperature kPa (psi)
Hot Pressed Silicon Nitride	869000 (126000)	294000 (42600) HP-130 (Ref. 16)	317 x 10^6 (45 x 10^6 (Ref. 20)	3.2	3.2 x 10^{-6} (Ref. 10) (3.73 x 10^{-6} at 1800°F) (Ref. 26)	28 (17) (Ref. 12)	0.17 (0.30 at 1800°F) (Ref. 20)	650 (Ref. 21) Lucas Material	26 (Ref. 22)	138000 (20,000) HS-130 at 1149°C (2100°F) (Ref. 19)
Hot Pressed Silicon Carbide	676000 (98000)	239000 (34700) (Ref. 16)	441 x 10^6 (64 x 10^6) (Ref. 20)	3.2	4.3 x 10^{-6} (Ref. 20)	81 (47) (Ref. 20)	0.15	144 (Ref. 21) Norton Material	23 (Ref. 22)	(only 619 hours) 103000 (15,000) at 1260°C, (2300°F) (Ref. 28)
Reaction Bonded Silicon Nitride	317000 (46000)	—	172 x 10^6 (25 x 10^6)	2.4	3.2 x 10^{-6} (Ref. 20)	15.5 (9) (Ref. 20)	0.17	256 (Ref. 21) Lucas Material	5 (Ref. 22)	—
Recrystallized Silicon Carbide	186000 (27000)	—	207 x 10^6 (30 x 10^6) (Ref. 20)	2.6	4.3 x 10^{-6} (Ref. 20)	43 (25) (Ref. 20)	0.15	92 (Ref. 21) Norton Material	5 (Ref. 22)	—
713LC Nickel Base Superalloy	—	(68500) 19.7% elongation (Ref. 18)	206 x 10^6 (29.9 x 10^6) (Ref. 18)	7.91 (Ref. 18)	16.4 x 10^{-6} (Ref. 18)	21 (12) (Ref. 20)	—	Do not Apply to Ductile Materials		96500 (14000) at 982°C (1800°F) (Ref. 18)

*All information from Reference 17 unless indicated otherwise.

Table 3

Erosion of Candidate Nozzle Materials Versus Impingement Velocity

Material	Impingement Angle	Mean Particle Impingement Velocity, fps		
		190	520	840
		Erosion Volume Loss x 10^3 cc		
713 LC Superalloy	30°	0.09	2.60	-
				-
	90°	0.21	1.79	30.0
				26.8
Hot Pressed Silicon Nitride	90°	-	0.12	0.22
				0.63
				0.56
Hot Pressed Silicon Carbide	90°	-	0.32	1.59
				1.28
				1.34
Recrystallized Silicon Carbide, Silicon Filled (NC-430)	90°	0	0.39	2.34
				3.08
Reaction Bonded Silicon Nitride	90°	0	2.88	21.7
				28.2

Test Conditions: 15 minutes at room temperature with 80 mg/ft^3 of 43-74 micron Arizona road dust and 3/8 in. (0.95 cm) diameter nozzle. Gas velocity 200 fps (190), 600 fps (520), 1000 fps (840)

Table 4

Erosion of Candidate Nozzle Materials Versus Angle

Material	Erosion Volume Loss x 10^3 cc 30 Degree Impingement Angle	Erosion Volume Loss x 10^3 cc 90 Degree Impingement Angle
713 LC Superalloy	2.60	1.79
Hot Pressed Silicon Nitride	0	0.12
Hot Pressed Silicon Carbide	0.04	0.32
Reaction Bonded* Silicon Nitride	1.65**	2.88
NC-430	0.08	0.39

*Ground surface. ** Derived from previous results.

[520 fps mean particle impingement velocity, 15 minutes at room temperature, 80 mg/ft^3 of 43-74 Micron Arizona road dust and 3/8 in. (0.95 cm) diameter nozzle]

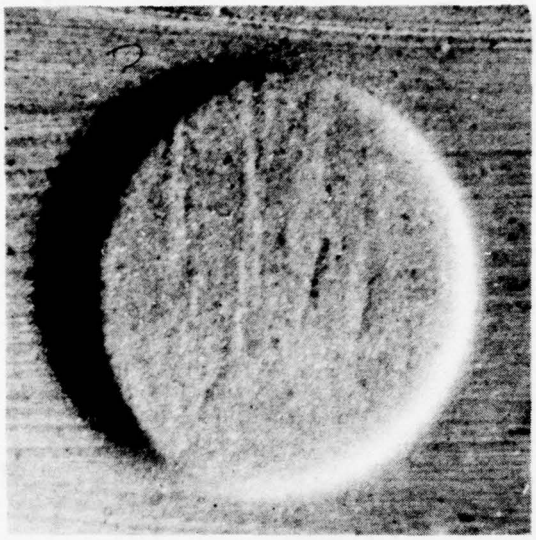

713LC Nickel-Base Superalloy
0.017 inch Penetration
30.3 cc x 10^{-3} Volume Removal

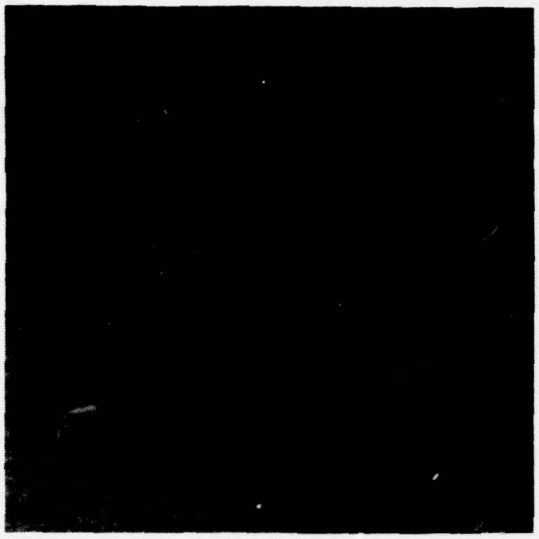

Hot Pressed Silicon Nitride
0.0003 inch Penetration
0.6 cc x 10^{-3} Volume Removal

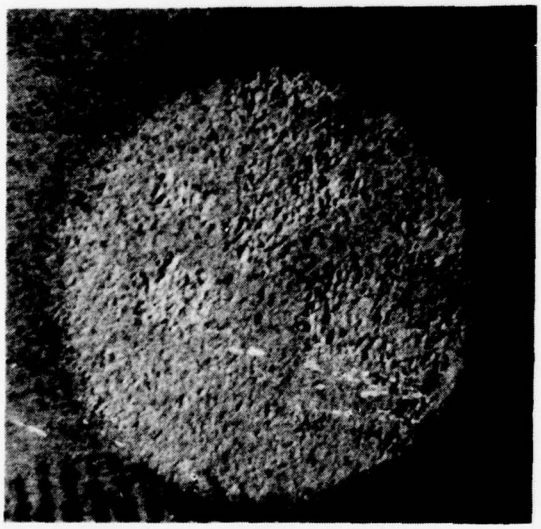

Hot Pressed Silicon Carbide
0.0007 inch Penetration
1.3 cc x 10^{-3} Volume Removal

Silicon Filled Recrystallized
Silicon Carbide (NC-430)
0.0013 inch Penetration
2.3 cc x 10^{-3} Volume Removal

Figure 8. Eroded Surfaces of 713LC Nickel-Base $HPSi_3N_4$, HPSiC Superalloy and NC-430; 3/8 Inch Nozzle Diameter; 90 Degree Impingement Angle; 15 Minutes at Room Temperature; 840 fps Particle Velocity; and 80 mg/ft^3 of 43-74 Micron Arizona Road Dust. (Volume removal and penetration calculated from weight changes)

Reaction sintered silicon nitride shows only a slight erosion advantage over 713LC at 30 degree impingement angle and inferior erosion in relation to 713LC at a 90 degree impingement angle. This disqualifies consideration of a reaction sintered silicon nitride for use as a vane material in this program since erosion is the first priority material property for vanes. (However, it should resist erosion acceptably as a shroud material since the lower gas velocity at most surfaces of shrouds makes erosion less critical. Also, particle impingement angles to shrouds are very low near nozzle throat and turbine contour regions where gas velocities are higher.)

HPSiC shows slightly less erosion resistance compared to $HPSi_3N_4$ but is still considerably superior to 713LC superalloy under these test conditions. The silicon filled recrystallized silicon carbide has surprisingly good erosion resistance for a lower strength ceramic.

Thermal Stress Resistance. Good thermal stress resistance is considered to be important for a vane material. Reference 11 cites two thermal stress resistance parameters for ceramics, R_1 and R_2, which depend upon bend strength, σ_B, elastic modulus, E, thermal expansivity, α, and thermal conductivity k.

$$R_1 = \sigma_B/E\alpha$$

$$R_2 = k\sigma_B/E\alpha$$

R_1 applies to rapid thermal cycling and R_2 to slow thermal cycling.

The values of these parameters are given in Table 2 for the four materials under consideration. The terms are in indices of relative resistance to thermal stresses of different ceramic materials assuming the same geometry and surface heat loading in a monolithic structure. Larger values of R_1 and R_2 suggest greater thermal stress resistance.

Based upon the values of R_1 and R_2 listed in Table 2, hot pressed silicon nitride would be expected to perform better than the other materials under rapid or slow thermal transient conditions. This is in good agreement with thermal shock experiments conducted by a number of researchers, including Solar. Even though experimental thermal shock performance of hot pressed silicon carbide is substantially less than that of hot pressed silicon nitride, the parameter R_1 best describes its relative merit for gas turbine applications. R_1 also agrees with experimental evidence which shows both reaction bonded silicon carbide and recrystallized silicon carbide to have inferior thermal shock resistance to either hot pressed form.

Beck (Ref. 12) reported results from comparative thermal shock tests of the four ceramic types in Table 2. Each of these materials was fabricated into simulated airfoil sections with various edge radii and exposed to a 1316°C

(2400°F) maximum temperature laboratory thermal shock schedule with the following results.

Hot Pressed Silicon Nitride (Grades 130 & 110)	Both survived all tests for all radii (grade HS-130 (Norton Co.) provided better oxidation resistance).
Hot Pressed Silicon Carbide	Crack sensitive with one of four possible radii to 1316°C (2400°F). Survivied all tests to 1260°C (2300°F). Oxidation resistance good only for short term exposure. Vane tests conducted later on an improved grade (NC-203) showed good oxidation resistance but continued subcritical cracking when exposed to peak temperatures.
Reaction Bonded Silicon Nitride	One grade exhibited poor thermal shock resistance for all size radii. A second grade performed well in thermal shock but considerable edge loss (oxidation) was experienced for all test specimens.
Recrystallized Silicon Carbide	Showed an early tendency toward cracking but little progression of cracks. Oxidation resistance was good.

Mumford and Booker (Westinghouse, Ref. 13) reported simultaneous high temperature (1371°C [2500°F]) thermal shock tests of hot pressed silicon nitride and hot pressed silicon carbide vanes. (The maximum surface heat transfer coefficient on the vane airfoils was about 2840 W/M^2 °C (500 Btu/hr sq. ft °F).

After three cycles the silicon carbide airfoils were cracked whereas the nitride parts were undamaged. Subsequent failure of the combustor impacted both types of vanes with metal debris. All of the silicon carbide vanes were shattered while the silicon nitride vanes remained intact.

Simulated gas turbine environment thermal shock tests to 1200°C (2200°F) conducted by Sanders and Probst (Ref. 14) are shown in Table 5. (Figure 9 summarizes these findings in the form of a bar chart for clarity.)

These data support the concept that the hot pressed silicon nitride is superior in high temperature thermal shock to the other three ceramic forms considered here, and that hot pressed silicon carbide performs better than reaction bonded silicon nitride or recrystallized silicon carbide. Refel SiC shows good thermal shock resistance, possibly better than HPSiC.

Corrosion Resistance. Figure 10 taken from Reference 15 gives corrosion-erosion behavior of hot pressed Si_3N_4 and SiC compared to that of commonly used superalloys, X-45 and Udimet-500. The ceramic materials were exposed to

Table 5

Summary of Test Results for SiC and Si_3N_4 Simulated Vane Shape Specimens Evaluated at 1200°C in a Mach 1 Simulated Gas Turbine Environment

Materials reaching 100 cycle goal	Materials failing in thermal fatigue (cycle range to failure)	Materials failing in mechanically in holder (cycle range to failure)
Norton HP SiC	A.C.E. HP SiC (41-43)	Norton low-fired RS SiC (26)
U.K.A.E.A. (Refel) RS SiC	AVCO HP SiC (1-47)	A.M.E. RS Si_3N_4 (7-49)
Norton HP HS130 Si_3N_4	Ceradyne HP SiC (1-11)	Norton NC350 RS Si_3N_4 (54-92)
Ceradyne HP Si_3N_4	Carborundum-KT-RS SiC (1-10)	U.K.A.E.A. (Refel) RS SiC (89)
AVCO HP Si_3N_4	Norton low-fired RS SiC (22)	E.R.C. CVD SiC (1-52)
	Norton high-fired RS SiC (0-1)	
	A.M.E. RS Si_3N_4 (9-24)	
Test Cycle: 1 hour at 1200°C, 5 minute still air cool (Ref. 14)		

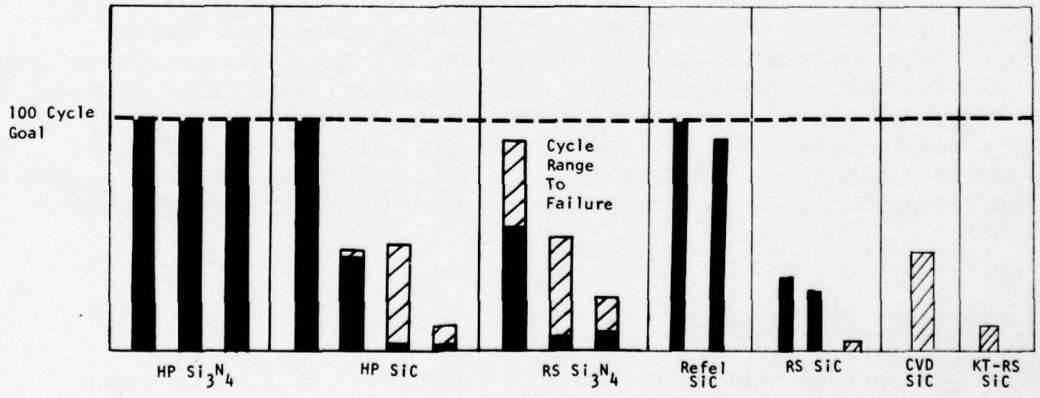

Figure 9. Summary of Test Results for SiC and Si_3N_4 Simulated Vane Shape Specimens Evaluated at 1200°C in a Mach 1 Simulated Gas Turbine Environment. Test Cycle: One Hour at 1200°C, 5 Minutes Still Air Cooled (Ref. 14)

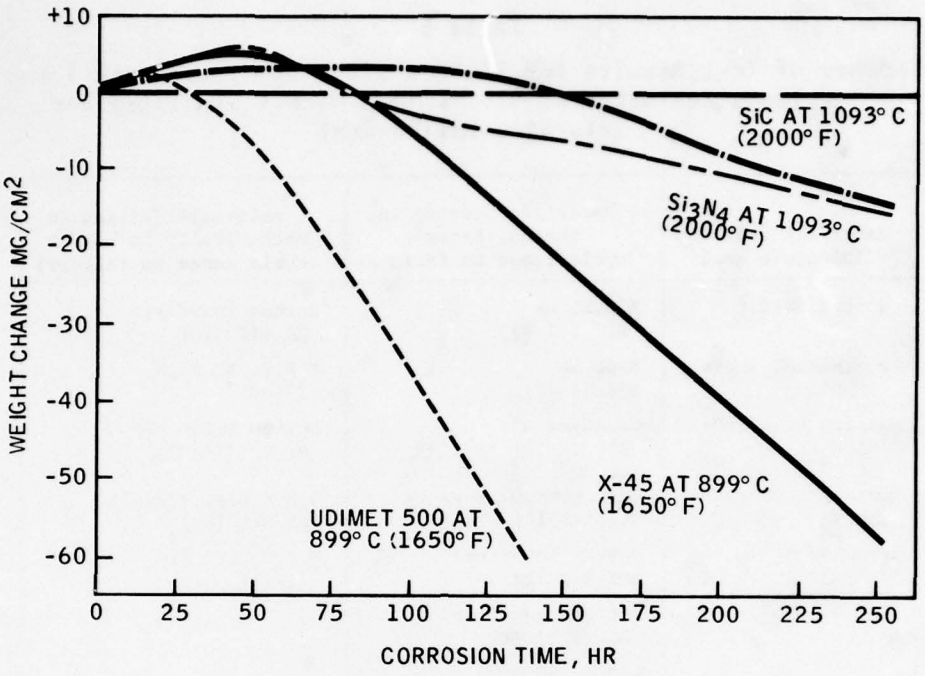

Figure 10. Corrosion of Various Materials in Turbine Test Passage Exposed to Combustor Gas Contaiminated With 0.5% S, 5 ppm Na, 2 ppm V, and 0.6 ppm Mg

1093°C (2000°F) diesel oil combustion gas containing S, Na, V and Mg. The superalloys showed greater weight loss even though they were exposed to a lower temperature of 908°C (1650°F). No appreciable degradation in strength was noted for either of the ceramics.

Later work by the same researchers (Ref. 16) determined that barium introduced into the diesel fuel to inhibit smoke and prevent gum formation played a major role in accelerating corrosion-erosion behavior. Tests with a barium free fuel showed corrosion-erosion weight loss to be even less than corrosion weight loss alone cited in Figure 10. On the basis of these results, corrosion (plus mild erosion) are not expected to present a problem with the assumption that certain deleterious additions are not present in fuels.

High Temperature Strength/Fracture Strength. Figure 11 (from Ref. 17 and 18) includes the flexural strength (3 point bend) of hot pressed silicon nitride (NC-132), hot pressed silicon carbide (NC-350), and tensile strength of 713C superalloy as a function of temperature. High temperature bend strengths are superior to the tensile strengths of high temperature turbine alloys. (Tensile strengths of ceramic materials are typically less than bend strengths as can be seen from data in Table 2. This is due to the statistical nature of failure in these materials. A tensile specimen has more potential sites for failure under load than a bend sample, therefore

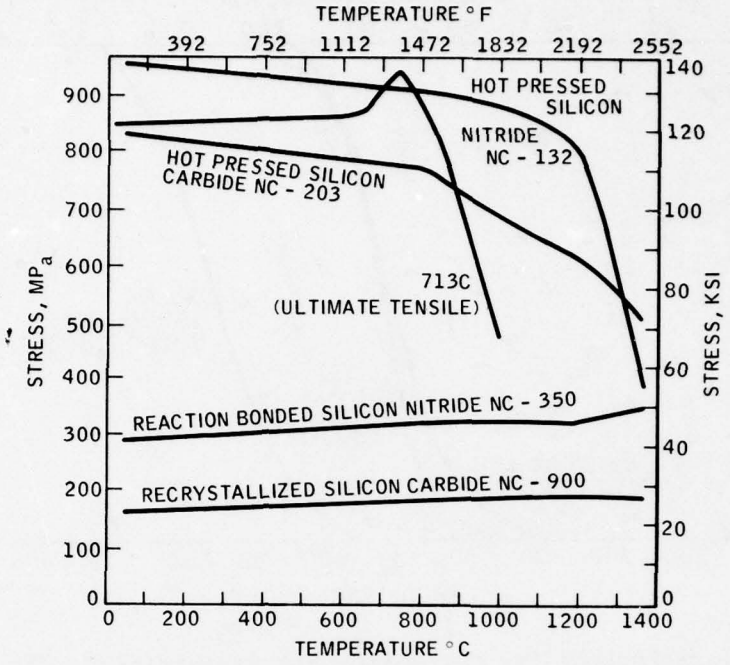

Figure 11. Three Point Bend Strength of Ceramic Materials and Ultimate Tensile Strength of 713C Nickel Base Alloy

failure is more probable at a lower stress. However, bend test results are appropriate for consideration in this program for nozzle vanes since pure tensile loads are not expected to be encountered.) A failure probability curve shown in Figure 12 for hot pressed silicon nitride and silicon carbide taken from Reference 19 shows that despite high mean failure stresses, ceramic materials must be designed to a lower stress which depends upon the statistical nature of failure.

Figure 13 (Ref. 20) gives unnotched Charpy impact strengths for HPSiC (NC-203) and HPSi_3N_4 (NC-130) as a function of temperature. The difference in the high temperature impact strength between these materials is substantial, and offers a possible correlation to better thermal shock resistance in HPSi_3N_4.

Summary of Ceramic Material Selection for 10 kW Nozzle Vanes. Good erosion resistance is the highest priority material selection factor for ceramic vane materials to be considered in rig tests. Hot pressed Si_3N_4 has superior erosion resistance whereas reaction bonded Si_3N_4 offers no improvement over metals. RBSi_3N_4 is therefore eliminated from consideration for vane materials on this basis. HPSiC and silicon filled RCSiC both resist erosion well.

Thermal shock resistance is the next important material selection factor. HPSi_3N_4 appears to be significantly more resistant to thermal shock than the

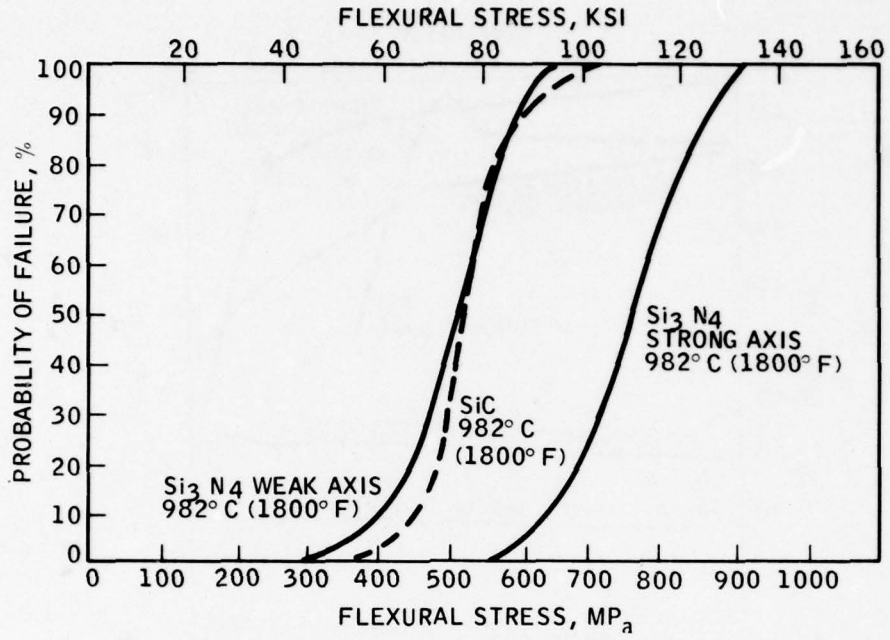

Figure 12. Failure Probability for Norton Hot Pressed Si_3N_4 HS-130, and Norton Hot Pressed Silicon Carbide at 982°C (1800°F) (Ref. 19)

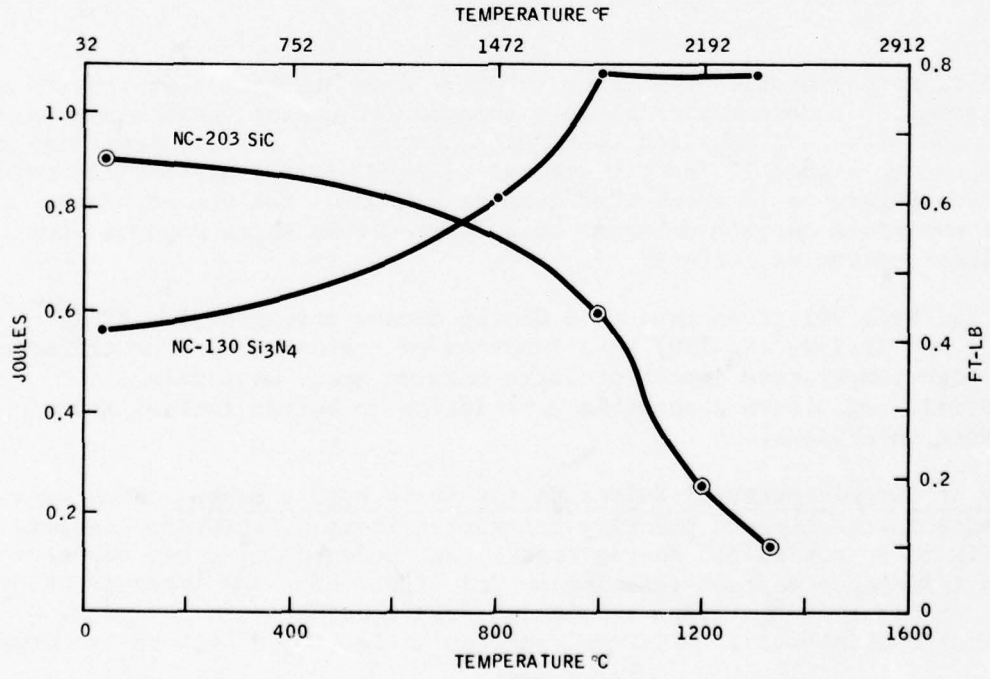

Figure 13. Unnotched Charpy Impact Strength (Ref. 20)

other ceramics considered. Refel SiC (similar to silicon filled RCSiC) shows good thermal shock characteristics, possibly better than HPSiC. Both of the hot pressed ceramics show good high temperature corrosion and strength properties, but $HPSi_3N_4$ shows a higher impact resistance at elevated temperature than HPSiC.

Based upon the above factors, hot pressed silicon nitride was selected as the nozzle vane material for rig testing. Silicon filled RCSiC has an attractive combination of good erosion, and thermal shock resistance while still being a low cost form of ceramic. This material (as well as others) is now being considered as a cost saving alternative to $HPSi_3N_4$ for nozzle vanes (Ref. 21).

Shroud Materials

Ease of Fabrication. Since both inner and outer shrouds for the 10 kW are relatively large and are complex shapes compared to vanes, they must be made from materials capable of being fabricated easily to avoid prohibitive costs. Reaction bonded silicon nitride has the advantage over hot pressed forms because it can be fabricated by injection molding and other low cost fabrication methods. Injection molding is a convenient and inexpensive fabrication method in relation to hot pressing. Lower strength forms of silicon carbide also offer good fabrication properties since they can be slip cast or formed by some other means prior to final firing.

$RBSi_3N_4$ offers advantages over RCSiC because of very minimal distortion or shrinkage upon firing. SiC has some tendency to distort during firing. In addition, surface finish is not as good. Si_3N_4 can be fired to a very good surface finish with negligible distortion of any type.

Hot pressing of either SiC or Si_3N_4 requires graphite dies which must function at temperatures in the range of 1700°C (3092°F) and 1800°C (3272°F) and pressures of 3000 to 4000 psi for one to two hours (Ref. 22). Usually parts must be diamond ground after hot pressing because of process limitations. There is a significant difference in the cost and capabilities of these two techniques (Refs. 10 and 22).

High Temperature Strength. Strength of reaction bonded silicon nitride and recrystallized silicon carbide is substantially less than hot pressed forms (see Fig. 11). In the case of reaction bonded silicon nitride there is some advantage over hot pressed at very high temperatures [>1400°C (2552°F)] because it is free of grain boundary silicates resulting from the addition of MgO necessary as a bonding agent in the hot pressed silicon nitride. However, within the temperature range to be studied in this program, strength is still inferior to hot pressed materials.

Thermal Shock Resistance. Experimental evidence cited in "Thermal Stress Resistance" above shows the low strength forms of Si_3N_4 and SiC to be less resistant to thermal shock in bench tests. These data do not disqualify the

lower strength materials from consideration since thermal conditions at the 10 kW shrouds are not necessarily as severe as the test exposure cycles cited.

Erosion/Corrosion Resistance. Very little erosion resistance is required for the 10 kW turbine shrouds since very little, if any, damage is observed here due to dust ingestion. Vanes typically suffer most of the erosion damage.

Shrouds experience low angle of impingement from dust particles traveling at low velocities. Erosion studies at Solar indicated in Table 3 show that reaction sintered silicon nitride performs at least as well as 713LC superalloy at low impingement angles.

Reference 12 indicates poor oxidation resistance for reaction bonded silicon nitride and good oxidation resistance for recrystallized silicon carbide in laboratory thermal shock tests with temperature excursions up to 1316°C (2400°F).

Summary of Material Selection for 10 kW Turbine Shrouds. Reaction bonded silicon nitride was selected as the candidate shroud material to be tested in Phase I rig tests. This selection was primarily based upon ease of fabrication, capability of making more complex shapes with good tolerance control and resultant lower final cost. Other properties such as strength and thermal shock resistance are lower for $RBSi_3N_4$ than for hot pressed forms, but increased fabrication capability and less severe material requirements allow consideration of $RBSi_3N_4$ as a shroud material.

Erosion and corrosion properties of these less dense materials are also inferior to hot pressed forms but are anticipated to at least equal the durability of the current shroud material, 713LC, and therefore perform acceptably.

3.2.3 Fabrication Studies

The objective of fabrication studies was to develop ceramic joining methods for the nozzle vane to shroud interface which could be evaluated in rig testing. The joint is expected to perform two functions: (1) seal gas leakage around ceramic inserts; and (2) provide uniform support of ceramic parts such that localized stress concentrations are avoided.

Ceramic to Ceramic Joint

"T" samples, as pictured in Figure 14 were used to evaluate bonds. The samples were fired and then evaluated for strength and stability after 60 hours air furnace exposure at 1093°C (2000°F).

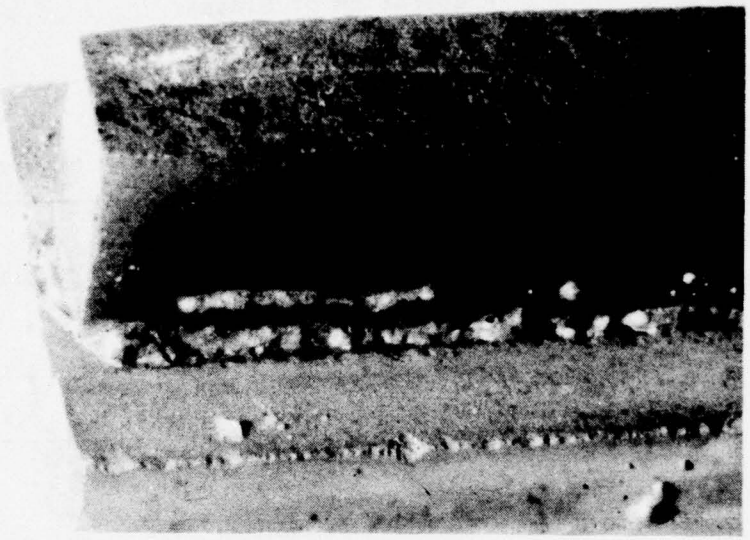

Figure 14. 40% GN19, 20% B402, 40% Cr_2O_3 After 60 Hours, 2000°F Exposure in Air ($RBSi_3N_4$ to $HPSi_3N_4$)

The "T" samples consisted of $RBSi_3N_4$ pieces (corresponding to shrouds) with dimensions of 1 inch x 0.25 inch x 0.180 inch and $HPSi_3N_4$ pieces (corresponding to vanes) with dimensions of 1 inch x 0.25 inch x 0.15 inch. The shroud pieces used 0.170 inch wide 0.020 inch deep lengthwise slots to contain the test joint material and vane pieces.

The glass mixture compositions were mixed from dry weights of basic glass ingredients shown in Table 6. Distilled water was added in appropriate amounts to make a thick slurry. The slurry was applied to both surfaces to be joined after they were cleaned by light bead blasting. The assembly was oven dried and then fired for one hour in air at the specified firing temperature.

Table 7 lists the eight types of relaxing joint materials that were studied.

The joint materials that are underlined, i.e., 40% GN19, 20% B402, 40% Cr_2O_3, and 60% GN19, 40% Cr_2O_3 were selected as the materials to be used for rig test joints. They are stable and have good bond quality. Joints made from these materials are shown in Figures 14 and 15.

Of the other materials listed in Table 7, B402 with 20% Cr_2O_3 was rejected because of instability and 50% GN19 with 50% B402 was rejected because it lacked a filler material to prevent extrusion from the joint under pressure. Both Pyrex and GN19 were unstable at temperature and silicon sintering was rejected because it offers no relaxation and relatively low strength. Thirty percent GN19, 30% B402 and 40% Cr_2O_3 also showed instability at the bond surface and was eliminated.

Table 6

Preparation of Glasses

Glass Type	Weight of Constituents (gm)			Milling Time (Hours)
	Glass Frit	*Green Label Clay	KNO_2	
*S5210	300	18	-	6
†B402	95	5	-	1.5
†GN-19	95	5	-	4
Pyrex	95	5	1	1.5
x332	95	5	-	1.5

*Ferro Corporation Designation

†Solar Designation

xNational Bureau of Standards Designation

Table 7

Summary of $RBSi_3N_4$ Shroud to $HPSi_3N_4$ Vane Fill Materials Exposed to Temperature

Fill Material	Firing Temperature (°C (°F)	As-Fired Condition	After Exposure 60 hrs @ 1093°C (2000°F)	Bond Quality at Room Temperature After Exposure
B402, 20% Cr_2O_3	1093 (2000)	OK	Unstable	Good
50% GN19, 50% B402	1093 (2000)	OK	Good	Stronger than $RBSi_3N_4$
Pyrex	1149 (2100)	OK	Unstable	Good
Si (325 mesh)	1100 (2012) 40 min.; 1400 (2552) 16 hrs; in N_2 atmosphere	OK	Good	Weak
30% GN19, 30% B402, 40% Cr_2O_3	982 (1800)	OK	Unstable	Fair
40% GN19, 20% B402, 40% Cr_2O_3	1038 (1900)	OK	Good	Good
GN19	1149 (2100)	OK	Unstable	Weak
GN19, 40% Cr_2O_3	1149 (2100)	OK	Good	Good

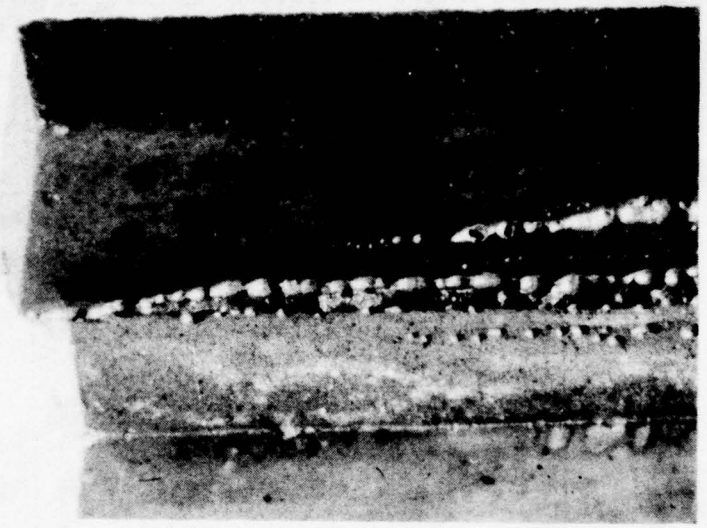

Figure 15. 60% GN19, 40% Cr_2O_3 After 60 Hours, 2000°F Exposure in Air ($RBSi_3N_4$ to $HPSi_3N_4$)

The mixtures chosen for rig testing show little tendency to deteriorate with time at temperature. They contain a significant amount of filler material (Cr_2O_3) and have relatively strong bonds at room temperature.

Ceramic to Metal Joint

Ceramic to metal joint filler materials were considered here to find three types suitable for rig testing.

The test samples consisted of $HPSi_3N_4$ pieces which simulate vanes and 713LC superalloy shroud material with a 0.030 inch depth groove to receive the simulated vane.

Twenty-three different combinations of glass, glass filler and firing temperatures as listed in Table 8 were considered as metal-shroud ceramic-vane rig test candidate materials. The three candidates shown in Figures 16 to 18 which include: 30% B402, 30% GN19, 40% Cr_2O_3, 1093°C (2000°F) fire; 35% B402, 35% GN19, 30% Cr_2O_3, 1093°C (2000°F) fire; and 20% GN19, 40% B402, 40% Cr_2O_3, 927°C (1700°F) fire, showed promise in meeting all of the functional requirements of a glass filler and were selected for rig test. The two basic material requirements are to seal gas leakage around ceramic inserts and to provide uniform contact surface for ceramic parts such that localized stress concentrations are avoided. The three compositions above appear capable of meeting sealing requirements since they survived

Table 8

Summary of Metal Shroud to $HPSi_3N_4$ Relaxing Joint Materials Exposed to Temperature Cycling

Material	Firing Temperature (°F)	As-Fired Condition	After Exposure Cycle		Appearance and Comments
			1300°F Air Cool Two Times	1300°F Water Quench Two Times	
S5210	1700	OK	Vebonded	--	Poor adherence and cracking
S5210, 47% Cr_2O_3	1700	Loose	Debonded	--	Poor adherence and cracking
B402	1500	OK	OK	OK	Crazed and excessive wetting
B402, 5% Cr_2O_3	1500	Debonded	--	--	
B402, 10% Cr_2O_3	1500	Debonded	--	--	
B402, 5% Cr_2O_3	1800	Debonded	00	00	
B402, 10% Cr_2O_3	1800	OK	OK	OK	Too soft at temperature
50% B402, 50% GN19	1800	OK	OK	OK	Will not resist extrusion
40% B402, 40% GN19, 20% Cr_2O_3	2000	Debonded	--	--	
35% B402, 35% GN19, 30% Cr_2O_3	2000	OK	OK	2 of 3 Samples OK	Resists extrusion
30% B402, 30% GN19, 40% Cr_2O_3	2000	OK	OK	OK	Resists extrusion
60% Pyrex, 40% Cr_2O_3	2100	Debonded	--	--	
40% GN19, 20% B402, 40% Cr_2O_3	2100 1900	-- OK	 Debonded	 --	Glass unstable --
20% GN19, 40% B402, 40% Cr_2O_3	2100 1700	-- OK	-- OK	-- 1 of 3 Samples OK	Glass unstable
332 (NBS)	1700	Debonded	--	--	Poor adhesion to ceramic
332 (NBS), 40% Cr_2O_3	1800	Debonded	--	--	Poor adhesion to ceramic
332 (NBS), 40% Cr_2O_3	1800	Debonded	--	--	Poor adhesion to ceramic
GN19	2100	OK	Debonded	--	Unstable
GN19, 40% Cr_2O_3	2100	OK	Debonded	--	
B402, 40% Cr_2O_3	1500	Debonded	--	--	

differential strains associated with temperature cycling, as shown in Table 8, with severe cracking or spalling, while still adhering to both metal and ceramic surfaces. In addition, no tendency for these materials to migrate from fill interface due to excessive wetting was evident. The second function which requires the material provide a uniform contact surface should be met because of the large quantities of Cr_2O_3 fill. This prevents the glass from flowing out of the metal-ceramic interface, since this quanitity of nonviscous fill material appears to all but eliminate viscous newtonian fluid behavior.

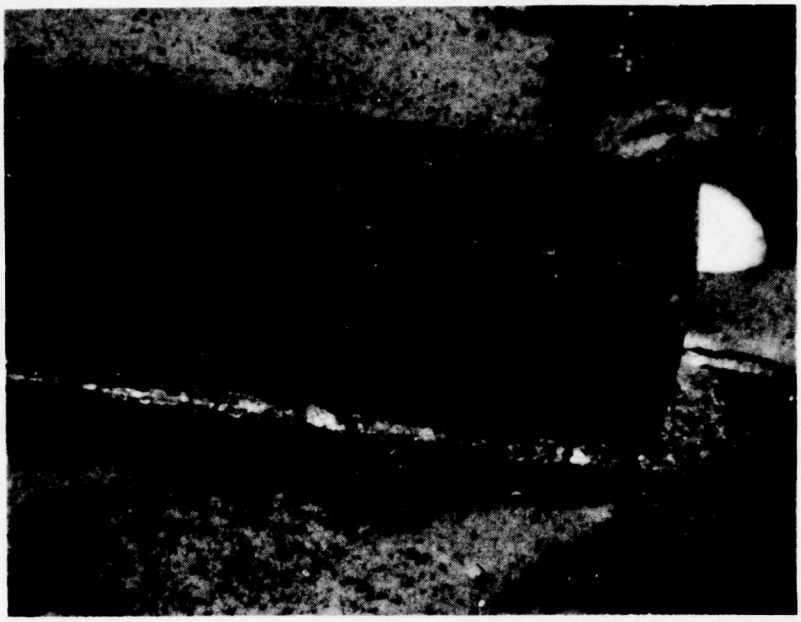

Figure 16. 30% B402, 30% GN19, 40% Cr_2O_3 After Exposure Cycle (713LC to $HPSi_3N_4$

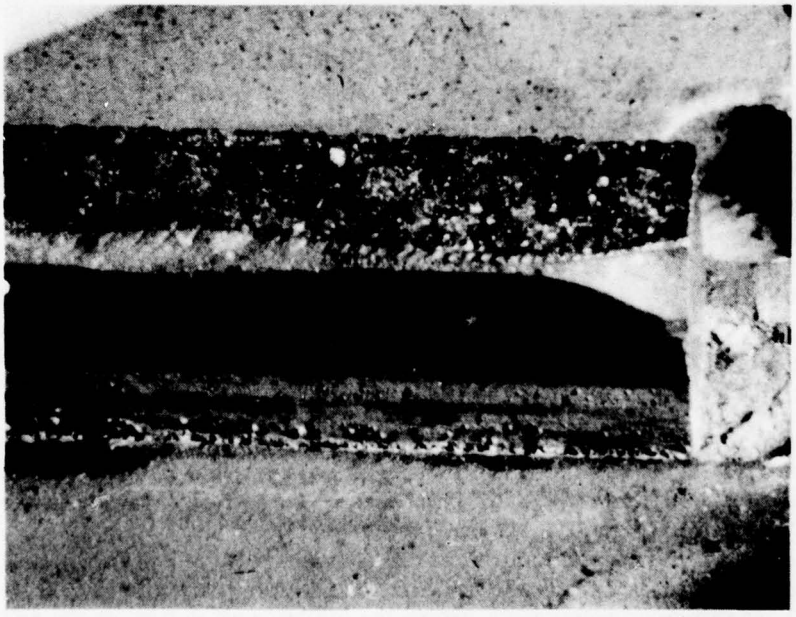

Figure 17. 35% B402, 35% GN19, 30% Cr_2O_3 After Exposure Cycle (713LC to $HPSi_3N_4$)

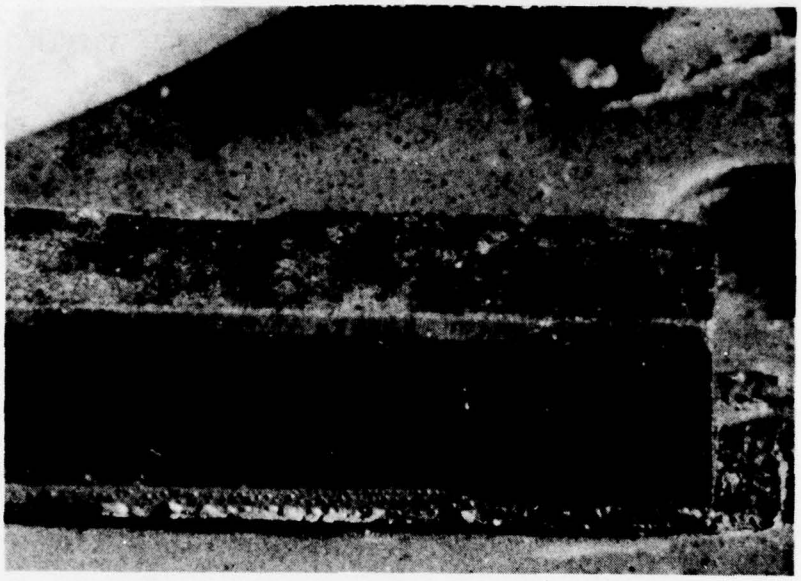

Figure 18. 20% GN19, 40% B402, 40% Cr_2O_3 After Exposure Cycle (713LC to $HPSi_3N_4$)

3.2.4 Design and Analysis for Rig Test of Ceramic/Superalloy Nozzle

Design

Figure 19 illustrates the 10 kW nozzle design selected for engine simulator evaluation. The shrouds are made from 713LC superalloy and vanes are part 713LC (leading edge) and part ceramic (trailing edge). This type of bimaterial vane design is possible for improved erosion resistance because almost all vane erosion occurs at the trailing edge. This obviates the need for through holes in the ceramic because the 713LC leading edge will accommodate these.

The ceramic trailing edge is recessed into the shrouds. A glass adhesive may be applied at the ceramic interface for sealing and support of these ceramic vane sections or the vane sections might be supported strictly by direct entrapment between shroud recesses.

Figure 20 shows details of the ceramic/metal nozzle vane design for engine simulator rig testing. The lip on the inboard side of the leading edge results from an aerodynamic analysis which shows that static pressure forces will locate the ceramic insert at the downstream portion of shroud recess and against the inside surface (towards the axis of the engine). Clearance between recess size and ceramic insert size necessary to accommodate assembly dimensional stack-ups amount to between 0.010 and 0.030 inch in the lengthwise direction. In addition, differential expansion between 713LC nickel-base superalloy shrouds and hot pressed silicon nitride vanes amount

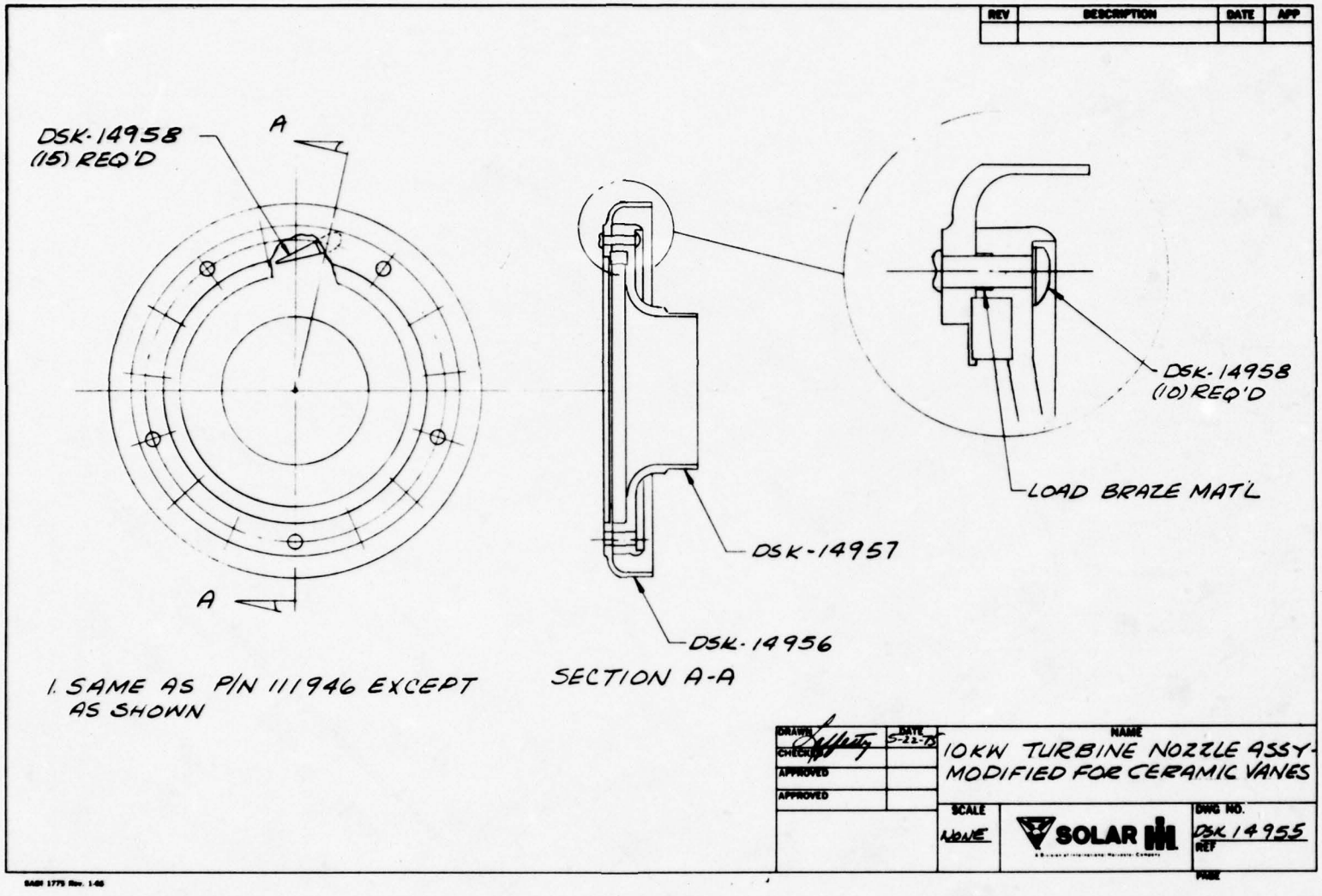

Figure 19. 10 kW Turbine Nozzle Assembly With Ceramic Vane Inserts

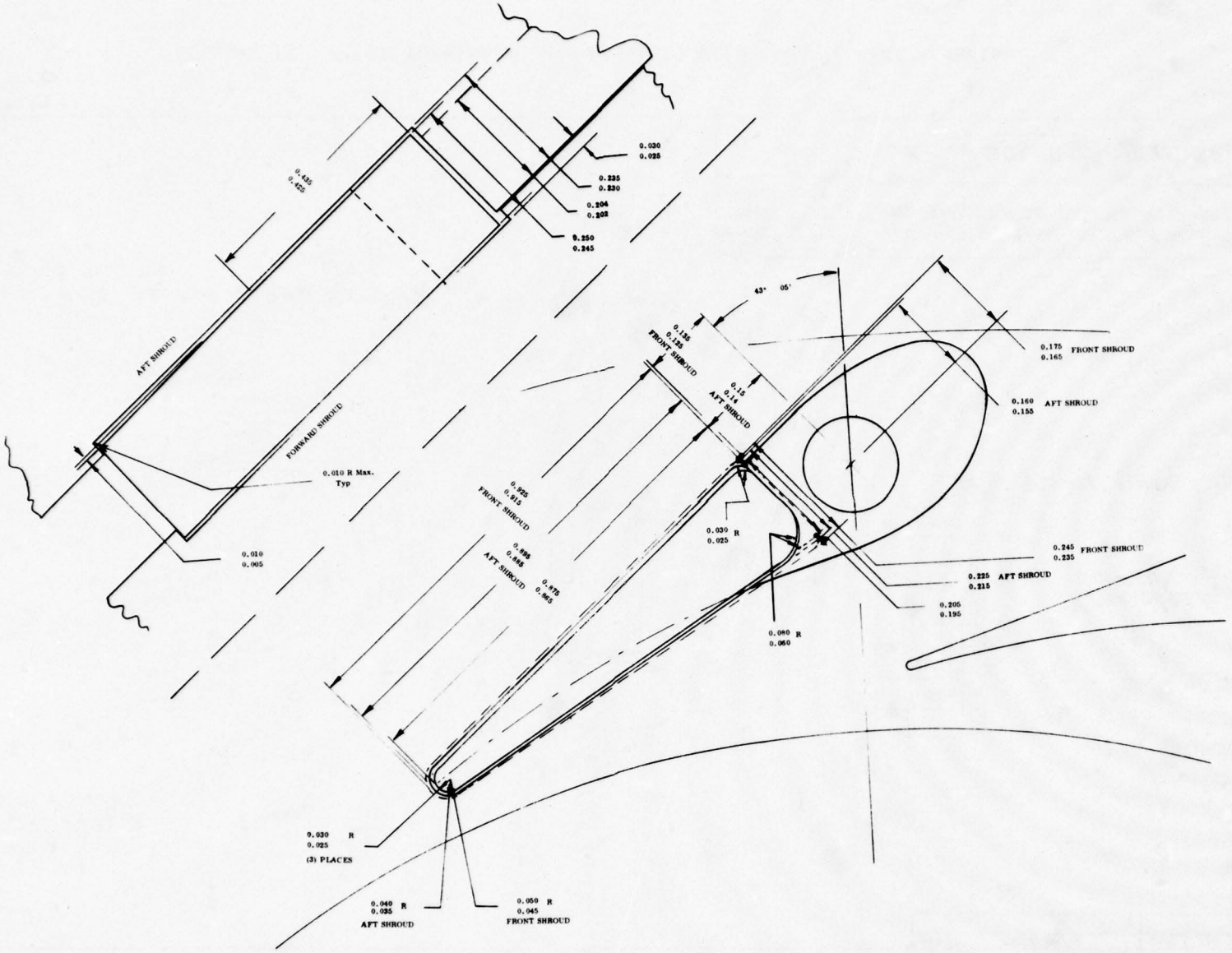

Figure 20. Layout Drawing of Vane ($HPSi_3N_4$ Ceramic) Trailing Edge Insert

to an additional 0.010 inch clearance. In the assembly where ceramic adhesives will not be used, a clearance will occur at the interface between vane metal section and ceramic section. Therefore, a total gap between 713LC leading edge and $HPSi_3N_4$ trailing section which can vary between 0.020 and 0.040 inch will result. This would cause substantial leakage through this interface since nearly the entire 18 psi static pressure differential taken across the nozzle exists across this surface at rated engine load. The lip provides a seal necessary for acceptable nozzle performance.

Thermal stresses developed at the section change of the metal tab in this latest design were suspected as a possible difficulty, however, engine simulator rig tests subsequently showed this not to be a problem.

Drawings of the nozzle components for this bimaterial design chosen for rig test are given in Figures 19 and Figs. 21 through 24.

3.2.5 Analysis

An analysis of static thermal stresses in the ceramic vane of the metal/ceramic nozzle as installed in the 10 kW engine was performed. It showed that under peak temperature conditions the forward (outer) shroud could possibly yield and generate compressive loads on the ceramic vane trailing edge. For this reason the forward side of the ceramic vane was tapered to avoid trailing edge loading. A finite element analysis of the ceramic vane per DSK-14958 indicated that internal stresses in the vane would be no greater than 8600 psi assuming the loads were evenly distributed by glass joint filler material. In the event that a filler material were not used and shroud yielding did occur, contact stresses applied to the ceramic vane piece as high as the yield strength of 713LC superalloy could occur.

No other significant stresses were expected to be applied to ceramic vanes during engine operation, except those generated internally in the vane due to thermal shock.

3.2.6 Design and Analysis for Rig Test of All-Ceramic Nozzle

Design

A simplified design of an all-ceramic nozzle was decided upon for erosion, corrosion and thermal shock evaluation purposes in a turbine simulator rig. The rig test nozzle components are shown in Figures 25 through 27.

The $HPSi_3N_4$ ceramic nozzle vanes as shown in Figure 25 are mechanically held in the shroud recesses. The entire shroud vane assembly is held in place for rig tests with three piloted spring loaded Hastelloy X pins. Glass joining materials were applied at the vane shroud interfaces. (The assembly is pictured in Section 3.2.7).

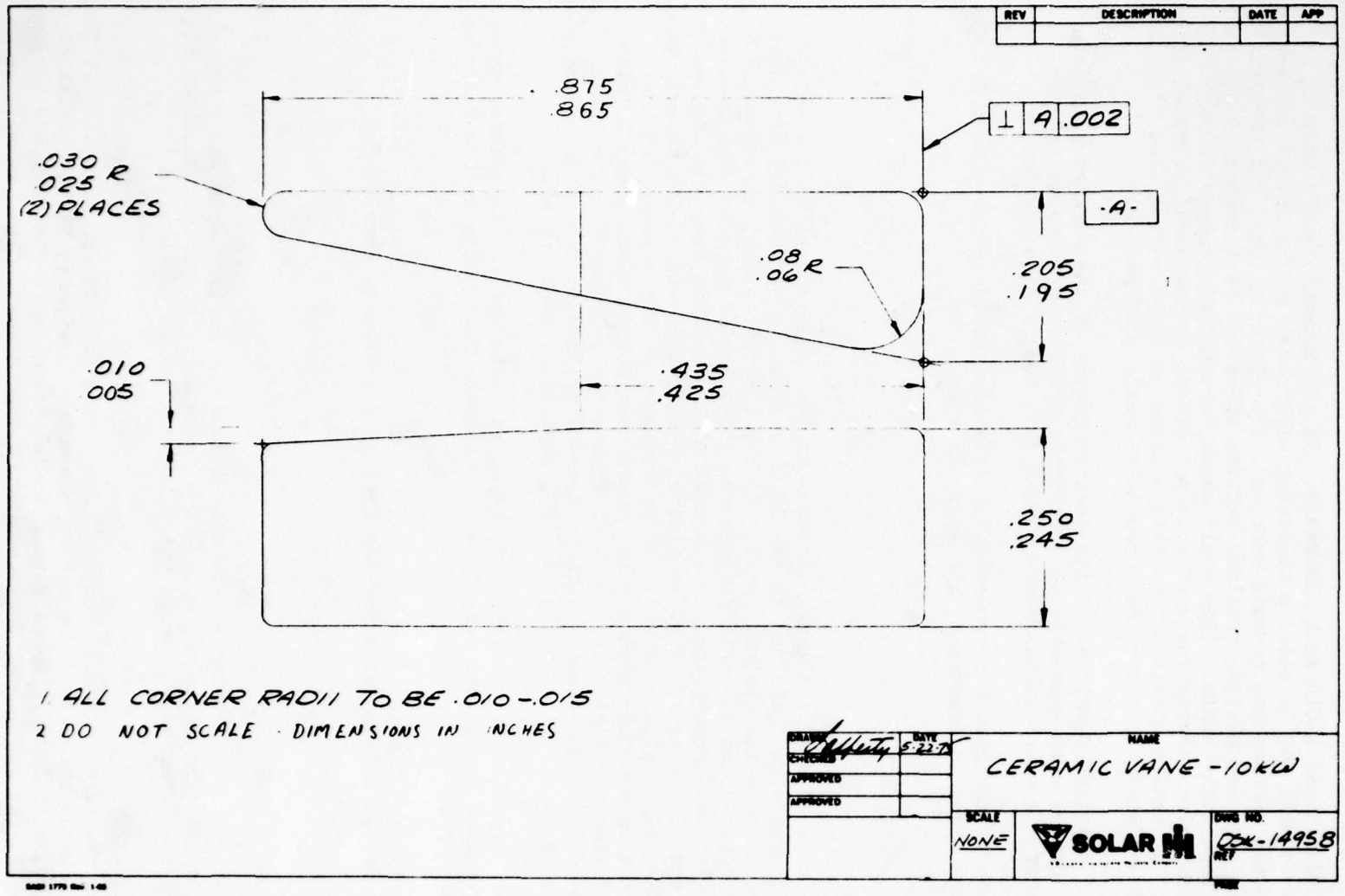

Figure 21. Ceramic Vane Section - 10 kW

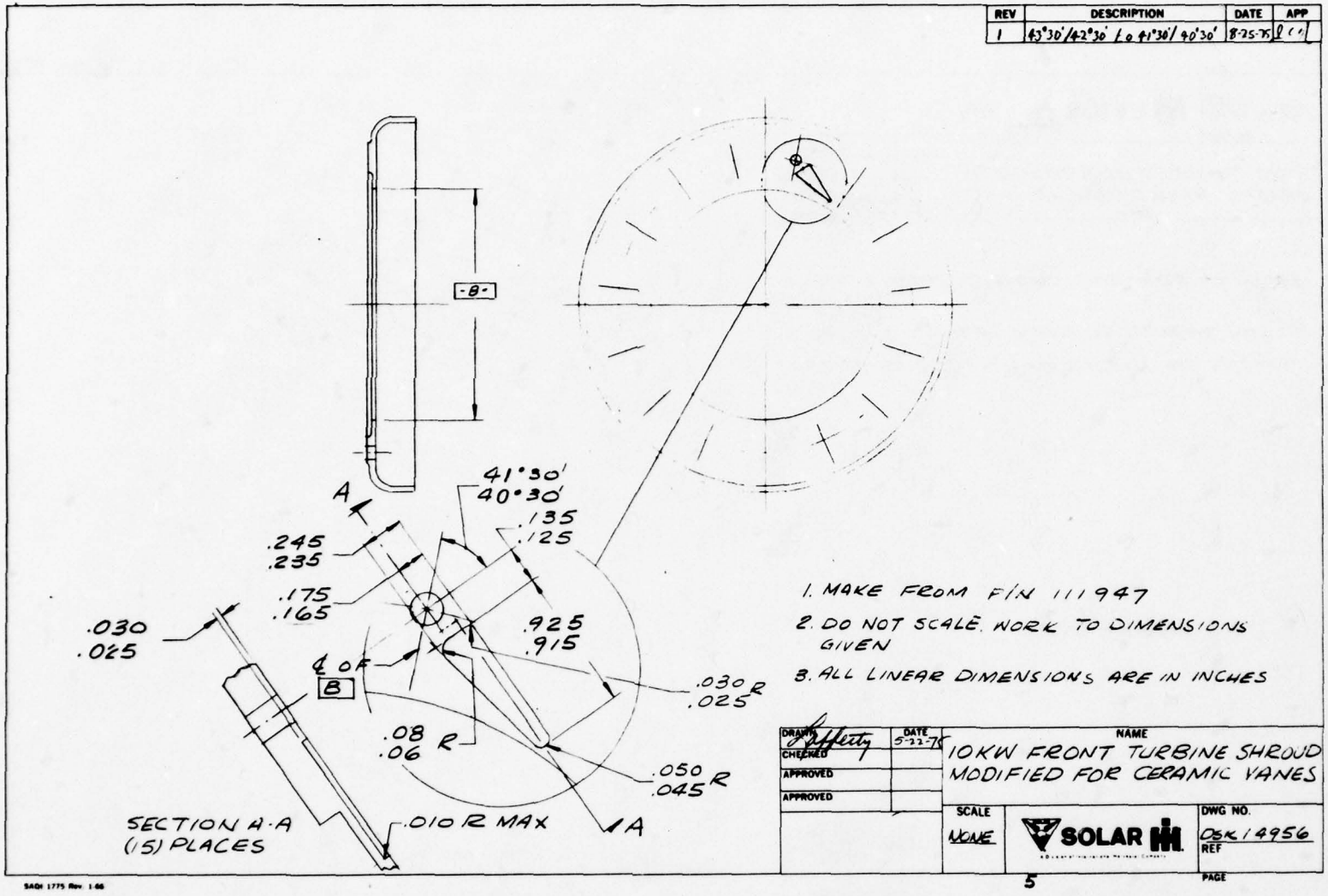

Figure 22. 10 kW Front Turbine Shroud Modified for Ceramic Vanes

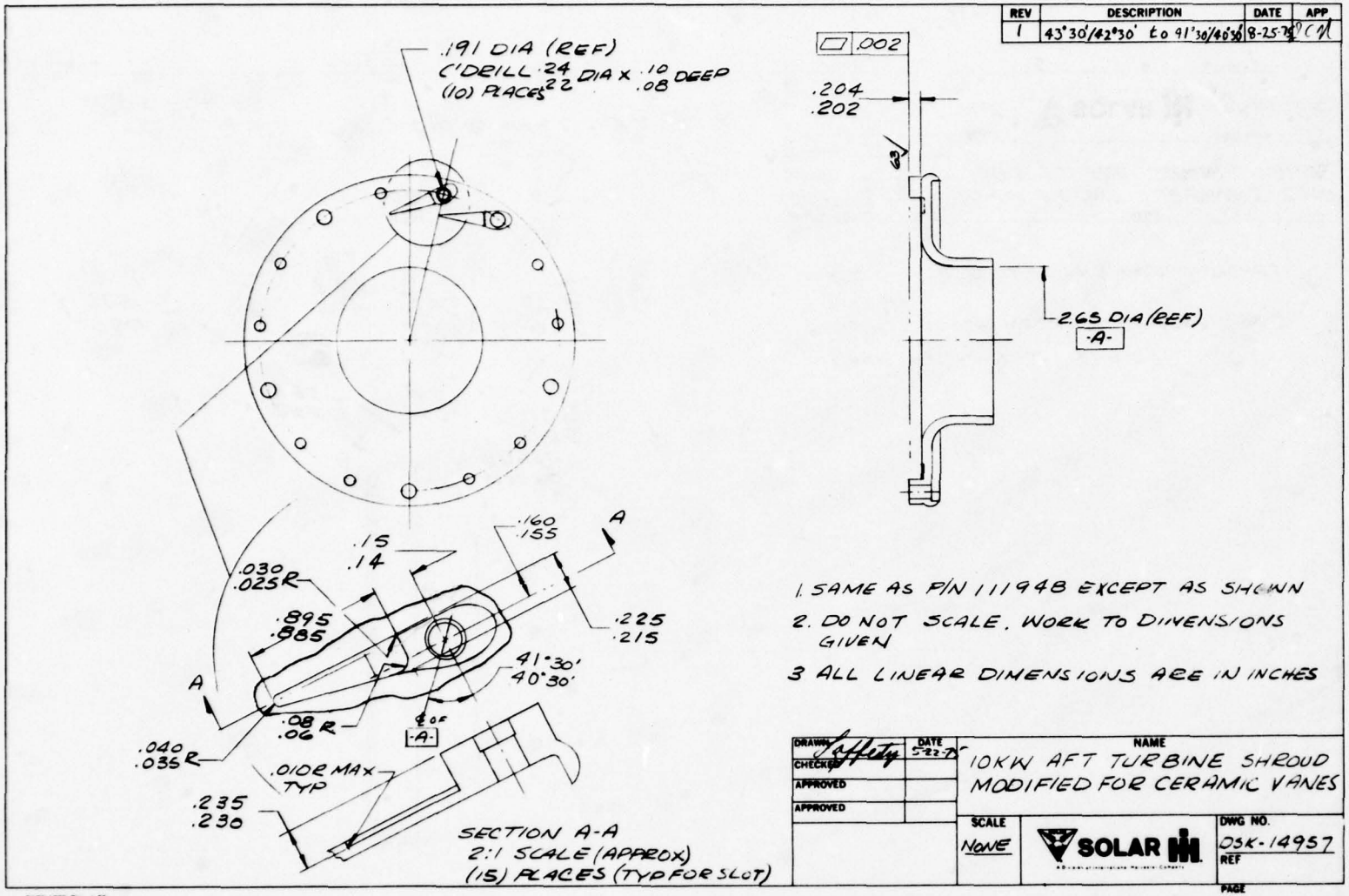

Figure 23. 10 kW Aft Turbine Shroud Modified for Ceramic Vanes

SOLAR PART NO.	REVISIONS			
	LTR	DESCRIPTION	DATE	APPROVED

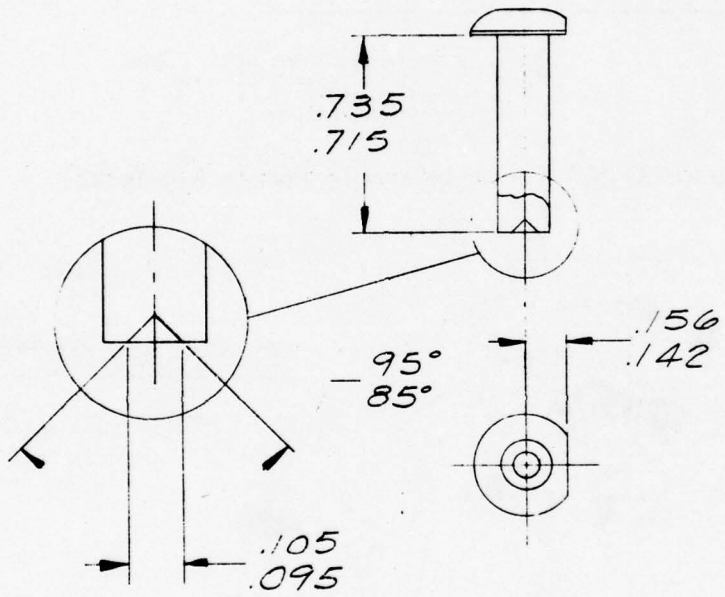

1. MAKE FROM P/N 45118
2. DO NOT SCALE DWG. WORK TO DIM'S GIVEN
3. ALL DIM'S IN INCHES

APPROVED BY	SOLAR — DIVISION OF INTERNATIONAL HARVESTER COMPANY, 2200 PACIFIC HIGHWAY · SAN DIEGO, CALIFORNIA 92112	
GOVT. CONTRACT NO.		
PROJ	DRAWING TITLE: RIVET, TURBINE NOZZLE	
DES		
CH		
DR [signature] 5-27-75		
DESIGN ACTIVITY	SIZE: A	CODE IDENT NUMBER: 55820 — DRAWING NUMBER: DSK-14959
CUSTOMER	SCALE 2:1	TOTAL WT. — SHEET 1 OF 1

Figure 24. Rivet, Turbine Nozzle

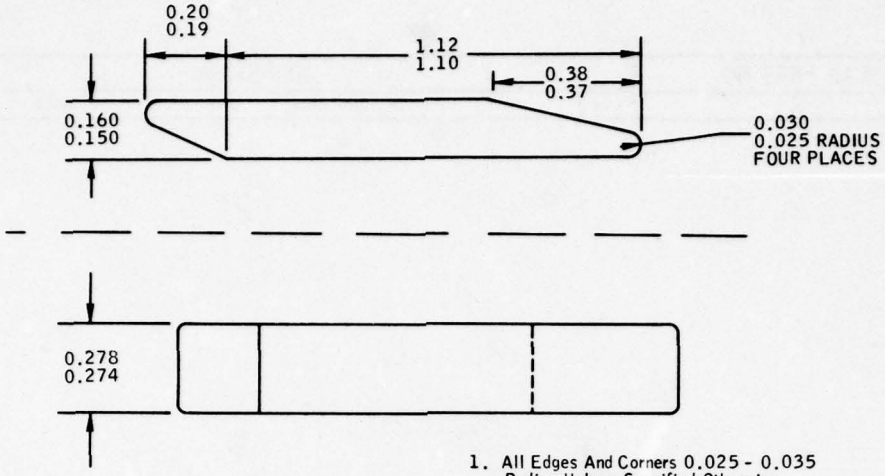

Figure 25. Vane ($HPSi_3N_4$) for All-Ceramic Nozzle Rig Tests

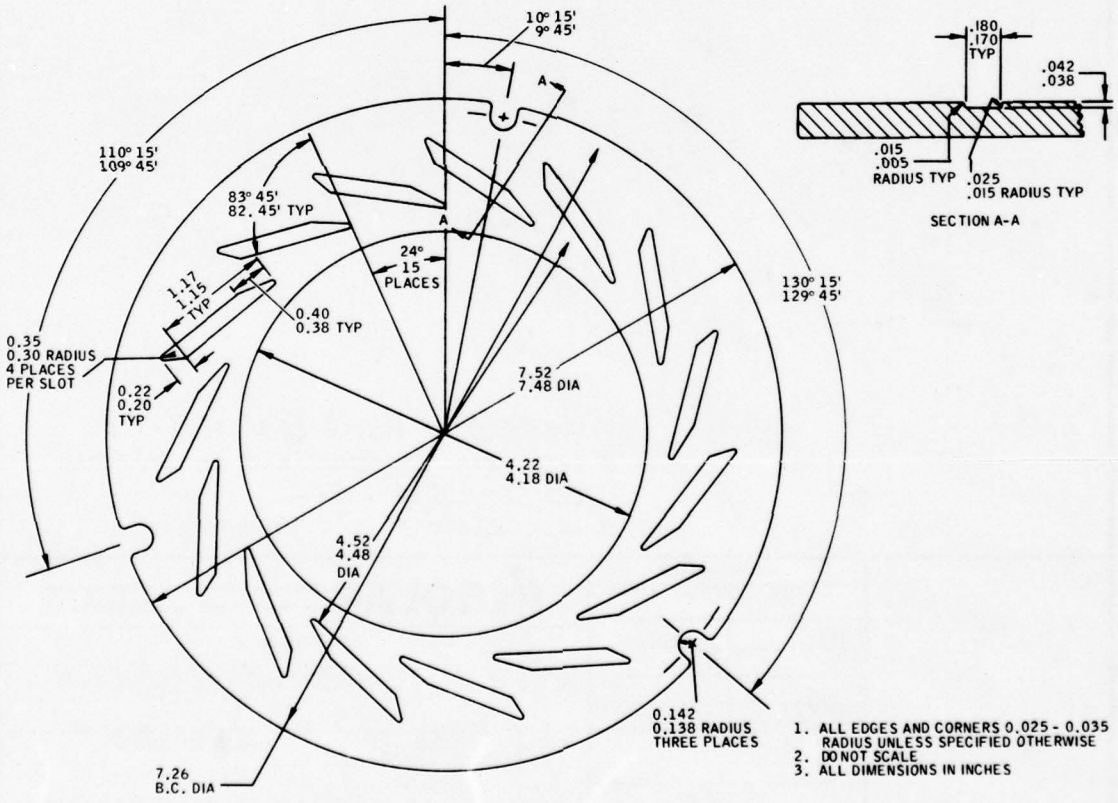

Figure 26. Forward Shroud Ring ($RBSi_3N_4$) to be Used in All-Ceramic Nozzle Rig Test

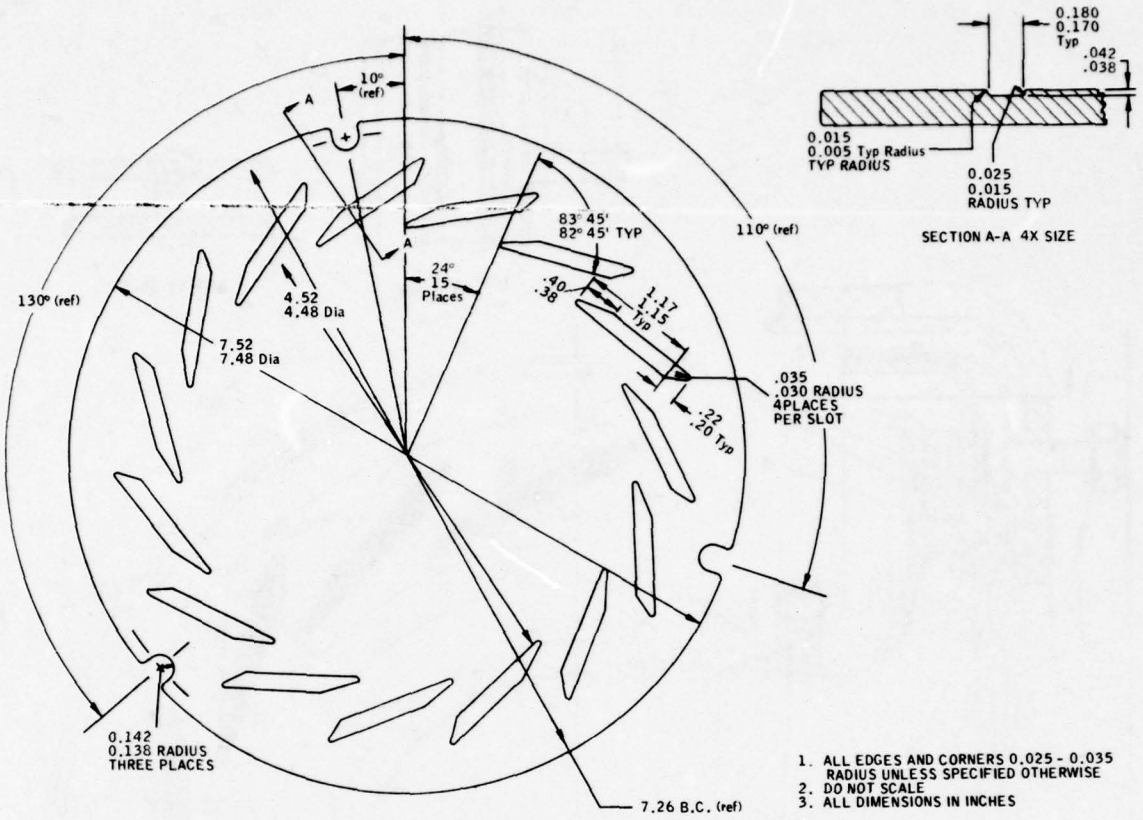

Figure 27. Aft Shroud Rings ($RBSi_3N_4$) to be Used in All-Ceramic Nozzle Rig Tests

Vane Design

The shroud recess must restrict the vane from moving laterally, longitudinally and from rotating. View B-B of Figure 28 shows a recess type that could accomplish this, however the square sides of the recess which prevent rotation result in sharp radii and high stress concentration. (Total groove depth at sides is only approximately 0.030 inch which implies bottom corner radii to be less than 0.010 inch. This results in approximately a 2.5 stress concentration factor for a transverse tensile load [Ref. 23].)

A variation on this design which is the design chosen for rig test, is given in Figure 29. The flat region at recess bottom offers resistance to rotation. Since the recess shape is not cylindrical the recess is deeper at the sides thus allowing for a greater radii. A 0.030 radius results in approximately 1.8 stress concentration factor. This configuration is regarded to be the least complex to fabricate of those considered here. Good vane location tolerances can also be achieved because static aerodynamic forces will locate the vane downstream and against the surface toward the engine axis.

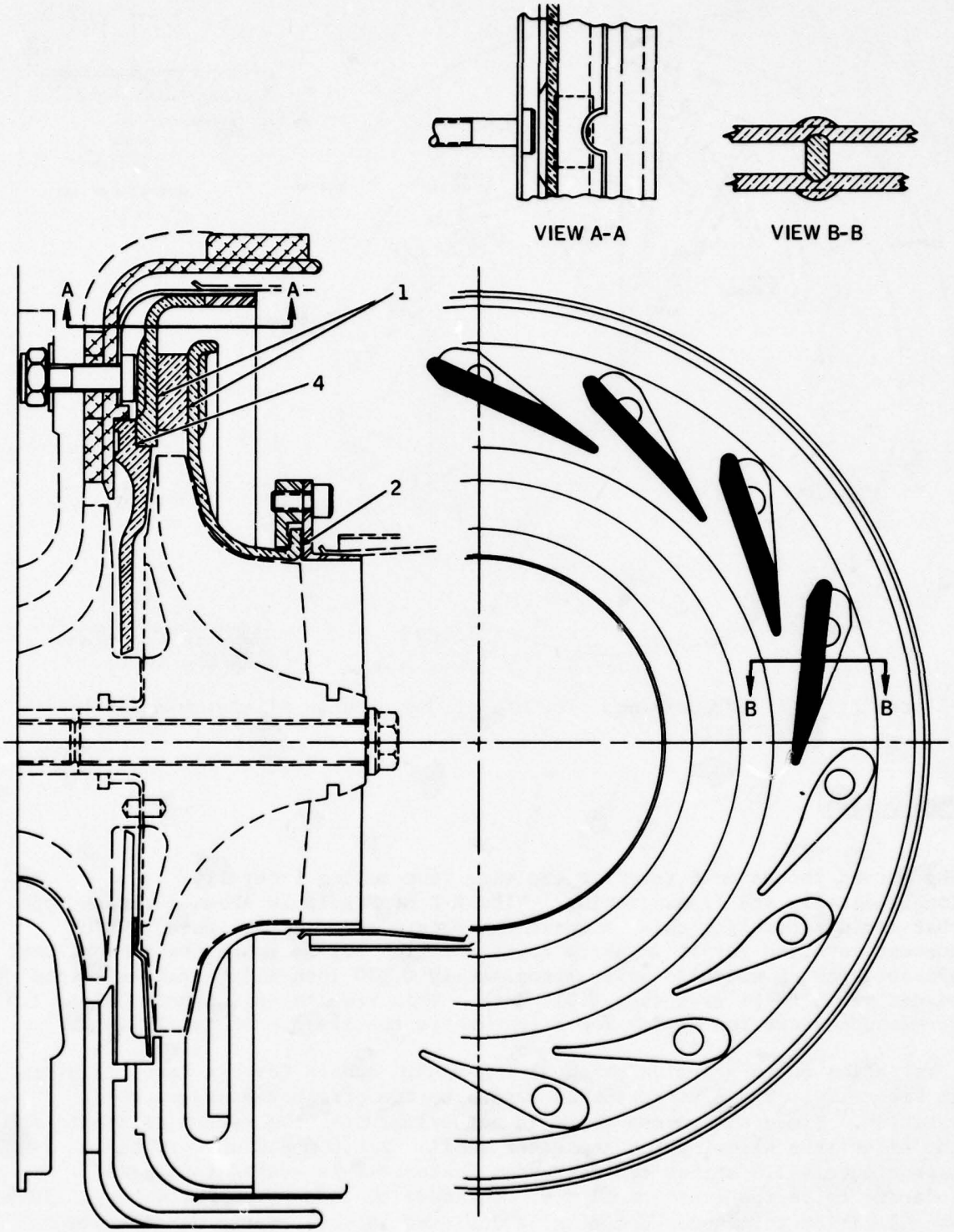

Figure 28. Comparison of Present Metallic Nozzle Design (lower) With Preliminary Design for Ceramic Vanes, Shrouds and Seal Plate (upper)

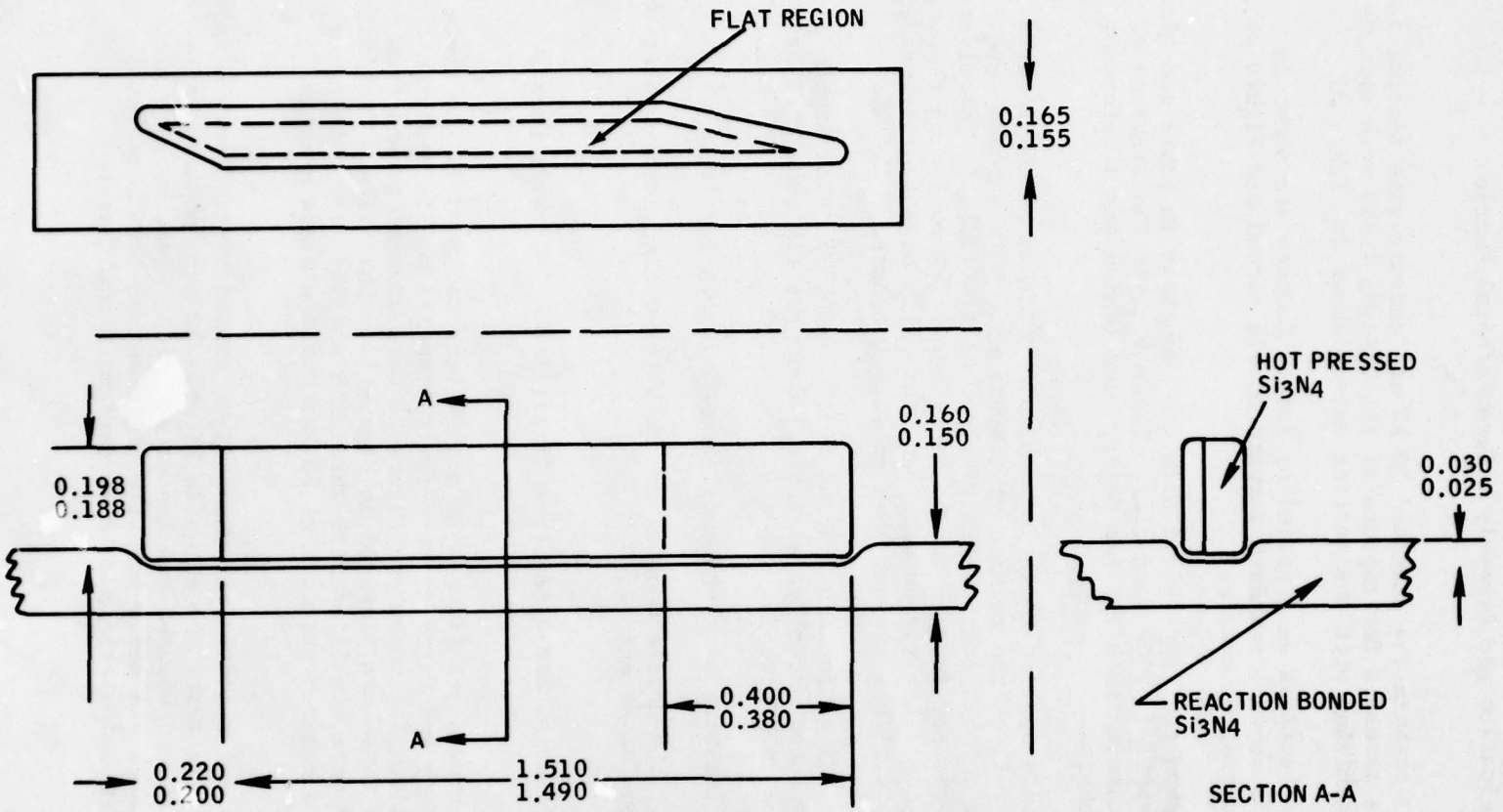

1. All Corners and Edges 0.030-0.040 Radius for Shroud
2. All Corners and Edges 0.020-0.030 Radius for Vane

Figure 29. Shroud Recess and Vanes for Simplified All-Ceramic Nozzle For Rig Test Evaluation

3.2.7 Rig Test Fabrication and Assembly - Ceramic/Metal Nozzle

Figures 30 A and 30B compare the standard 10 kW and ceramic vane section rear nozzle shrouds. The recesses for capture of the HPSi_3N_4 vanes were made by Electro Discharge Machining with the tooling set-up shown in Figure 31.

Typical ceramic vane sections as supplied by Norton Company are shown in Figure 32. Figure 33 shows a standard forward nozzle shroud and Figure 34 shows the ceramic/superalloy nozzle.

Figure 34A and 34B show the rear shroud with vane sections in place and glass interface material applied prior to firing. Table 9 gives the sequence of glass application starting with the top center vane (which has a reference arrow) counting clockwise.

The glass slurries were applied to the appropriate recesses of the forward and rear shrouds as well as the ceramic vane sections. Both shrouds were then bolted together through each of the 15 rivet or bolt holes. The rivets were then progressively set in each of the ten rivet holes following removal of the bolts one by one. The rivets were set statically on a tensile machine at ambient temperature with a maximum load of 15,000 pounds.

The assembly was then fired for one hour at 1038°C (1900°F) in an Argon atmosphere. The completed assembly, as installed in the rig test chamber before test, is shown in Figure 35.

Figure 36 shows the location of thermocouples used in rig testing.

Figure 37 illustrates the nozzle mounted to the water-cooled test chamber and location of thermocouples #1 and #2.

3.2.8 Rig Test Fabrication and Assembly - Simplified All-Ceramic Nozzle

The ceramic nozzle shrouds per Figures 26 and 24 were machined in the green state by Norton Company and fired to make their standard NC-350 reaction bonded silicon nitride. The vanes per Figure 24 were diamond ground from NC-132. As-received vanes are pictured in Figure 32. The billets from which the vanes originated were qualified with three MOR samples each which were specified as having a minimum strength of 80 ksi and a minimum average strength of 110 ksi.

The assembly details and sequence for the RBSi_3N_4 shroud HPSi_3N_4 vane nozzles for engine simulator rig tests are shown in Figures 38 through 41. Refrasil insulation has been placed between the cooled stainless steel support plate and the nozzle. Figures 42A and B show the placement of thermocouples between the insulation and nozzle such that they will read nozzle temperatures.

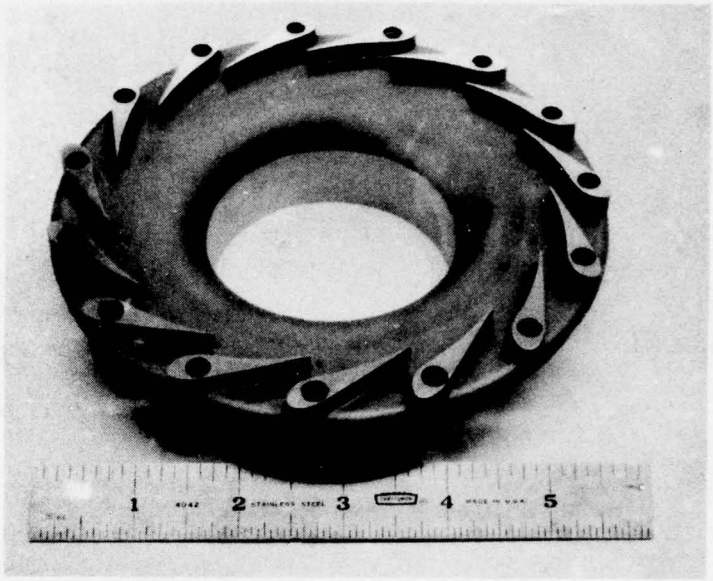

A.

Standard 10 kW Rear Nozzle Shroud (Part #107726-1)
(Turbine Seal Surface Not Machined)

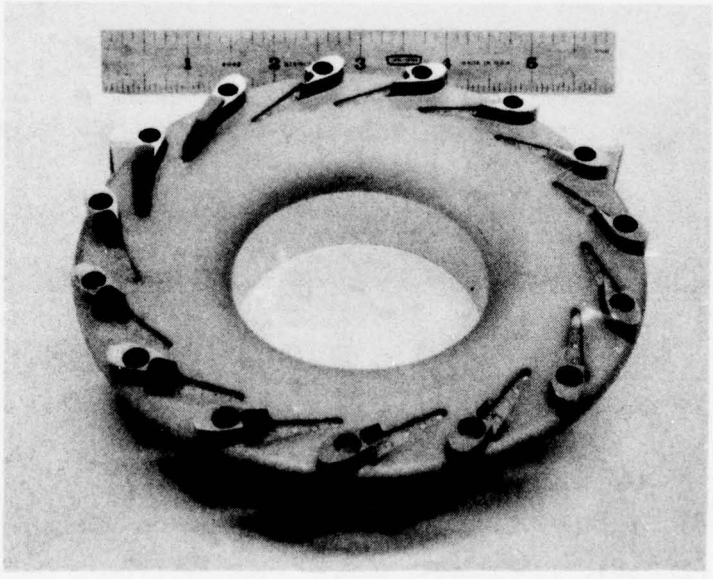

B.

Figure 30. 10 kW Rear Nozzle Shroud With Two HPSi_3N_4 Trailing Vane Sections Inserted (Per Drawing DSK 14957)

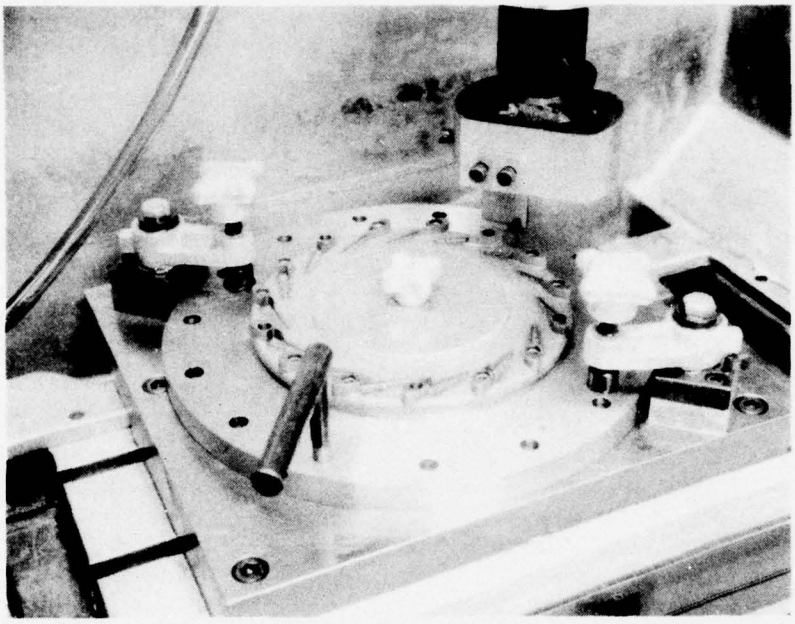

Figure 31. Tooling Set-Up for EDM of Recesses in Nozzle Shrouds

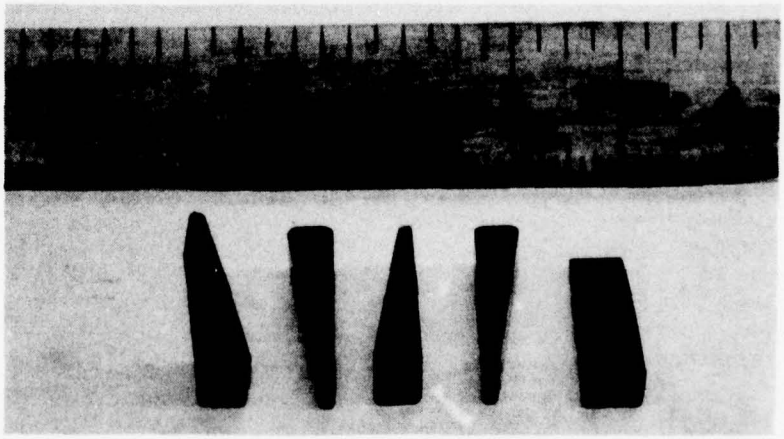

Figure 32. $HPSi_3N_4$ (NC-132) Nozzle Vane Trailing Edge Sections (per Drawing DSK 14958)

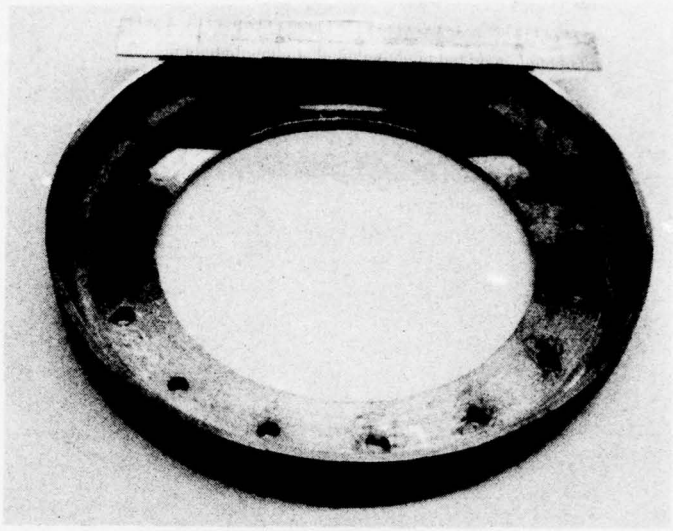

Figure 33. Standard 10 kW Forward Nozzle Shroud (Part #74-8006)

Spring loaded Hastelloy X pins hold the assembly in place. Spacer washers of Hastelloy X are located between the shrouds and allow a net height clearance for vanes between the shrouds.

Relaxing glasses were applied to vane shroud interfaces for thermal shock testing according to the sequence in Figure 43. They were not applied during assembly for dust erosion and corrosion testing so the nozzle could be easily disassembled for inspection after these tests.

Thermocouple locations are also shown in Figure 43.

3.2.9 Rig Tests - Standard Nozzle Baseline, Ceramic Vane Nozzle and Preliminary All-Ceramic Nozzle

The rig test facility used for thermal cycling, dust erosion and corrosion testing of ceramic nozzles was calibrated using the standard 10 kW nozzle configuration (Assembly #74-8005) prior to test of the ceramic vane nozzle and the preliminary all-ceramic nozzle.

The test facility is pictured in Figure 44. Inlet air is heated to 538°C (1000°F) in the preheater with natural gas. The main combustor provides additional heat to bring combustion gases to operating temperatures and can be fired with either liquid fuel or natural gas. The rig experiments were conducted using natural gas in order to avoid low temperature flameout during thermal cycling.

A

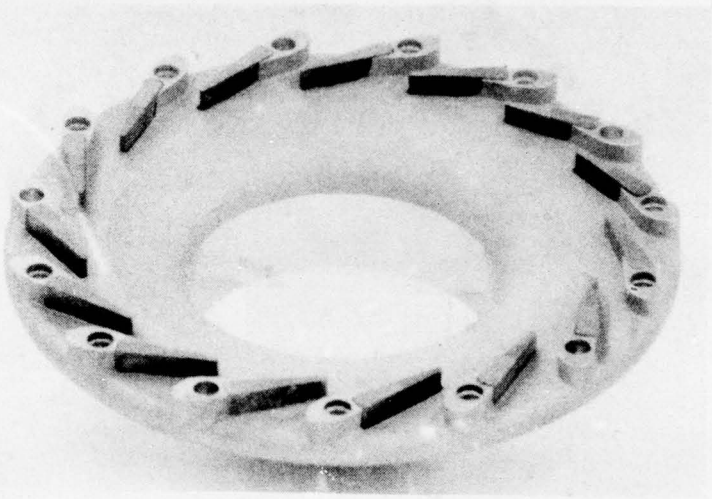

B

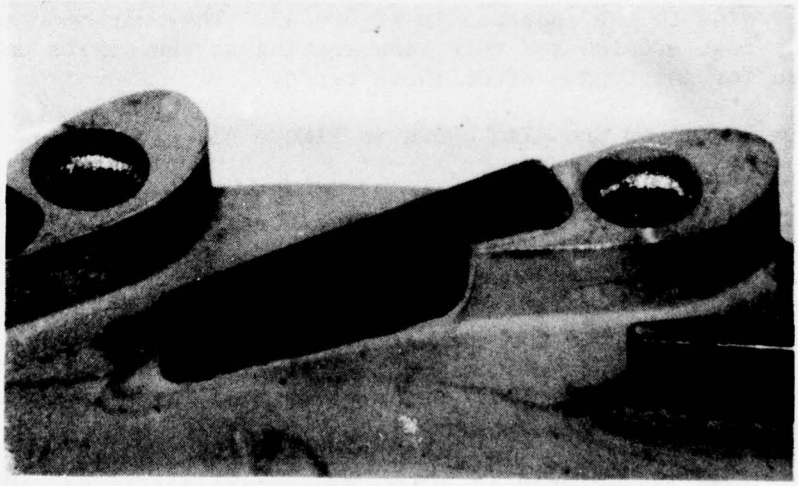

Figure 34. Ceramic/Superalloy Nozzle Partially Assembled Prior to Firing Glass Interface

Table 9

Assembly Schedule for Ceramic/Superalloy 10 kW Nozzle for Rig Test

Vane Location Number	Ceramic Vane Identification	Glass Interface Type		
		30% B402 30% GN19 40% Cr_2O_3 (A)	35% B402 35% GN19 30% Cr_2O_3 (B)	40% B402 20% GN19 40% Cr_2O_3 (C)
1 (Top Center Fig. 34A)	B	X		
2 (Clockwise)	G		X	
3	H			X
4	I		No Glass Fill	
5	J	X		
6	K		X	
7	L			X
8	M		No Glass Fill	
9	N	X		
10	S		X	
11	P			X
12	Q		No Glass Fill	
13	R	X		
14	O		X	
15	T			X

The test chamber which holds the nozzle section was water cooled. This provides the facility for test temperatures up to or beyond 1400°C (2552°F). The position of the turbine nozzle in the test chamber is shown in Figure 45. The nozzle holder has been removed and turned such that the nozzle upstream side is seen.

Figure 46 shows the location of thermocouples at upstream, downstream and forward shroud positions used in the test of the standard nozzle and the ceramic vane nozzle. Figure 37 shows the position of thermocouples #1 and #2.

This rig test configuration closely simulates actual turbine temperature and gas flow conditions. The major rig pressure drop is taken across the nozzle. Table 10 lists temperatures, pressures, and flows observed for the test rig with the standard 10 kW and ceramic vane section nozzles installed.

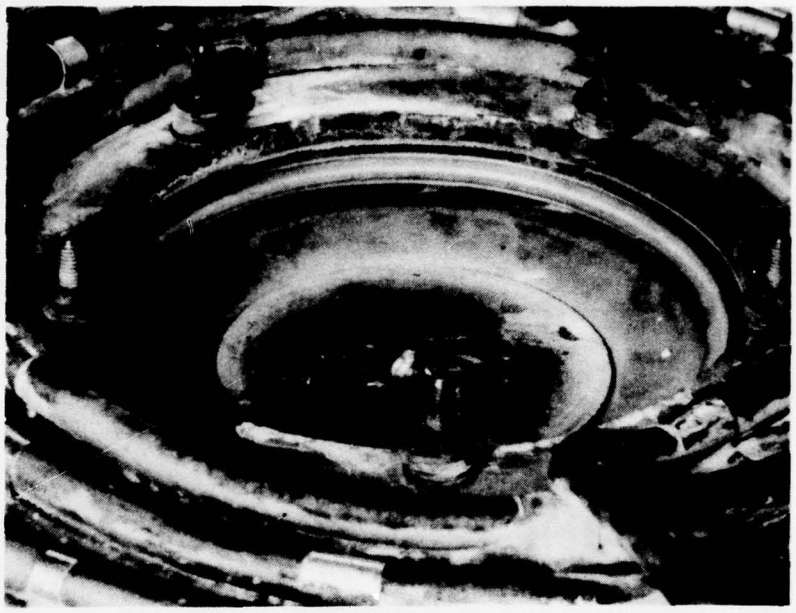

Figure 35. Cooled Nozzle Test Chamber With Ceramic Vane Nozzle Installed

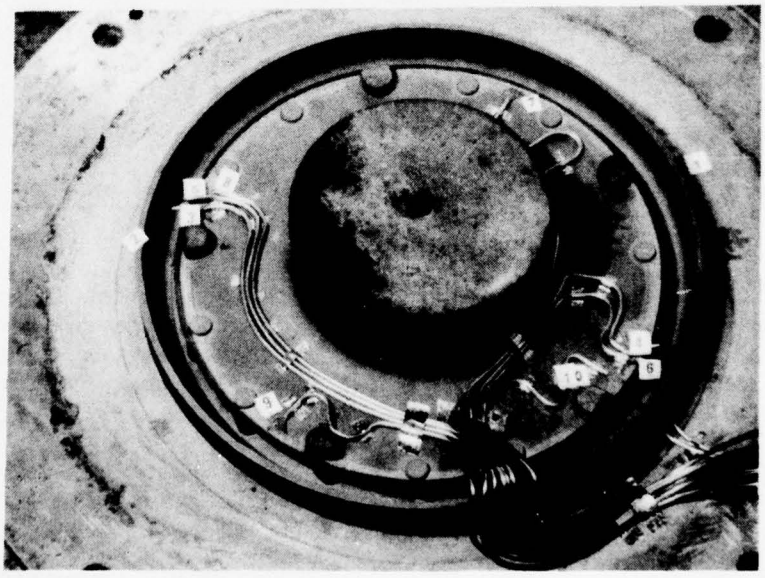

Figure 36. 10 kW Nozzle Test Rig Thermocouple Location

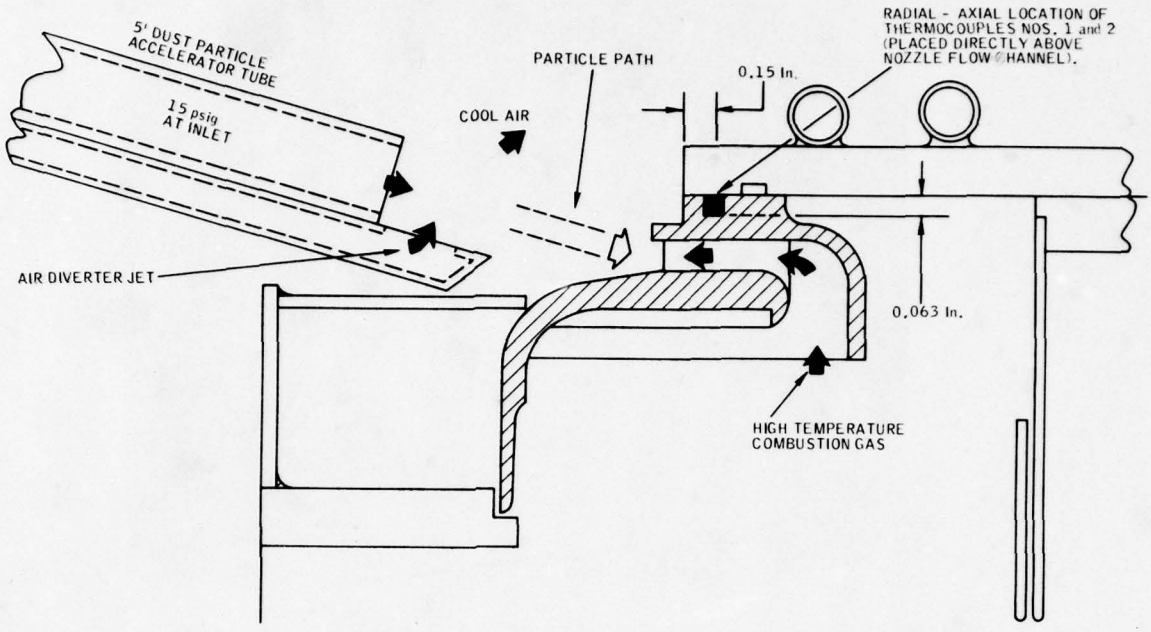

Figure 37. Location of Thermocouple #1 and #2 in Rig Tests and Sketch of Dust Erosion Device

Thermal Shock

The thermal shock test cycle consists of a rapid up-shock and slower cool down cycle designed to simulate the most severe thermal cycle condition which occurs for the 10 kW on shutdown from full power with no load as illustrated in Figure 47. (Thermocouple #95 is located at the same forward shroud position as thermocouples #1 and #2 in rig tests as shown in Figure 37. Temperature of the forward shroud at engine position 95 as indicated in Figure 47 undergoes an excursion of 300°C (540°F) at a maximum rate of 33°C/sec (60°F/sec).

Temperatures experienced during the rig test thermal shock cycle of the ceramic vane nozzle are shown in Figures 48A and 48B. The forward shroud temperature ramp rate and temperature excursion have been adjusted to closely match that experienced on engine shutdown, with the only difference being that an up-shock rather than down-shock is used.

An optical pyrometer was used to measure peak temperature of vane trailing edge. (The signal function depends upon the ninth through tenth power of temperature and therefore is biased heavily towards peak material temperatures.) Also, pyrometer measurement threshold is 716°C (1320°F). Direct measurement of unlinearized pyrometer signal shows minimum cycle vane temperature to be 588°C (1092°F).

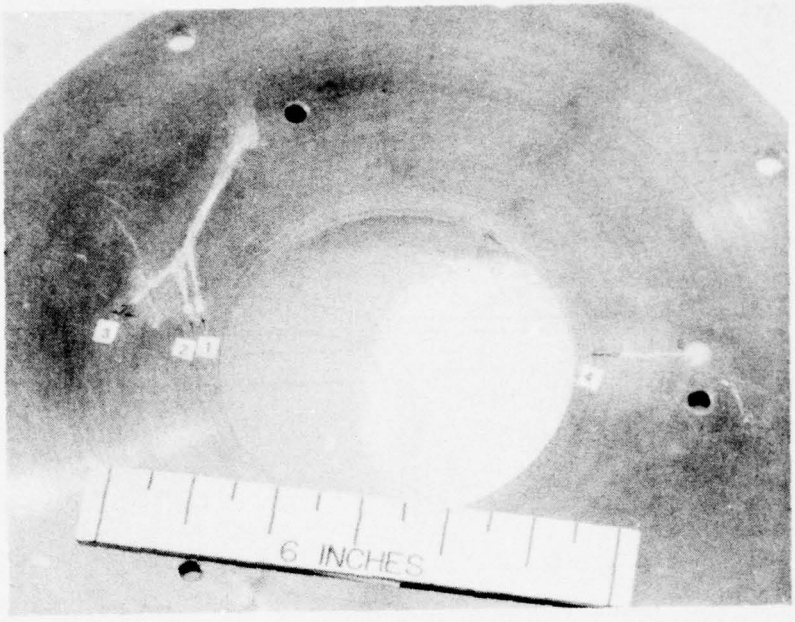

A. Cooled Mounting Plate for All-Ceramic Nozzle

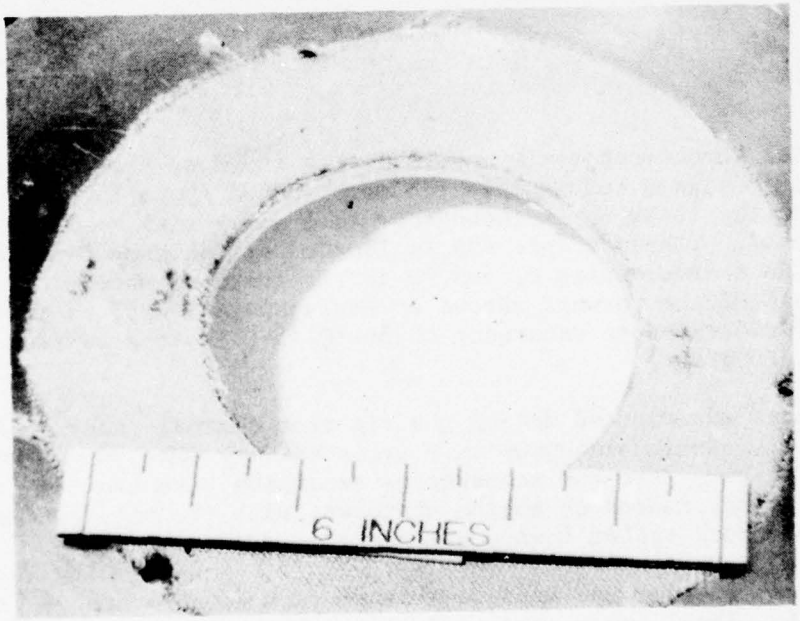

B.

Figure 38. Plate With Refrasil Insulation in Place

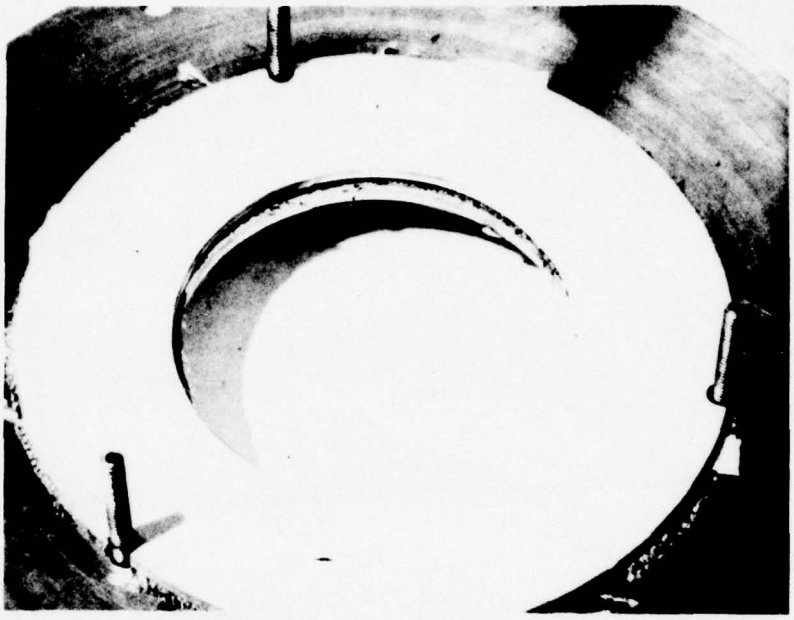

A.

$RBSi_3N_4$ Exit Shroud Installed

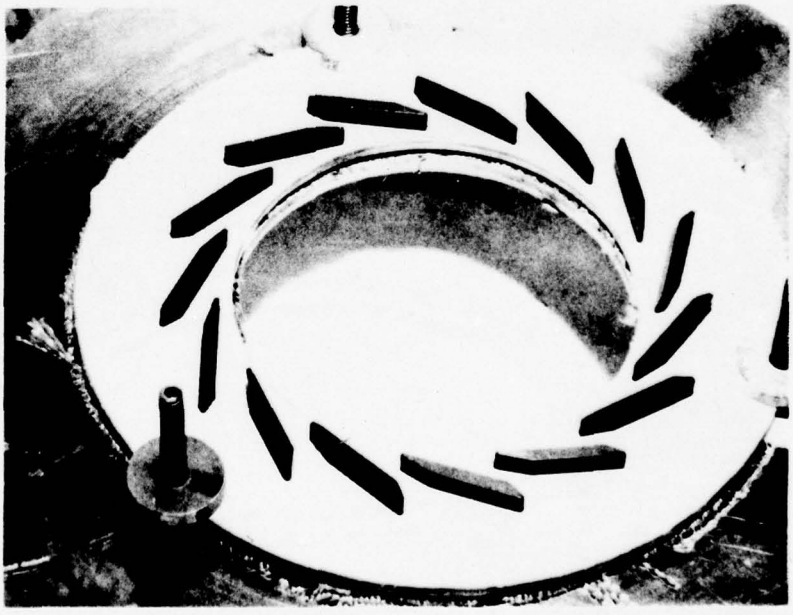

B.

Figure 39. $HPSi_3N_4$ Vanes Installed With Hastelloy X Spacer Washers and Pins

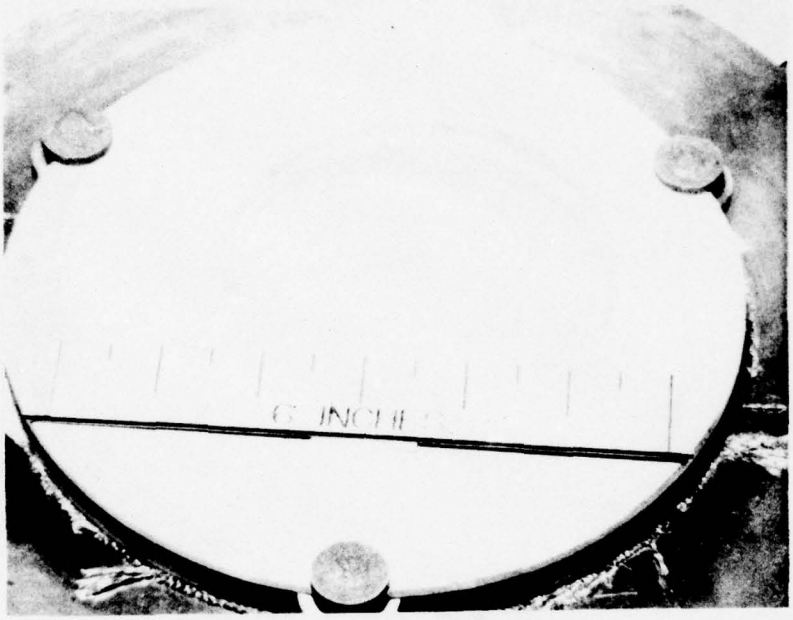

A.

$RBSi_3N_4$ Upstream Shroud Installed

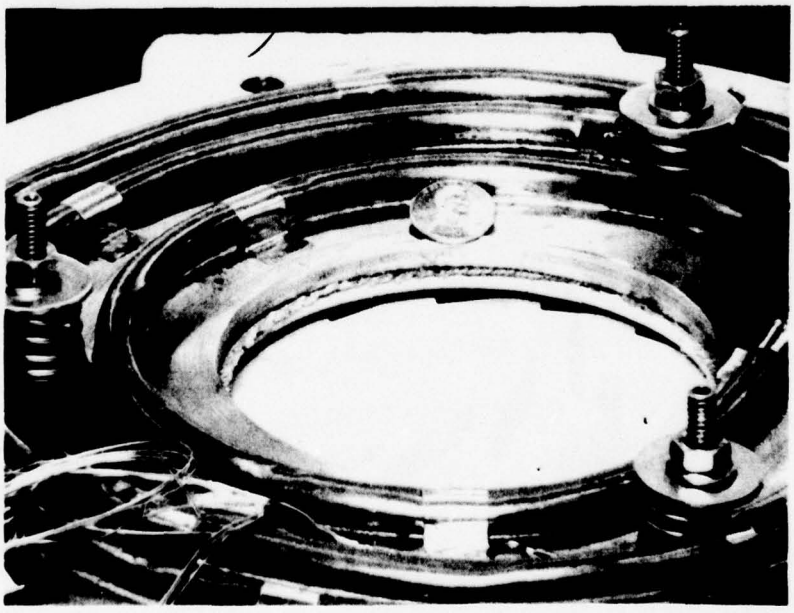

B.

Figure 40. Downstream View of All-Ceramic Nozzle in Cooled Test Chamber

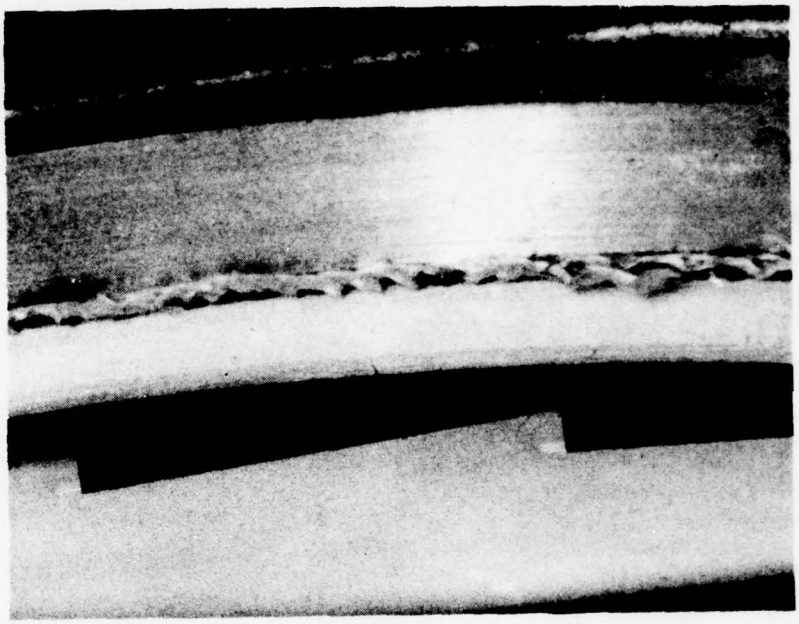

A.

Downstream View of Typical Vane

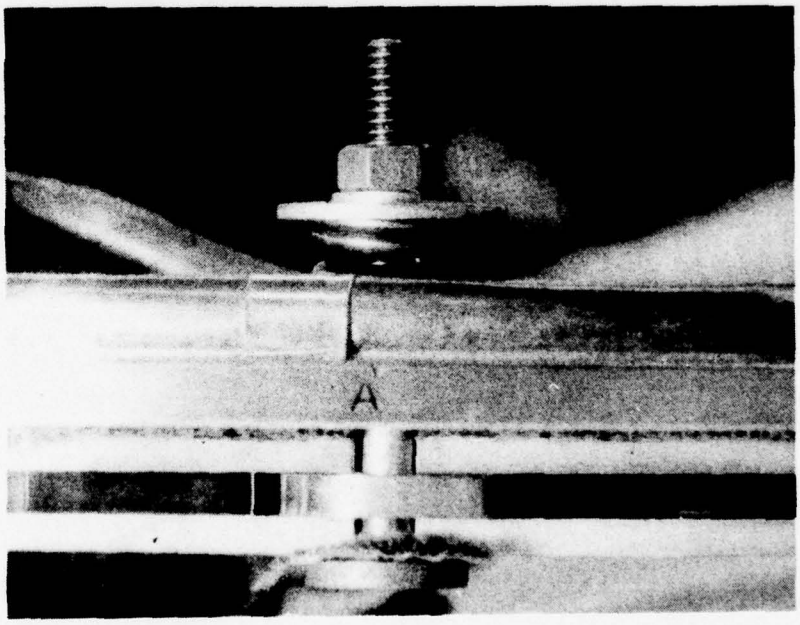

B.

Figure 41. Upstream View of Spring Loaded Hastelloy Nozzle Support Pin 'A'

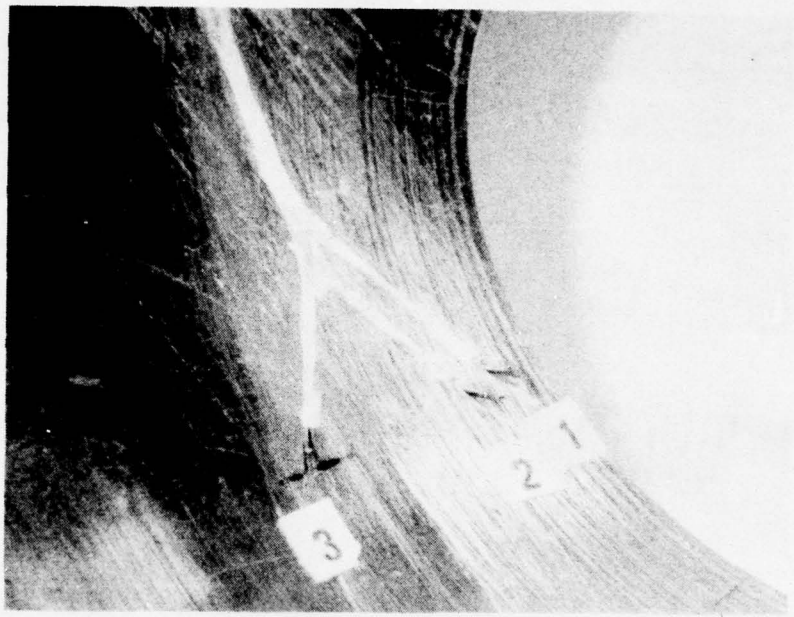

A.

Type K Thermocouple Location

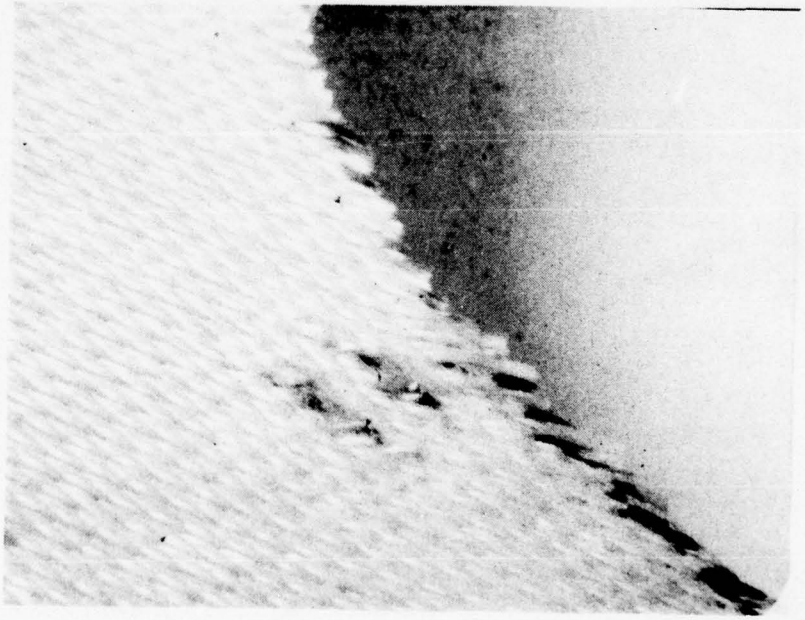

B.

Figure 42. Thermocouple Inserted Through Insulation

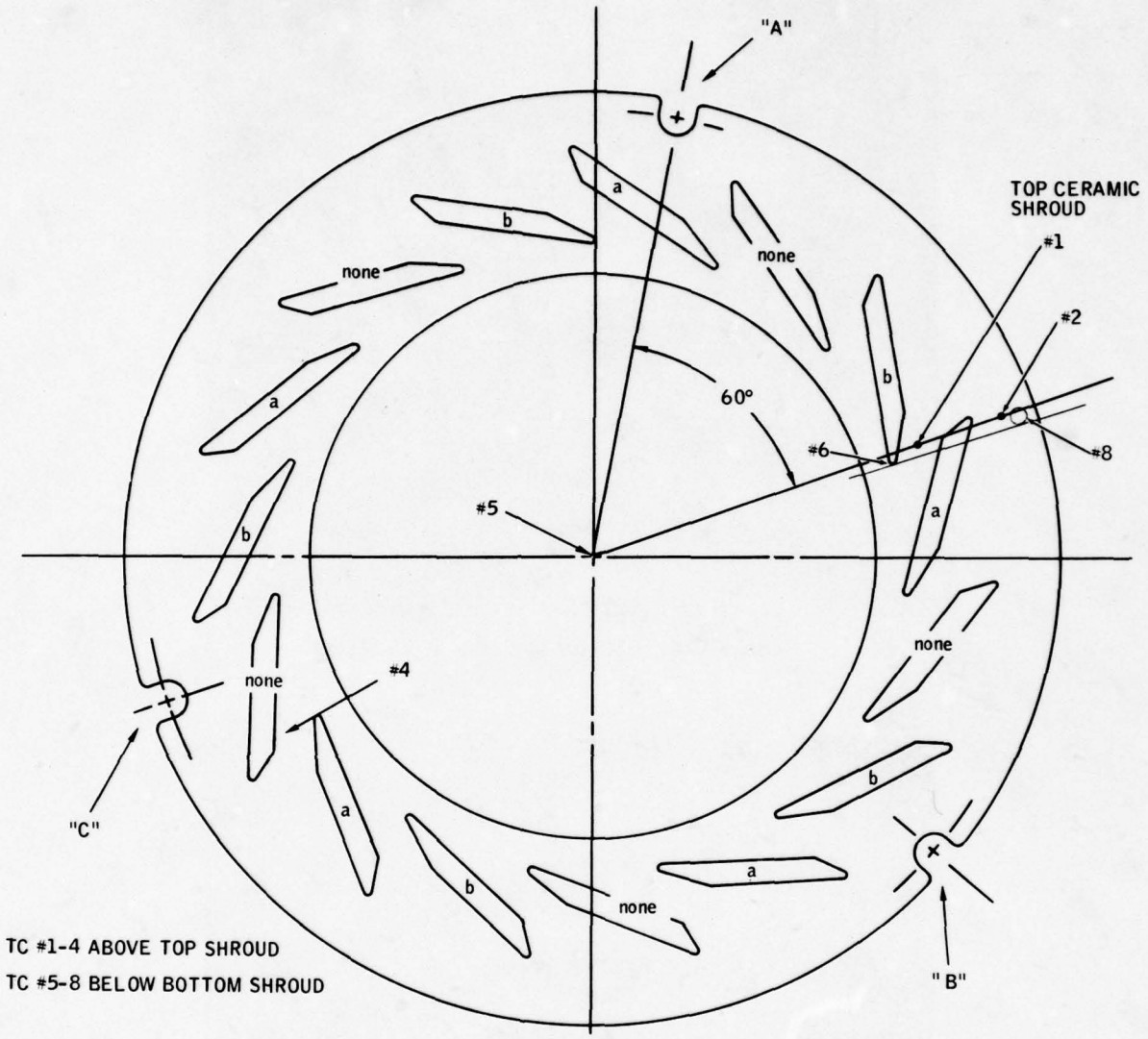

Figure 43. Thermocouple Location and Glass Joint Filler Material Location

The standard 10 kW shroud is shown in Figures 49A and 49B after exposure to 500 thermal cycles. Thermal cracking initiating at the sharp edged lip of the rear shroud is evident in Figure 49B. One of the cracks has proceeded through a rivet hole and vane. Some maldistribution of temperature was noted with this nozzle quadrant experiencing highest temperatures. This location was instrumented. The time temperature profile at the shroud lip is shown in Figure 48A (TC #7). Since temperature here was approximately 93°C (200°F) higher than other sections monitored during the test, the thermal cracking can be attributed to overtemperature. The rig was modified to reduce this maldistribution to less than 38°C (100°F) during corrosion and thermal shock tests of ceramic nozzles.

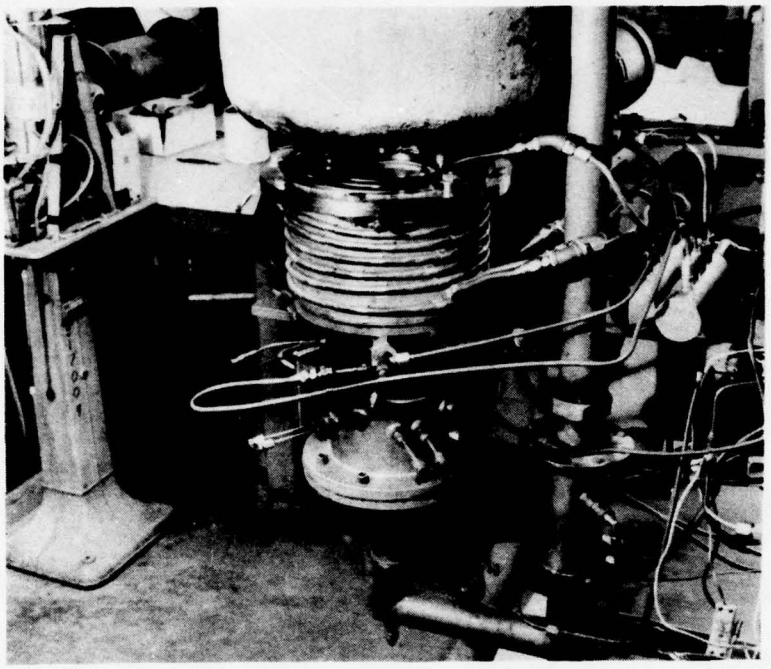

Figure 44. 10 kW Nozzle Test Rig

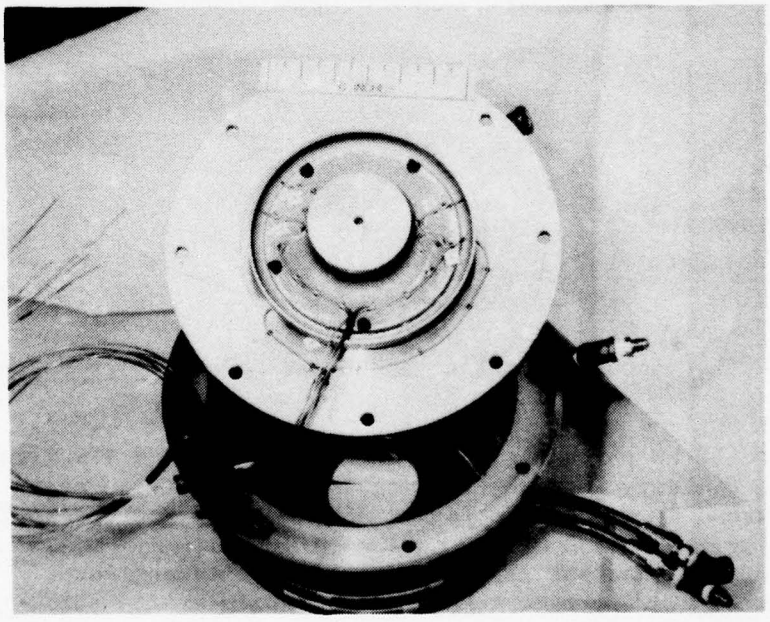

Figure 45. Cooled Nozzle Test Chamber With Lid Inverted to Show Upstream Section of Nozzle

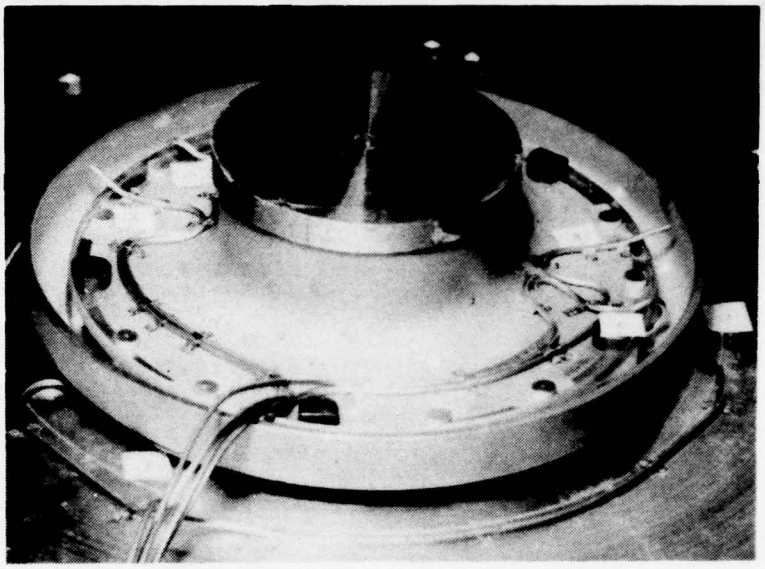

Figure 46. 10 kW Nozzle Test Rig Thermocouple Location

Table 10

Test Rig Flow Conditions for Standard and Ceramic Vane Nozzle Tests

Test Condition	Nozzle Upstream Flow		Nozzle Throat Conditions			
	Total Pressure psia	Total Gas Temperature °F	Mach Number	Gas Velocity ft/sec	Gas Density (lb/ft^3)	Total Mass Flow ÷ Nozzle Coefficient of Discharge (lb/sec)
Thermal Shock High Fire	25.4	2500	0.919	2269	0.0157	0.173
Thermal Shock Low Fire	22.4	1160	0.80	1486	0.0276	0.1995
Dust Erosion or Hot Corrosion	22.9	1725	0.82	1768	0.0206	0.177

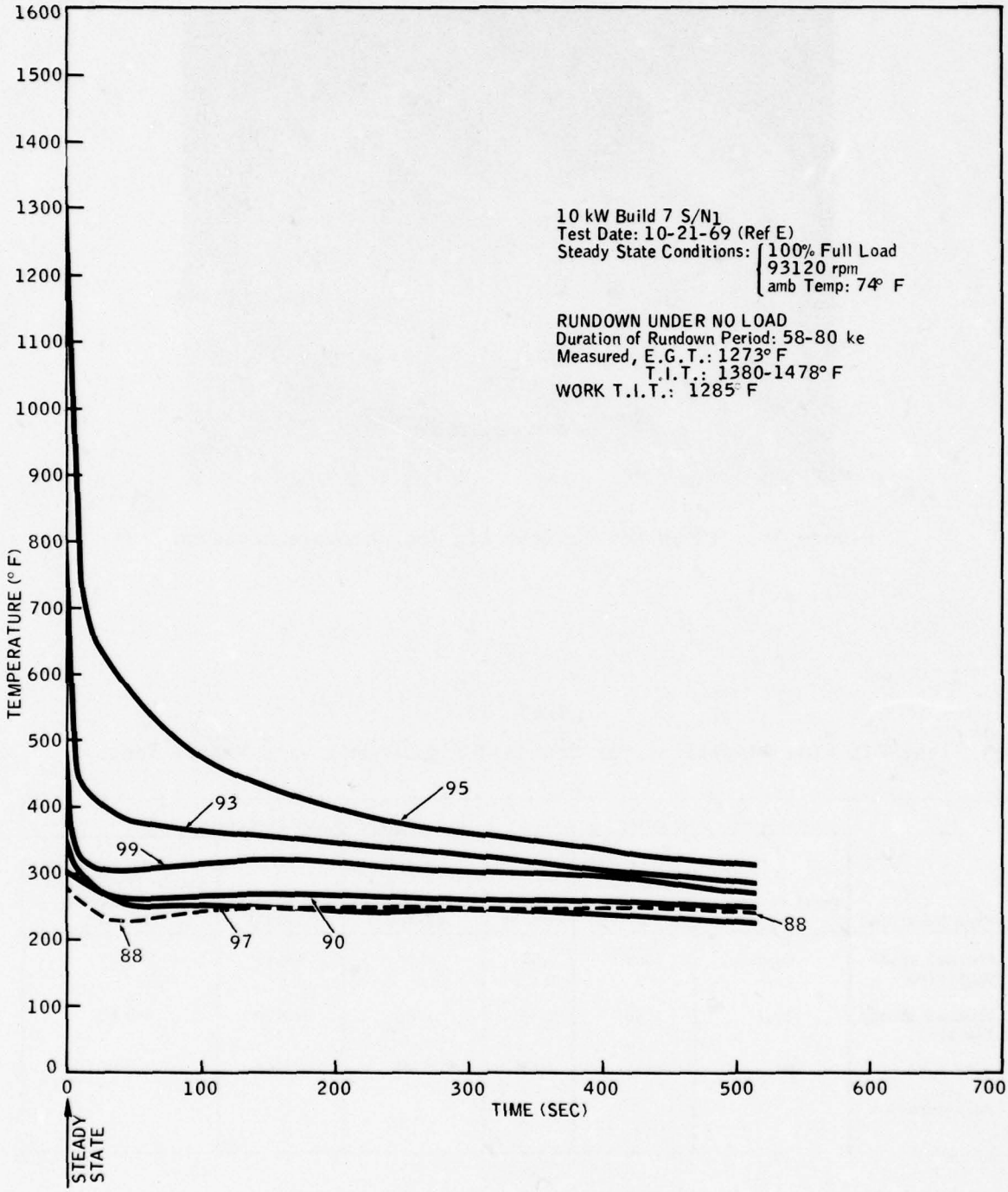

Figure 47. 10 kW Soakback Temperatures; Run Down Under no Load

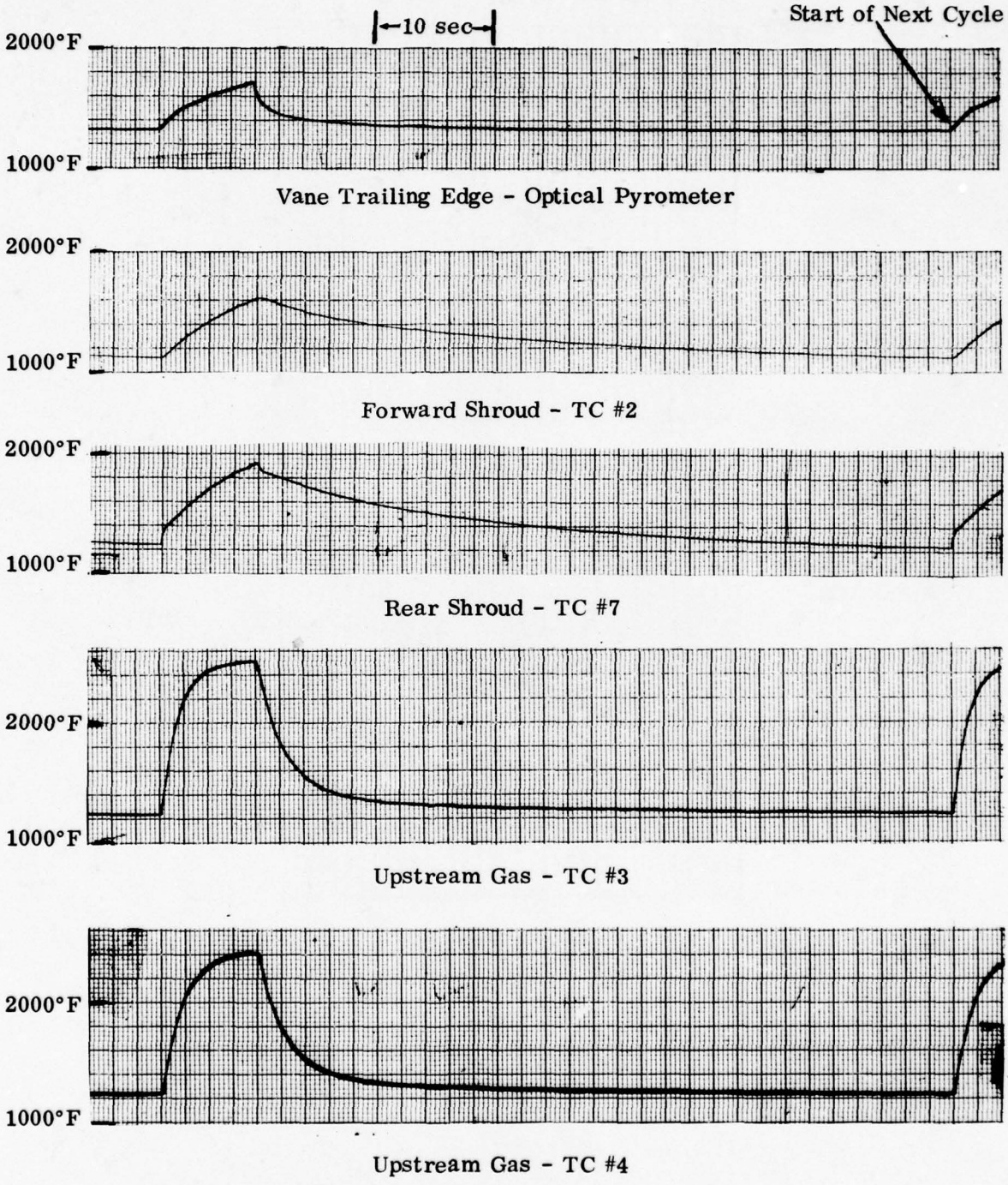

A.

Figure 48A. Time Temperature Profiles of Various Shroud Locations During Thermal Shock Cycle

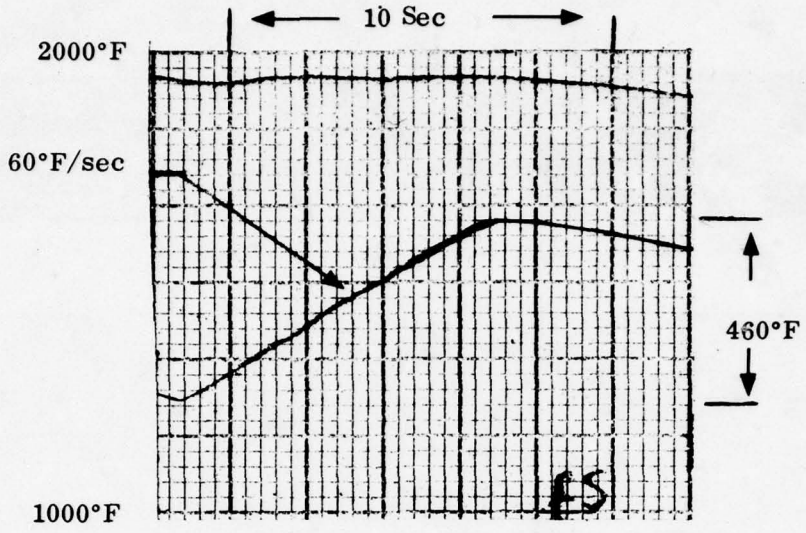

Forward Shroud TC #1

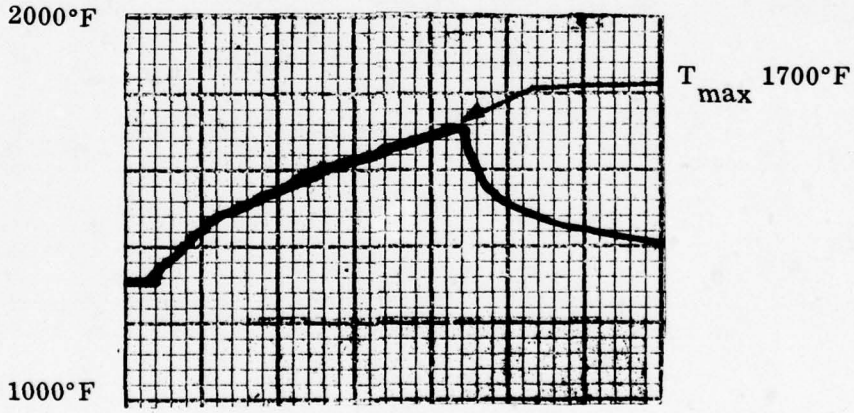

B.

Vane Trailing Edge
Optical Pyrometer

Figure 48B. Thermal Up-Shock of Forward Shroud and Vane Trailing Edge

A

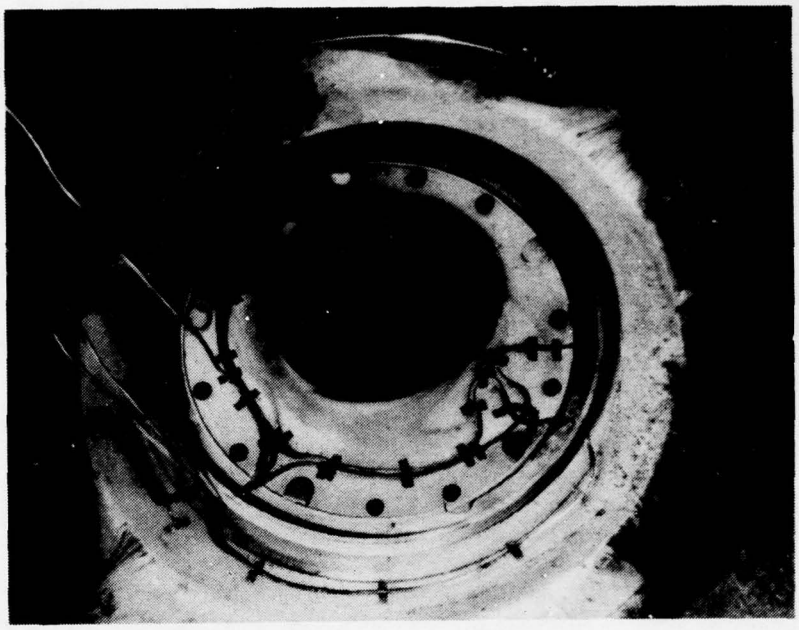

B

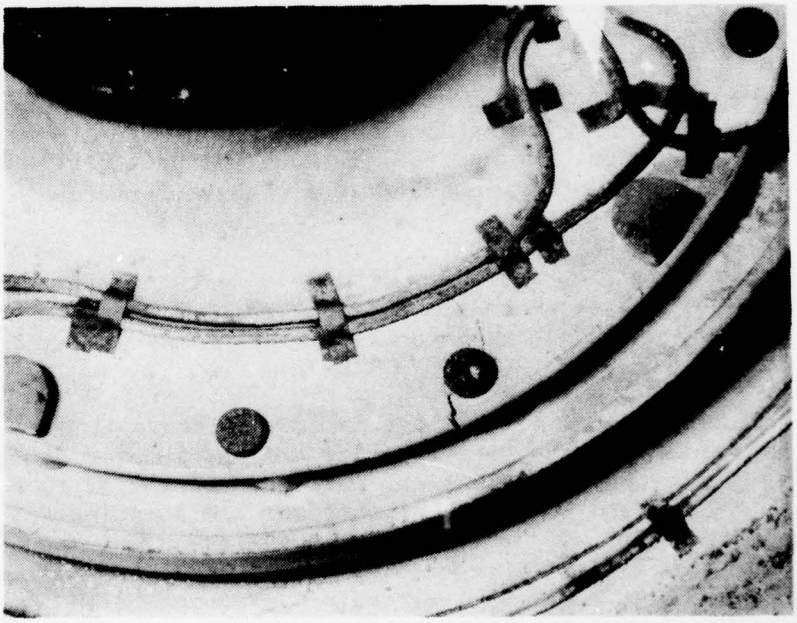

Figure 49. Standard 10 kW Nozzle After 500 Rig Test Cycles

Five hundred rig test thermal shock cycles, as described above were also applied to the ceramic vane superalloy shroud nozzle assembly. Figure 50 shows vane location #7, #8 and #14, which evidence no damage after the 500 cycles. This condition is typical of ceramic vane sections located in positions #1 through #14.

Figure 51 shows vane position #15 where the ceramic vane piece sustained a crack at the trailing edge location. The lowest temperature glass (40% B402, 20% GN19, 40% Cr_2O_3) which has a nominal 927°C (1700°F) firing temperature, was applied to this vane. No flaws or defects were evident in the hot pressed silicon nitride vane insert from Zyglo inspection done prior to the test.

The failure initiates at the contact point between the vane trailing edge and the lip of the forward shroud recess, and appears to be due to longitudinal compressive forces. It is believed that shear resistance of the glass at lower temperature tended to support compressive differential thermal loads on the trailing edge which resulted in this failure.

Only one of the four vanes using this low temperature glass failed at this stage of testing. This probably reflects the statistical nature of failure of ceramics. Subsequent disassembly of this nozzle showed no other probable cause for this failure.

Figures 52A and 52B show the rear shroud section of the ceramic vane superalloy shroud test nozzle after 500 thermal cycles. The general condition of the nozzle is good except that each of the bolt or rivet holes has a thermal crack propagated from the shroud outer lip as shown typically in Figure 52B. Thermal cracking is also observed on the lip section of the forward shroud (see Figs. 50A and 50B) at each end of the vane trailing edge sections. These cracks are arrested at the change of section and do not continue into the forward shroud.

The thermal damage to the superalloy shrouds attests to the severity of the rig test thermal shock sequence since this type of damage has not been encountered on any of the 10 kW turboalternator engine packages that have been operational.

The thermal shock sequence for the preliminary all-ceramic nozzle was run in four 125 cycle sets of increasing severity and checked for damage or cracks after each set. Temperature transient rate was controlled to 8, 17, 25 and 33°C/sec (15, 30, 45 and 60°F/sec) at thermocouple locations #1 and #2 which corresponds to location #95 in the 10 kW engine transient trace shown in Figure 47. Maximum cycle temperature was 1093°C (2000°F) at vane trailing edge as monitored with an optical pyrometer. Figures 53 and 54 shown temperature time traces for the least severe (15°F/sec) and most severe (60°F/sec) thermal cycles. Table 11 gives gas flow conditions for these thermal shock tests.

The RBSi_3N_4 shroud HPSi_3N_4 vane nozzle survived this test series without sustaining any damage.

A.

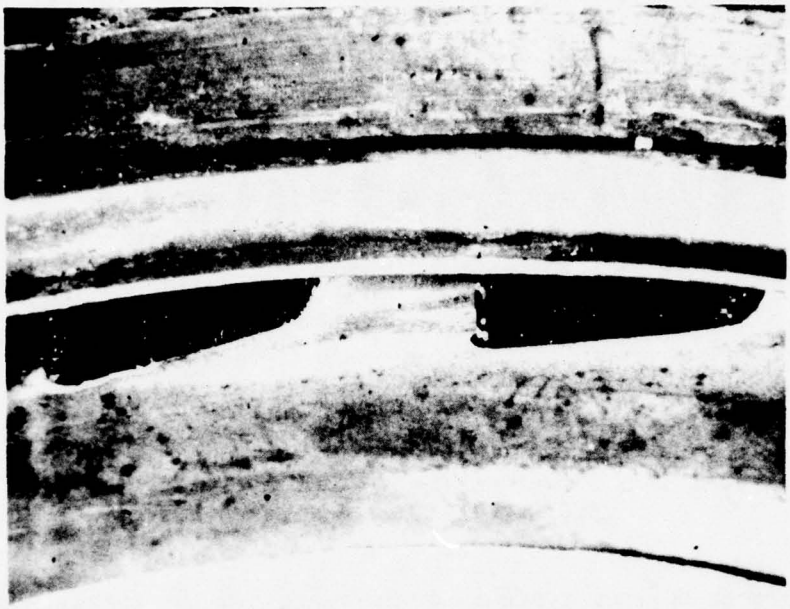

B.

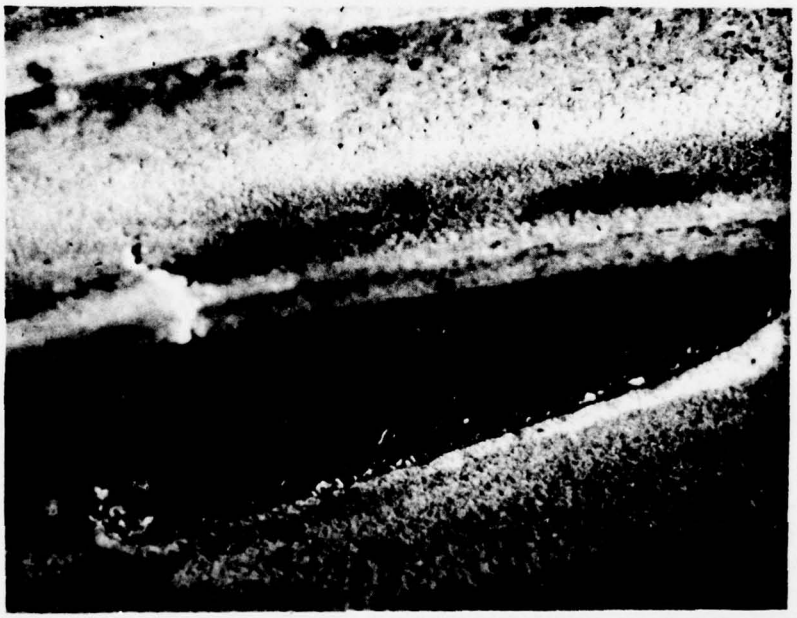

Figure 50. Close-up View of Nozzle Vane Locations (A) 7 and 8, (B) 14, After 500 Rig Test Thermal Shock Cycles

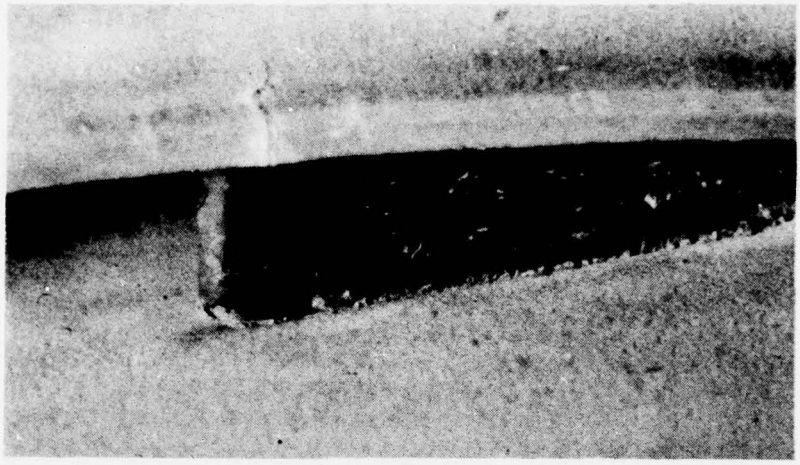

Figure 51. Close-Up View of Vane Location #15 After 500 Rig Test Thermal Shock Cycles

Figures 55 through 60 show typical nozzle vanes and the nozzle shrouds after the 500 cycle thermal shock test was complete. Dye penetrant inspection showed no evidence of cracks.

All of the vanes were intact after the test regardless of type of glass joint material used or whether any was used at all.

Dust Erosion

Since all experimental and analytical evidence for vane erosion on the 10 kW turbine engine shows that erosion occurs due to secondary impingement of particles projected radially outward from the turbine wheel, it was decided that erosive particles would not be introduced in the upstream gas in rig tests. Instead, an impinger was devised which simulates the type of erosive attack that occurs in the engine. Figure 37 shows the design and arrangement of this device. Dust particles are accelerated in the airstream traveling in a five foot tube toward the vane to be eroded. A diverter jet of air redirects the particle accelerating stream so the hot gas nozzle flow would not be disturbed. Particles of Arizona Road dust classified to include the 43-74 micron size range were used as the erosive media. These particles are large enough that they are not redirected from their path toward the nozzle vane by the diverter air jet. The impinger outlet was located 4 cm (1.6 in.) from nozzle vane surface and particles impinged at a 60 degree angle from orthogonal to the vane.

A ten hour test was run on the referenced 713LC superalloy nozzle vane shown in Figure 61. The vane trailing edge temperature was monitored with an optical pyrometer and controlled to 927°C (1700°F). Dust concentration in the impinging gas stream was 0.0018 mg/cm^3 (50 mg/ft^3) with this stream

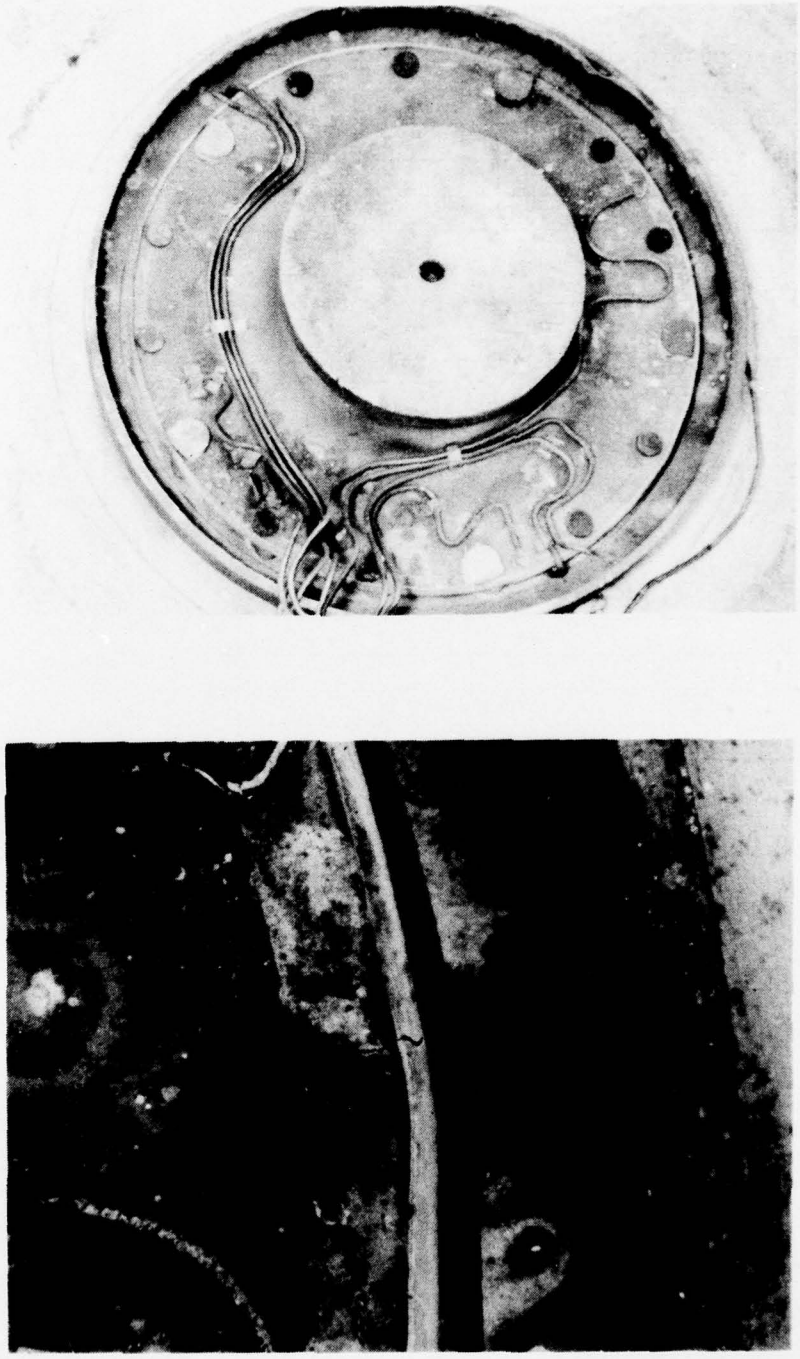

Figure 52. Rear Shroud of Bi-Material Nozzle After 500 Rig Test Thermal Shock Cycles Showing Thermal Cracking at Holes

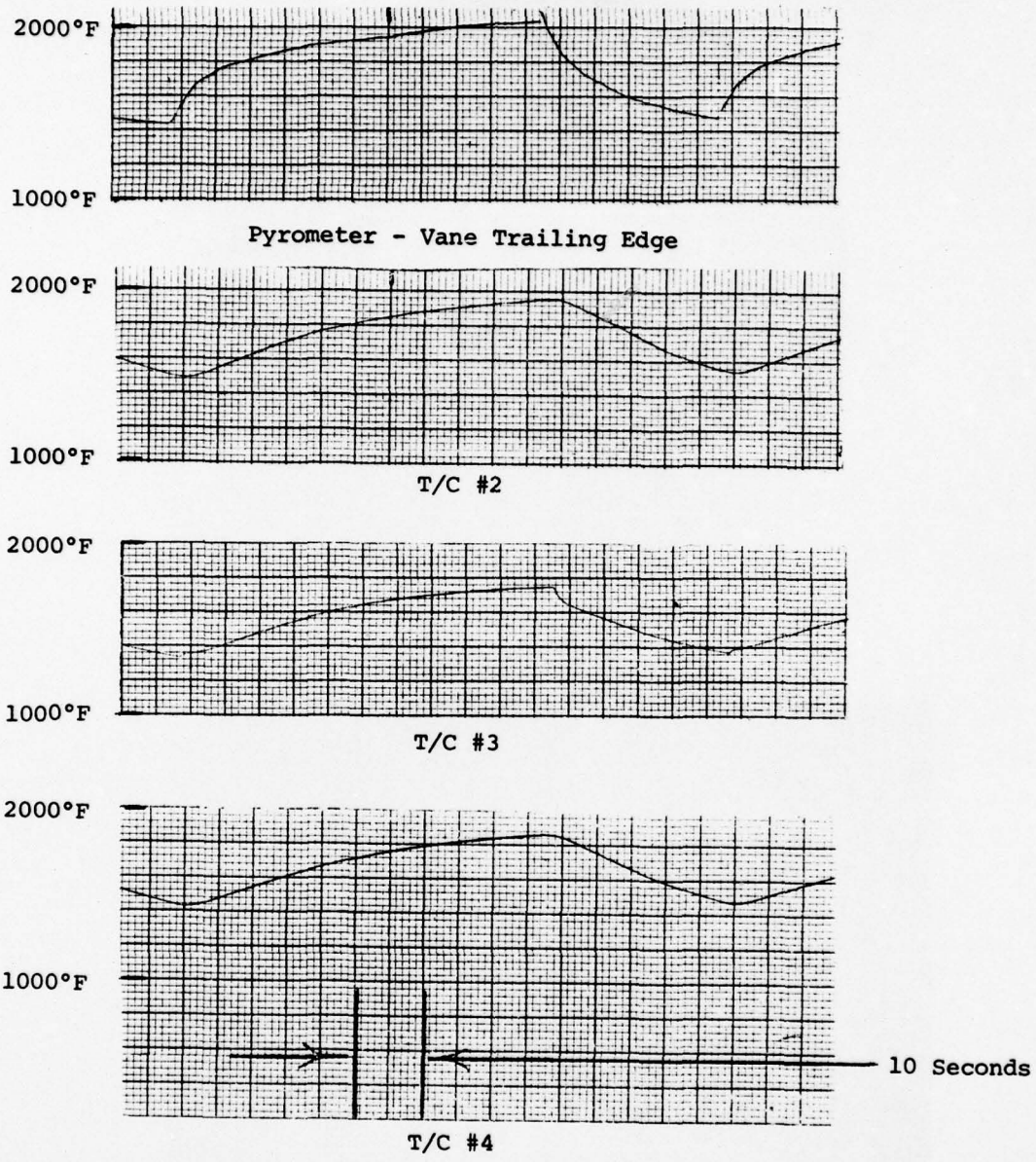

Figure 53a. Thermal Shock Cycle - 15°F/Sec at T/C #2 - All-Ceramic Nozzle

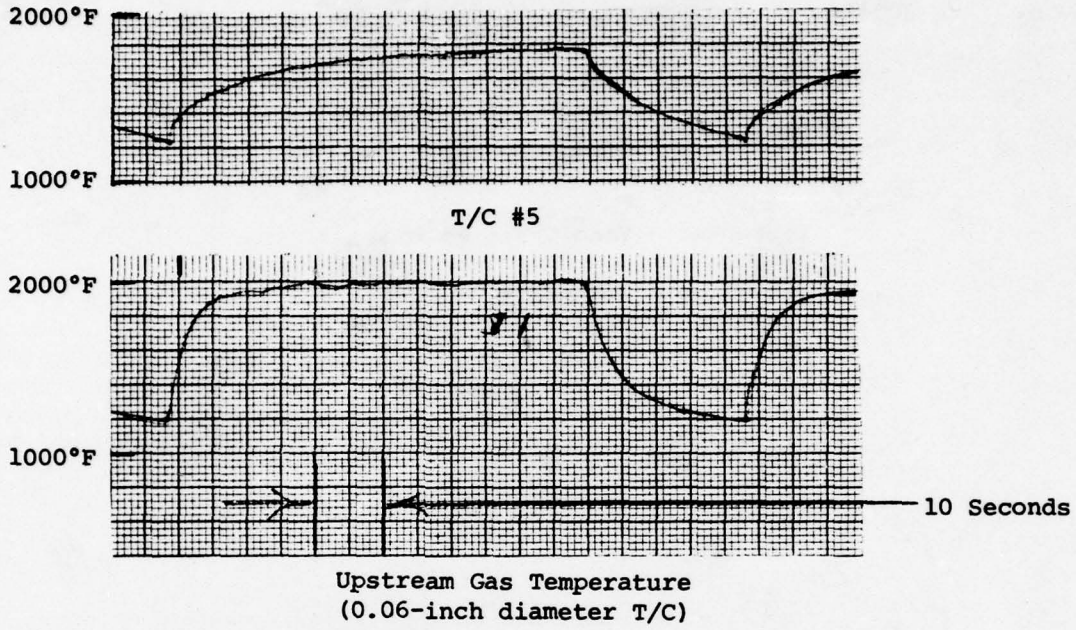

Figure 53b. Thermal Shock Cycle - 15°F/Sec at T/C #2 - All-Ceramic Nozzle

flowing at 305 m/sec (1000 ft/sec). The particle velocity upon impinging the vane trailing edge falls in the range of 251-274 m/sec* (800-880 ft/sec) depending on particle size.

The ceramic superalloy nozzle was also exposed to 10 hours of dust erosion with vane temperature controlled by pyrometry to 927°C (1700°F). Vane #1 was subjected to erosion.

Figures 62A and 62B show the vane at location #1 after the 10-hour erosion test. Microscopic examination of the trailing edge shows 0.005 in. maximum erosion at the vane trailing edge and 0.0035 inch of erosion at ceramic vane midpoint 0.19 inch from the trailing edge. This location is comparable to the location on the standard 10 kW nozzle which suffered 0.055 inch erosion in the same test sequence (see Fig. 63). This implies a 16:1 erosion advantage for HPSi$_3$N$_4$ over 713LC at 927°C (1700°F) at a 60 degree impingement angle. Examination of nozzles eroded in engine tests suggests that erosive particle impingement angle is less than 60 degrees and approaches a more oblique angle of 30 degrees. Ambient temperature tests show an erosion ratio

*These values were calculated using the method described in Appendix I of Reference 24.

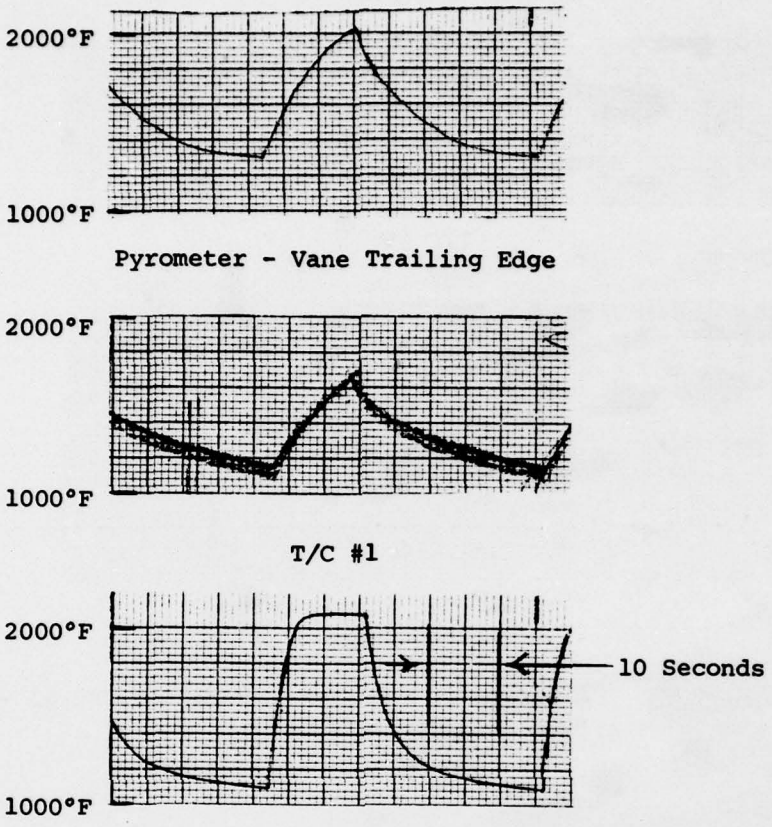

Figure 54. Thermal Shock Cycle - 60°F/Sec at T/C #1 - All-Ceramic Nozzle

comparison of 60:1 for these materials at 30 degrees. Therefore it can be assumed that the 16:1 erosion ratio measured here is conservative. Values of 60:1 might be expected in actual engine tests.

The simplified all-ceramic nozzle was tested with upstream dust ingestion to look at the effect of erosive particles on ceramic shrouds as they pass through the nozzle throat. Arizona road dust in the 43-74 micron size range was injected upstream to the nozzle during 1093°C (2000°F) rig testing. Total dust flow through the nozzle during a five hour erosion run was 557 gm. Average particle velocity upon impact with vanes has been estimated to be 600 fps. The nozzle exit gas velocity in this test is approximately 1800 fps.

Figures 64 through 66 show the nozzle after this test. Erosion of vanes was not measurable. The shrouds exhibited slight rounding of edges on the

Table 11

Engine Simulator Rig Flow Conditions With All-Ceramic Nozzle

Test Condition		Nozzle Upstream Flow		Nozzle Throat Conditions			
		Total Pressure (psia)	Total Gas Temperature (°F)	Mach Number	Gas Velocity (ft/sec)	Gas Density (lb/ft^3)	Total Mass Flow * Nozzle Coefficient of Discharge (lb/sec)
Dust Erosion or Hot Corrosion		21.6	2000	0.76	1742	0.0180	0.173
Thermal Shock							
15°F/sec	High Fire	20.7	2100	0.72	1693	0.0171	0.160
	Low Fire	19.5	1200	0.65	1242	0.0259	0.178
30°F/sec	High Fire	22.2	2240	0.79	1890	0.0165	0.172
	Low Fire	20.4	1120	0.70	1297	0.0276	0.200
45°F/sec	High Fire	23.9	2250	0.863	1983	0.0168	0.184
	Low Fire	21.4	1240	0.75	1432	0.0260	0.206
60°F/sec	High Fire	26.3	2250	0.951	2358	0.0173	0.225
	Low Fire	22.8	1110	0.820	1489	0.0287	0.236

inboard side of vane holding recesses. The shrouds might be expected to exhibit more erosion, except that dust particles impinge on the shrouds with a very shallow angle of incidence and as a result cause very little material removal.

The erosion experiment was stopped after five hours due to the failure of the dust feed system. In light of the time delay and expense required to continue this test, it was terminated at this point. Since erosion is expected to continue at a linear rate with time, results can therefore be scaled. The five hour exposure yields the same conclusions concerning erosion as would be reached by continuing testing for the prescribed 10 hours, i.e., neither ceramic vanes or shrouds are significantly eroded by dust injection.

Corrosion Tests

Corrosion testing of both test nozzles was done with three parts per million of simulated sea salt per total stream mass flow. Salt constituents are given in Table 12. Vane trailing edges were monitored with an optical pyrometer to 927°C (1700°F) in a 60-hour test for the ceramic vane nozzle and to 1093°C (2000°F) in a 70-hour test for the preliminary all-ceramic nozzle. (The standard nozzle was not corrosion tested since the ceramic vane nozzle uses the 713LC superalloy material.)

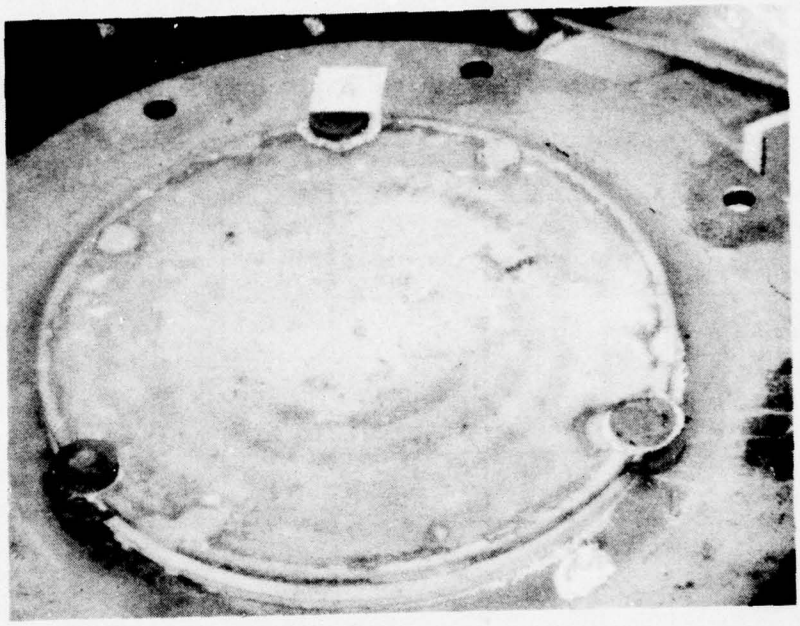

A. Upstream

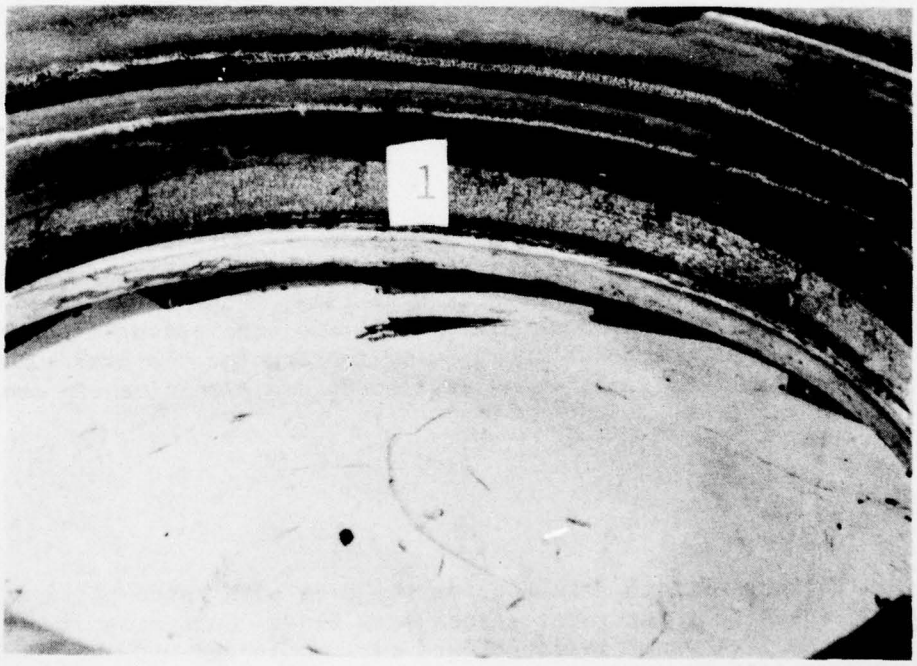

B. Downstream

Figure 55. All-Ceramic Nozzle After 500 Thermal Shock Cycles

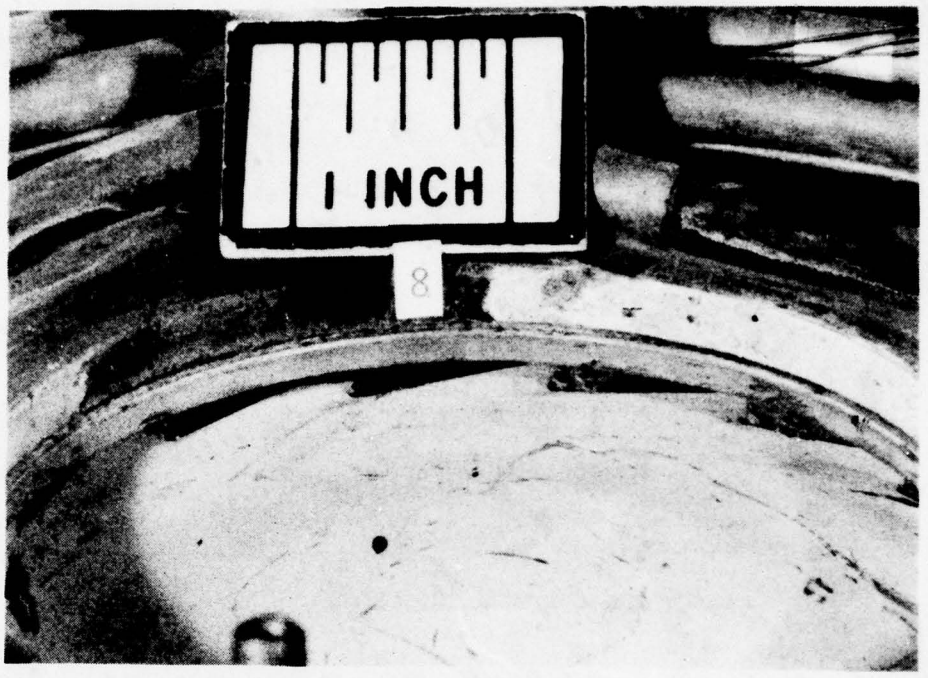

Figure 56. All-Ceramic Nozzle After 500 Thermal Shock Cycles - Downstream

Figures 67A and 67B show vanes #7 and #8 of the ceramic vane nozzle after this test. The HPSi$_3$N$_4$ ceramic vane shows no evidence of attack whereas the superalloy shrouds do, as seen in Figures 68A and 68B. Figure 69 gives a cross section of a ceramic vane and a superalloy vane leading edge for a comparison of relative corrosion in this test.

After erosion testing, the simplified all-ceramic nozzle was exposed to 70 hours of 3 ppm simulated sea salt corrosion (separate component pieces were exposed to the 500 cycle thermal shock sequence). The nozzle is shown after test in Figures 70 and 71. Molten deposits formed on most of the nozzle surfaces.

A crack developed at locating pin 'B' during test and propagated towards the center of the upstream shroud. It is shown in Figures 72 and 73. Other cracks occurred at locating pin 'A' (see Fig. 74) but did not propagate beyond the pin region. It appears that the cracks resulted from localized thermal stresses since the pins run relatively cool because of direct mounting to the water cooled stainless steel plate. The refrasil insulation wafers between the holding pin head and lower shroud were found to be impregnated with molten products at locations 'A' and 'B'. The insulating wafer at location 'C' was relatively free of molten materials. Since location 'C' on the lower shroud showed no cracking it seems probable that the short circuiting of the thermal insulation at location 'A' and 'B' was the primary cause of high thermal stresses and shroud cracking. The appearance of the crack (shown in Figure 75) as it follows the circumference of the pin head strongly supports this conclusion.

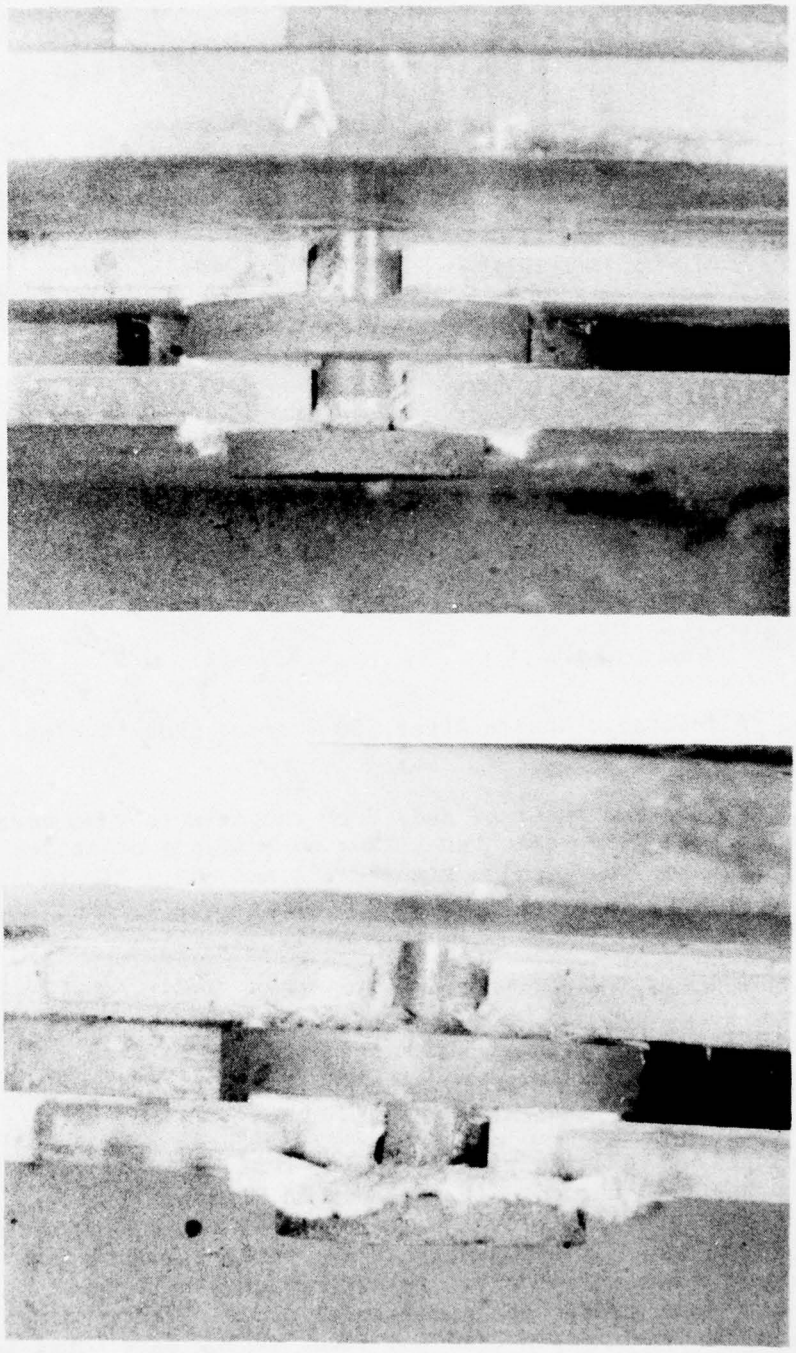

Figure 57. All-Ceramic Nozzle at Pin Locations 'A' and 'B' After 500 Thermal Cycles

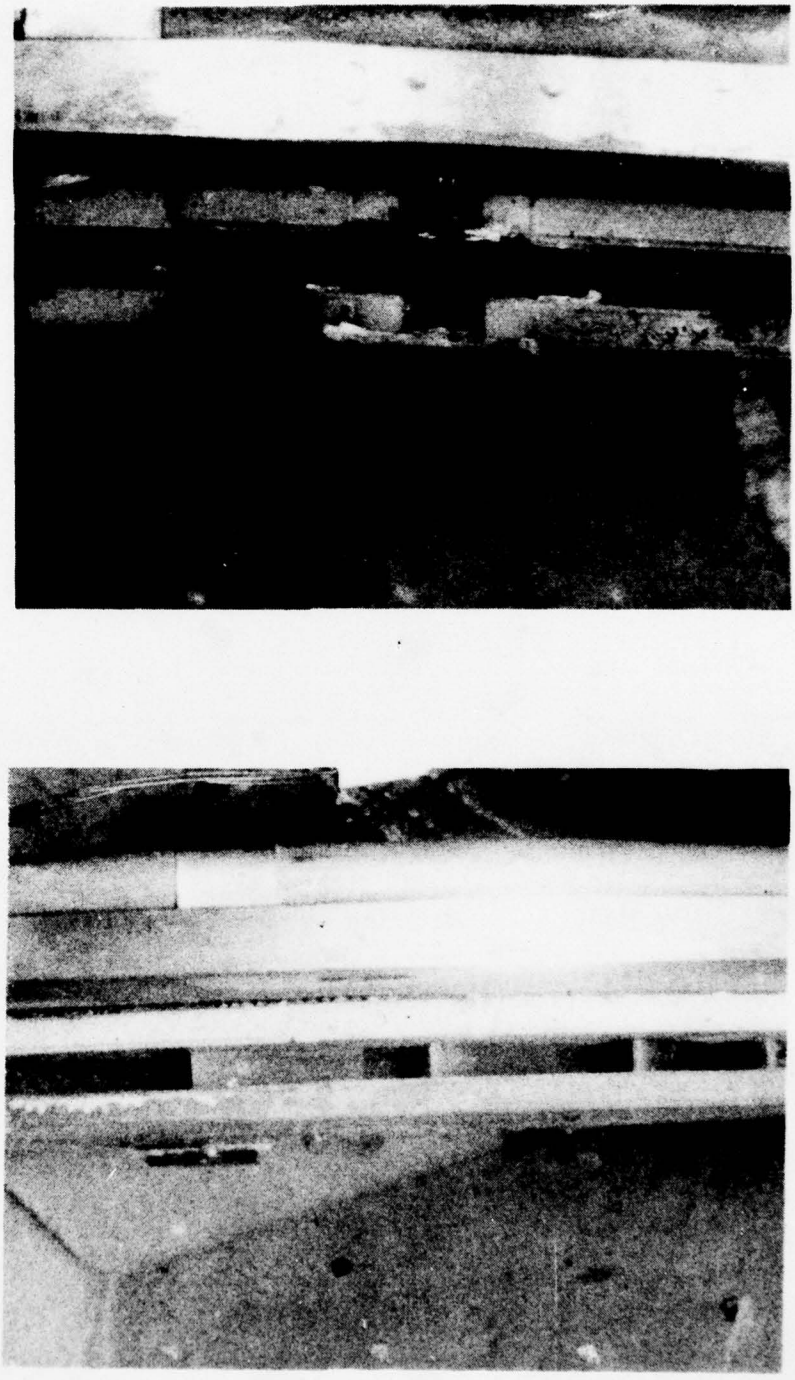

Figure 58. All-Ceramic Nozzle at Pin Location 'C' and Between Pins 'A' and 'C' After 500 Thermal Shock Cycles

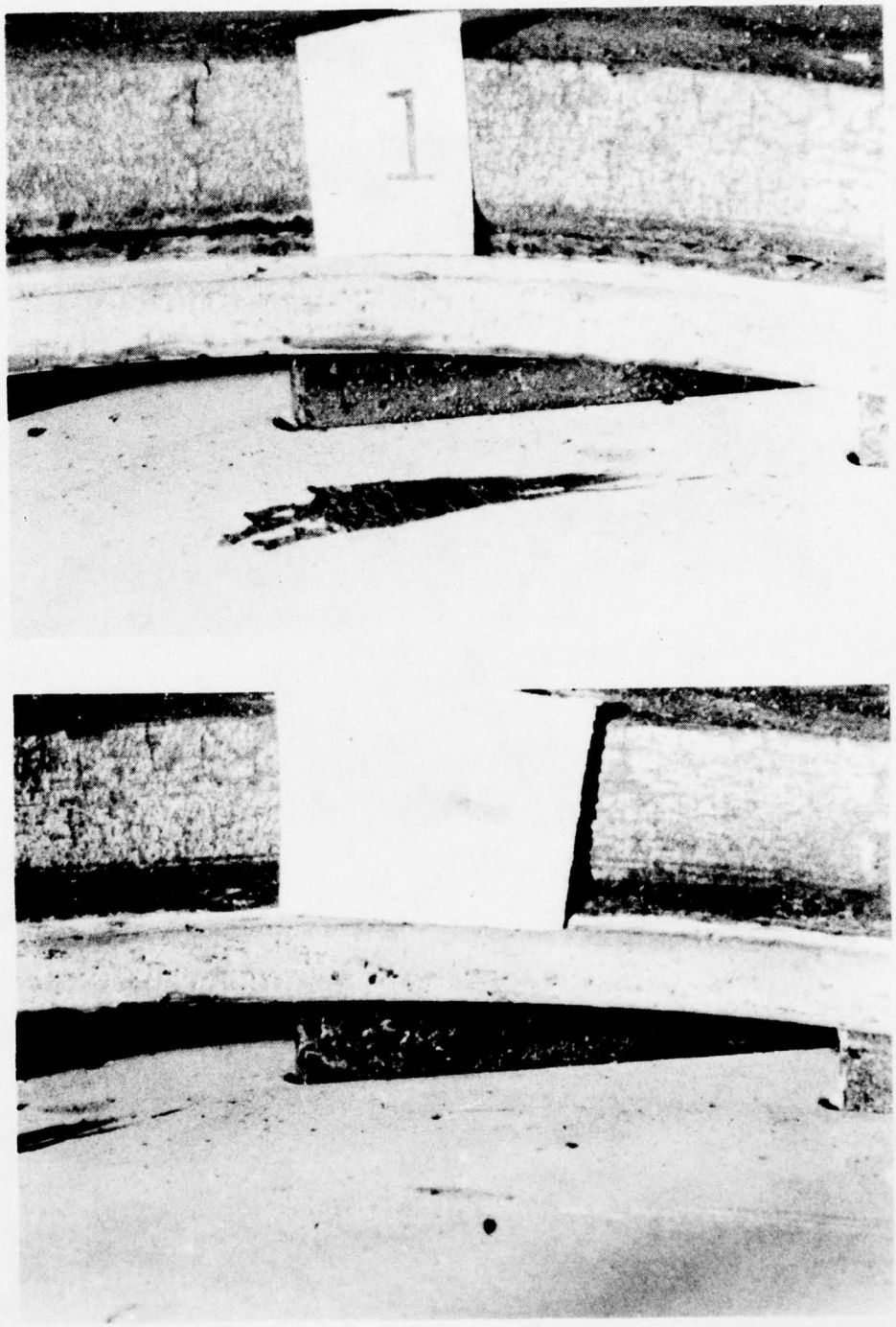

Figure 59. All-Ceramic Nozzle After 500 Thermal Shock Cycles - Locations #1 and #2

Figure 60a. All-Ceramic Nozzle After 500 Thermal Shock Cycles - Vane Location #3

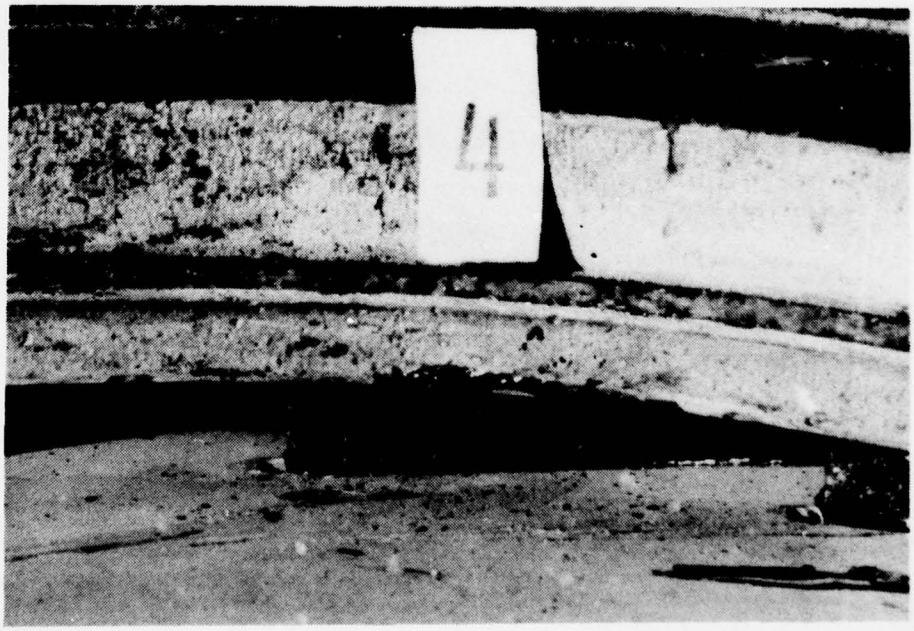

Figure 60b. All-Ceramic Nozzle After 500 Thermal Shock Cycles - Location #4

AD-A081 184 SOLAR TURBINES INTERNATIONAL SAN DIEGO CA F/G 21/5
APPLICATION OF CERAMIC NOZZLES TO 10 KW ENGINE.(U)
DEC 78 J C NAPIER, A G METCALFE, T E DUFFY DAAK02-75-C-0138
UNCLASSIFIED SR80-R-4375-43 NL

2 OF 3
AD-
A081184

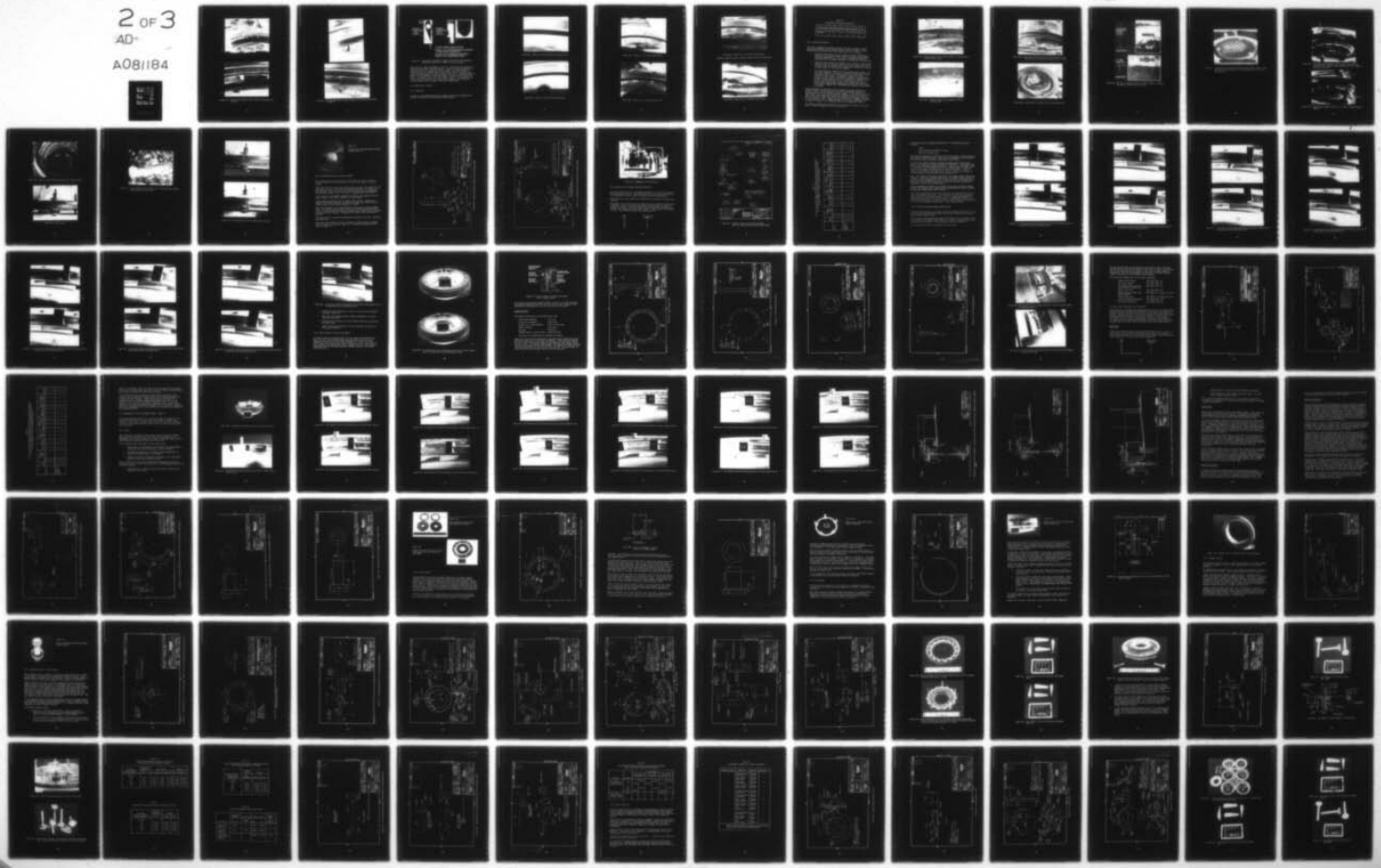

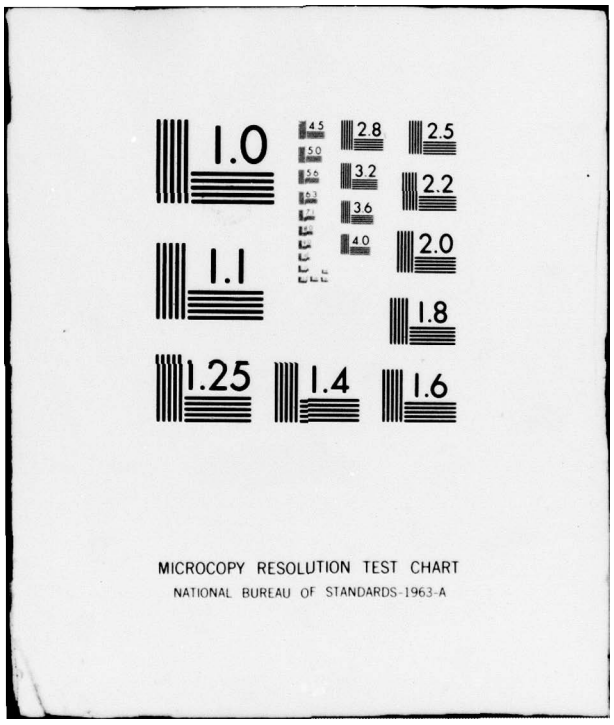
1.0
1.1
1.25
1.4
1.6
1.8
2.0
2.2
2.5
2.8
3.2
3.6
4.0
4.5
5.0
5.6
MICROCOPY RESOLUTION TEST CHART
NATIONAL BUREAU OF STANDARDS-1963-A

A.

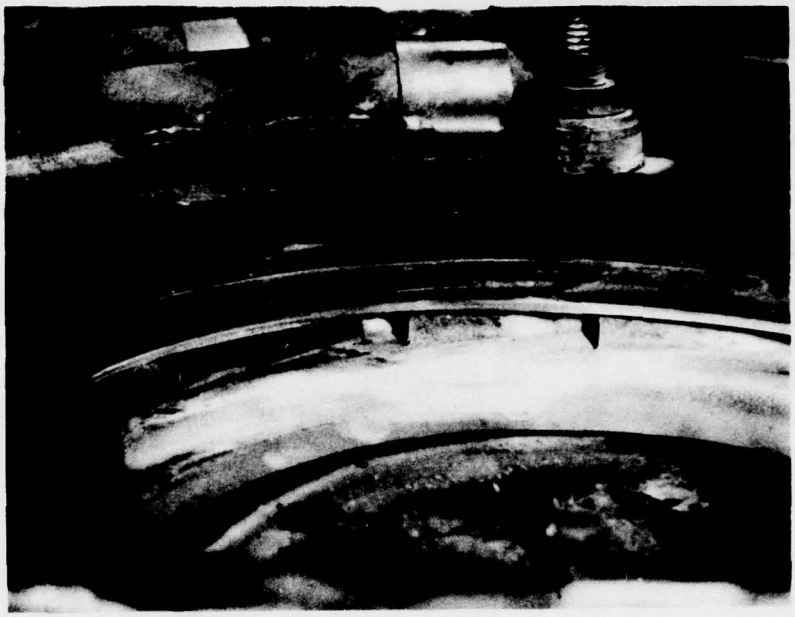

B.

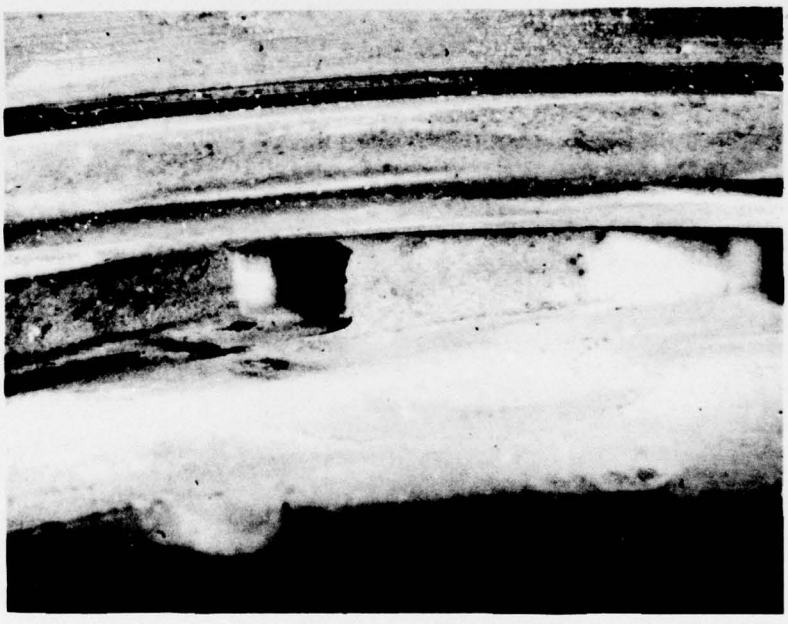

Figure 61. Standard 10 kW Nozzle After 10-Hour Rig Erosion Test at 1700°F

A

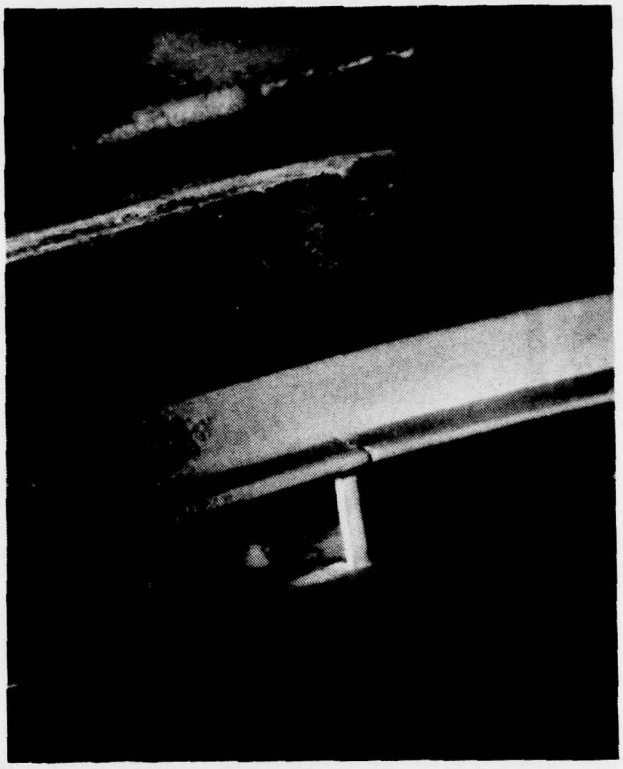

B

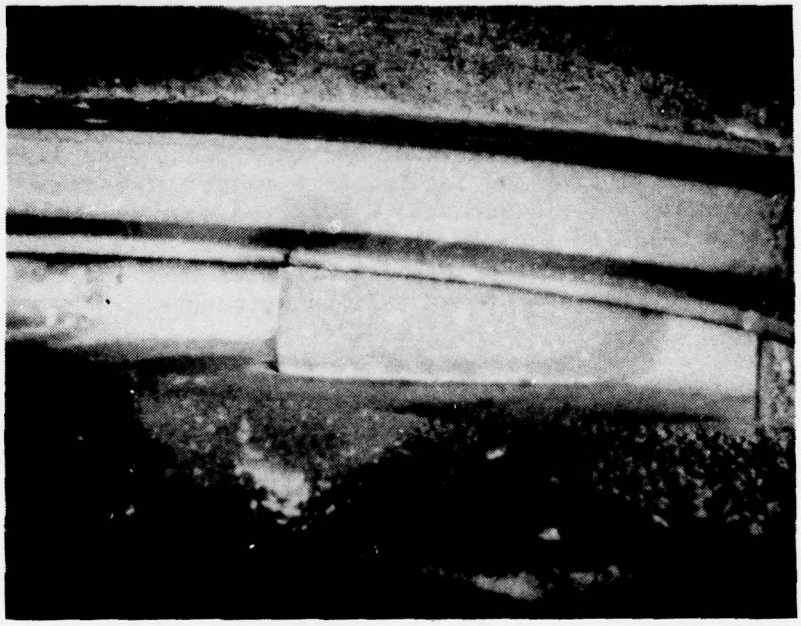

Figure 62. $HPSi_3N_4$ Vane Section After 10 Hours of Rig Test Dust Erosion at 1700°F

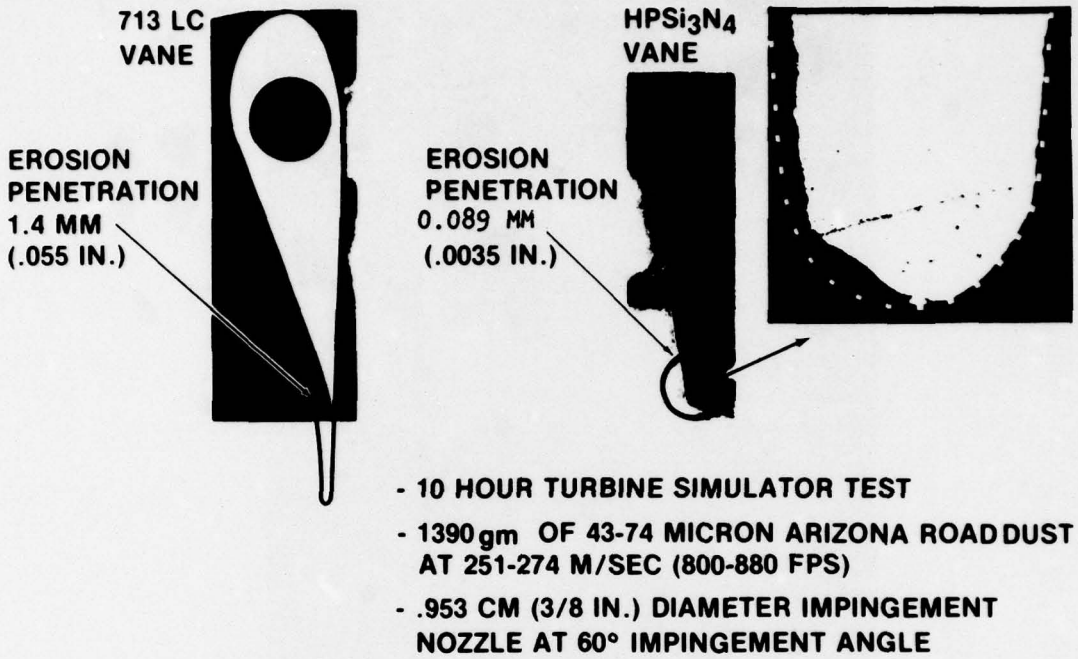

Figure 63. Comparison of Erosion of Nozzle Vanes From 713LC Superalloy and $HPSi_3N_4$ (NC-132) at 1700°F in Engine Simulator

Some attack of vanes (approximately 0.010 in. penetration) was observed on inboard surfaces after corrosion testing. Since the products deposited in these areas were not soluble in water it appears that constituents of artificial sea salt combined with residual molten Arizona road dust from 1093°C (2000°F) erosion testing and reacted with vanes. Localized attack of shrouds to approximately a 0.015 inch depth occurred near the holding pin heads. The deposits found here were soluble in water. This region of the nozzle would be expected to run cooler which suggests that this attack occurred because of the presence of sea salt constituents.

3.3 ENGINE TEST - PHASE II

3.3.1 Objective

The goal of this program phase was to design, fabricate and engine test a ceramic vane nozzle in the 10 kW gas turbine engine.

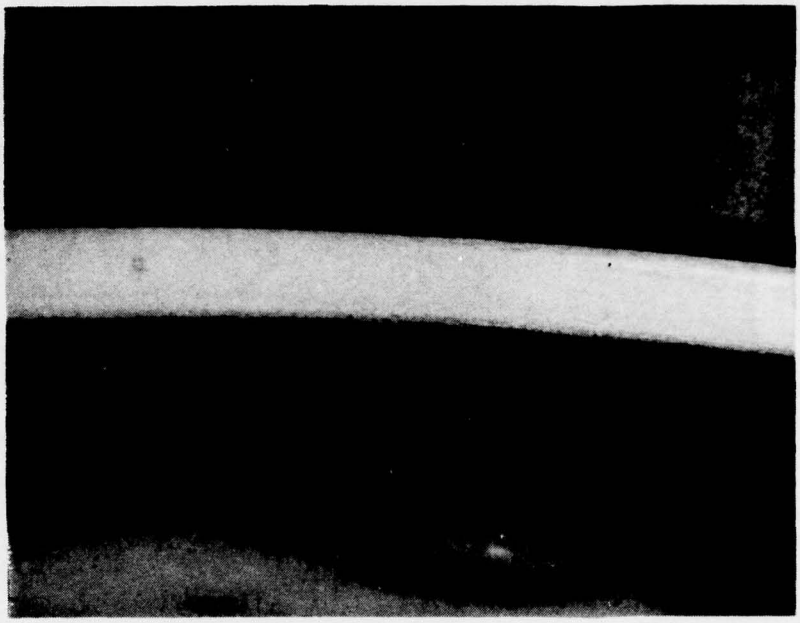

Figure 64a. Vanes 5 & 6 After 5 Hour Dust Erosion Test

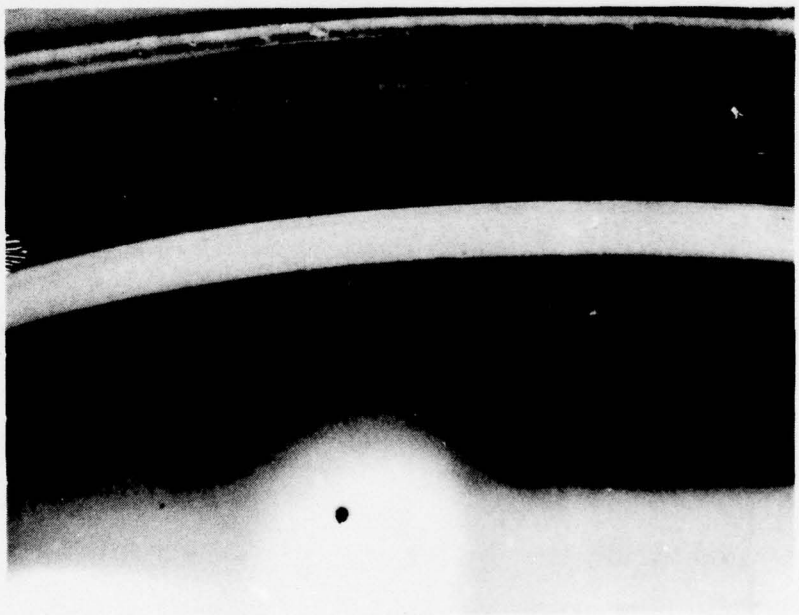

Figure 64b. Vanes 1, 2 and 3 After Erosion Test

Figure 65a. Vanes 4, 5 & 6 After Erosion Test

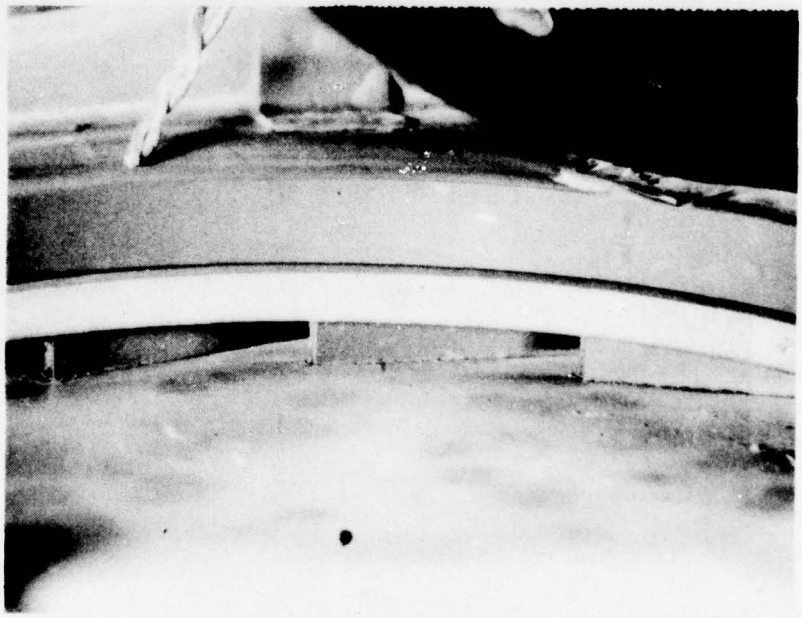

Figure 65b. Vanes 7, 8 & 9 After Erosion Test

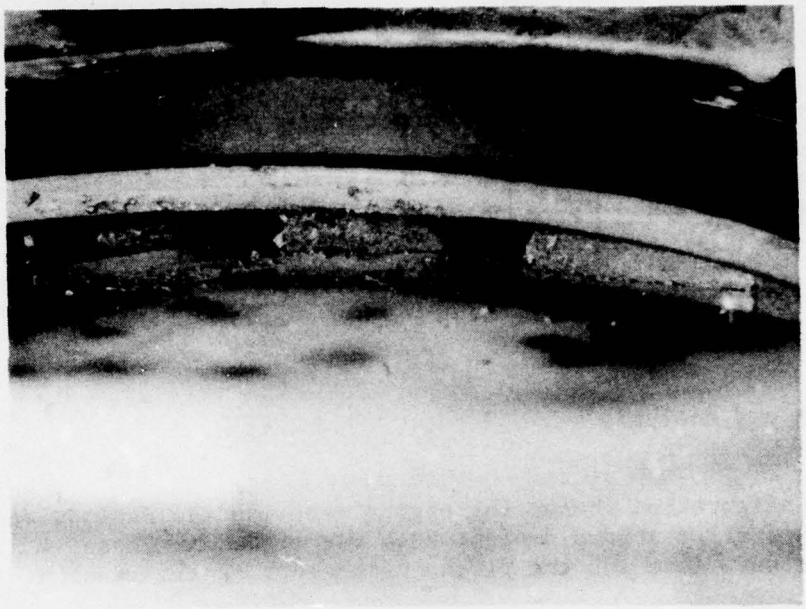

Figure 66a. Vanes 10, 11 & 12 After Erosion Test

(Surface Irregularity Due to Molten Deposits of Arizona Road Dust)

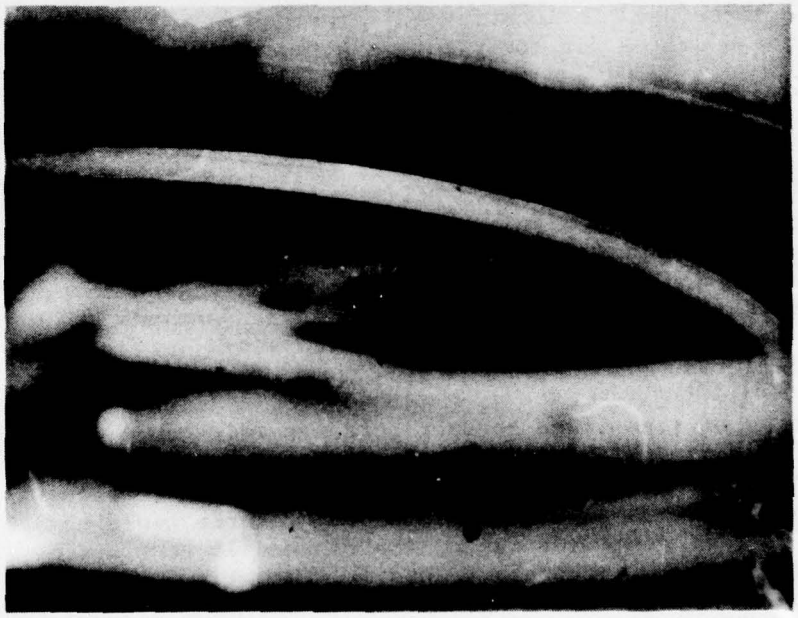

Figure 66b. Vanes 13, 14 & 15 After Erosion Test

Table 12

Constituents of Simulated Sea Salt

Constituent	NaCl	$MgCl_2$	Na_2SO_4	$CaCl_2$	KBr	KCl
ppm per total gas flow	2.04	0.455	0.310	0.099	0.080	0.018

3.3.2 Design and Analysis

The nozzle configuration chosen for engine test was the $HPSi_3N_4$ ceramic vane-713LC superalloy shroud design which was tested in Phase I. Three modifications were made for the first engine test of this design.

1. Flow data generated in rig test showed the nozzle coefficient of discharge to be slightly higher than the standard nozzle design. This was compensated for in the engine installation design by decreasing the vane height dimension of 0.204/0.202 to 0.185/0.184.

2. Since the nozzle throat area depends on the location of the inboard surface of the rear (inner) shroud nozzle vane recess, some of the tolerances used in locating this surface were tightened in relation to those called out for rig test hardware.

3. Rig tests showed one failure out of the fifteen vanes tested. The cause was assigned to constraint introduced between metal shrouds and ceramic vanes by the low temperature glass bond [927°C (1700°F)] in the surface. Differential strains on cooldown were believed to have caused an excessive longitudinal compressive load on vane trailing edge where it is contained in the recess. In order to avoid this type of failure in an engine test, it was decided that relaxing glass bonds between shrouds and vanes would not be used in engine test. Unbonded vanes survived rig test with no failures.

Even distribution of transverse contact stresses on ceramic vanes due to possible forward shroud distortion is the most significant function of relaxing glasses in this bimaterial nozzle design. It was expected that the engine tests at sea level and low ambient temperatures would not result in high turbine inlet temperatures during the planned 25 hour engine test run and 50 stop/start cycles. Therefore, nozzle distortion, because of yielding of shroud material due to thermal gradients and excessive temperature as predicted in Section 3.6.2, Analysis, would not be expected to occur.

The finalized design of the ceramic vane section nozzle tested in the 10 kW engine is shown in Figures 19, 21, 24, 76, and 77.

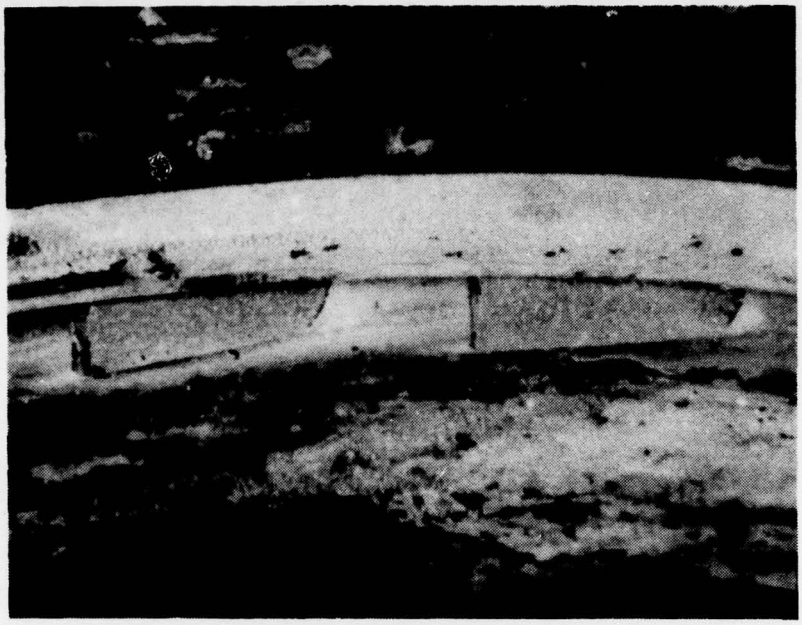

Figure 67a. Vane Locations 8 and 7 After 60 Hours, 3 ppm Sea Salt, 1700°F Corrosion Test

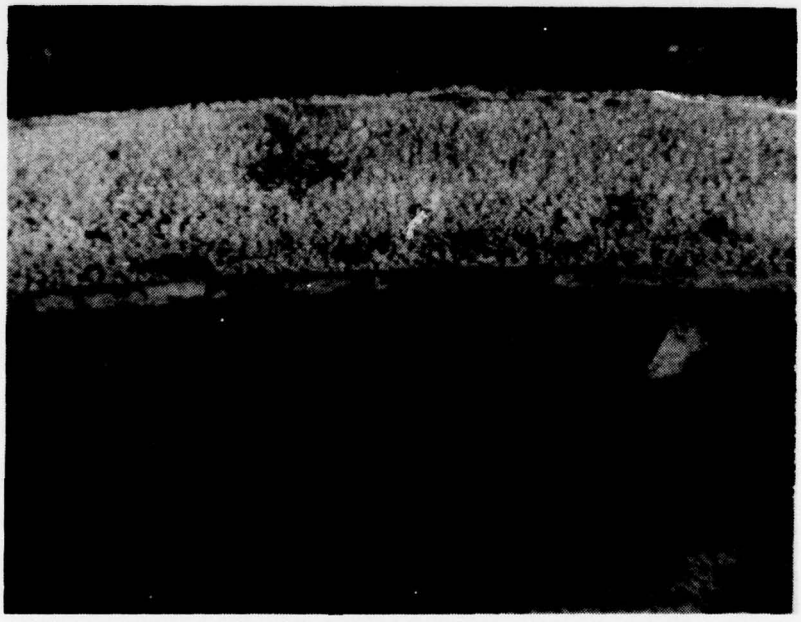

Figure 67b. Close-up View of Vane Location 7, After Corrosion Test

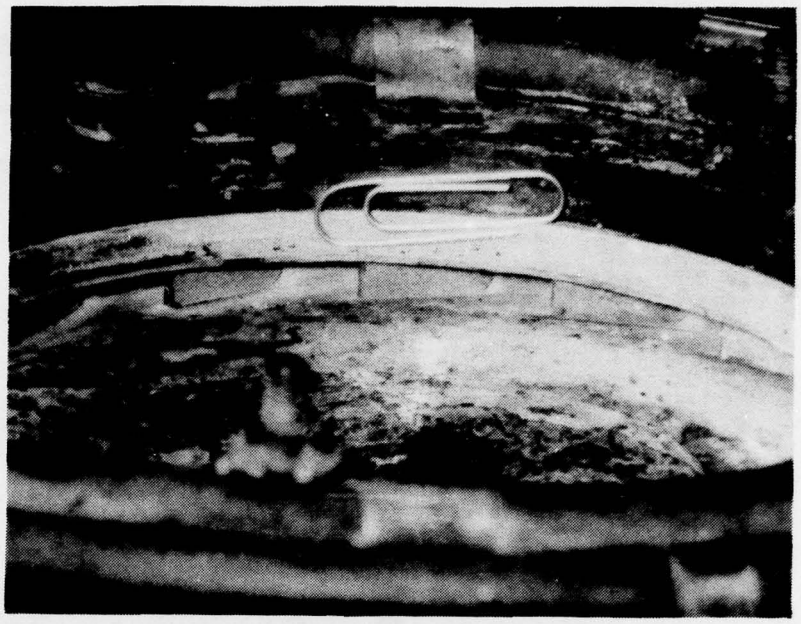

Figure 68a. Downstream Side of Nozzle After Rig Corrosion Test (Vanes Shown are From Left to Right 9, 8, 7, 6 & 5)

Figure 68b. Upstream Side of Nozzle After Rig Corrosion Test

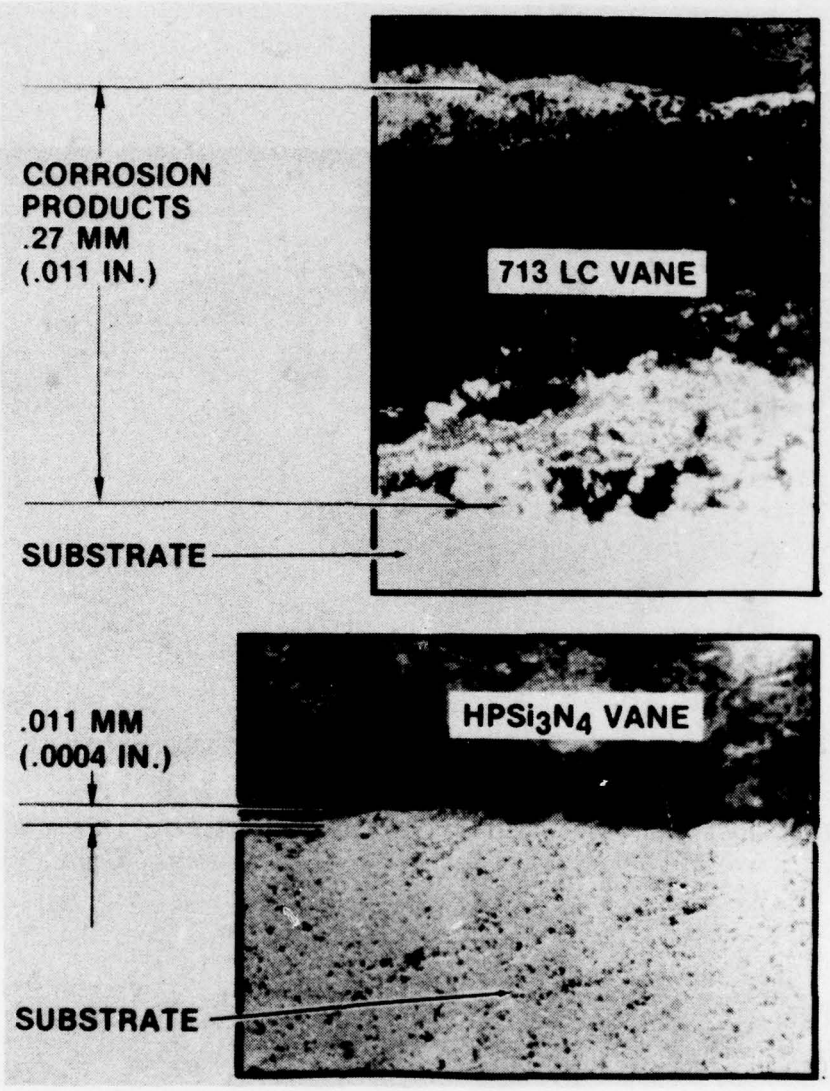

Figure 69. Sea Salt Corrosion; 60 Hours at 927°C (1700°F) in Turbine Simulator, 3 ppm Artificial Sea Salt

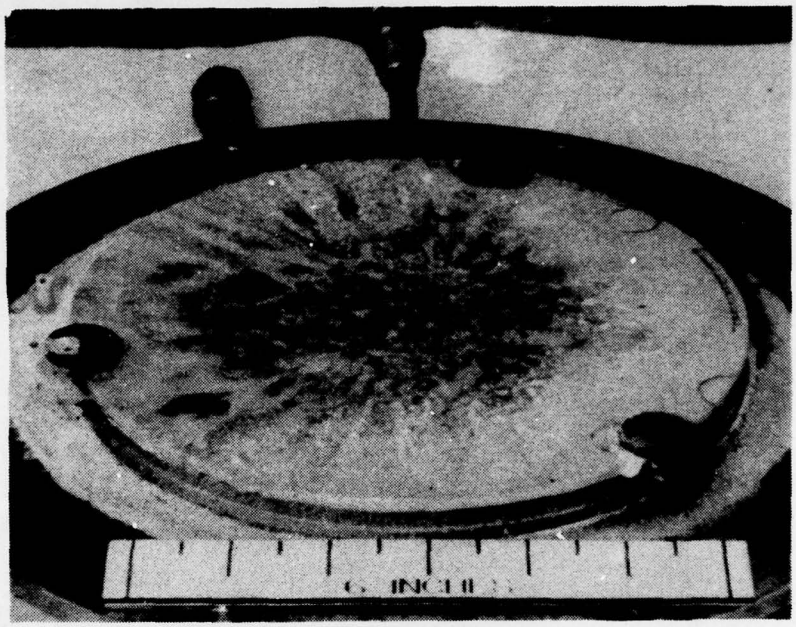

Figure 70. Upstream View of Simplified Ceramic Nozzle After 70 Hour, 3 ppm Sea Salt Corrosion Test (Pin 'A' at Bottom Right, Pin 'B' at Left Center)

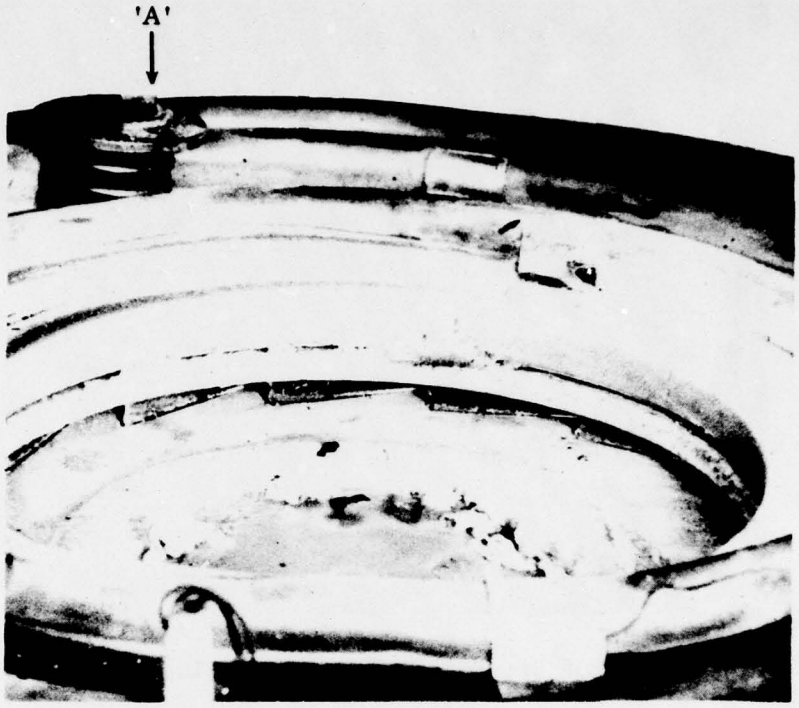

Figure 71A. Simplified Ceramic Nozzle After 70 Hours 3 ppm Sea Salt Corrosion Test. (Nozzle locating spring pin 'A' is shown in top left of picture)

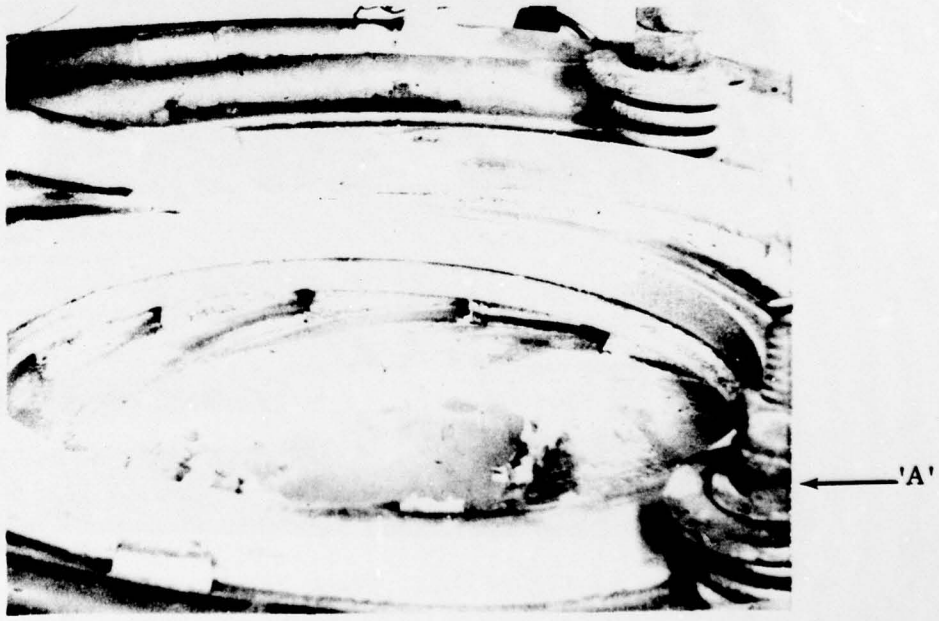

Figure 71B. Second View of Nozzle (Spring 'A' is Shown in Bottom Right of Picture)

Figure 72a. View of Crack From Downstream Side of Ceramic Nozzle

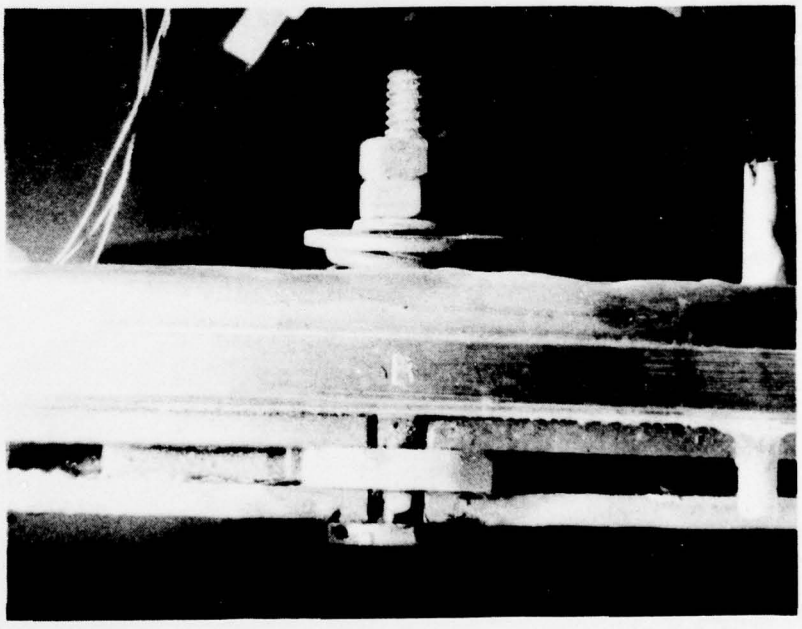

Figure 72b. Crack Origin

Figure 73. Crack Originating at Holding Pin 'B' (Dye Penetrant Applied for Visibility in this View)

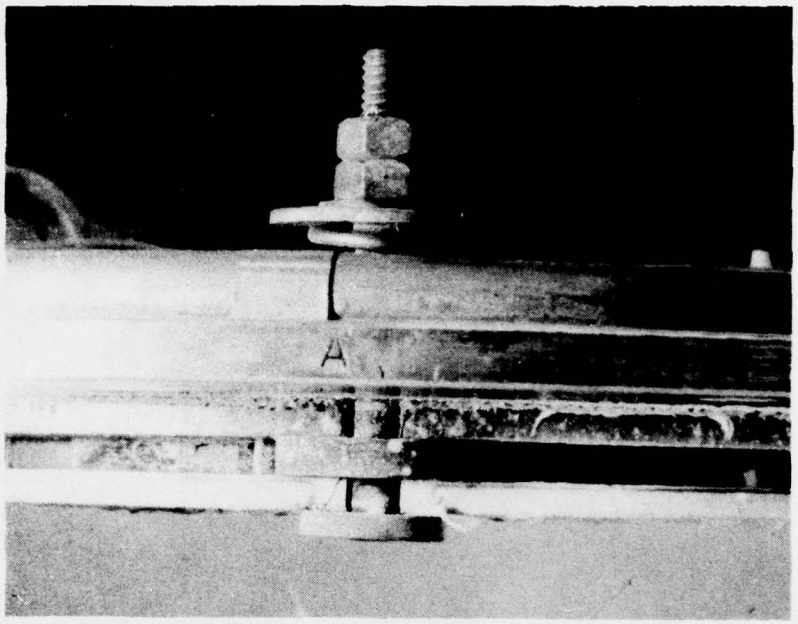

A

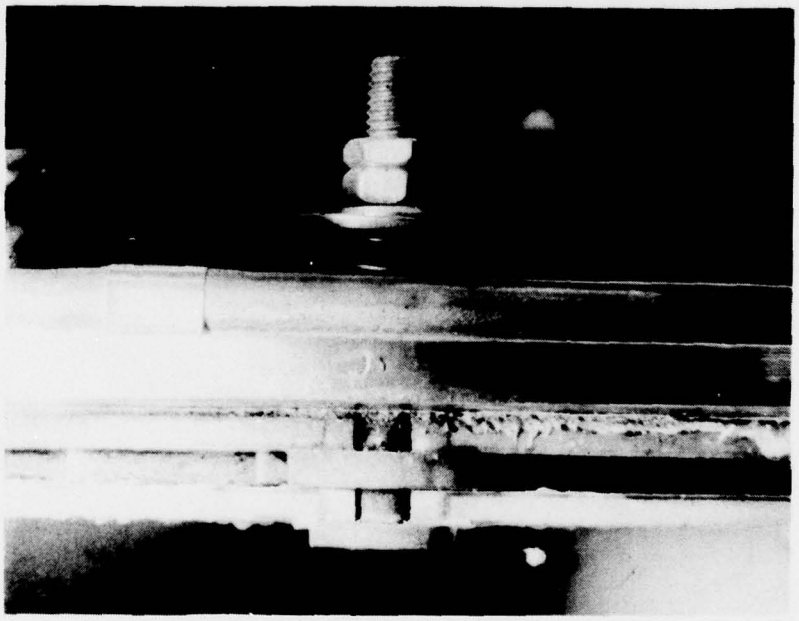

C

Figure 74. Pin Locations 'A' and 'C' After Corrosion Test

Figure 75.

Thermal Crack in Bottom Ceramic Shroud at Holding Pin 'B'

3.3.3 Nozzle Fabrication and Engine Assembly

The forward and rear nozzle shrouds per DSK 14956 and 14957 were electro-discharge machined from standards 10 kW castings (part numbers 11947 and 11948).

Vanes were placed in the recesses and AMI 100 braze alloy was loaded into the rear shroud at counter bore holes per standard procedure. The rivets per DSK 14959 were static cold set with 12,000 pound load and the assembly was vacuum furnace brazed at 1162°C (2125°F) for approximately five minutes.

At this point in the assembly procedure the $HPSi_3N_4$ vane segments were all loose. (This is the correct condition for this design.)

Final machining operations for the turbine wheel contour, combustor and exhaust pipe sealing diameters, and piloting surfaces were then done by an outside vendor per the standard drawing No. 74-8005.

After this operation it was observed that the vane sections were no longer loose. The forward (outer) shroud piloting lip (which is final machined to 0.040 to 0.050) had been distorted by machining tool pressure and had trapped the vanes in their recesses. No damage to the ceramic vane sections was observed.

This distortion was repaired by mechanically bending the lip back. The vanes were then loose.

The nozzle was assembled into the 10 kW engine in turboalternator package Serial #5 which is pictured in Figure 78. An assembly clearance chart is given in Figure 79.

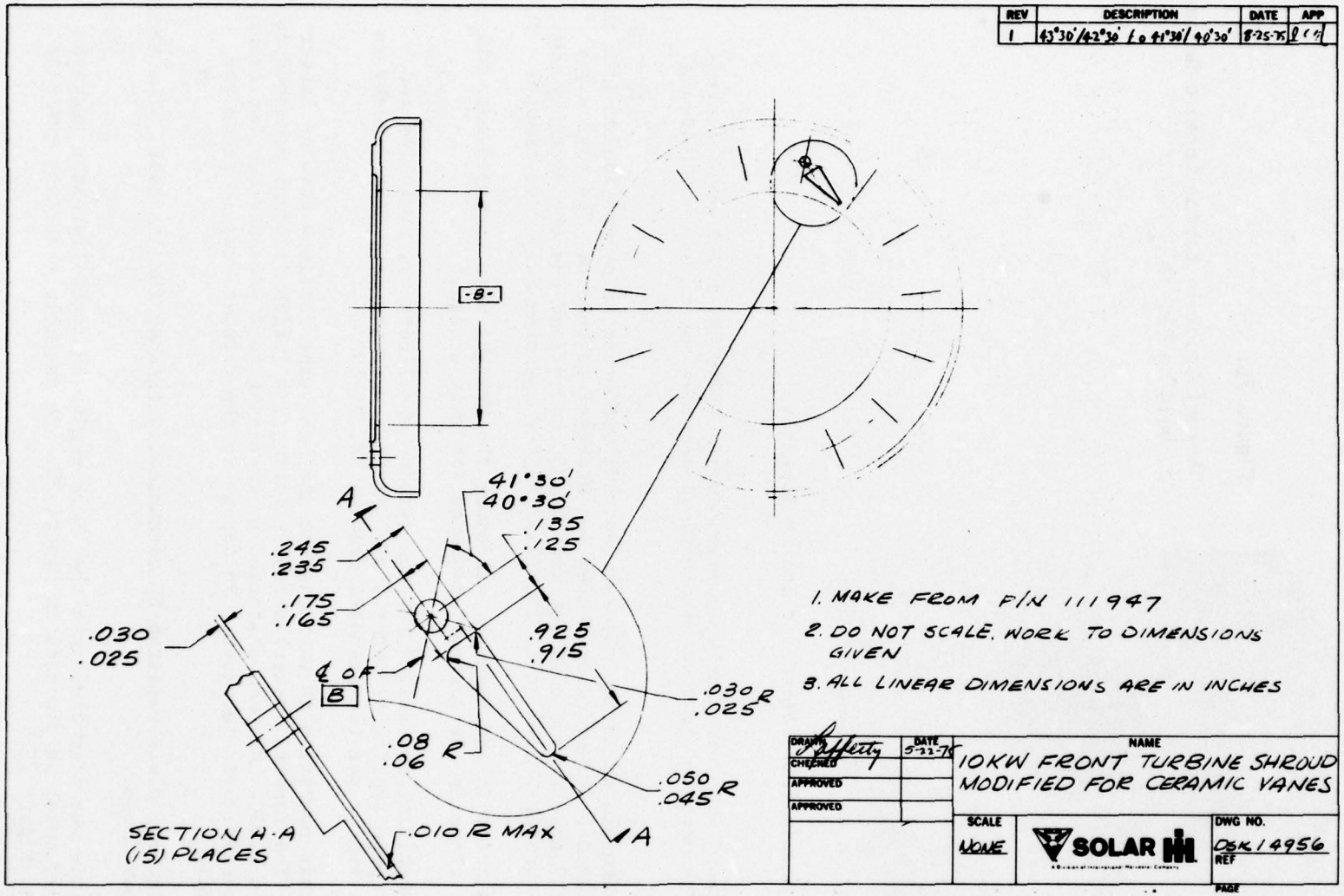

Figure 76. Forward Shroud for Engine Test of Ceramic Vanes

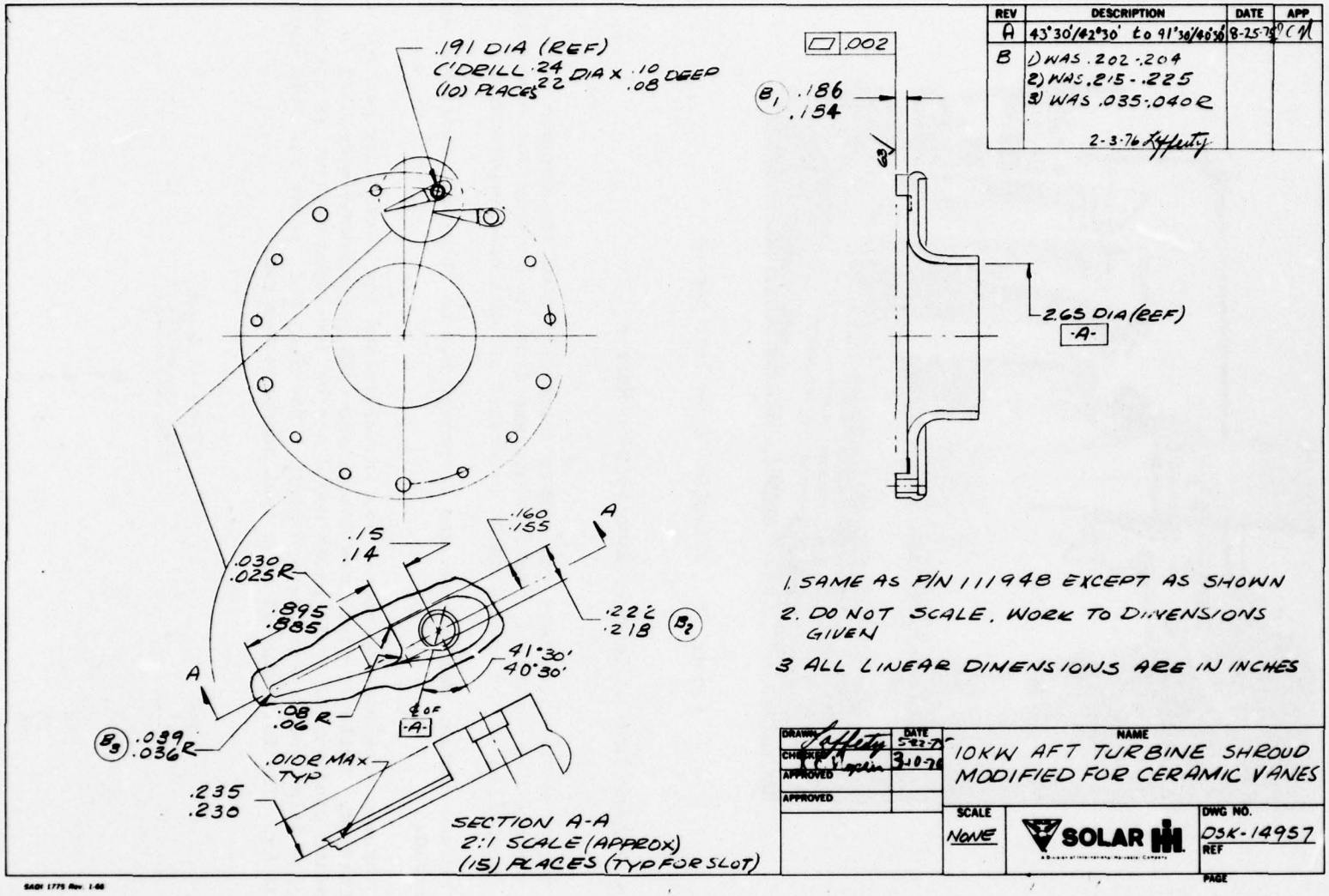

Figure 77. Rear Shroud for Engine Test of Ceramic Vanes

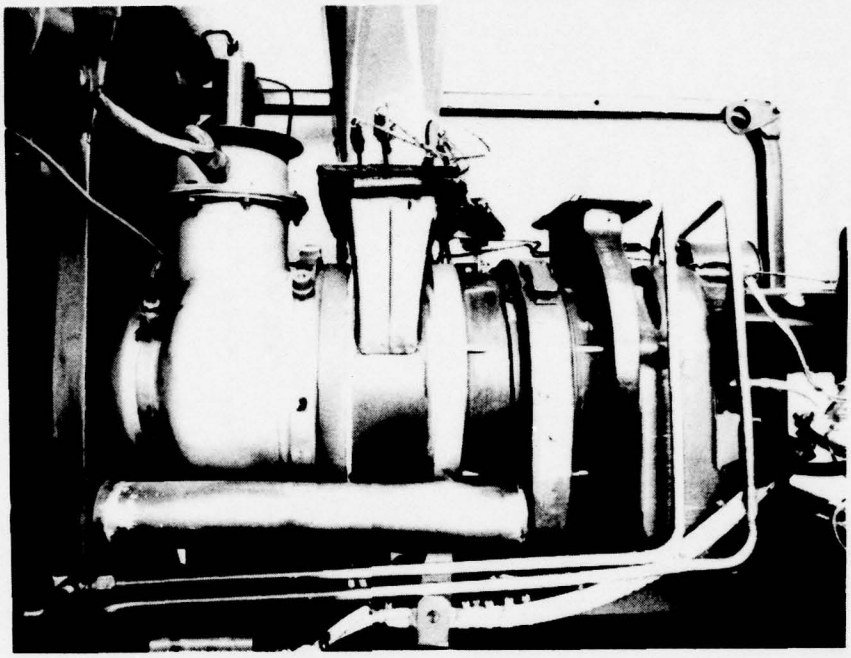

Figure 78. MERADCOM 10 kW Test Engine

3.3.4 Engine Test of Ceramic Vane Section Nozzle

The engine package was test run before installation of the ceramic nozzle in the as-received condition. Performance was found to be poor and load could not be applied to the unit without excessive exhaust gas temperature.

The nozzle section was removed and inspected but no abnormal conditions were observed.

The ceramic vane section nozzle was installed and the alternator package was calibrated. Table 13 gives raw data along with performance corrected to standard conditions. Full power could not be developed without generating turbine inlet temperature beyond 898°C (1650°F). Full power for this engine is 12 kW. The following 25 hour test sequence was run:

Load (%)	Time at Load (hrs)
75	6
0	1
50	6
25	6
75	6

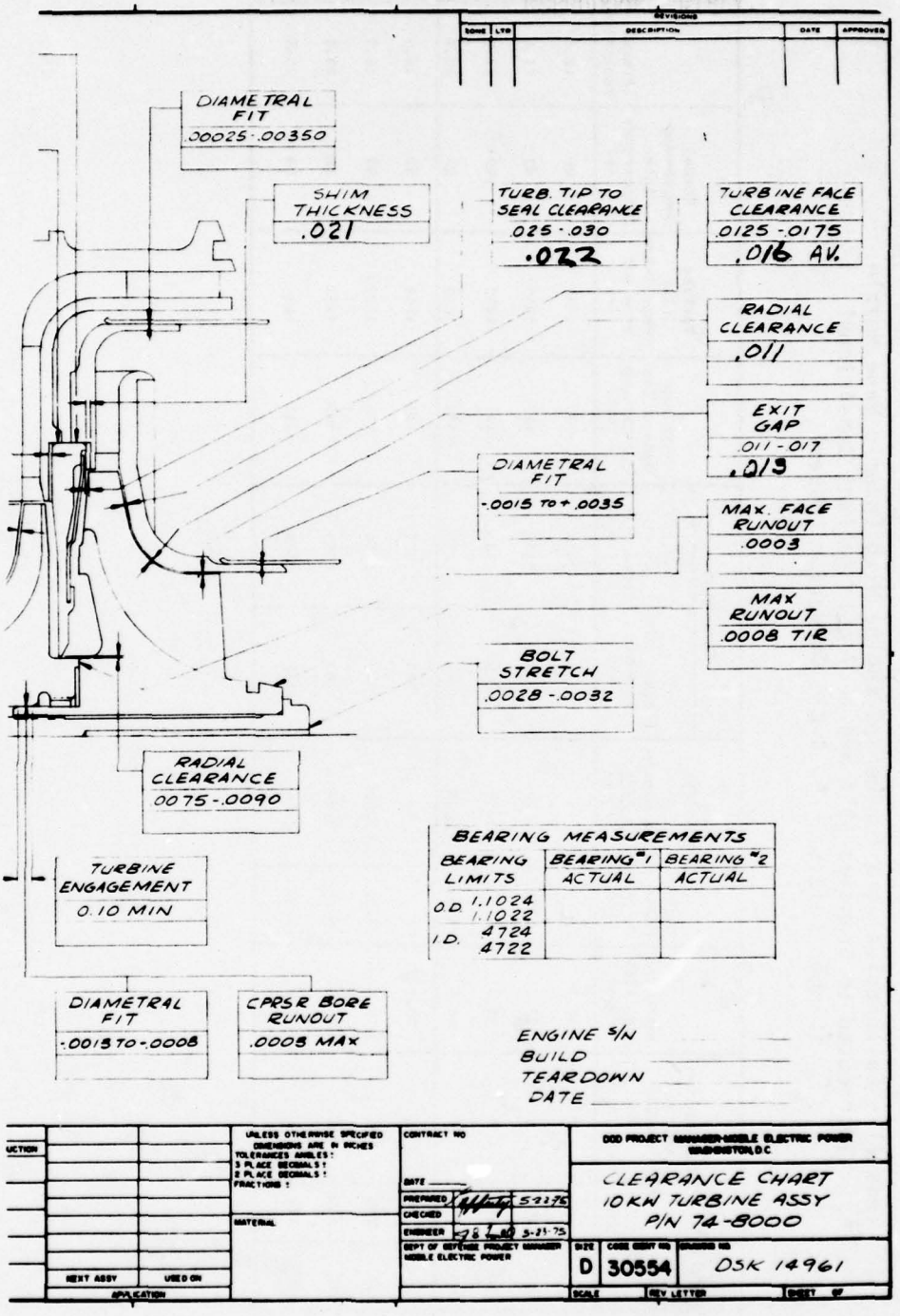

Figure 79. Clearance Chart 10 kW Turbine Assembly (June 15, 1976 Engine Serial #5) P/N 74-8000

Table 13

Test #1 - Calibration Data for Gemini Engine With Ceramic Vane Nozzle
(Corrected to Standard 59°F and 14.7 psia Ambient Conditions)
(Linear Loading - No Cycle Convertor Losses)

	Data Point No.	Load	Cummulative Engine Running Time (hours)	Corrected Fuel Flow (pph)	Shaft Power Output (kW)	Shaft Specific Fuel Consumption lb JP-4 / kW-hr	Corrected		Measured Exhaust Gas Temperature (°F)	Turbine Inlet Temp. Calc. From EGT (°F)	Actual Compressor Inlet Temperature (°F)	Actual Fuel Flow
							Exhaust Gas Temperature (°F)	Turbine Inlet Temperature (°F)				
Pre-Test	1	0%	0	14.2	0	--	716	1018	795	1102	88	15.6
	2	25%	0	17.3	3.32	5.22	834	1165	925	1269	92	18.6
	3	50%	0	21.3	6.23	3.42	979	1343	1070	1452	(90)	22.3
	6	75%	0	24.9	9.38	2.66	1080	1475	1174	1593	90	25.9
After 26 hour run and 50 start/stop cycles	154	0%	26	18.0	0	--	740	1057	828	1154	92	19.9
	157	25%	26	18.7	3.32	5.63	870	1204	975	1327	97	20.1
	156	50%	26	21.8	6.23	3.49	982	1349	1095	1487	98	23.0
	155	75%	26	24.8	9.38	2.64	1112	1508	1230	1658	98	25.9

Following this test the engine was subjected to 50 start/stop cycles as follows:

- Start
- Three minutes operation at no load.
- Stop for 12 minute soak.

The alternator package was recalibrated after this series. These results are also shown in Tables 13 and 14. Some loss in performance was noted between pre- and post-test calibrations, particularly at low load.

The nozzle was removed from the alternator package after the above test. series. The vanes are pictured in Figures 80 through 87. Two overall views of the nozzle are shown in Figure 88A and B. Four of the nozzle vanes (vane #7, #9, #11 and #15) sustained cracks at the trailing edge. A fifth vane (vane #5) was broken at mid-section and a piece was missing. (Vane #1 through #5 were Norton vanes and vane #5 was run in the rig test sequence. Vanes #6 through #15 were Ceradyne vanes [Ceralloy 147]).

All of the ceramic vane sections were found to be wedged tightly between the shrouds. A post test inspection showed that the forward (outer) shroud lip (0.040 to 0.050 dimension) and rivet bolt hole section were deformed inward. This leads to the conclusion that the ceramic vane sections failed due to compressive loads at the trailing edges.

Shroud deformation was shown to be probable by analysis because of thermal stresses and lowered yield strength of the shroud material (713LC) at higher turbine inlet temperatures ∿871°C (1600°F).

Also, forces generated by nozzle mounting bolts are counteracted at the lip which was deformed during test. It is believed that the shroud lip deformation that occurrd resulted primarily from this assembly arrangement which applies bending loads to this shroud section. The deformation could also have resulted partially from residual stresses induced during final machining of this lip and susequent bending back to its original position.

3.3.5 Ceramic Vane Nozzle Design Modifications

Following vane failures in the engine test of the ceramic vane nozzle, it was decided that design modification would be made and a second nozzle would be fabricated and engine tested.

Since the first failures were attributed to deformation of the forward shroud inner diameter lip, design modifications were aimed at preventing this. This approach proved successful in the subsequent engine test (Test #2).

The design modifications (illustrated in Fig. 89) were:

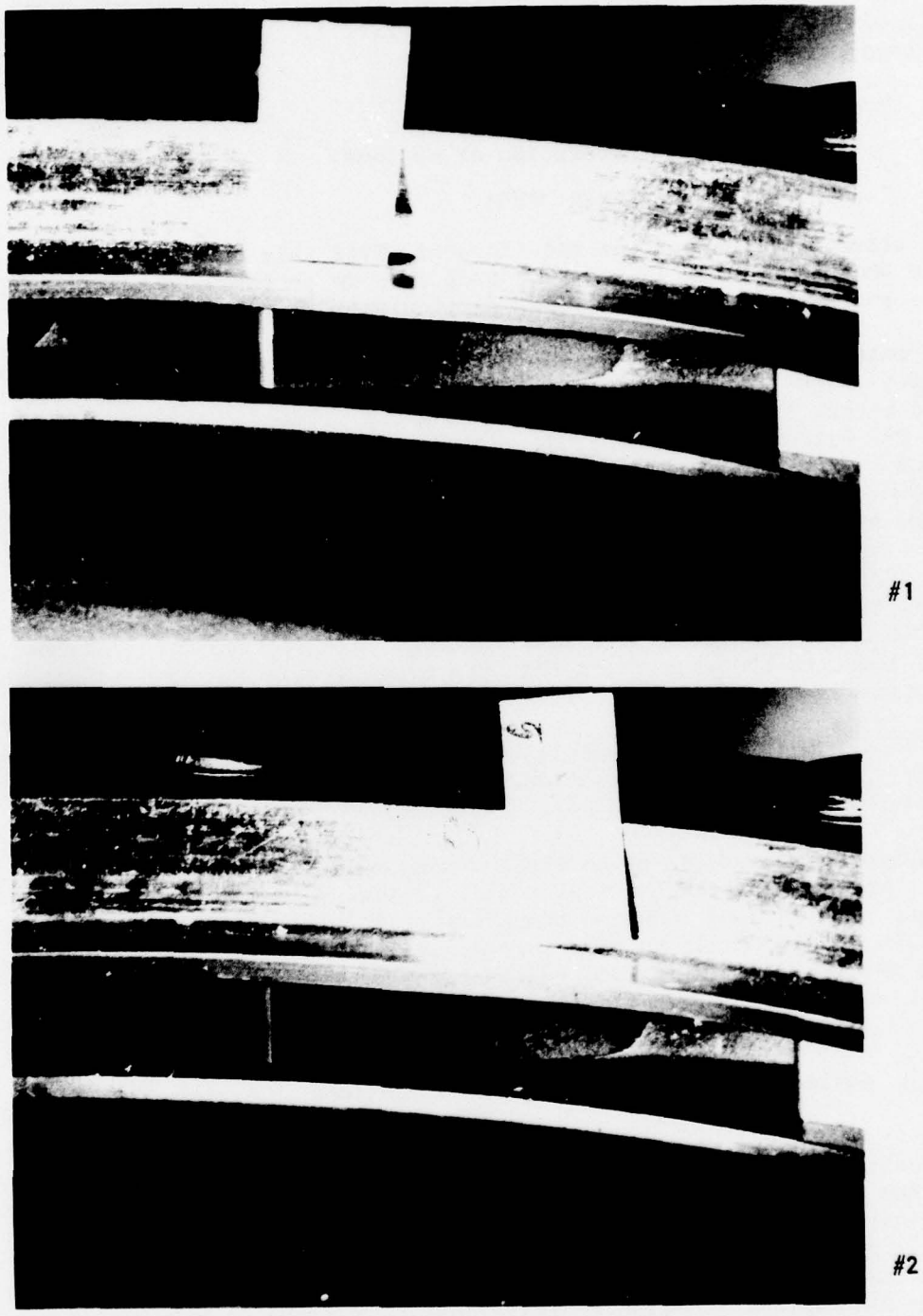

Figure 80. 10 kW Nozzle Ceramic Vane Sections #1 and #2 After Engine Test #1 25 Hour Run Plus 50 Start/Stop Cycles

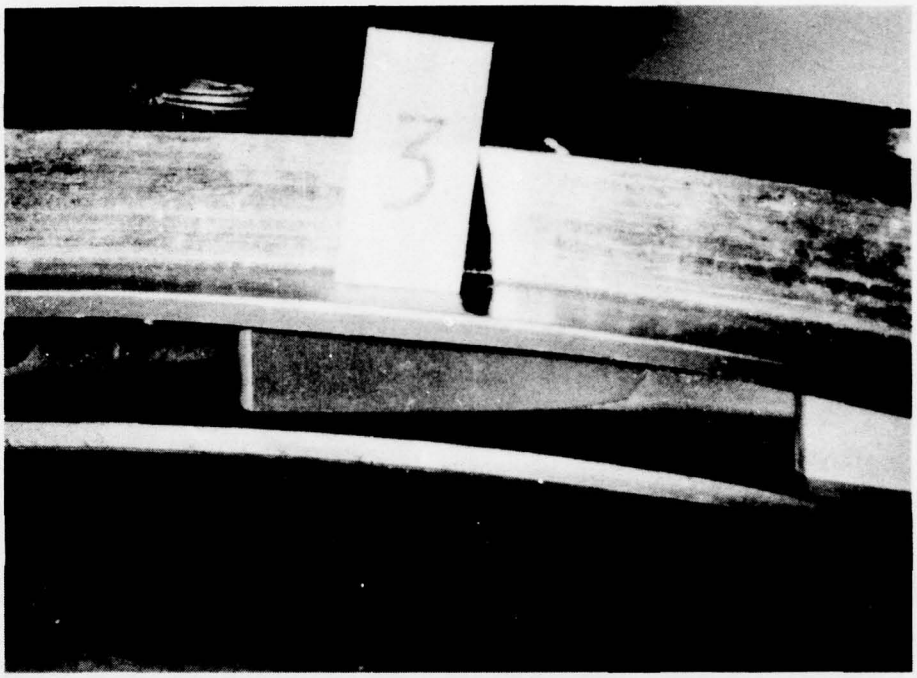

#3

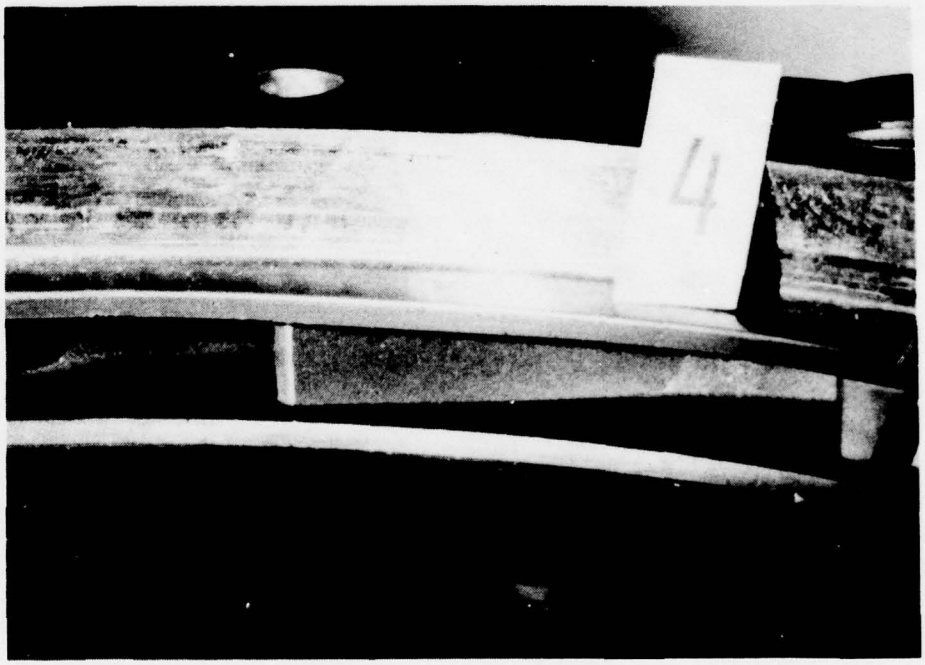

#4

Figure 81. 10 kW Nozzle Ceramic Vane Sections #3 and #4 After Engine Test #1 25 Hour Run Plus 50 Start/Stop Cycles

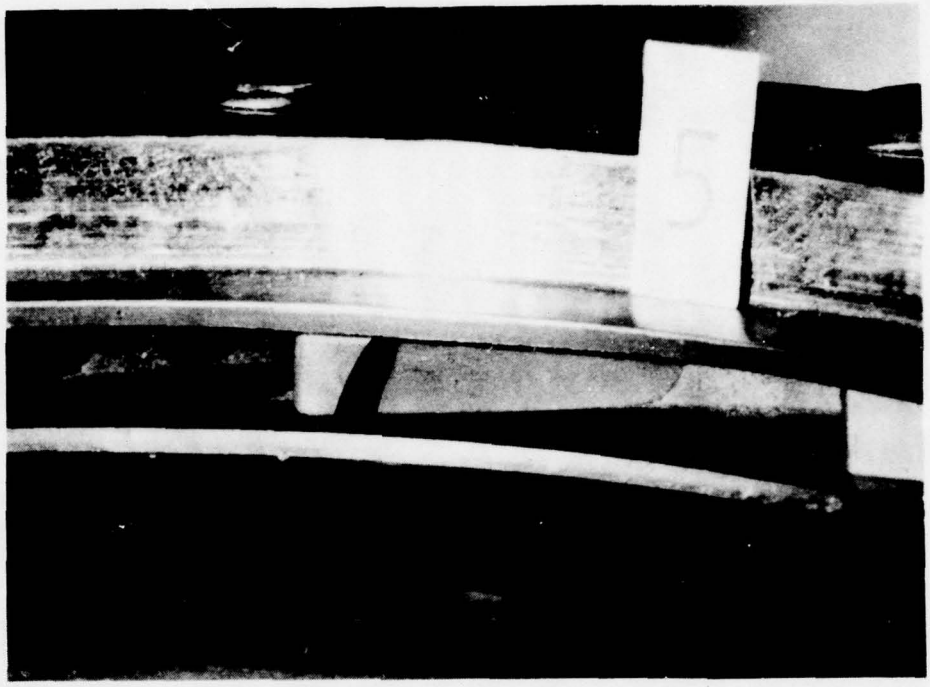

#5

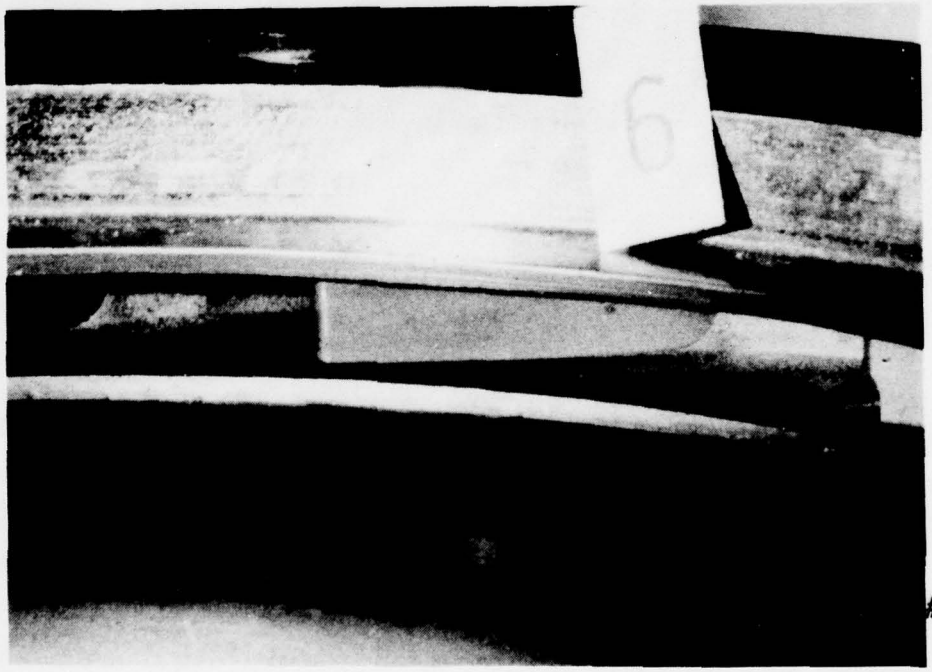

#6

Figure 82. 10 kW Nozzle Ceramic Vane Sections #5 and #6 After Engine Test #1 25 Hour Run Plus 50 Start/Stop Cycles

#7

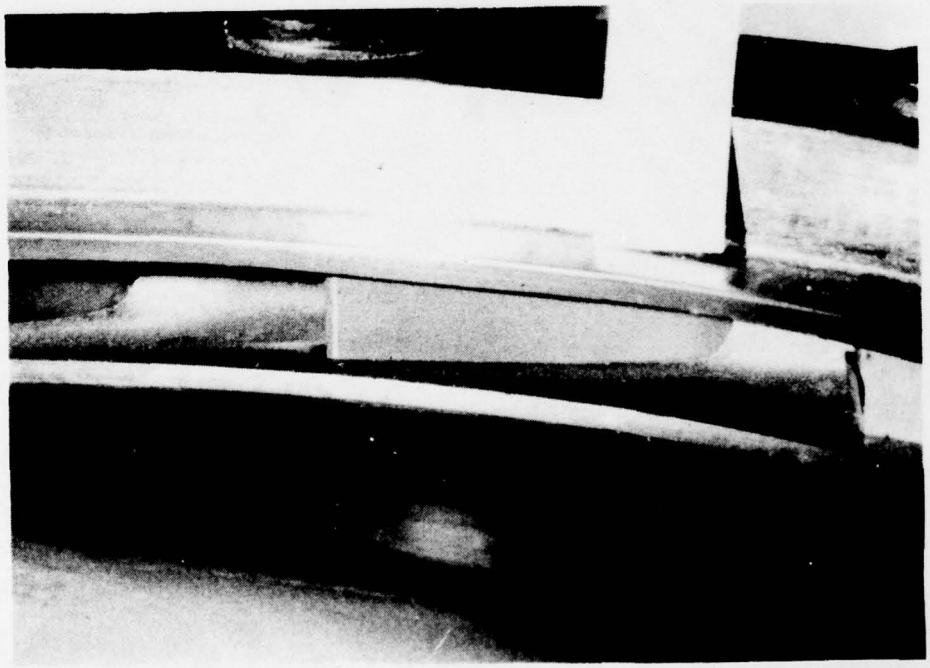

#8

Figure 83. 10 kW Nozzle Ceramic Vane Sections #7 and #8 After Engine Test #1 25 Hour Run Plus 50 Start/Stop Cycles

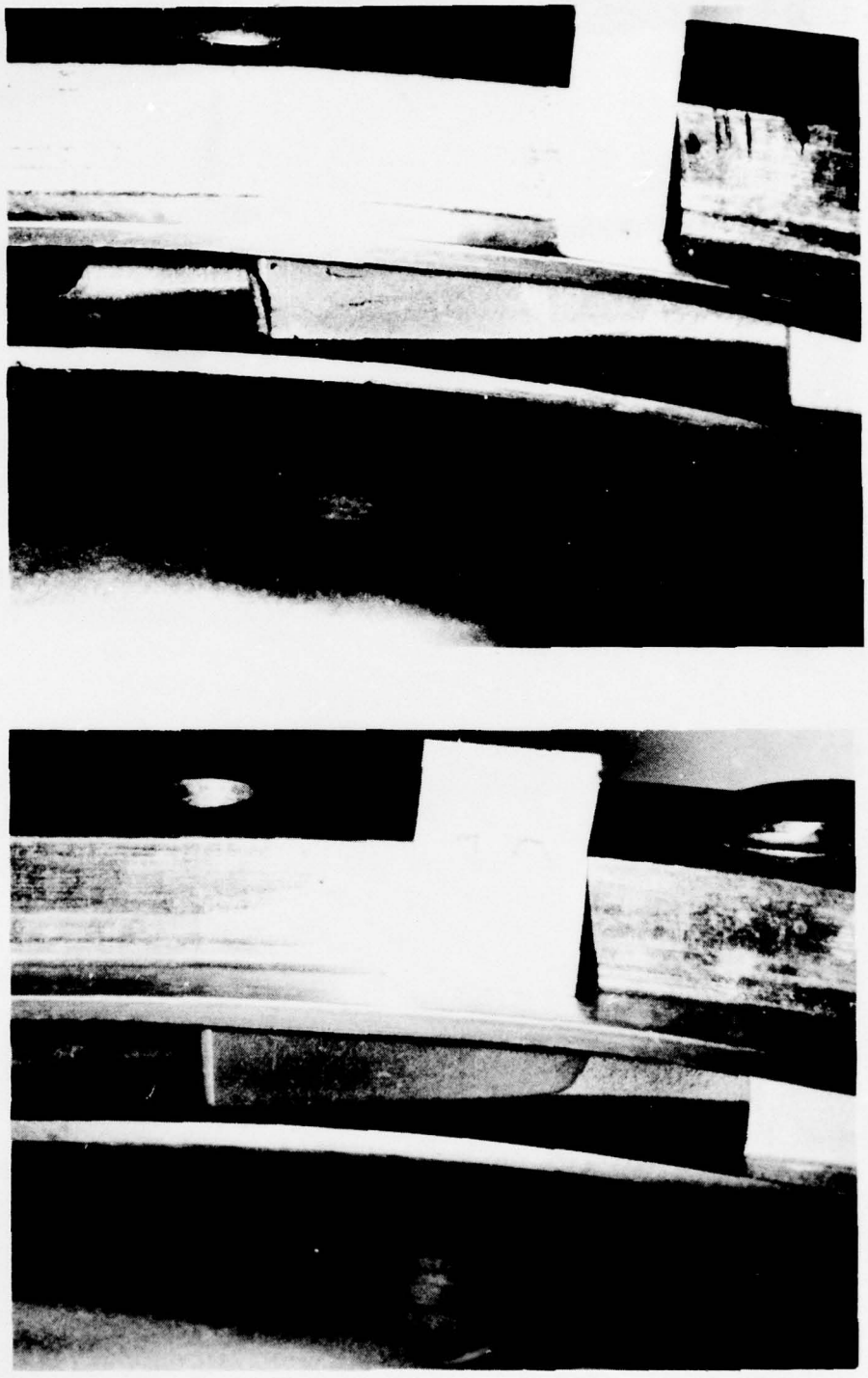

Figure 84. 10 kW Nozzle Ceramic Vane Sections #9 and #10 After Engine Test #1 25 Hour Run Plus 50 Start/Stop Cycles

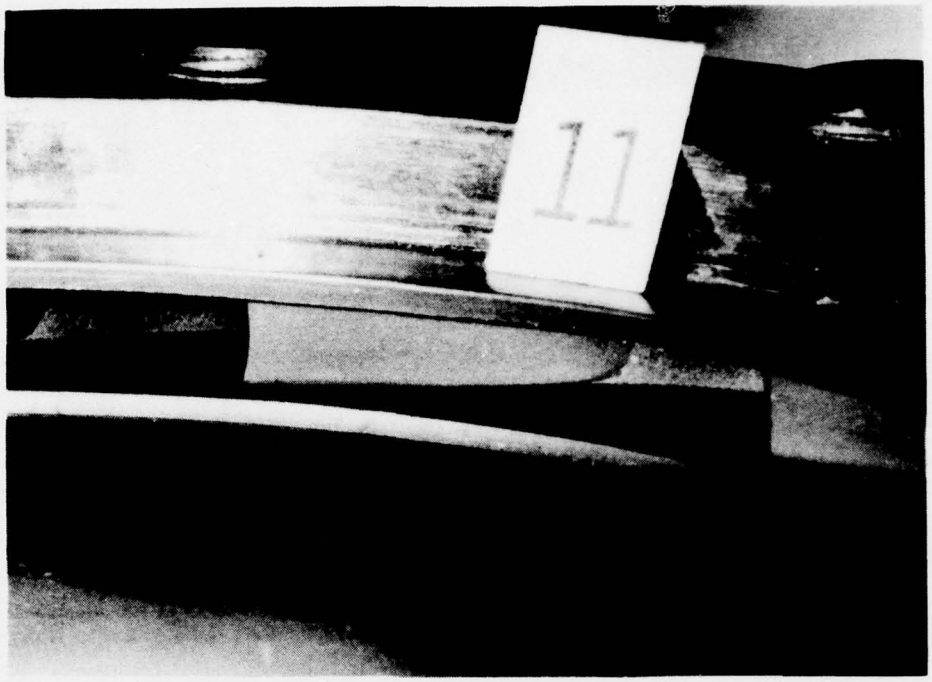

#11

#12

Figure 85. 10 kW Nozzle Ceramic Vane Sections #11 and #12 After Engine Test #1 25 Hour Run Plus 50 Start/Stop Cycles

#13

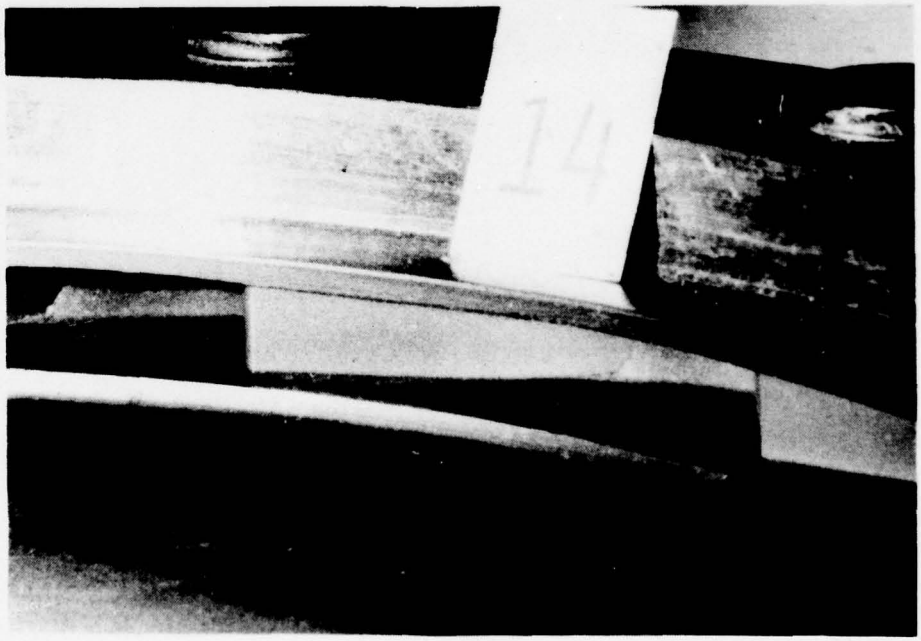

#14

Figure 86. 10 kW Nozzle Ceramic Vane Sections #13 and #14 After Engine Test #1 25 Hour Run Plus 50 Start/Stop Cycles

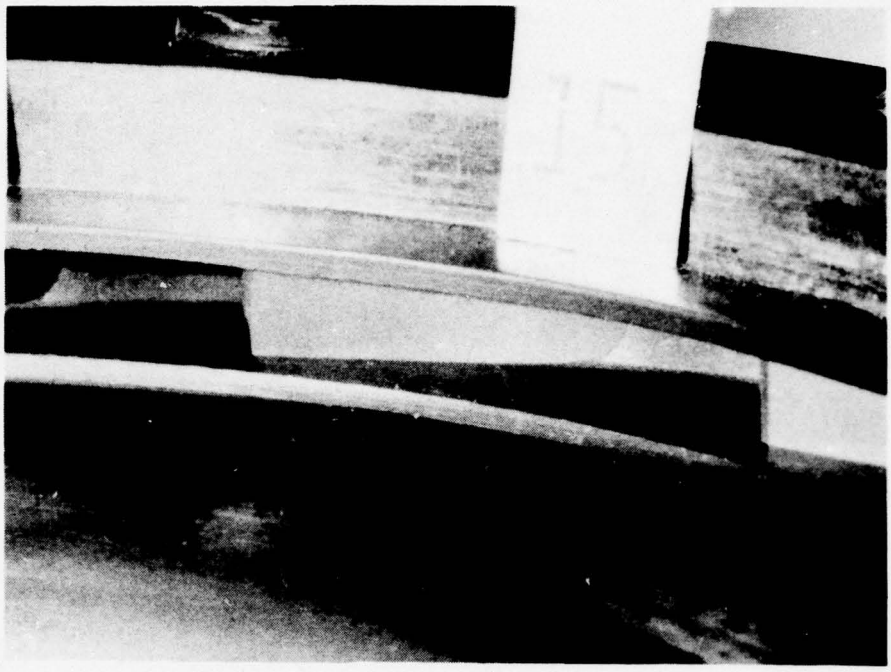

Figure 87. 10 kW Nozzle Ceramic Vane Sections #15 and #16 After Engine Test #1 - 25 Hour Run Plus 50 Start/Stop Cycles

1. Counteract nozzle mounting bolt forces at the bolt circle diameter (see Figs. 90 and 91).

2. Hold seal plate against diffusor housing independently of nozzle (see Figs. 92 and 93).

3. Relieve forward shroud lip to avoid thermal distortion in direction of ceramic vane.

4. Apply relaxing glass adhesive (30% B402, 30% GN19, 40% Cr_2O_3) to vane/shroud interface.

3.3.6 Engine Re-Test of Ceramic Vane Nozzle

An engine re-test was completed after the above design modifications were made. The test used the same engine operating cycle as the first test described above in Section 3.3.5 which consisted of 25 hours at various steady state operating conditions and 50 start/stop cycles. This engine run was successful and verified that initial problems with vane fractures were associated with the surrounding metallic assembly instead of the ceramic vanes themselves.

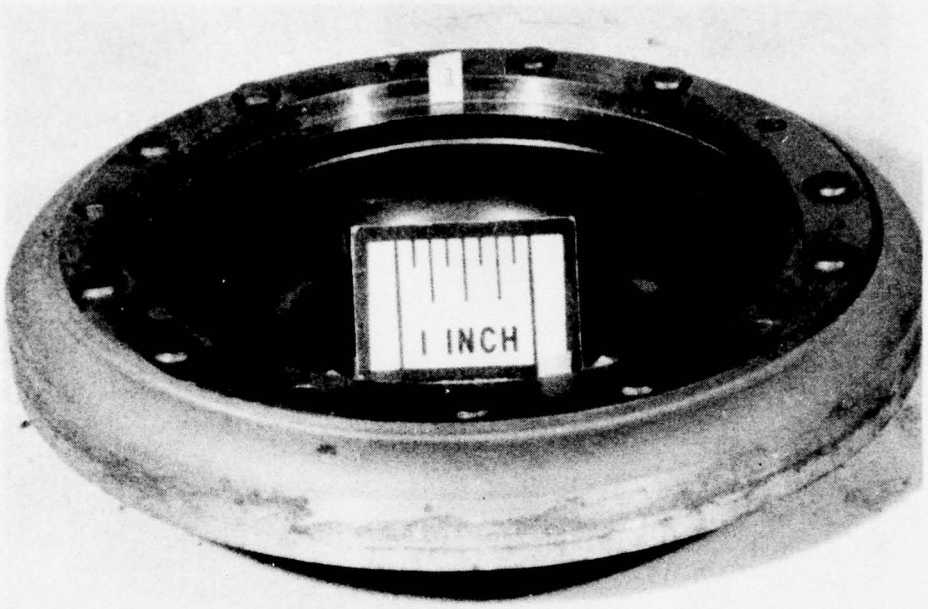

A.

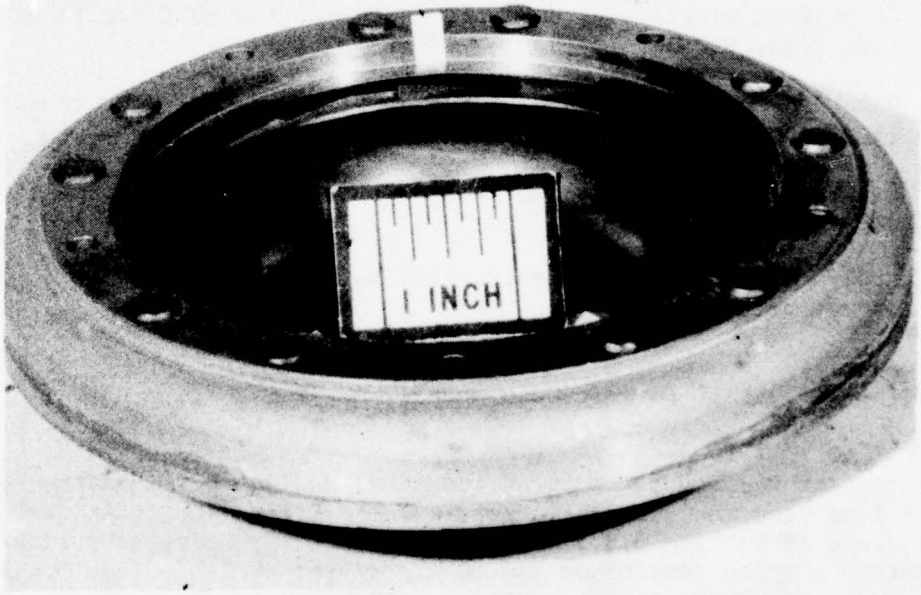

B.

Figure 88. 10 kW Nozzle With Hot Pressed Si_3N_4 Vane Sections After Engine Test #1 - 25 Hour Run Plus 50 Start/Stop Cycles

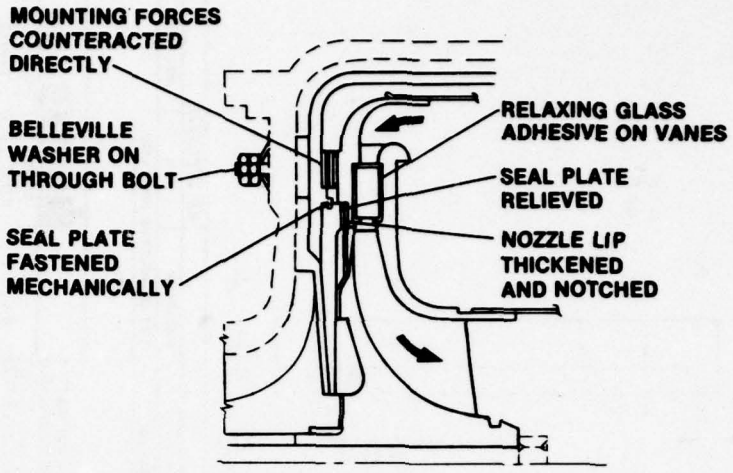

Figure 89. Design Changes to Ceramic Vane Nozzle Prior to Engine Test #2

The following gives engine assembly details, details of the test and engine performance calibration results at the start and the end of engine run #2. Documentation photographs of the nozzle and vane are also given.

Assembly Details

The assembly tolerances of the turbine nozzle were:

Nozzle shim thickness	0.116 inch
Turbine face clearance	0.0125 inch
Turbine tip to seal clearance	0.007 to 0.015 inch
Radial clearance	0.017 inch
Exit gap	0.013 inch
Maximum runout of turbine wheel	0.0003 inch TIR

(see Fig. 79 for definition of clearance locations.)

Figure 94 (A and B) shows the method of attaching nozzle through bolts with Belleville washers and a locking nut arrangement. Eight Belleville washers are used at each bolt and are stacked in two groups of four facing outward from the center. (The washers were obtained from Associated Spring (Gardena, CA) and are identified by part #BO-375-020S. The washers are stainless steel 0.020 inch thick with 0.375 inch OD and 0.190 inch ID. The free travel is 0.011 inch and yields 60 pounds load at the flat condition.)

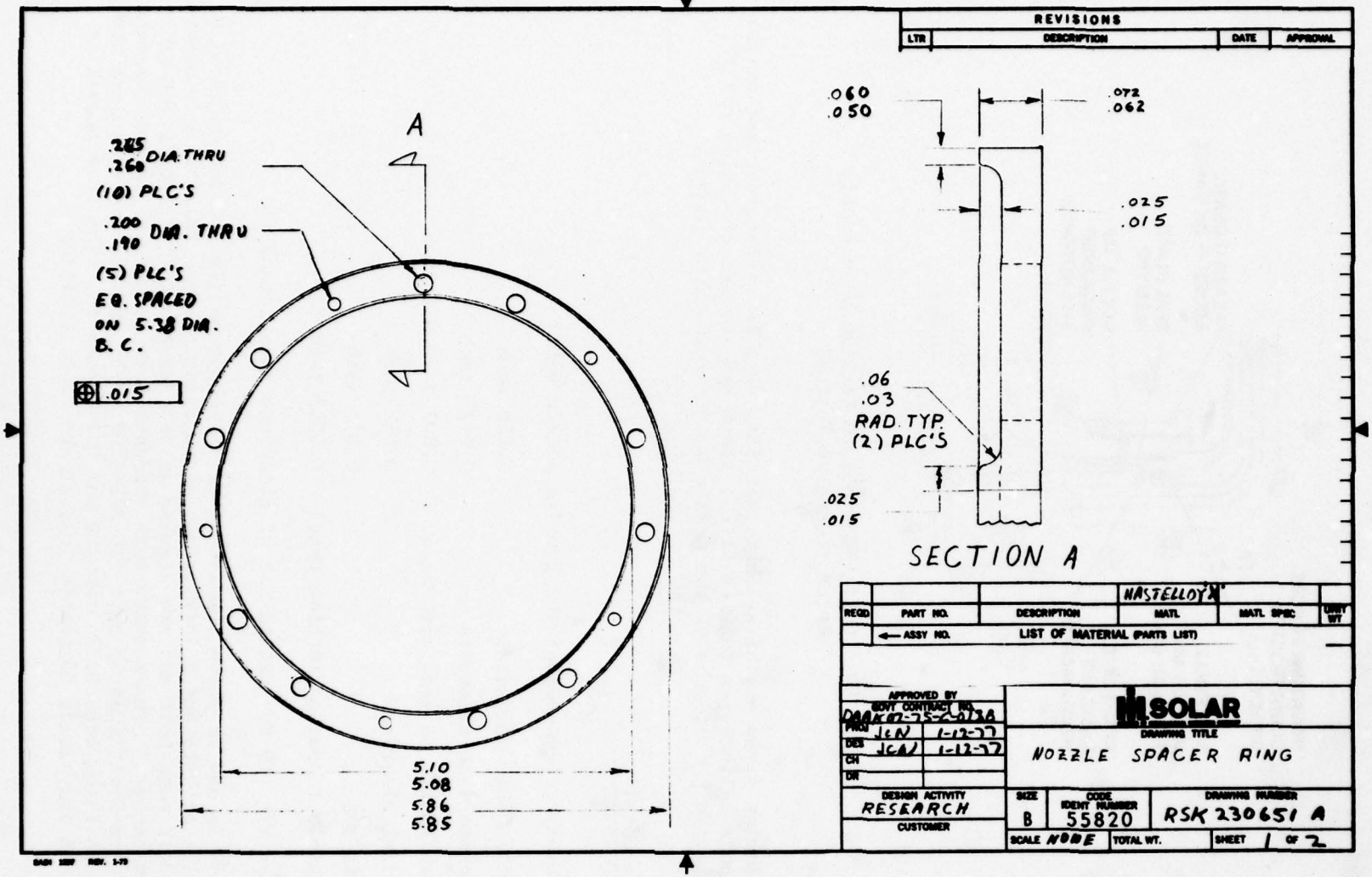

Figure 90. Nozzle Spacer Ring

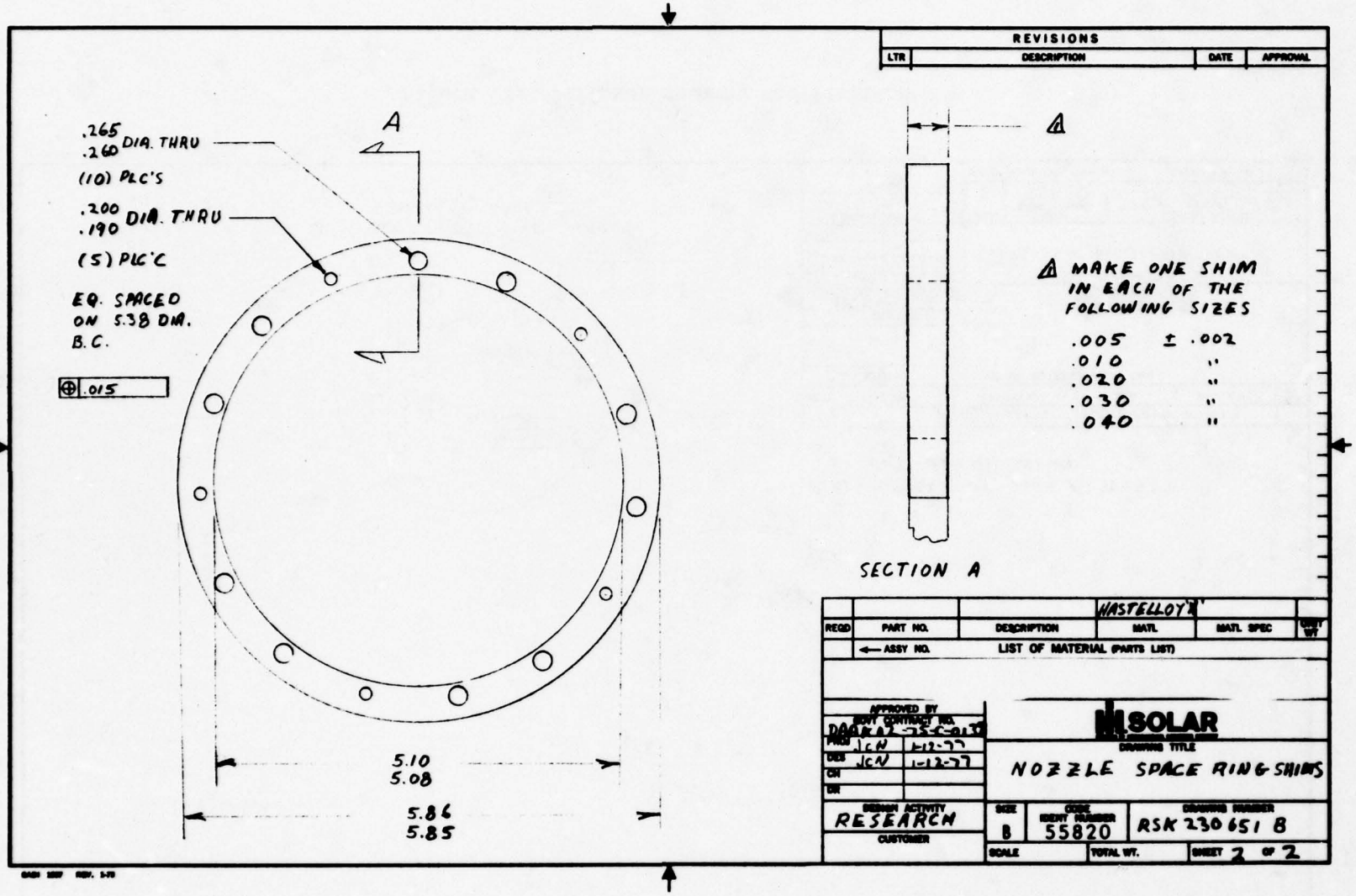

Figure 91. Nozzle Spacer Ring Shims

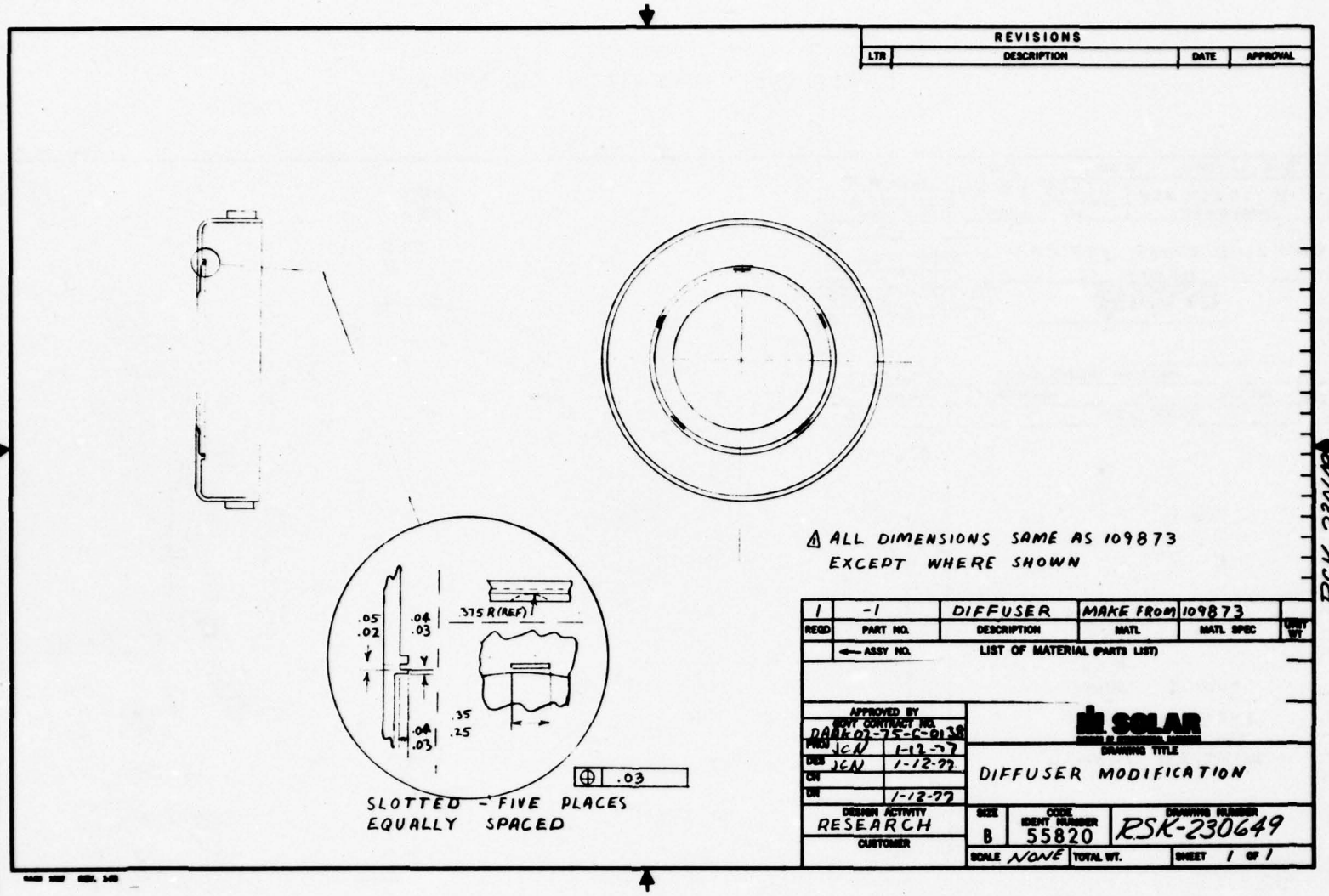

Figure 92. Diffuser Housing Modification

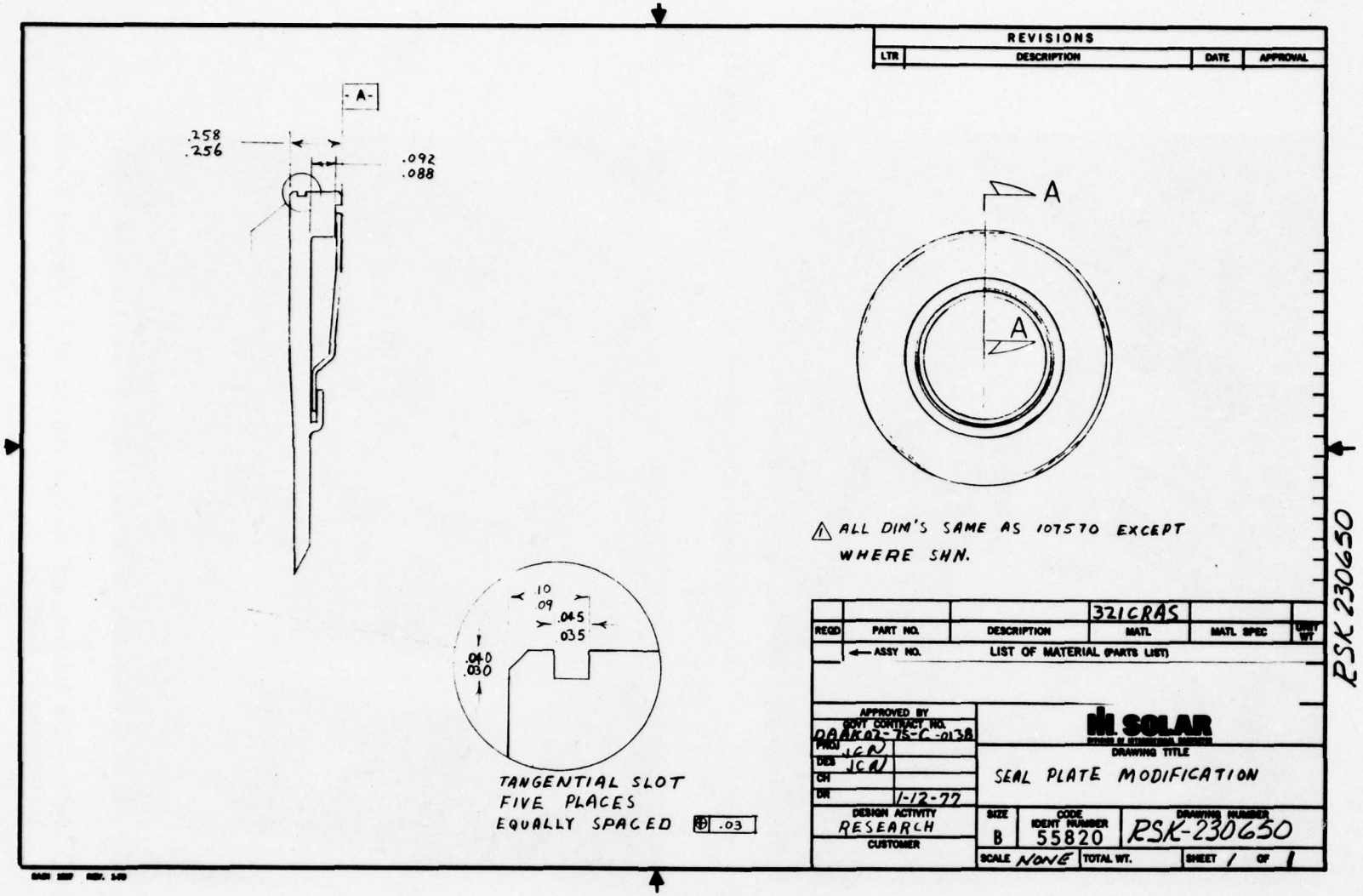

Figure 93. Seal Plate Modification

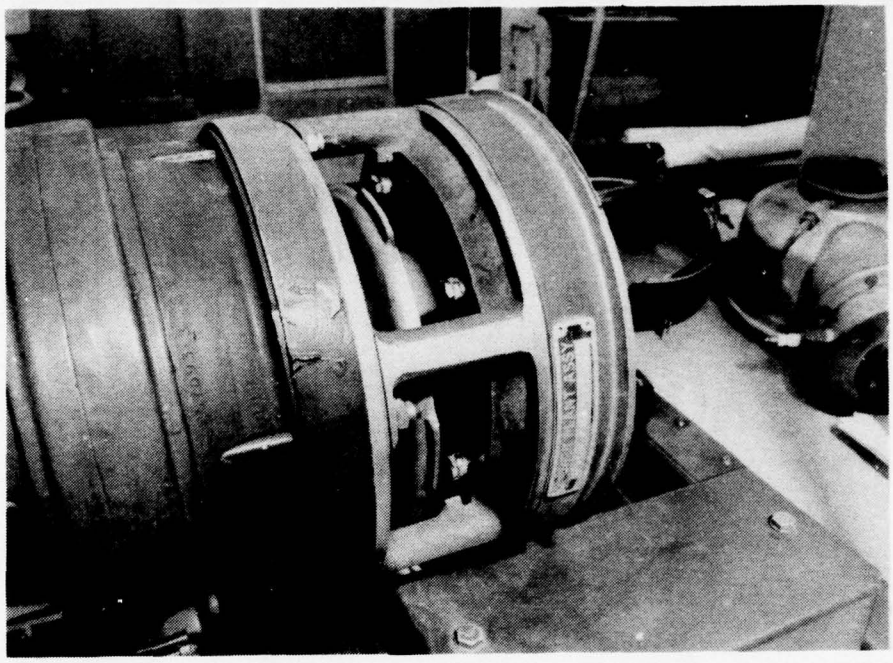

Figure 94a. Belleville Washer and Locknut Method of Fastening Nozzle D-Bolts to Compressor Housing

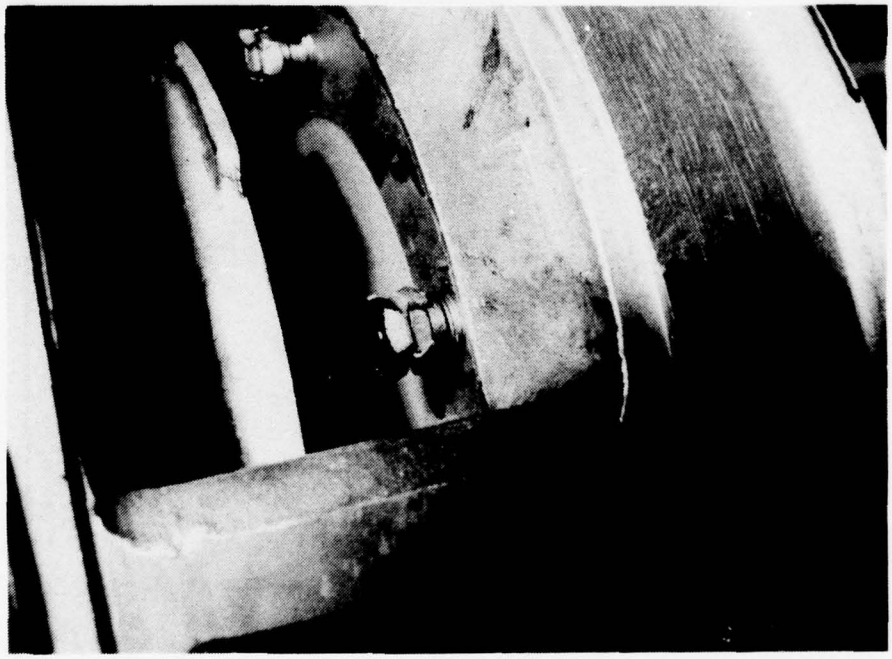

Figure 94b. Belleville Washer and Locknut Method of Fastening Nozzle D-Bolts to Compressor Housing

The eight washer stack as described above was tightened until the initial interior gap of 0.022 inch was reduced to 0.011 inch to yield a net load per bolt of 120 pounds with travel limits of 0.011 inch in either tension or compression. This bolt fixing method was essential in providing adequate thermal flexibility of the redesigned nozzle assembly.

The nozzle was assembled with the following components:

• Forward nozzle shroud	DSK 14956 (Fig. 76)
• Rear nozzle shroud	DSK 14957 (Fig. 77)
• Hot pressed silicon nitride vane sections - fifteen (15)	DSK 14958 (Fig. 21)
• Rivets - ten (10)	DSK 14959 (Fig. 24)
• Modification to ceramic vane nozzle assembly	RSK 230652 A & B (Figs. 95 & 96)
• Nozzle spacer ring	RSK 230651 A & B (Figs. 90 & 91)
• Diffuser housing modification	RSK 230649 (Fig. 92)
• Seal plate modification	RSK 230650 (Fig. 93)

All other engine components were unmodified.

The forward and rear shrouds were assembled and riveted with a relaxing glass adhesive (30% GN19, 30% B402 and 40% pigment grade Cr_2O_3) in all vanes containing recesses and AMI 400 braze alloy in the rear shroud counterbore (five places). Riveting was done in a press with maximum 12,000 pound static load. The assembly was then vacuum furnace brazed at 2125°F for five minutes. Final machining of the nozzle was completed. Assembly of the nozzle into the engine followed standard procedure except that shims (nozzle space rings per RSK 230651 A & B) were used to correctly locate nozzle axial position.

Engine Test

Table 14 shows the as-measured and corrected performance data for the 10 kW engine SN5 in test #2 with the redesigned ceramic vane nozzle installed. These results show that there was no signficiant change in engine performance after completion of the engine test which consisted of:

Load (%)	Time at Load (hours)
75	6
0	1
50	6
25	6
75	6
and 50 start/stop cycles	

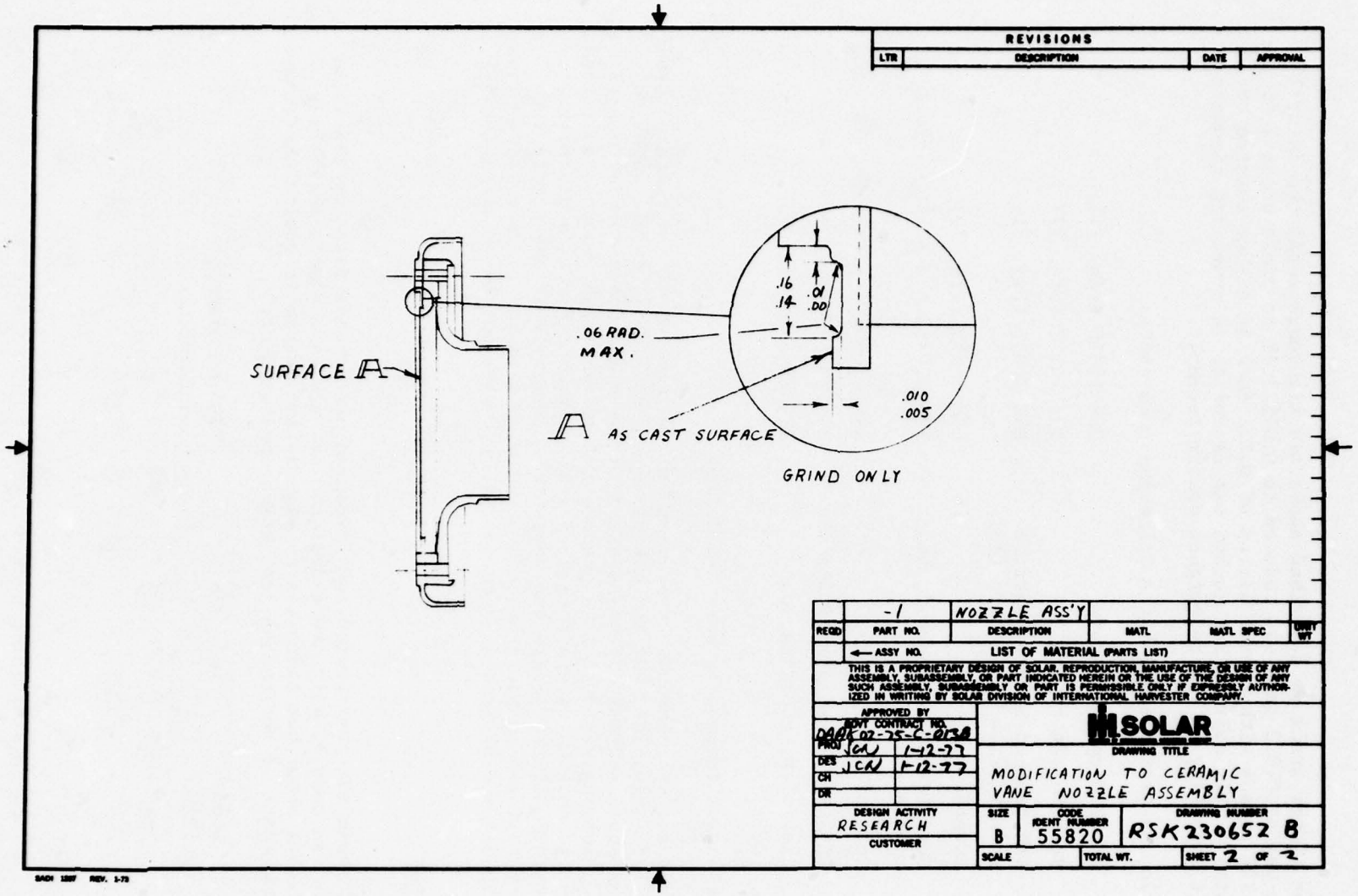

Figure 95. Modification to Ceramic Vane Nozzle Assembly

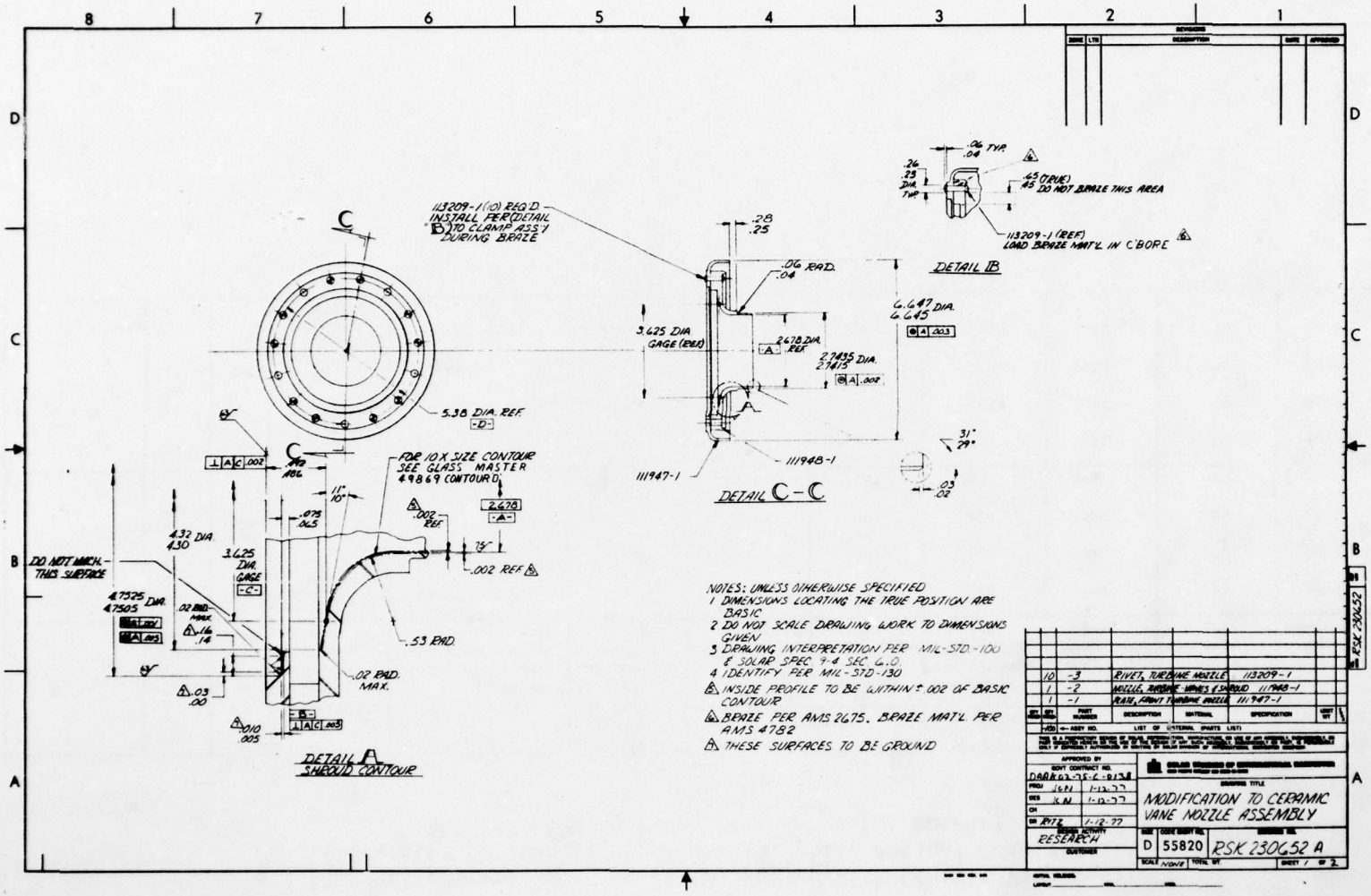

Figure 96. Modification to Ceramic Vane Nozzle Assembly

Table 14

Test #2 - Calibration Data for Gemini Engine With Ceramic Vane Nozzle
(Corrected to Standard 59°F and 14.7 psia Ambient Conditions)
(Linear Loading - No Cycle Convertor Losses)

	Data Point No.	Load	Cummulative Engine Running Time (hours)	Corrected Fuel Flow (pph)	Shaft Power Output (kW)	Shaft Specific Fuel Consumption lb JP-4 kW-hr	Corrected		Measured Gas Exhaust Temperature (°F)	Turbine Inlet Temp. Calc. From EGT (°F)	Actual Compressor Inlet Temperature (°F)	Actual Fuel Flow
							Exhaust Gas Temperature (°F)	Turbine Inlet Temperature (°F)				
Pre-Test	7	0%	1	16.9	0	--	750	1054	750	1054	65	17.3
	6	25%	1	19.5	3.13	6.24	802	1168	740	1168	70	20.1
	5	50%	1	21.0	5.95	3.52	896	1280	920	1280	65	21.2
	4	75%	1	23.7	9.05	2.62	1021	1447	1050	1447	65	23.9
After 25 hour run and 50 start/stop cycles	123	0%	51	17.4	0	--	730	1091	780	1091	75	18.3
	122	25%	51	19.6	3.17	6.18	834	1231	885	1231	75	20.3
	121	50%	51	22.2	5.95	3.73	940	1368	990	1368	75	22.8
	120	75%	51	24.1	9.05	2.66	1076	1544	1125	1544	75	24.6

Figure 97 (A through N) shows the nozzle with hot pressed silicon nitride vanes after the above engine test cycle. No flaws, defects or deterioration were noted in any vanes in a post test inspection.

It is concluded from the completion of this engine demonstration that ceramics have the potential of being applied to the 10 kW gas turbine for reduction in nozzle erosion. Before this concept is practical for consideration as a production item additional work in the area of cost reduction, which is now being supported by MERADCOM (Ref. 25), must be completed. This work will investigate alternative silicon based ceramic materials and associated fabrication methods for cost reduction. Additional engine test evaluation work is also scheduled for proposed latter stages of the referenced project.

3.4 DEVELOPMENT OF 10 kW ALL-CERAMIC NOZZLE - PHASE III

This program phase included all of the steps necessary to develop an all-ceramic nozzle section to the point that it was ready for engine test evaluation. The steps were design, design analysis, procurement, assembly mock-up, assembly analysis design update, static rig tests and engine simulator rig tests.

3.4.1 Design

Three alternative all-ceramic nozzle design concepts suitable for engine installation were defined in this task, each to be evaluated in rig experiments at the latter portion of this phase. Based upon these results a single design was selected for engine test in Phase IV.

Critical problem areas identified in nozzle design were:

1. Static seals at ceramic/metal alloy interfaces (nozzle/combustor, nozzle/seal plate and nozzle/exhaust scroll junctions).

2. Differential growths due to dissimilar thermal expansions and temperature differentials of the assembly.

3. Method of accurately locating and securing the rear shroud which includes turbine wheel matching contour.

Cross sections of the three design alternatives developed for study and analysis are shown in Figures 98 through 100. The three designs selected for evaluation include:

- Design Concept #1 - RBSi_3N_4 shrouds with HPSi_3N_4 vanes and 718 superalloy nozzle bolts

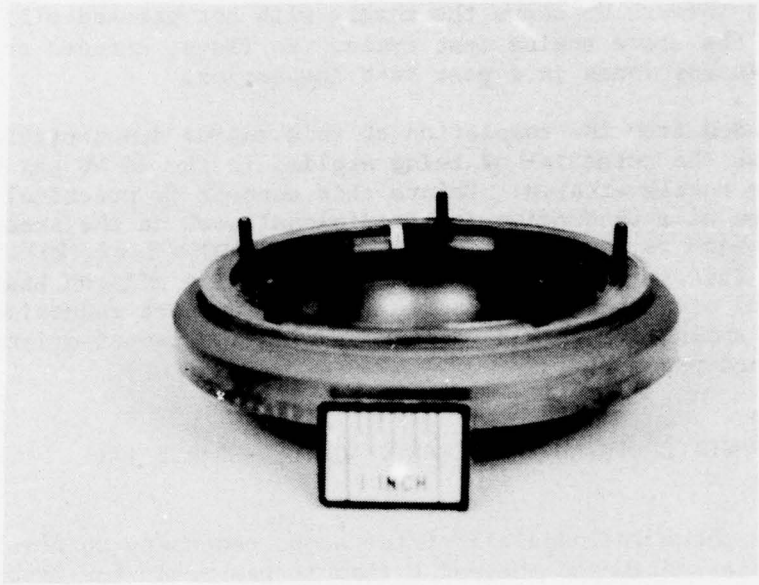

Figure 97a. Redesigned All-Ceramic Nozzle After Engine Test #2

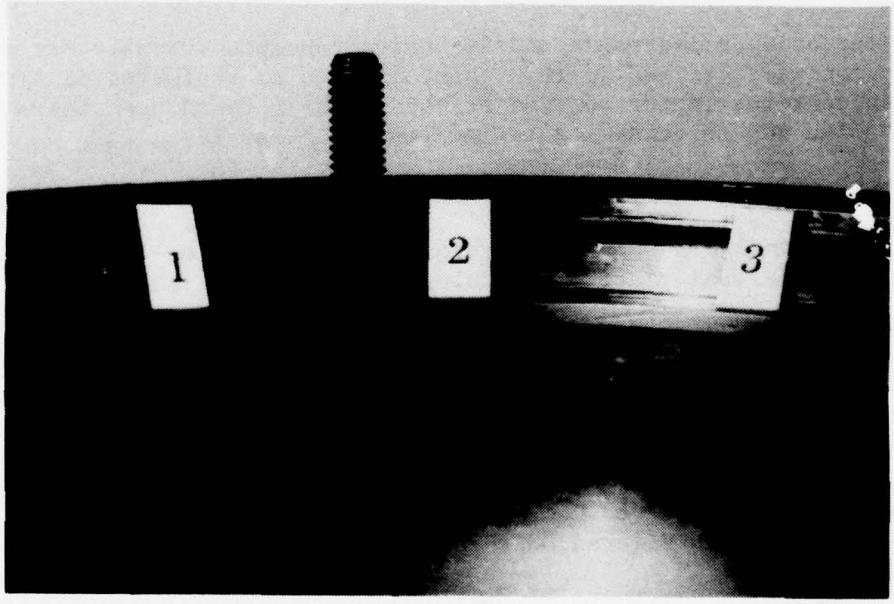

Figure 97b. Hot Pressed Silicon Nitride Vane Sections 1, 2 and 3 After Engine Test #2

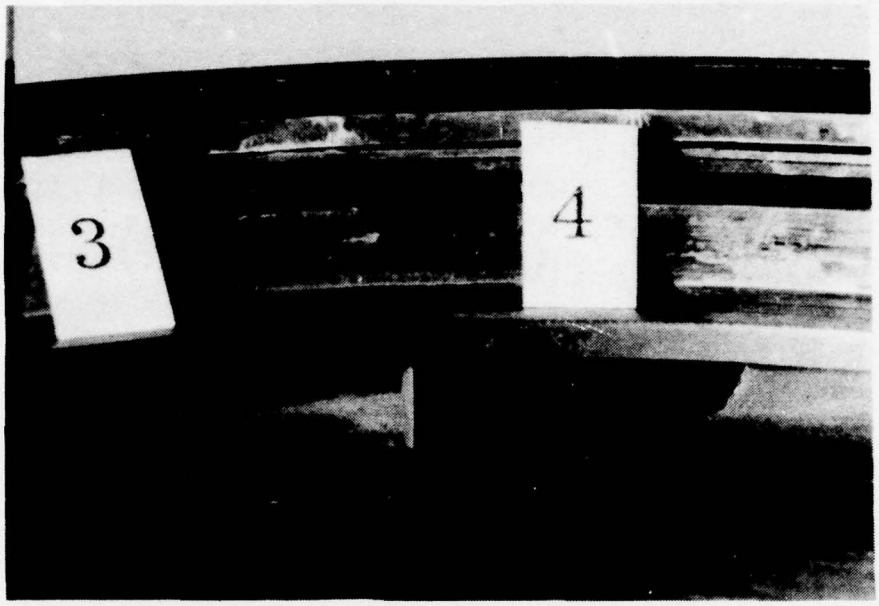

Figure 97c. Hot Pressed Silicon Nitride Vane Section 4 After Engine Test #2

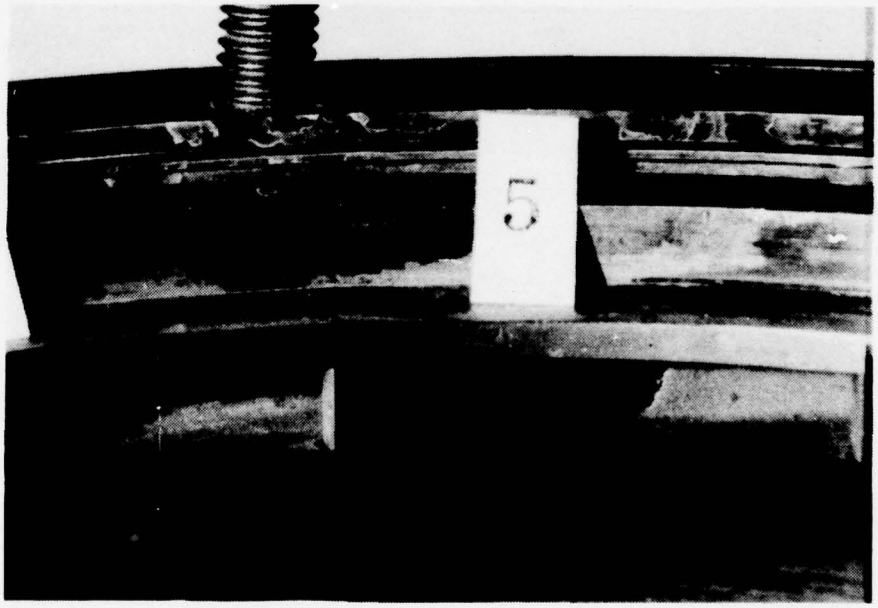

Figure 97d. Hot Pressed Silicon Nitride Vane Section 5 After Engine Test #2

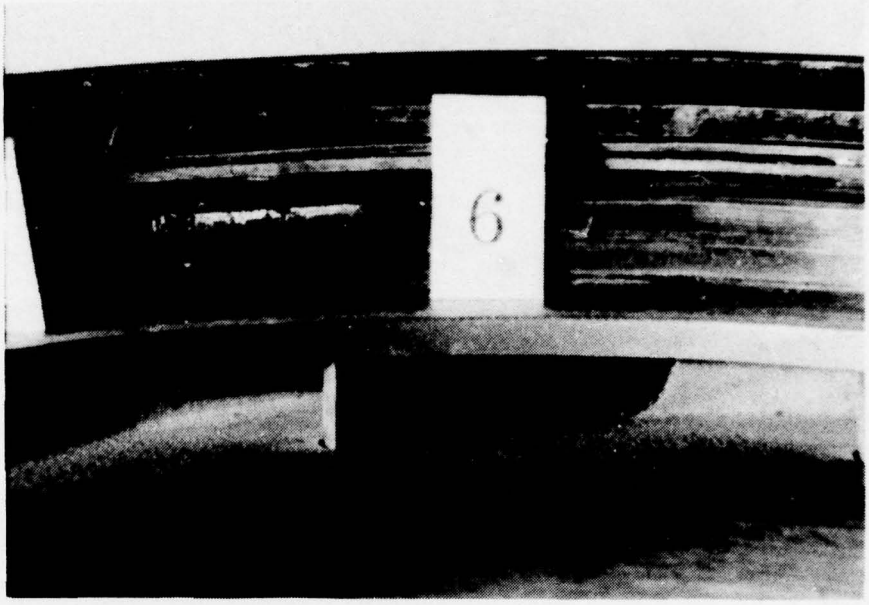

Figure 97e. Hot Pressed Silicon Nitride Vane Section 6 After Engine Test #2

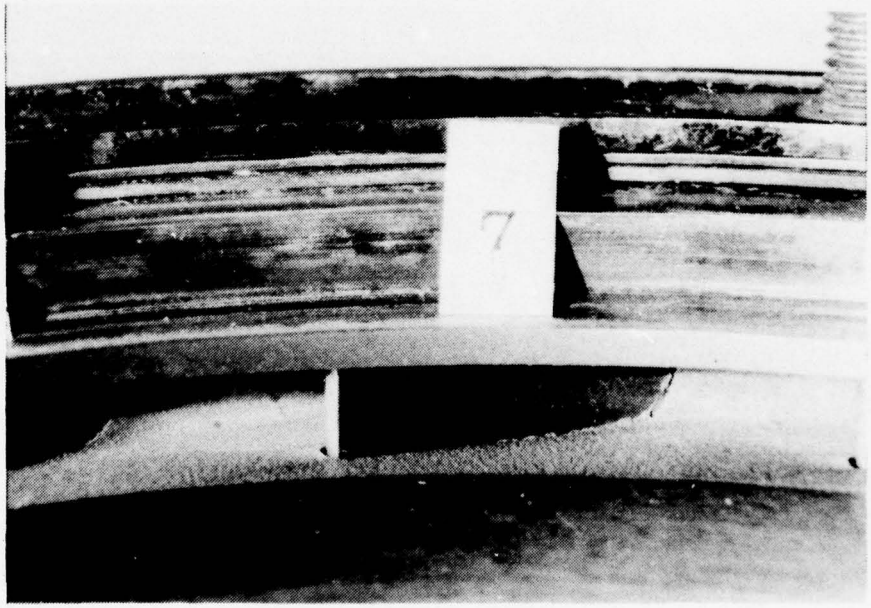

Figure 97f. Hot Pressed Silicon Nitride Vane Section 7 After Engine Test #2

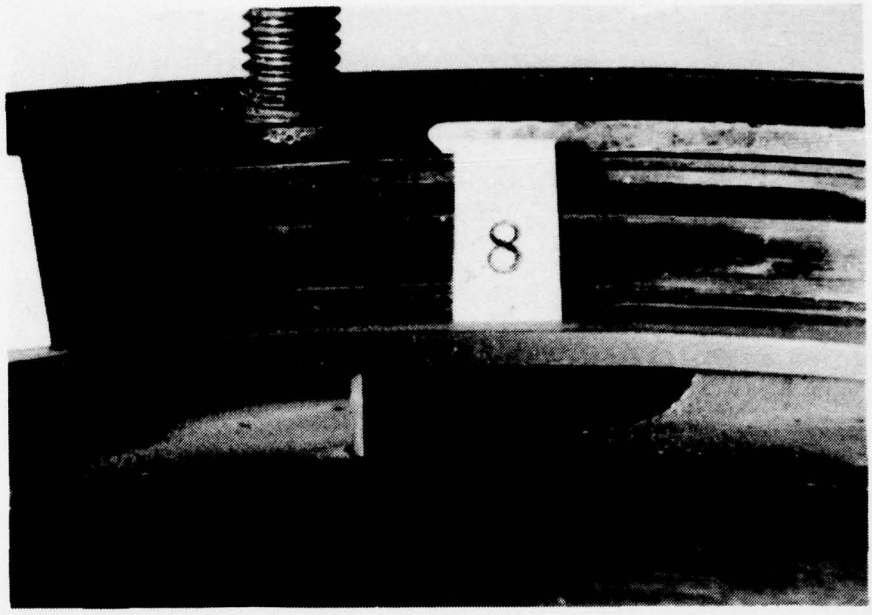

Figure 97g. Hot Pressed Silicon Nitride Vane Section 8 After Engine Test #2

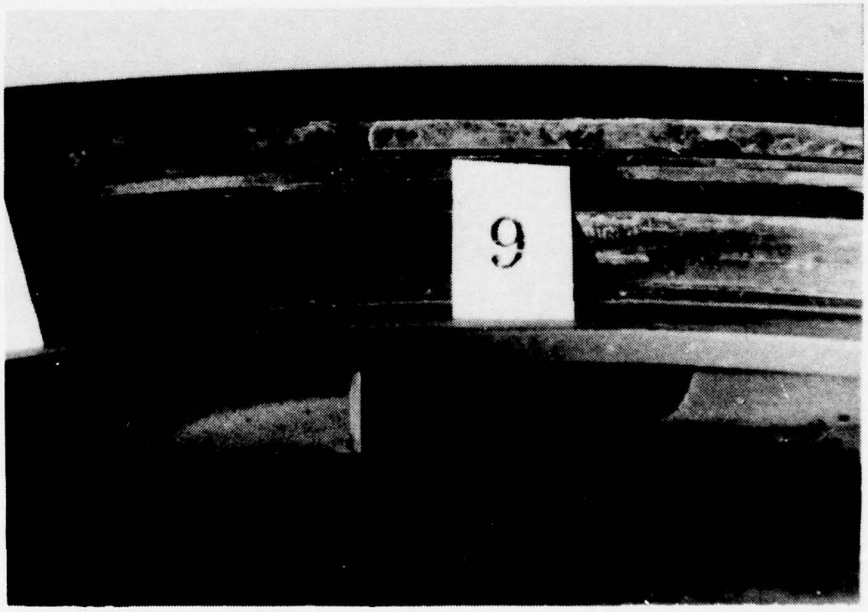

Figure 97h. Hot Pressed Silicon Nitride Vane Section 9 After Engine Test #2

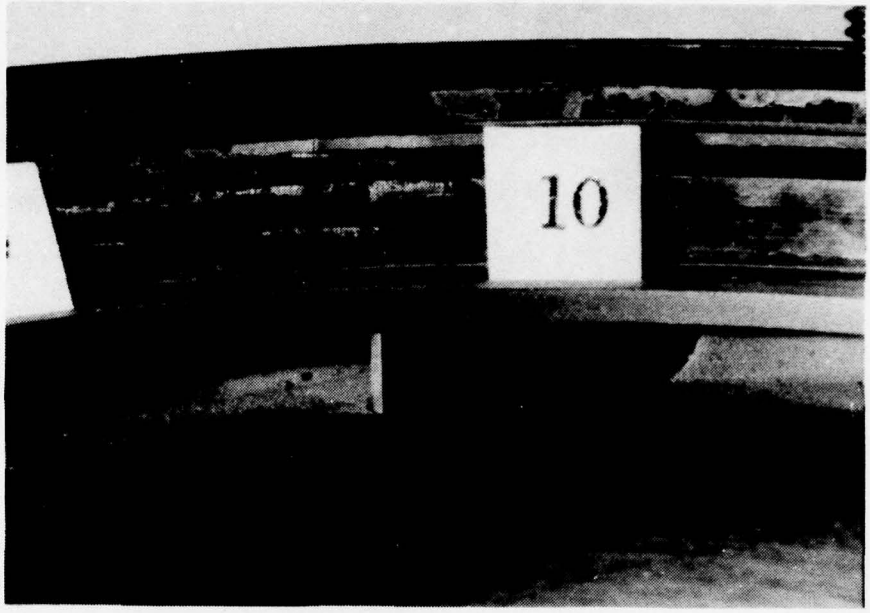

Figure 97i. Hot Pressed Silicon Nitride Vane Section 10 After Engine Test #2

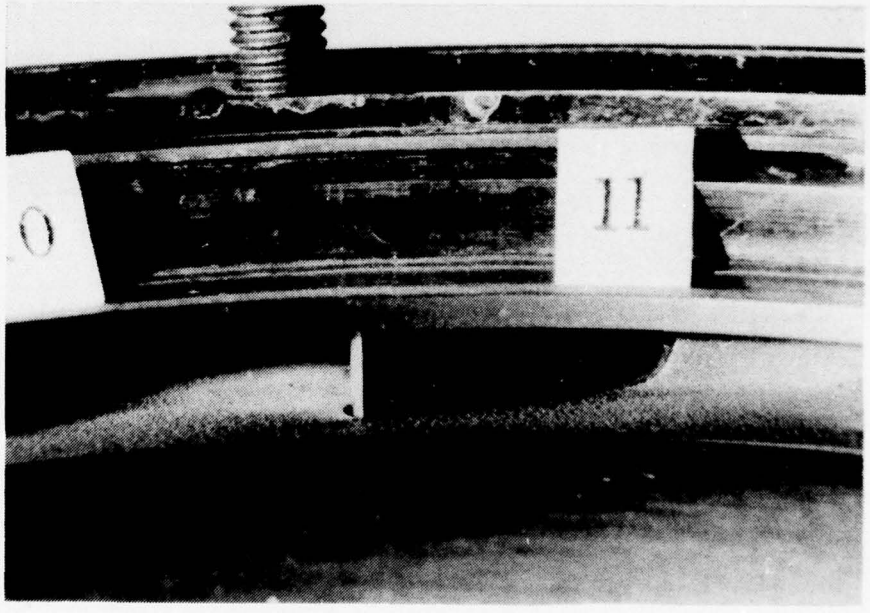

Figure 97j. Hot Pressed Silicon Nitride Vane Section 11 After Engine Test #2

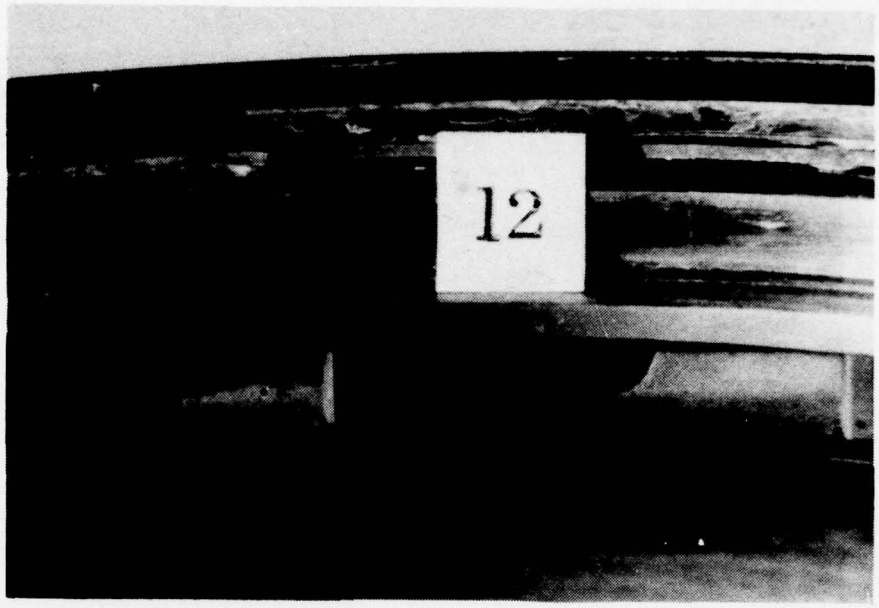

Figure 97k. Hot Pressed Silicon Nitride Vane Section 12 After Engine Test #2

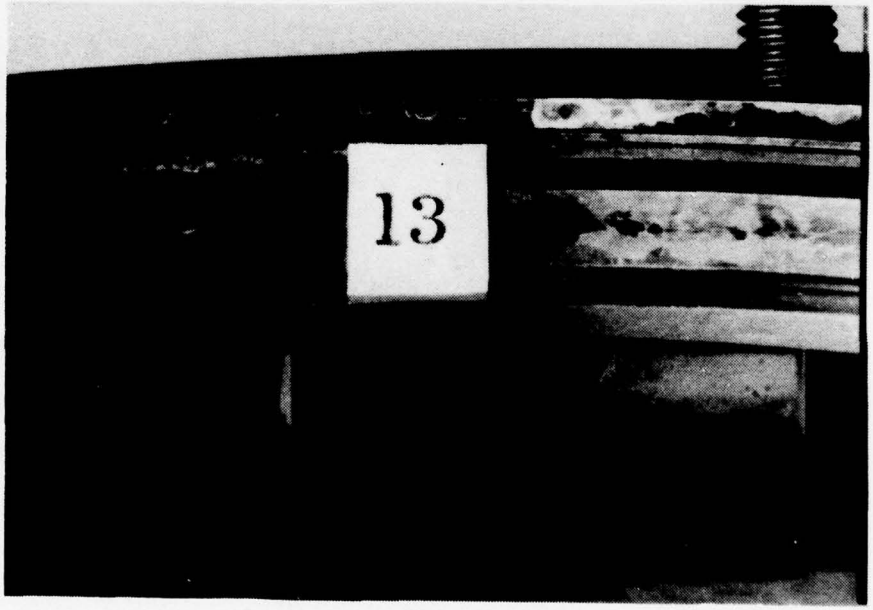

Figure 97l. Hot Pressed Silicon Nitride Vane Section 13 After Engine Test #2

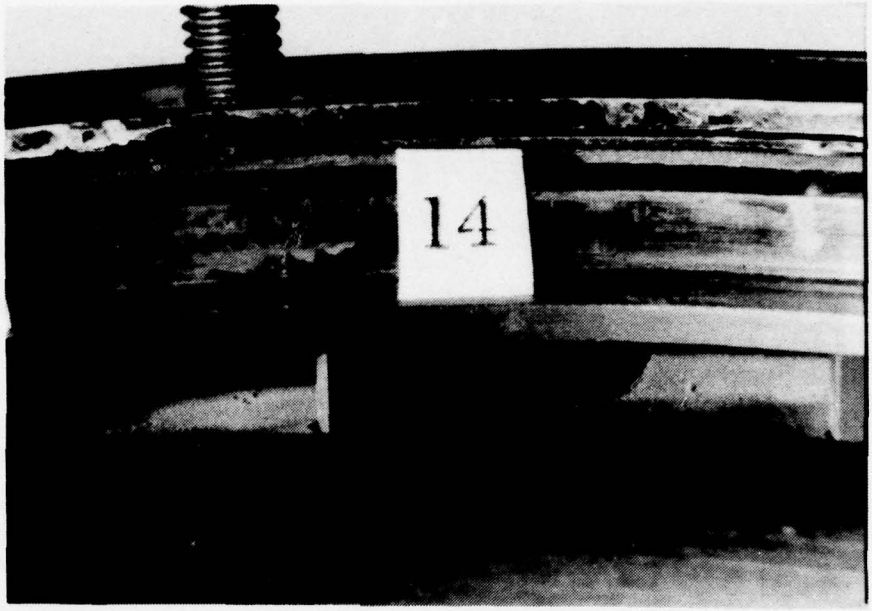

Figure 97m. Hot Pressed Silicon Nitride Vane Section 14 After Engine Test #2

Figure 97n. Hot Pressed Silicon Nitride Vane Section 15 After Engine Test #2

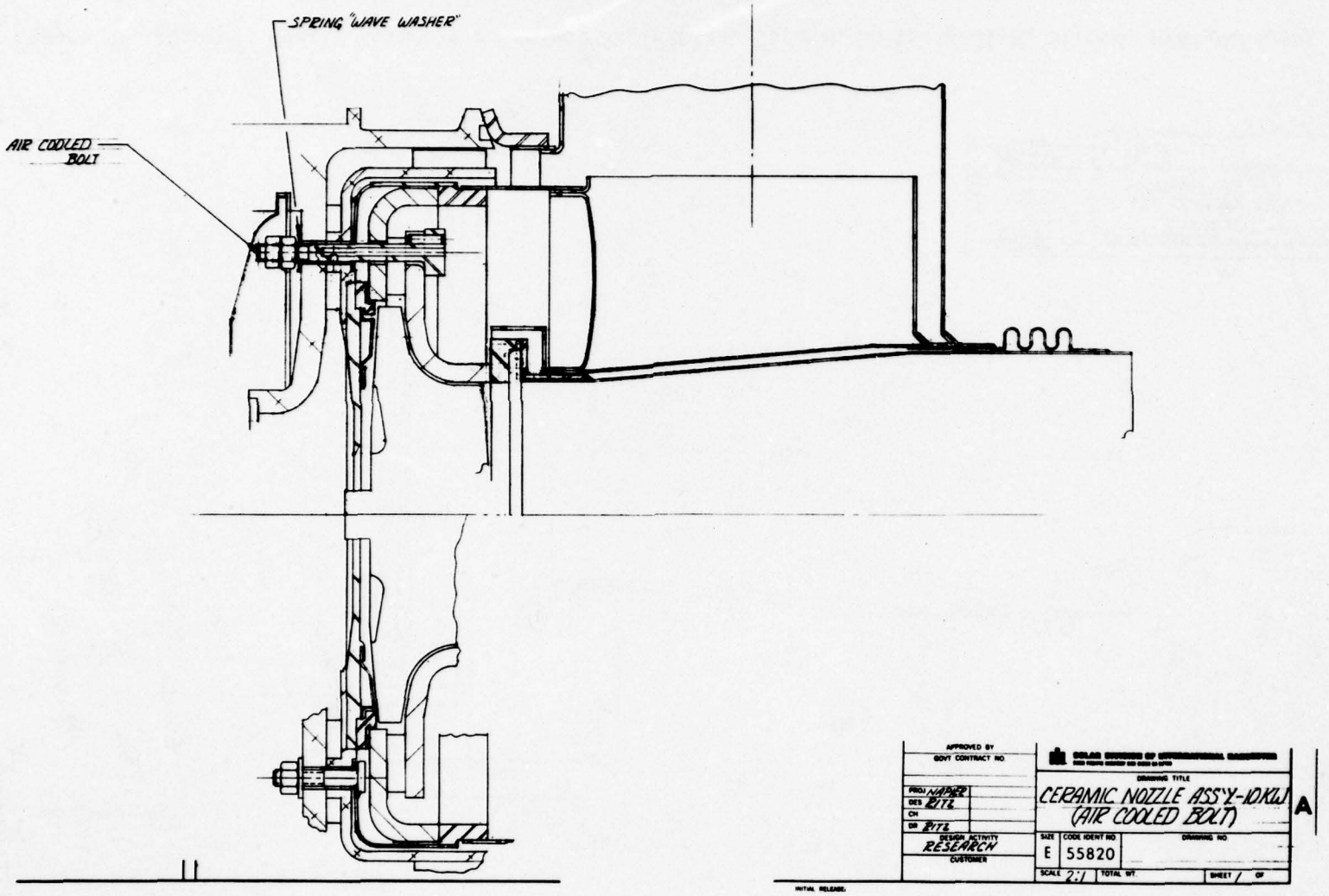

Figure 98. Ceramic Nozzle Assembly - Concept #1 (Air Cooled Superalloy Bolts, RBSi$_3$N$_4$ Shrouds, HPSi$_3$N$_4$ Vanes)

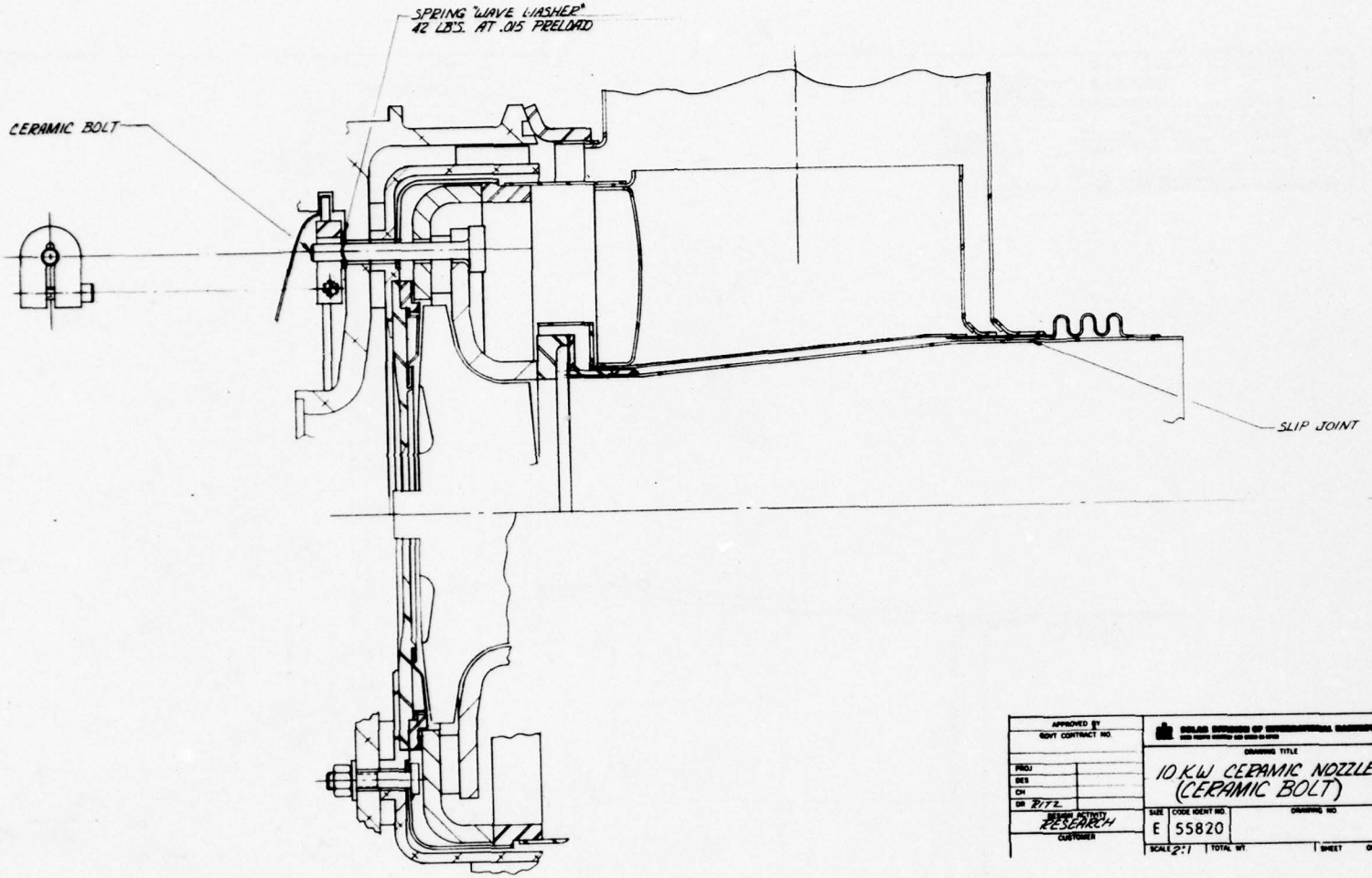

Figure 99. Cearmic Nozzle Assembly - Concept #2 ($HPSi_3N_4$ Ceramic Bolts, $RBSi_3N_4$ Shroud, $HPSi_3N_4$Vanes)

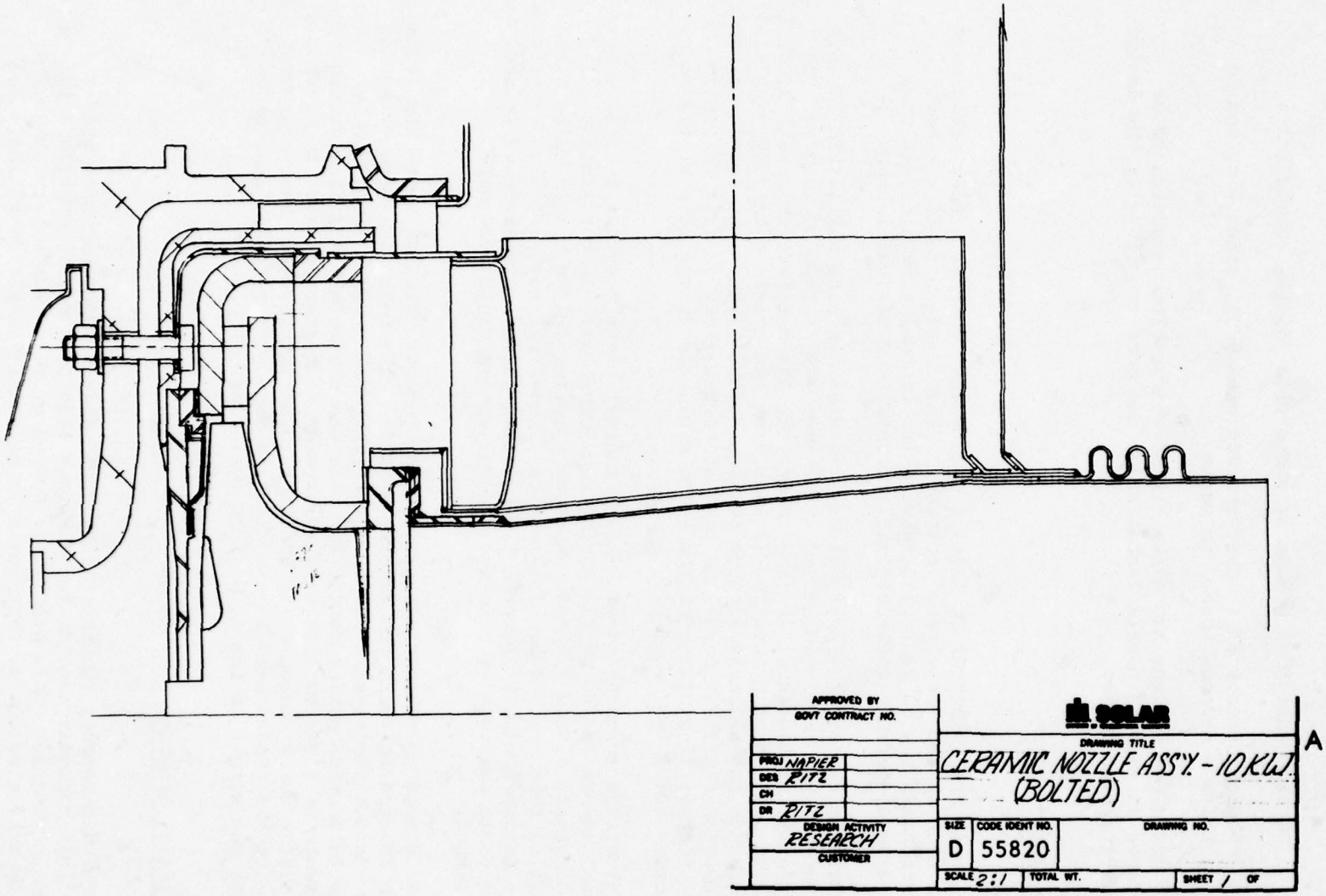

Figure 100. Ceramic Nozzle Assembly - Concept #3 (RCSiC Shrouds, SiC Vanes, Shroud and Vanes Bonded)

- Design Concept #2 - Same as above with HPSi_3N_4 nozzle bolts
- Design Concept #3 - RCSiC shrouds with HPSiC vanes - no nozzle bolts - shrouds bonded to vanes.

Each of the above designs addresses all of the problems expected to be encountered in ceramic nozzle installation and more specifically the design problems iterated above.

Static Seals

Static seals are identical in each of the design concepts. Face seals were used in each of the three seal locations. This appears to be the most straightforward way to deal with substantial thermal growth differences across a metal-ceramic interface while maintaining minimal leakage.

The nozzle to combustor liner seal uses nozzle retaining ring. (RSK 230782) which is spring loaded against the outer (forward) shroud by means of the spring retaining can (RSK 230773), to provide the metal-ceramic seal at that point. An additional transition is made from the nozzle retaining ring to the combustor can assembly with an overlap joint. (Since the initial design, the combustor can sheet metal has been slotted axially in five places to provide thermal flexibility of the sheet metal can in the hoop stress mode. See Section 3.4.5 for details.)

The seal at the forward (outer) shroud to seal plate junction functions as a face seal and is loaded by the spring retaining can. In the instance of design concepts #1 and #2 loads imposed by spring loaded nozzle bolts also transmit to this seal face. Initially a diametrical seal was also functional at this point, however, the seal plate mating surface diameter was reduced by 0.015 inch to assure that relative thermal growth would not cause interference.

The rear shroud to exhaust scroll seal is the most critical since its leakage path is in parallel with the turbine section. The face seal here is spring loaded through the exhaust scroll. Initially the design relied upon a bellows to provide spring forces but this was ultimately modified during rig experiments to a system that uses compressor discharge pressure to provide a small static force component in addition to spring forces. Seal alignment is insured by the presence of a thin flexible René 41 superalloy leaf which connects the scroll to the metal face seal ring.

Differential Growths

The large discrepancy in expansivities of silicon based ceramics and superalloys commonly used in gas turbines requires special consideration in the design process. This problem is solved at seal junctions as described above by exclusive use of face seals at material transition points. The diametrical growth component of the forward (outer) shroud to seal plate

junction is overcome by provision of adequate clearance and use of INCO 903, a new low expansion alloy, as the seal plate material.

Rear Shroud Location

The rear shroud mates with the turbine wheel contour and must be accurately located and centered for minimum clearance and optimum engine performance. In design concepts #1 and #2, the shroud is located in relation to the compressor diffusor housing via piloted bolts. The rear shroud uses radial slots to give good location and centering while allowing for differential growth. The forward shroud has clearance holes to account for differential growth. Design concept #3 does not use bolts and therefore centering of the rear shroud is accomplished by the diametrical centering of the forward shroud on the seal plate. The forward shroud and rear shrouds are bonded together through the nozzle vanes in this design.

Features common to each of the three designs included the seal plate/diaphragm assembly shown in Figures 101 through 106, spring-loaded retaining can shown in Figures 107 through 110, retaining ring for outer shroud shown in Figures 111 and 112, the rear shroud exhaust scroll seal shown in Figures 113 and 114, and the exhaust scroll shown in Figures 115 and 116.

Design concept #1, which employs RBSi$_3$N$_4$ shrouds, HPSi$_3$N$_4$ vanes and 718 superalloy nozzle bolts, includes relocation of one of three dowel pins and addition of holes and bosses in the air inlet housing and the compressor diffuser housing as appropriate for mounting the spring loaded retaining can and nozzle bolts. These modifications are shown in in Figures 117 and 118. The air cooled nozzle mounting bolt design is shown in Figure 119. An additional modification over the standard design includes spring load mounting of nozzle bolts with Belleville washers. The washers used are of the same type as described in Section 3.3.5. Seven washers were used on each bolt, with each adjacent washer facing in opposite direction. The washer nearest the nut was set such that its small diameter contacted the nut face. The stack was tightened half-way through free travel.

The design concept #1 ceramic shrouds and vanes are shown in Figures 120 through 124. The finished parts are seen in Figures 125 through 129.

Design Concept #2 differs from concept #1 only with respect to the nozzle mounting bolts. HPSi$_3$N$_4$ bolts are used in place of the air cooled 718 superalloy bolts of concept #1. The ceramic bolt is shown in Figure 130 and 131. A special collet design to be used with these bolts is given in Figures 132 through 134. The collet uses a 0.004 inch thick layer of platinum to protect the ceramic and uses two sets of Belleville washers for thermal flexibility. The washer configuration is the same as described above.

Design Concept #3 consists of silicon filled recrystallized SiC shrouds and HPSiC vanes. No mounting bolts are used in this design. No special modifications or hardware other than items common to the three ceramic alternatives are associated with this design.

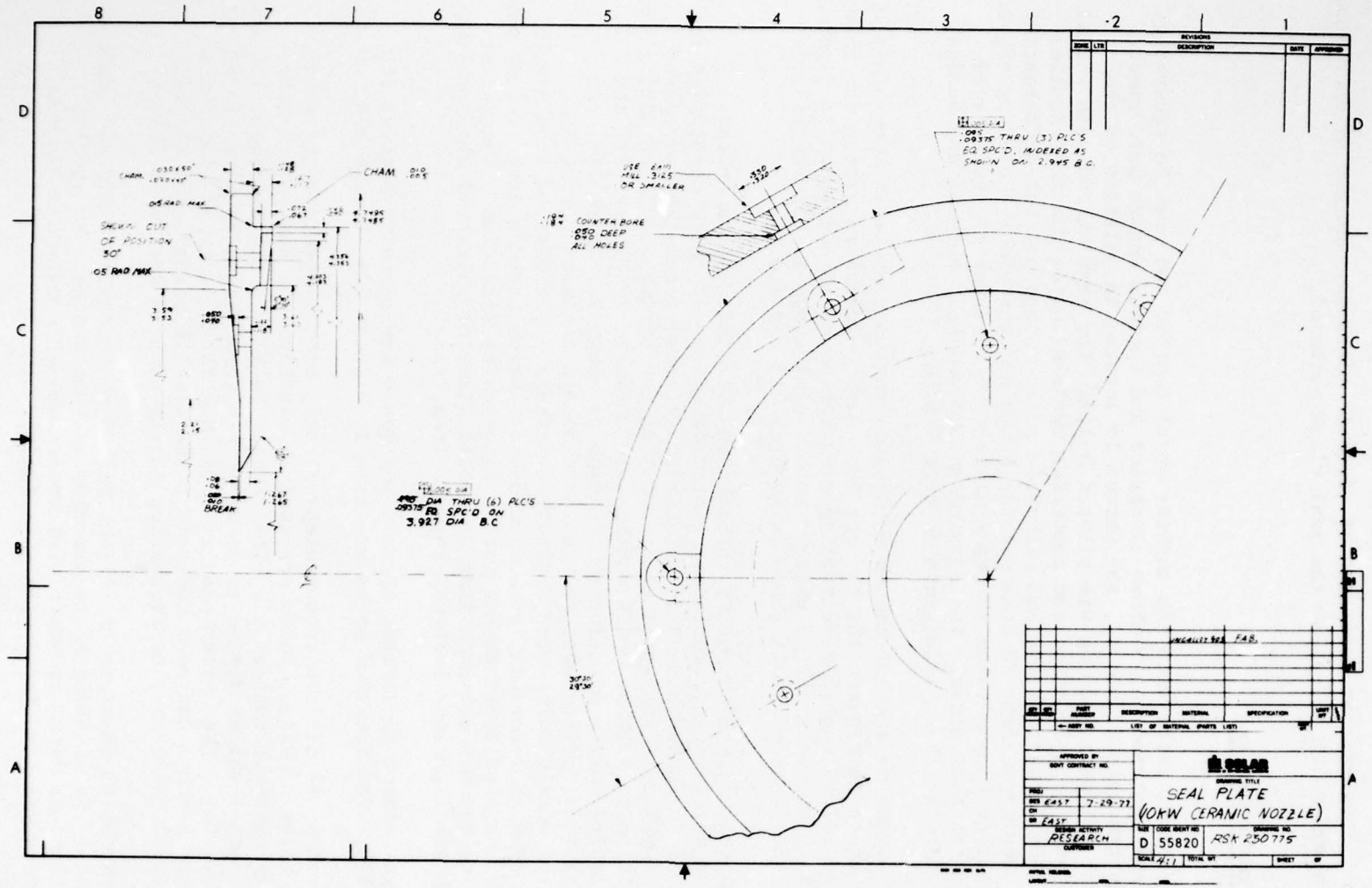

Figure 101. Seal Plate for Use With Si_3N_4 and SiC All-Ceramic 10 kW Nozzles

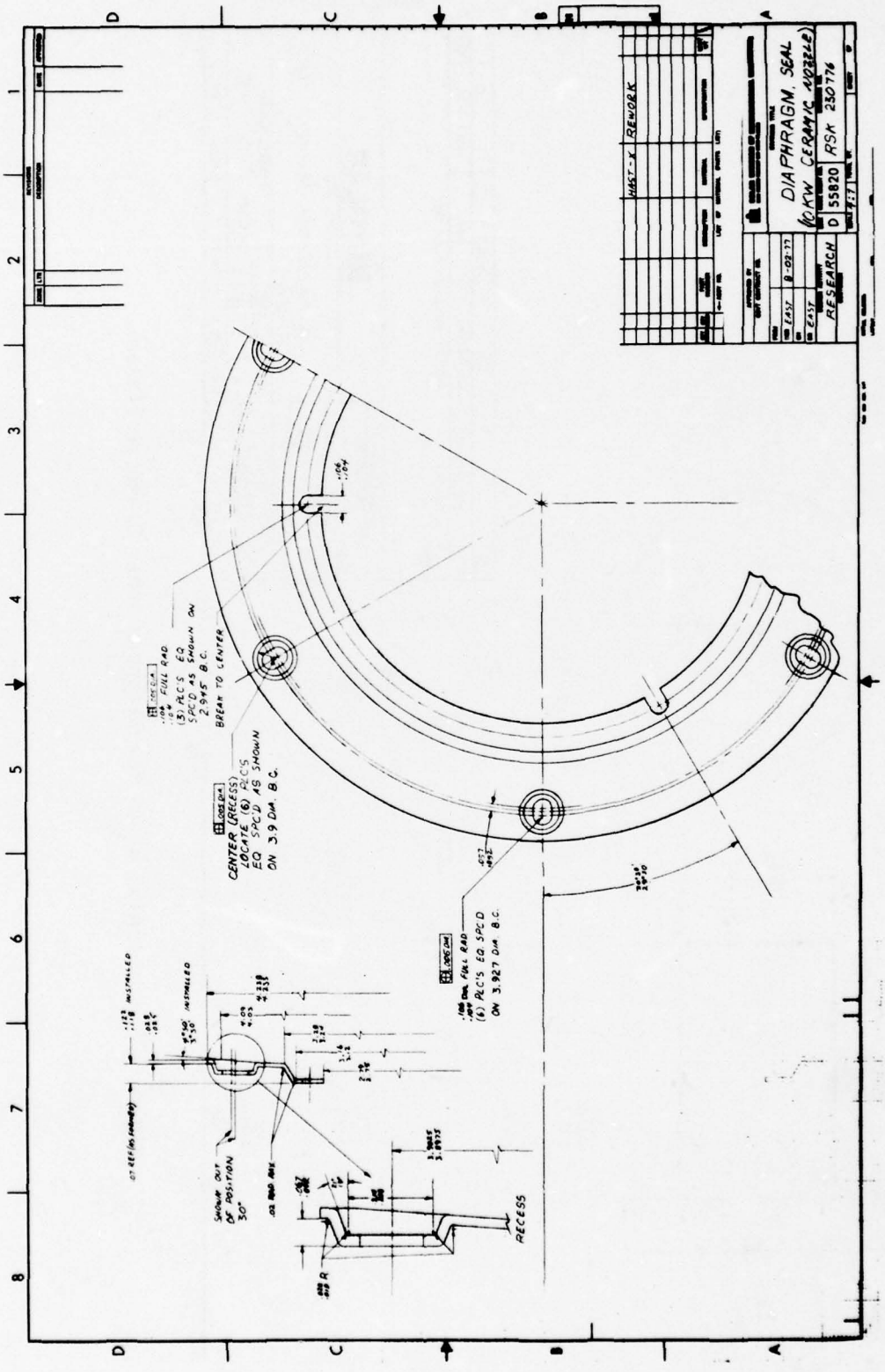

Figure 102. Seal Plate Diaphram for Use With Si_3N_4 and SiC Ceramic 10 kW Nozzles

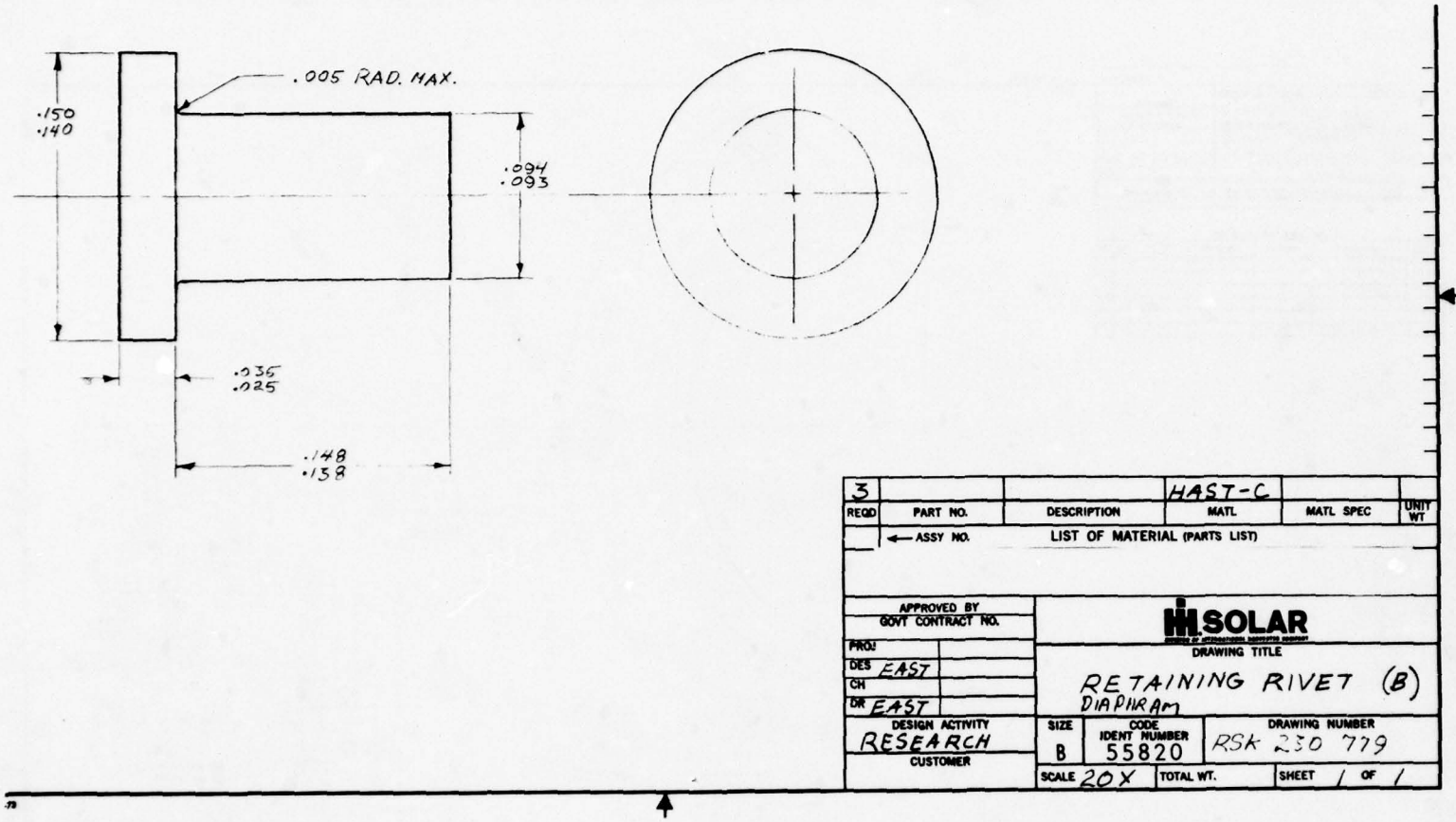

Figure 103. Retaining Rivet for Diaphram Inner Diameter (Three)

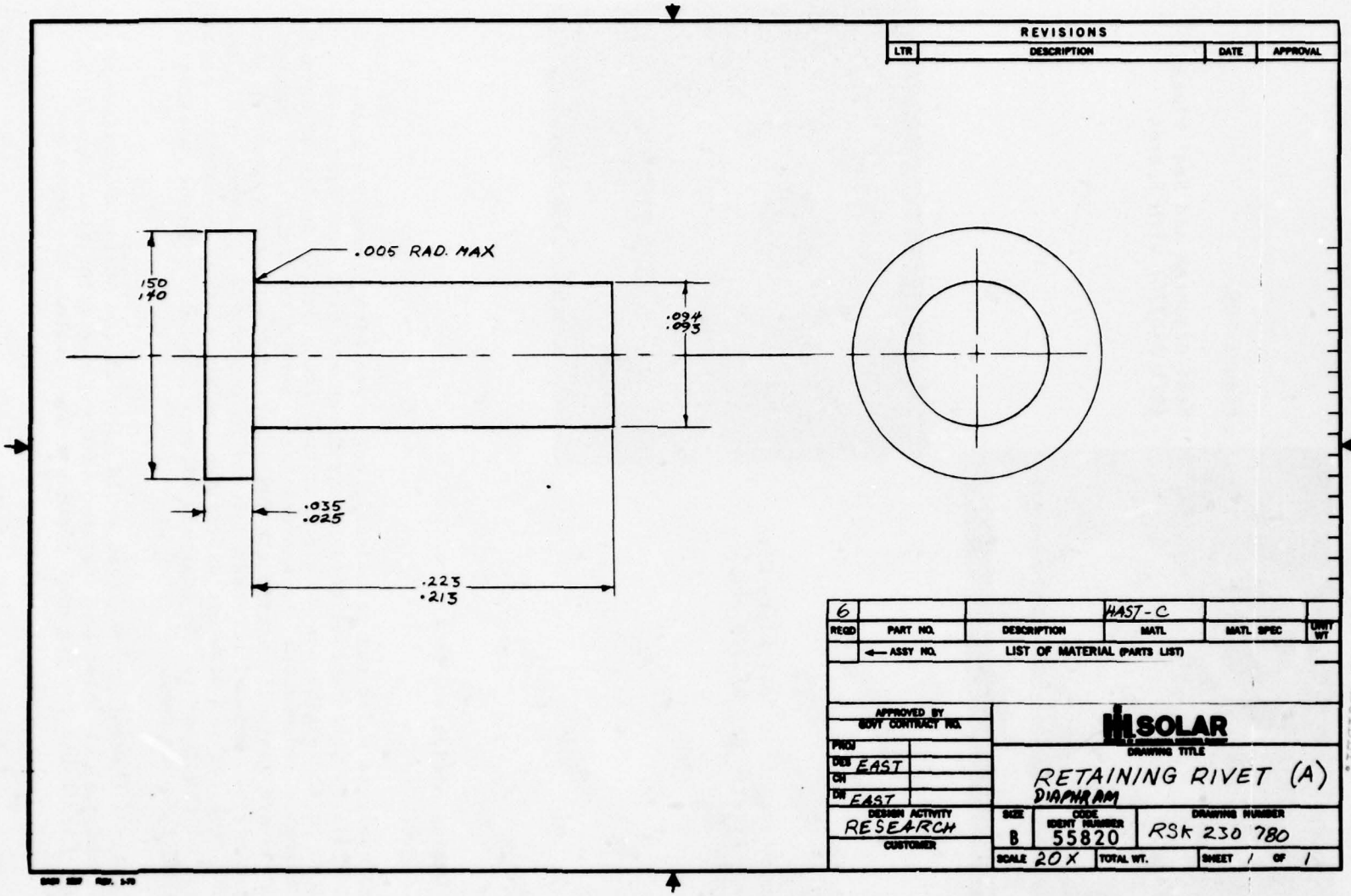

Figure 104. Retaining Rivet for Diaphram Outer Diameter (Six)

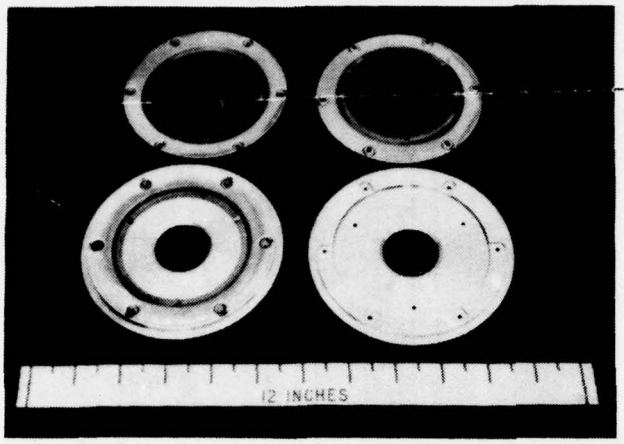

Figure 105.

Seal Diaphram and Seal Plate (RSK 230776) With Spares

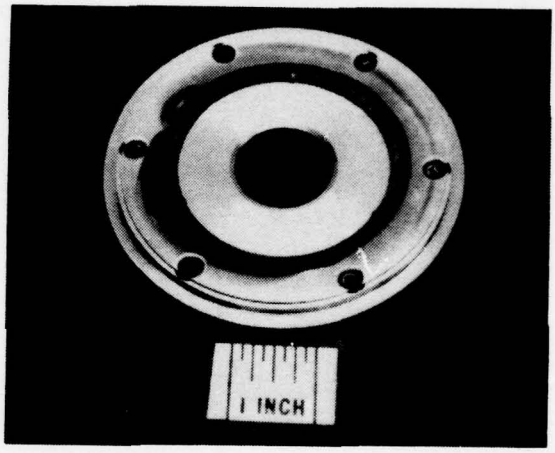

Figure 106.

Diaphram Attached to Seal Plate With Retaining Rivets (RSK 230779 and RSK 230780)

3.4.2 Design Analysis

A design analysis which was principally concerned with assembly compatibilities due to differential growths during steady state and transient conditions in the engine was done concurrently with detail design of ceramic nozzle assembly components. Mechanical loads were also considered, however, these loads are insignificant in the fully articulated designs used for these ceramic nozzles. Thermal stresses induced in components by steady state and transient temperatures were not determined analytically since this was beyond the scope of the program. An analysis of vane complexity versus fabrication cost of $HPSi_2N_3$ was done.

Table 15 lists thermal growths that would occur at the seal plate diameter for selected turbine inlet temperatures with various material alternatives which were available for the seal plate and the nozzle. The growths

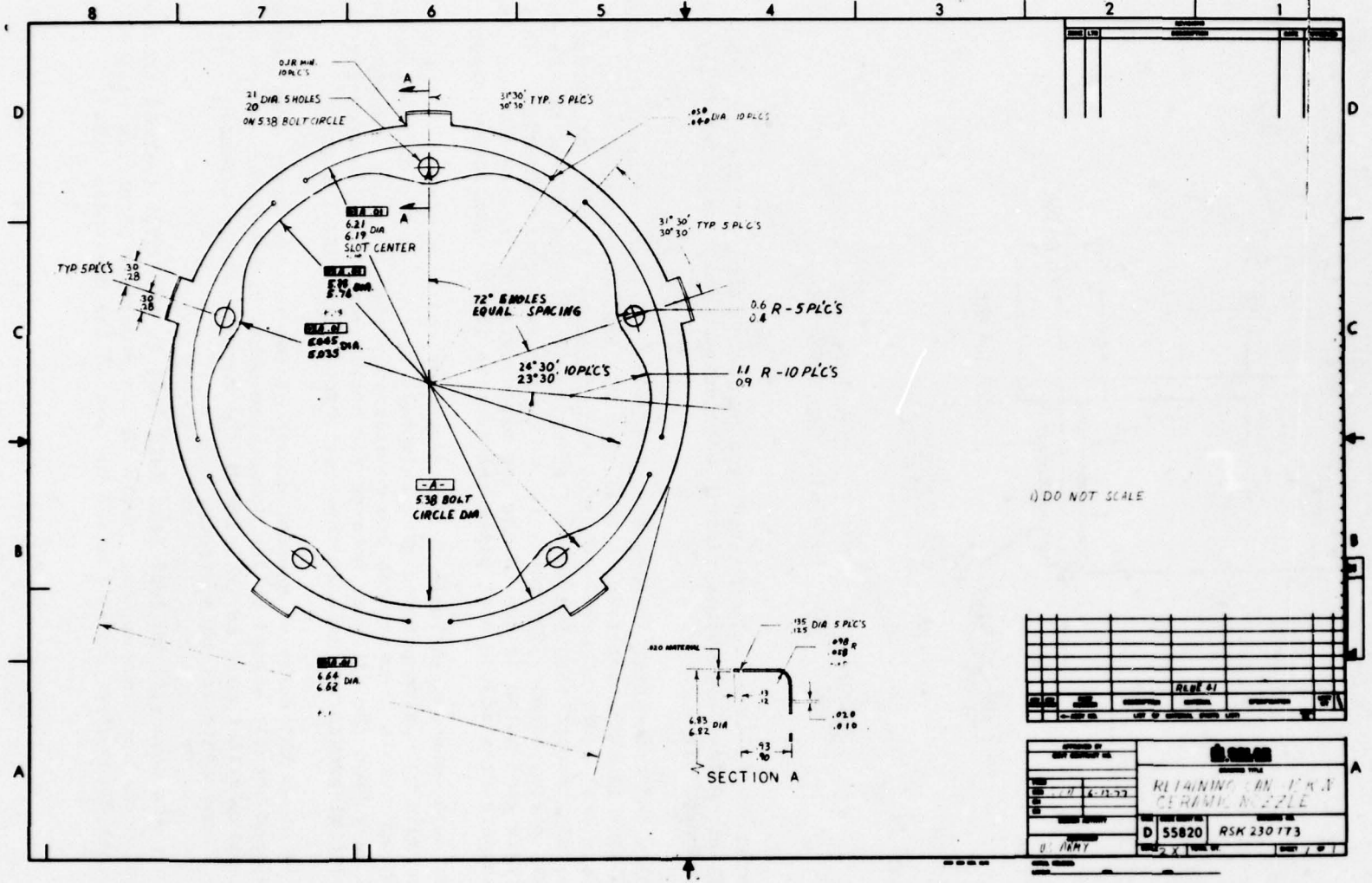

Figure 107. Outer Shroud Retaining Can for Use With Si_3N_4 and SiC Ceramic Nozzles

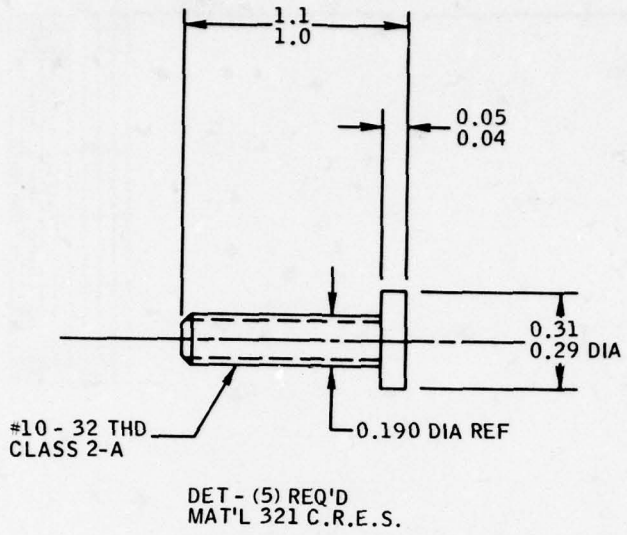

Figure 108. Bolt for Attachment of Nozzle Retaining Can (RSK 230785)

indicated in the table were derived from published expansivities of the materials, engine temperature distribution data measured experimentally and the component size.

The table indicates that Incoloy 903 used as a seal plate material has a net growth that is matched better to that of a SiC forward shroud than other candidate seal plate materials. Since design concept #3 uses SiC shrouds and is the only concept that relies upon diametrical piloting of the nozzle on the seal plate, Incoloy 903 was selected as the seal plate material. This relatively good match is due to the low expansivity of Incoloy 903 and lower mean temperatures of the seal plate relative to the forward nozzle shroud.

Similar data is shown in Table 16 for growth at the bolt circle. This shows that ceramic nozzle components grow only half as much as the diffusor housing even though nozzle temperatures are considerably higher. Since concepts #1 and #2 rely upon the diffuser housing for nozzle support, allowance for this differential growth was made at the rear shroud with radial slots.

Table 17 shows the relative thermal growth of the turbine wheel with respect to the rear ceramic shroud at its downstream outer diameter and additional cold clearance that must be included in the ceramic shroud dimensions in order to compensate for this effect.

Emergency shutdown with no load from full load is the worst thermal transient that can occur for this engine. Table 18 is an example of growth referenced to ambient datum that occurs towards the end of the downshock cycle.

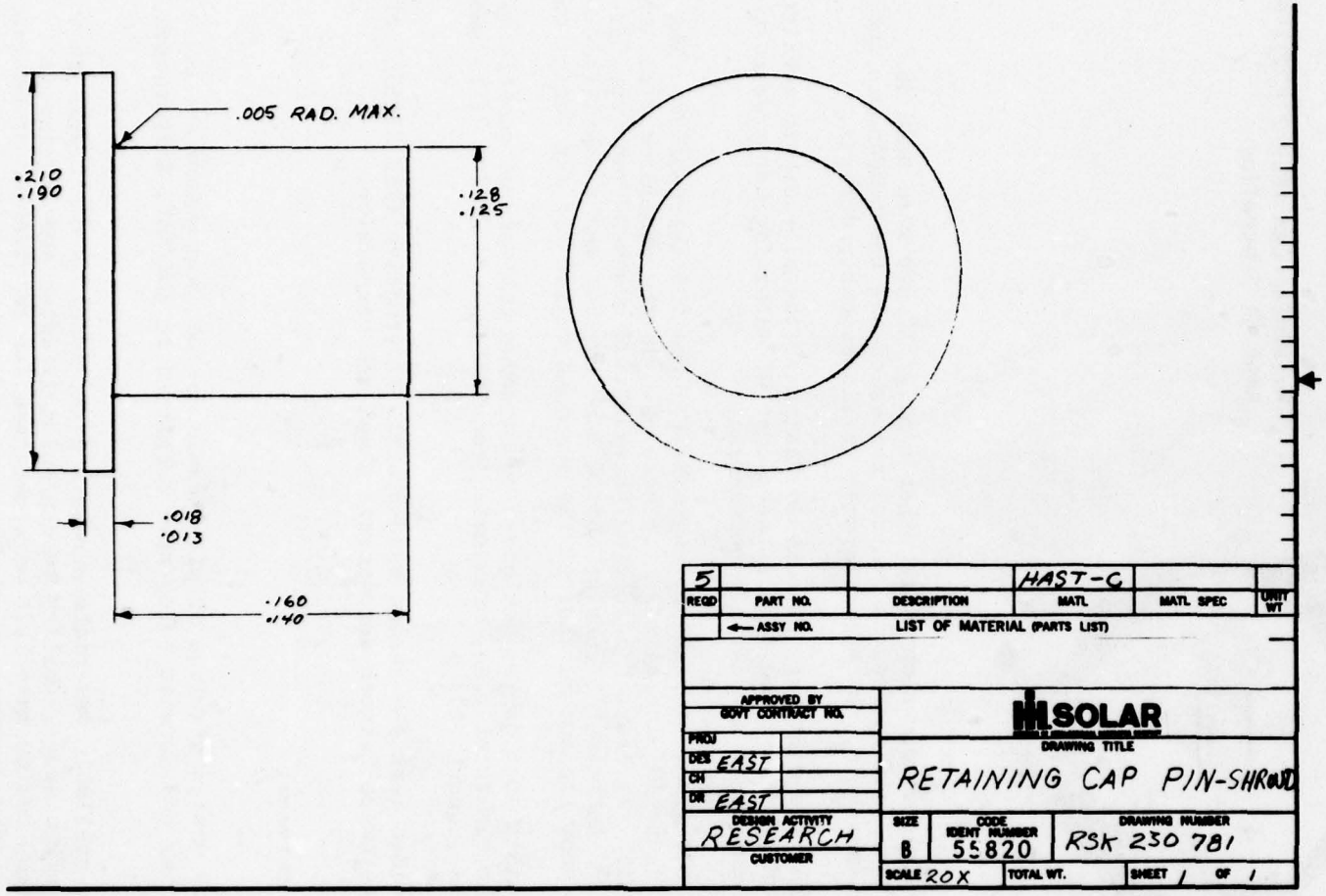

Figure 109. Retaining Cap Pins for Attachment of Nozzle Retaining Can to Nozzle Retaining Ring

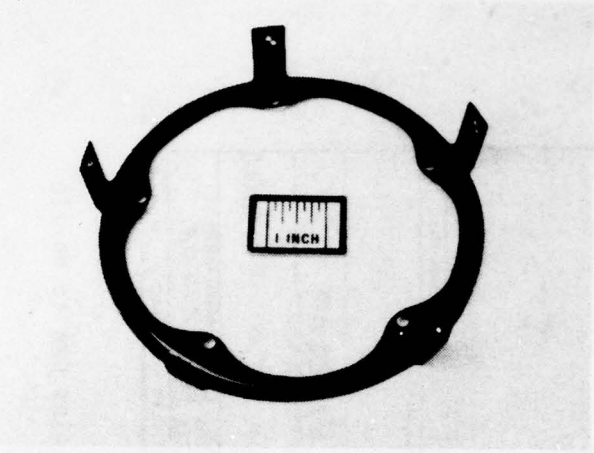

Figure 110.

Retaining Can (RSK 230773) From René 41 Superalloy

The above information along with other similar inputs were used in determining detail dimensions and tolerances of all the components included in, and adjacent to, the three ceramic nozzle assembly designs.

Vane profile was a primary concern in design of the all-ceramic nozzles. A design tradeoff had to be made between cost of machining hot pressed ceramic vanes and estimated aerodynamic performance.

The three alternate vane shapes shown in Figures 135 through 137. The vanes shown in Figure 135 are similar to those used in the preliminary all-ceramic nozzle design rig tested in Program Phase II. The second vane type presents a compromise between the current nozzle vane contour and a simplified vane. The third vane contour is that of the standard nozzle for the Gemini engine.

Table 19 lists cost quotations given by Ceradyne for various quantities of each of the six total vane forms made from $HPSi_3N_4$ and HPSiC. (The quotation was made in January 1977.)

It was decided that the second vane profile alternative (RSK 230630) offered a good compromise between aerodynamic shape and complexity.

3.4.3 Procurement

Preliminary design drawings of all-ceramic nozzle commponents including shrouds vanes and ceramic bolts were submitted to AME/KBI, Carborundum, Tylan and Norton.

Based upon available materials strength data, maturity of ceramic material fabrication processes, ability to control tolerances and fabrication capabilities, Norton materials were selected for fabrication of ceramic components. The items procured are listed in Table 20.

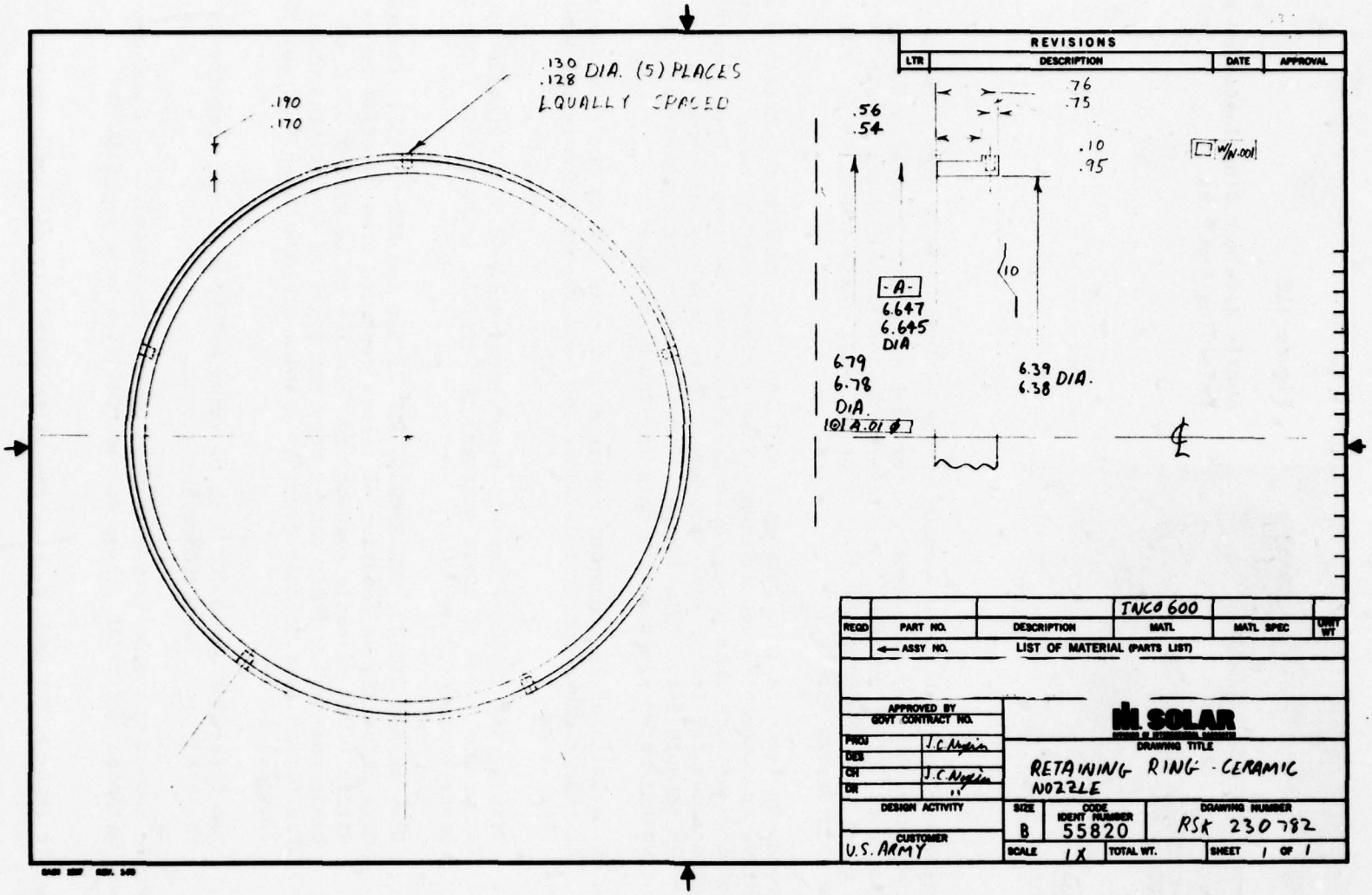

Figure 111. Retaining Ring for Attachment of Ceramic Outer Nozzle Shroud

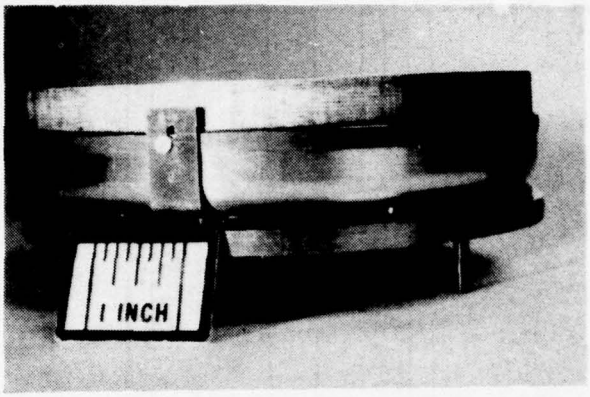

Figure 112.

Nozzle Retainer Ring Installed With Retaining Cap Pins

The last entry in Table 20 is bonding of one silicon carbide nozzle assembly. Norton declined to bond an assembly after fabrication of components due to anticipated difficulties in meeting tolerances specified for the nozzle throat diameter. (Bonding was done at Solar using glass adhesives in order to make this design viable.)

In response to feedback from personnel at Tylan Corp. to design concept #3 an alternative to concept #3 was defined. This included through holes in place of vane recesses such that vanes could form a sleeve joint with both forward and rear shrouds for better bond strength. These drawings are shown in Figures 138 through 141. This design was not selected for evaluation because of insufficient materials property data for the Tylan material.

Changes to ceramic nozzle component drawings were made during the procurement cycle. The change gives looser tolerances for vane recess contours and vane contours. They are:

1. Drawing RSK 230530 - Ceramic vane change note #2 from "Profile to be within 0.002 of basic contour" to "Profile to be within 0.005 of basic contour".

2. Drawing RSK 230632, RSK 230633, RSK 230636 and RSK 230637. Change note referring to location of recess contours from "Profile to be within 0.002 of basic contour" to "Profile to be within 0.005 of basic contour". (This change does not apply to the turbine wheel contour on rear shrouds given by drawing numbers RSK 230633 and RSK 230637.)

3. The tolerance of ±0.002 inch on vanes and vane recess contours is to be met on a best effort basis only.

All ceramic components were inspected upon receipt by visual, Zyglo and dye penetrant methods. No voids, flaws or abnormalities were noted in the materials.

Figures 142 through 145 show some of the as-received ceramic components.

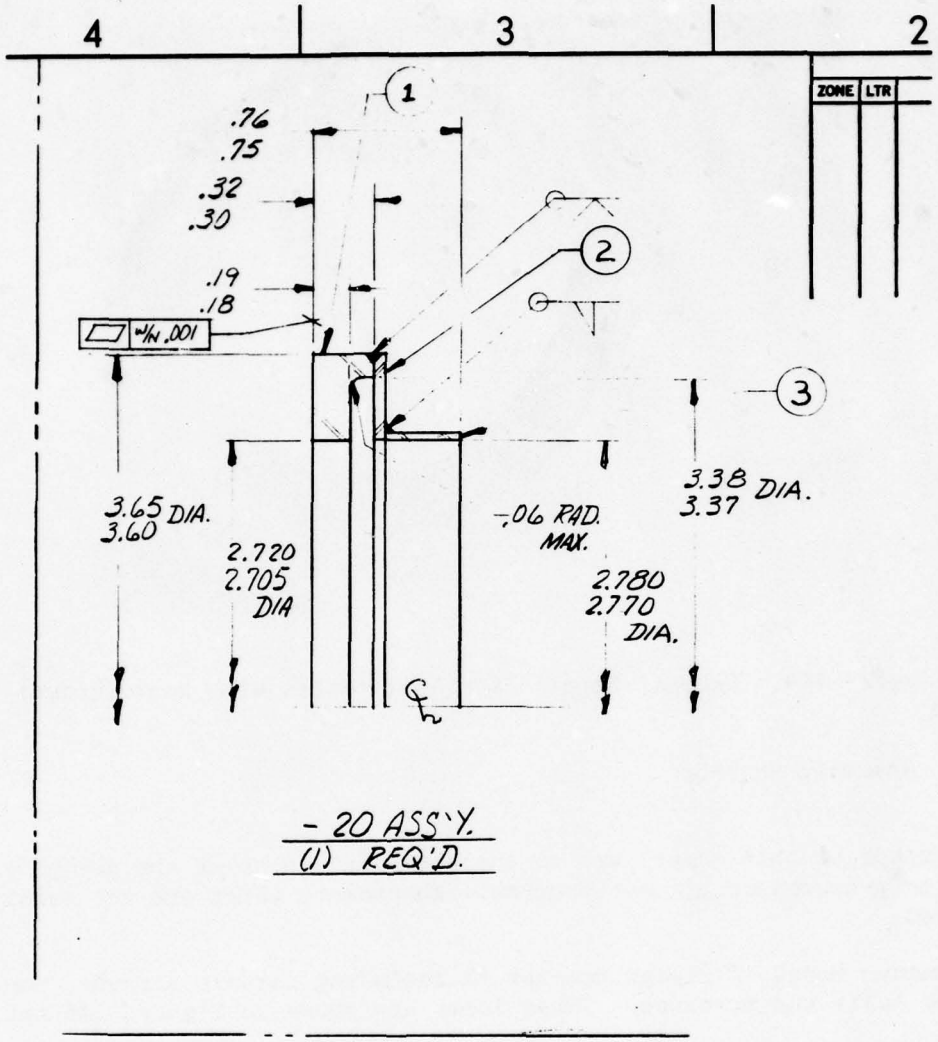

Figure 113. Rear Shroud to Exhaust Scroll Seal for Use With Si_3N_4 and SiC Ceramic Nozzles

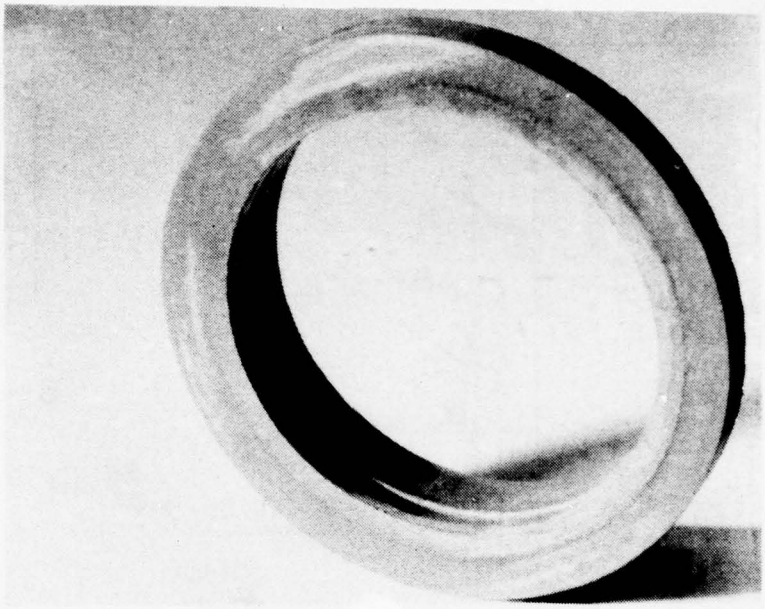

Figure 114. Exhaust Scroll Face Seal (Mates With Rear Shroud)

3.4.4 Assembly Mock-Up

The purpose of this effort was to check the soundness of the design assembly prior to procurement of costly ceramic components which are not easily modified.

An aluminum model of design concept #2 including ceramic shrouds, vanes and ceramic bolts was procured. These items are shown in Figures 146 and 147.

Figure 148 shows nozzle assembly components prior to assembly mock-up. Figures 149 through 155 show the assembly sequence. (The parts are attached to a fixture used to simulate the diffusor housing in rig tests so that the assembly can be seen more clearly.) Figure 156 views the nozzle assembly installed in the actual diffusor inlet housing. The turbine wheel is also in place in this figure. Figure 157 shows an exploded view of the assembly components which include Si_3N_4 shrouds, vanes and bolts.

Assembly analysis revealed that there were no dimensional or tolerance problems in matching component pieces. The only difficulty noted in assembly was insufficient elastic range of the bellows which spring loads the rear shroud/exhaust scroll face seal. The solution to this problem is given in the next section Assembly Analysis - Design Update.

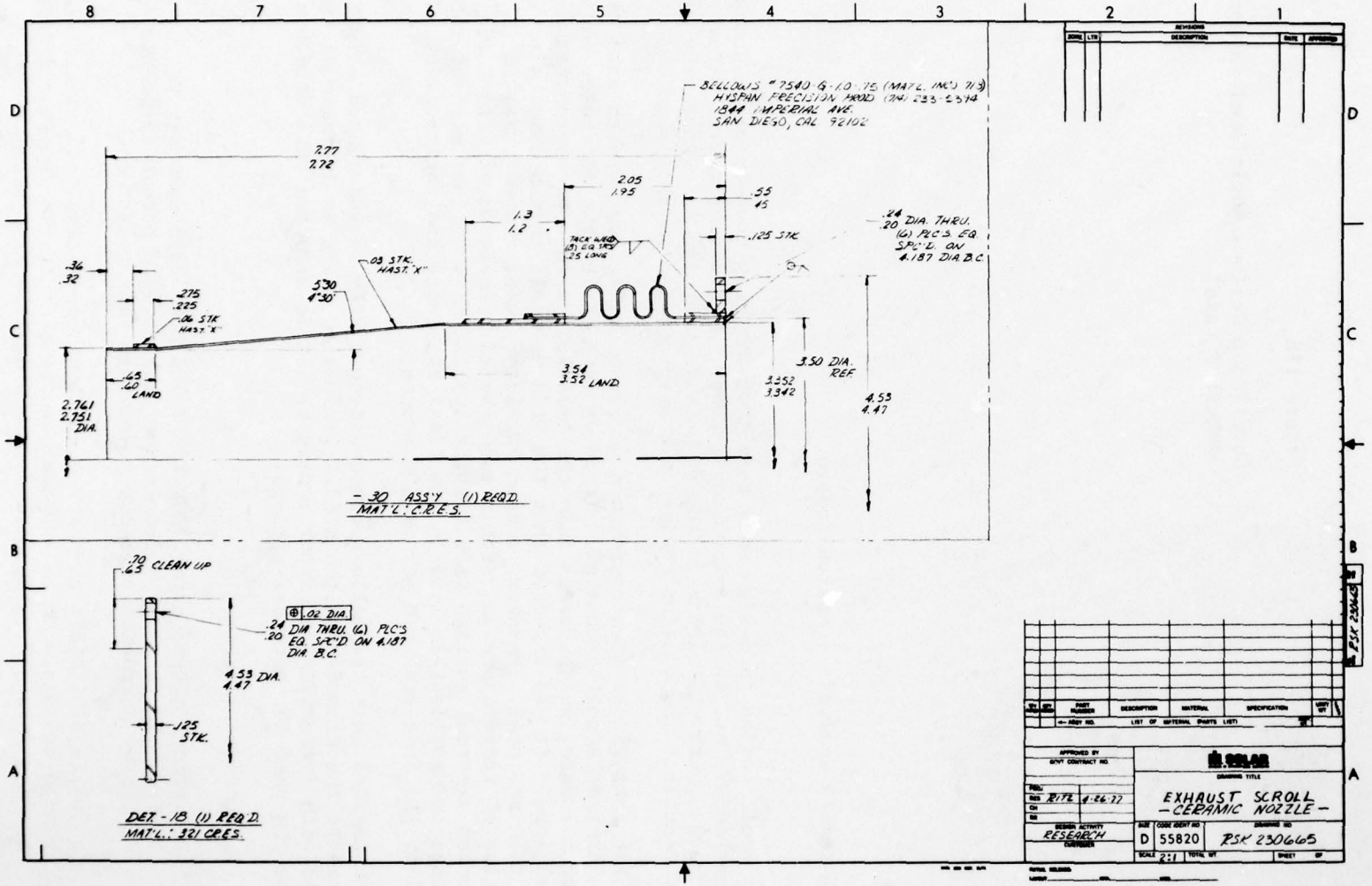

Figure 115. Exhaust Scroll for Use With Si_3N_4 and SiC Ceramic Nozzles

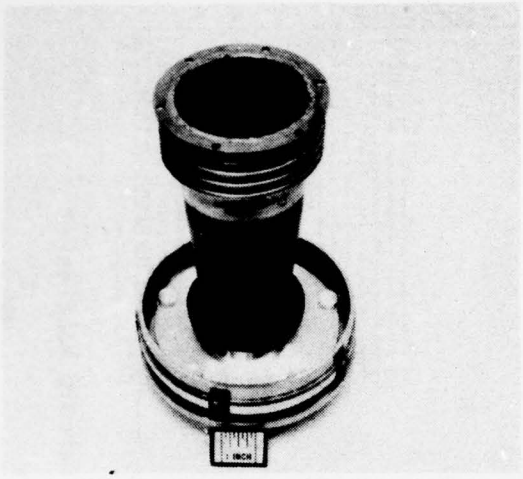

Figure 116.

Scroll and Bellows Positioned (Without Combustor Case)

3.4.5 Assembly Analysis - Design Update

The only modification in design as a result of assembly mock-up was a change in the method of loading the rear shroud/exhaust scroll face seal. Other design changes were made later in the project in response to engine simulator rig test results. These later changes are also covered in this section.

Figures 158 through 165 show a pressure compensating bellows system used to load the exhaust scroll face seal. It is designed such that increases in combustor pressure, which bleeds into the bellows, yield a net zero change in face seal load. It was expected that the bellows would then provide a spring load on the face seal. However, engine simulator tests showed that the combination of temperature and static load caused relaxation of this load. Three cooled external springs were finally applied at the right side of the last flange to provide this load in the final rig tests and engine test. The net load on the face seal was set at 100 pounds.

It is recommended that the bellows compensating system be redesigned slightly by increasing the diameter of the middle bellows to yield an increase in face seal load with increasing combustor pressure. It is expected that this would eliminate the need for external springs.

Other design changes include:

1. Reduction in seal plate (RSK 230775) 4.356/4.353 diameter to 4.341/4.338 to avoid interference with forward shroud ID due to debris or corrosion products present in this interface.

2. A two layer 0.002 inch thick Hastelloy X radiation heat shield was placed at nozzle OD to avoid excessive heat at the aluminum diffusor housing during high temperature 1066°C (1950°F) running.

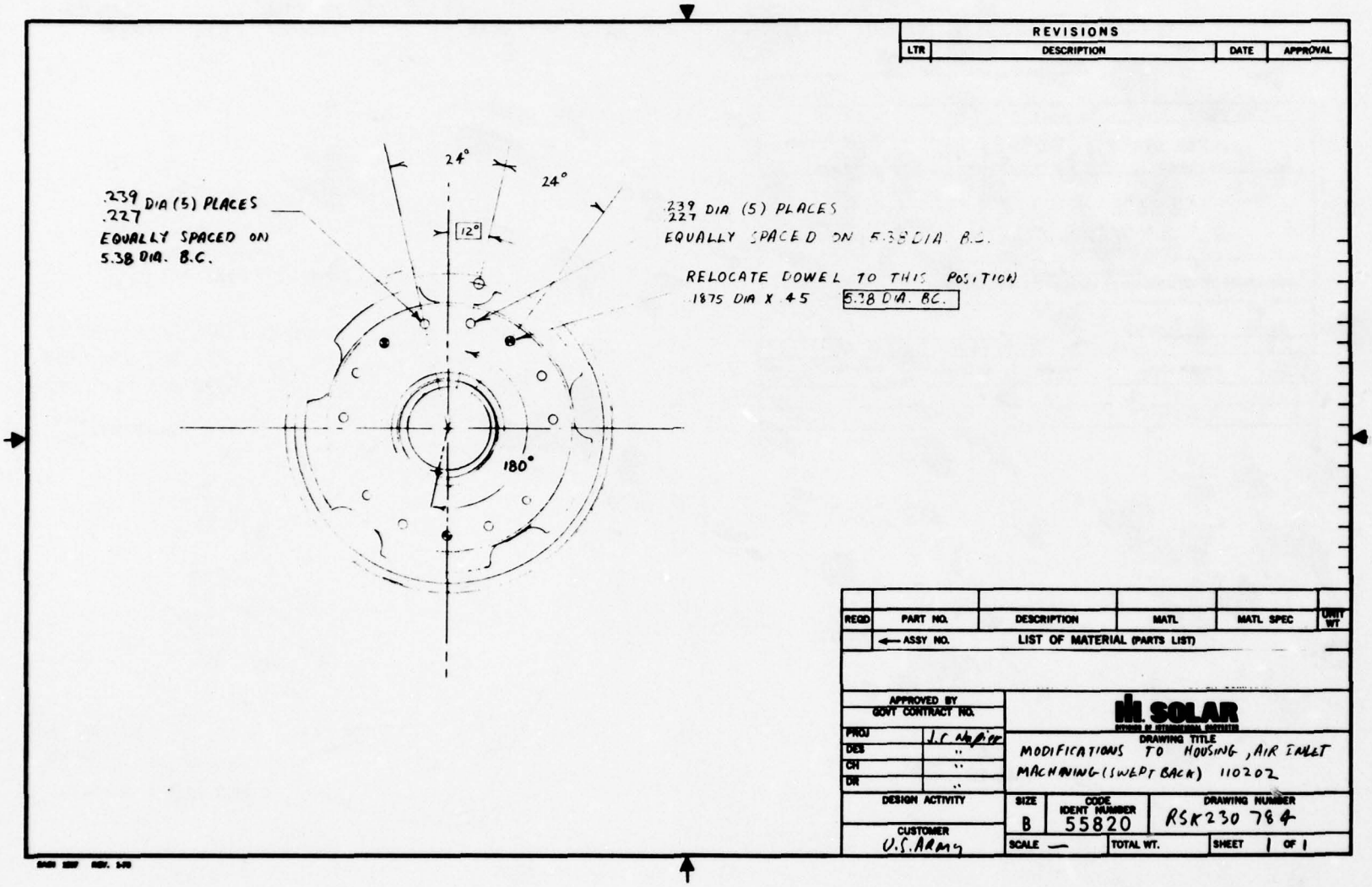

Figure 117. Modification of Air Inlet Housing (DSK 110202) for Ceramic Nozzle Design Concept #1 and #2

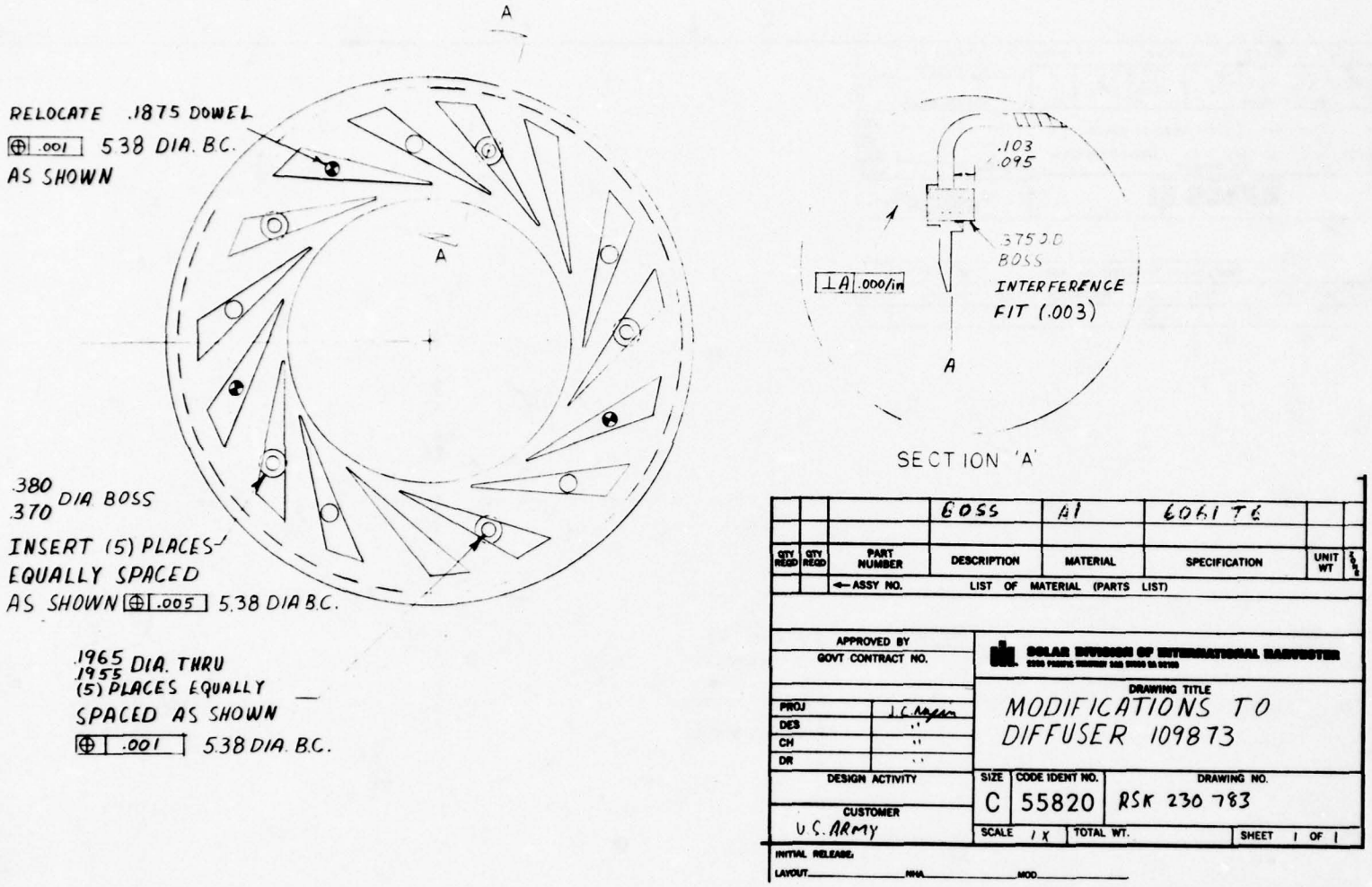

Figure 118. Modification to Standard Diffuser Housing (DSK 109873) for Ceramic Nozzle Design Concepts #1 and #2

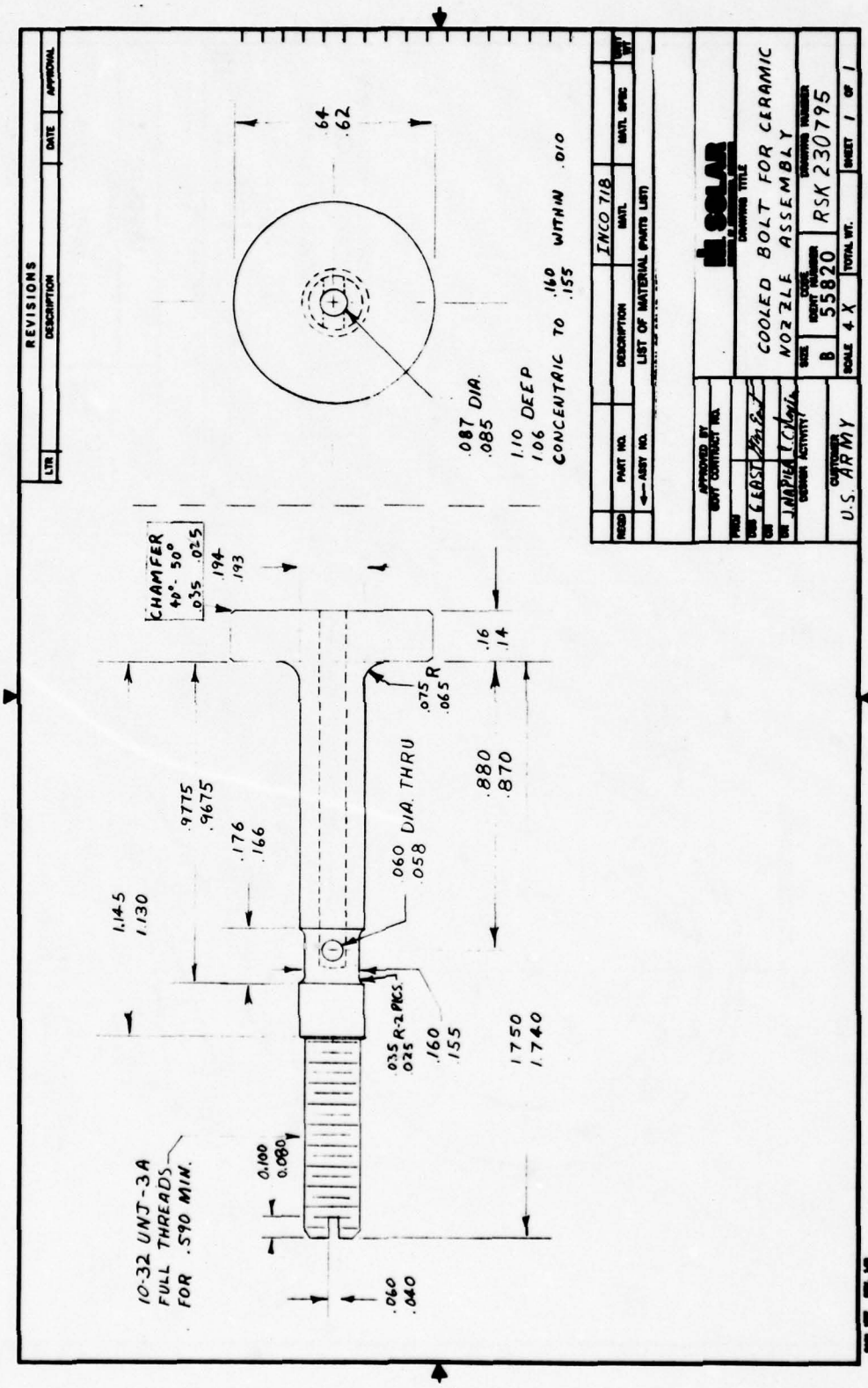

Figure 119. Cooled Superalloy Bolt for Ceramic Nozzle Assembly

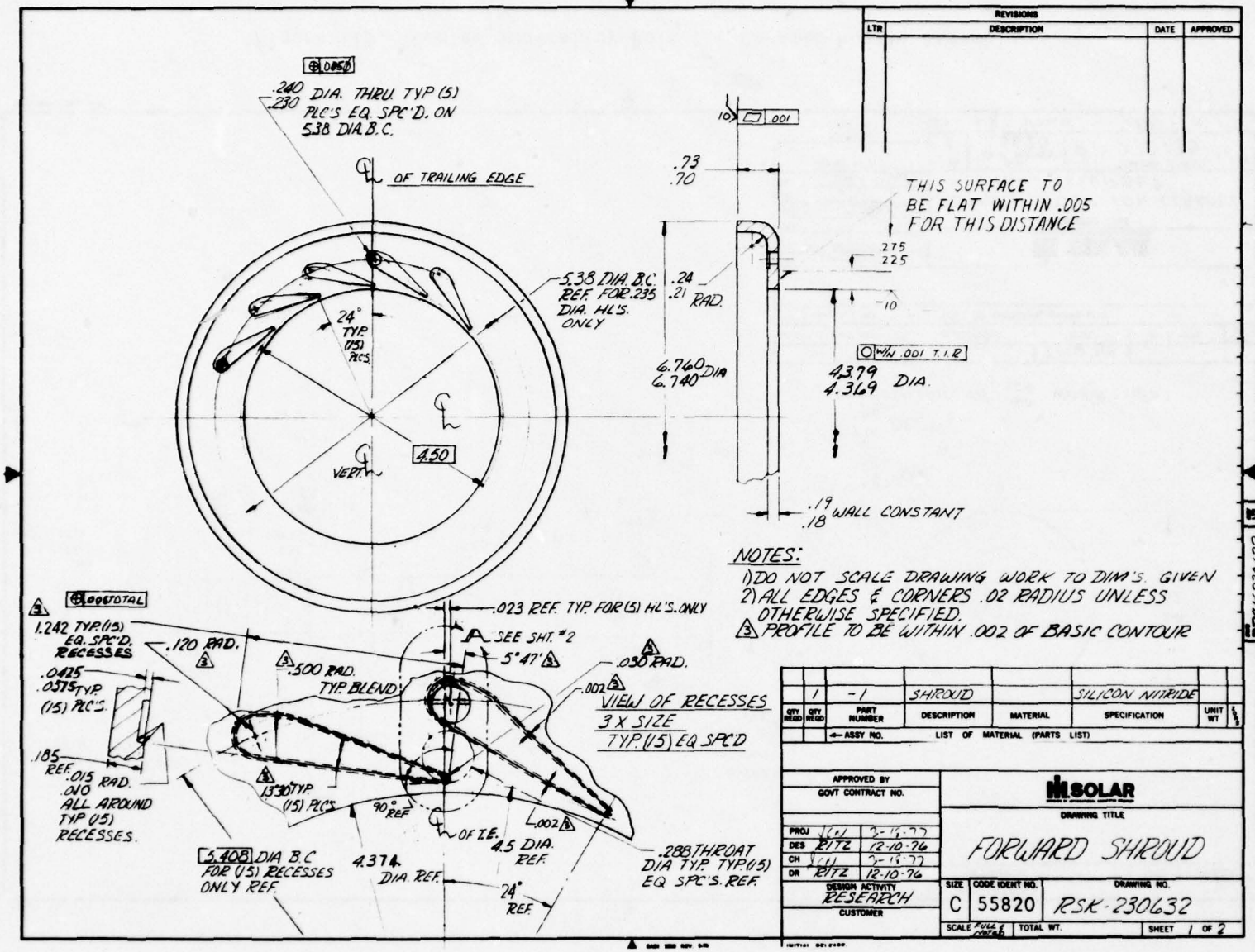

Figure 120. Forward Shroud

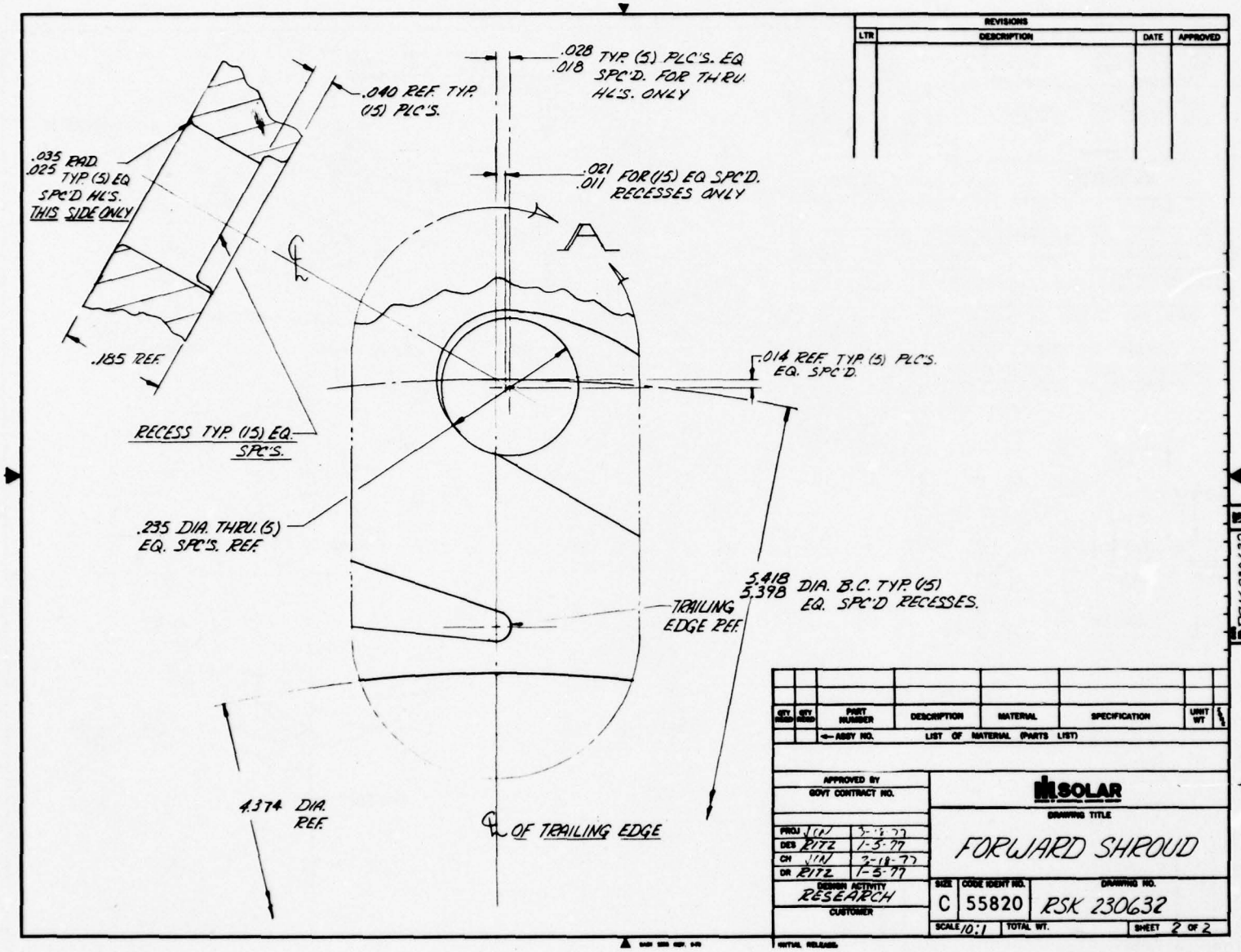

Figure 121. Forward Shroud

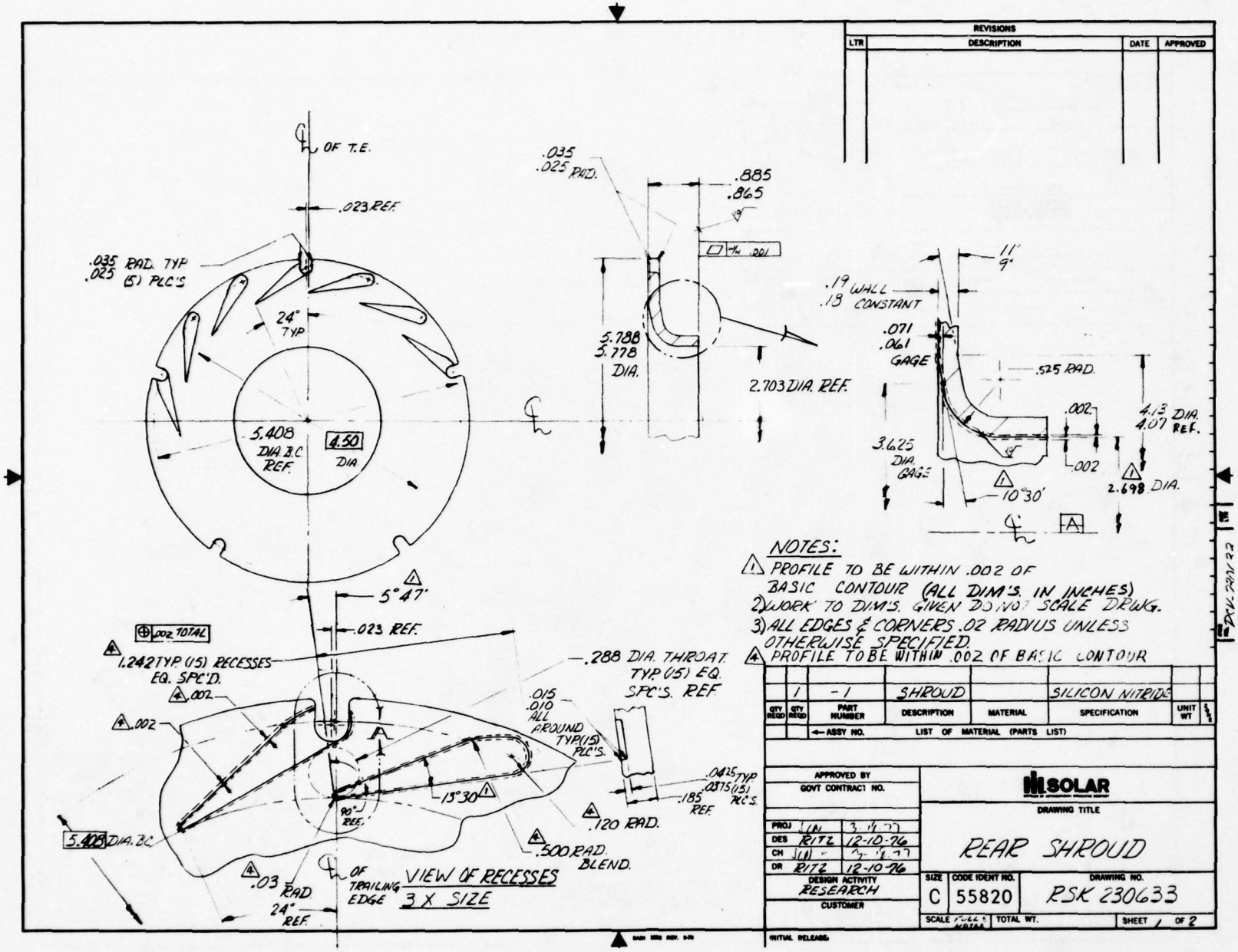

Figure 122. Rear Shroud

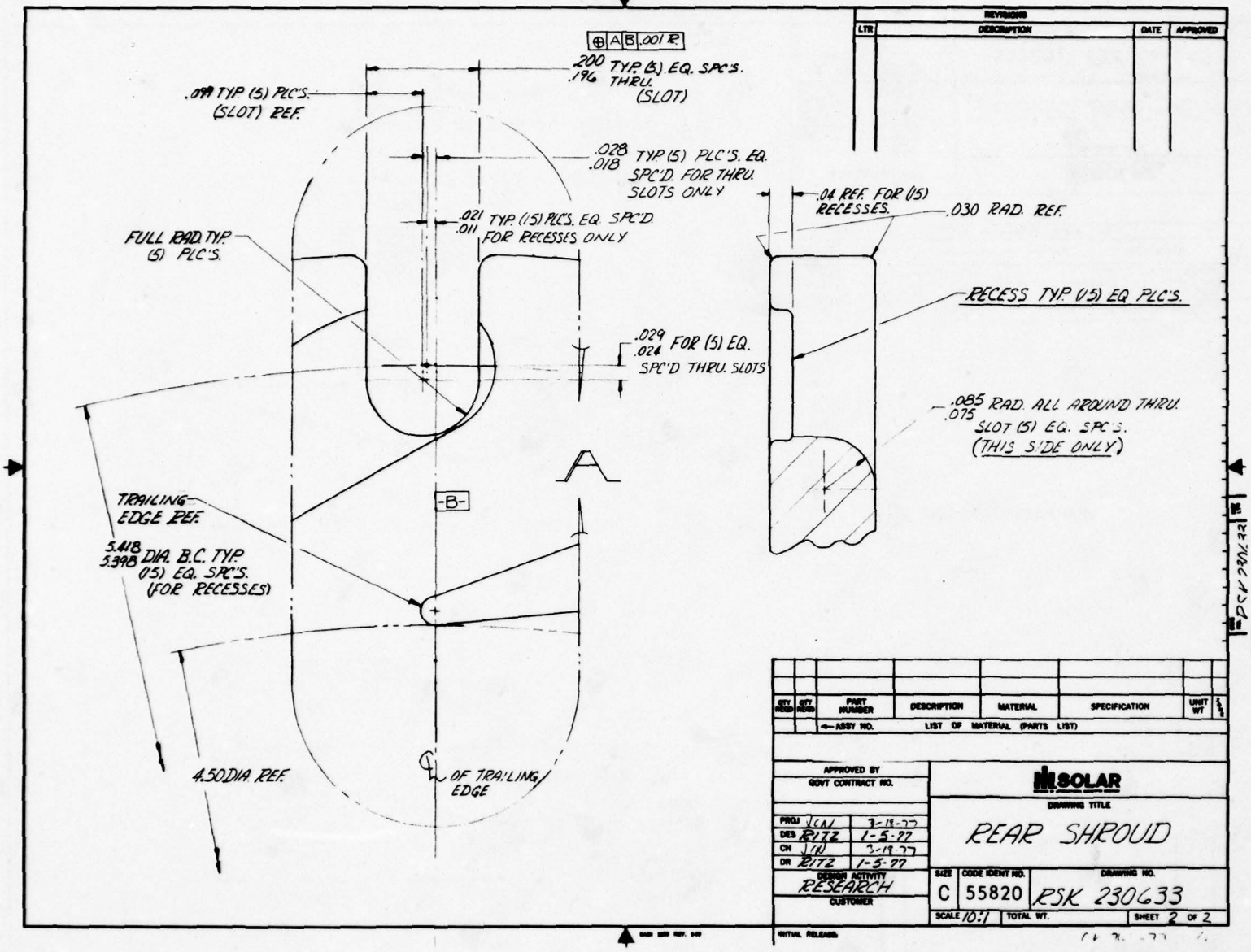

Figure 123. Rear Shroud

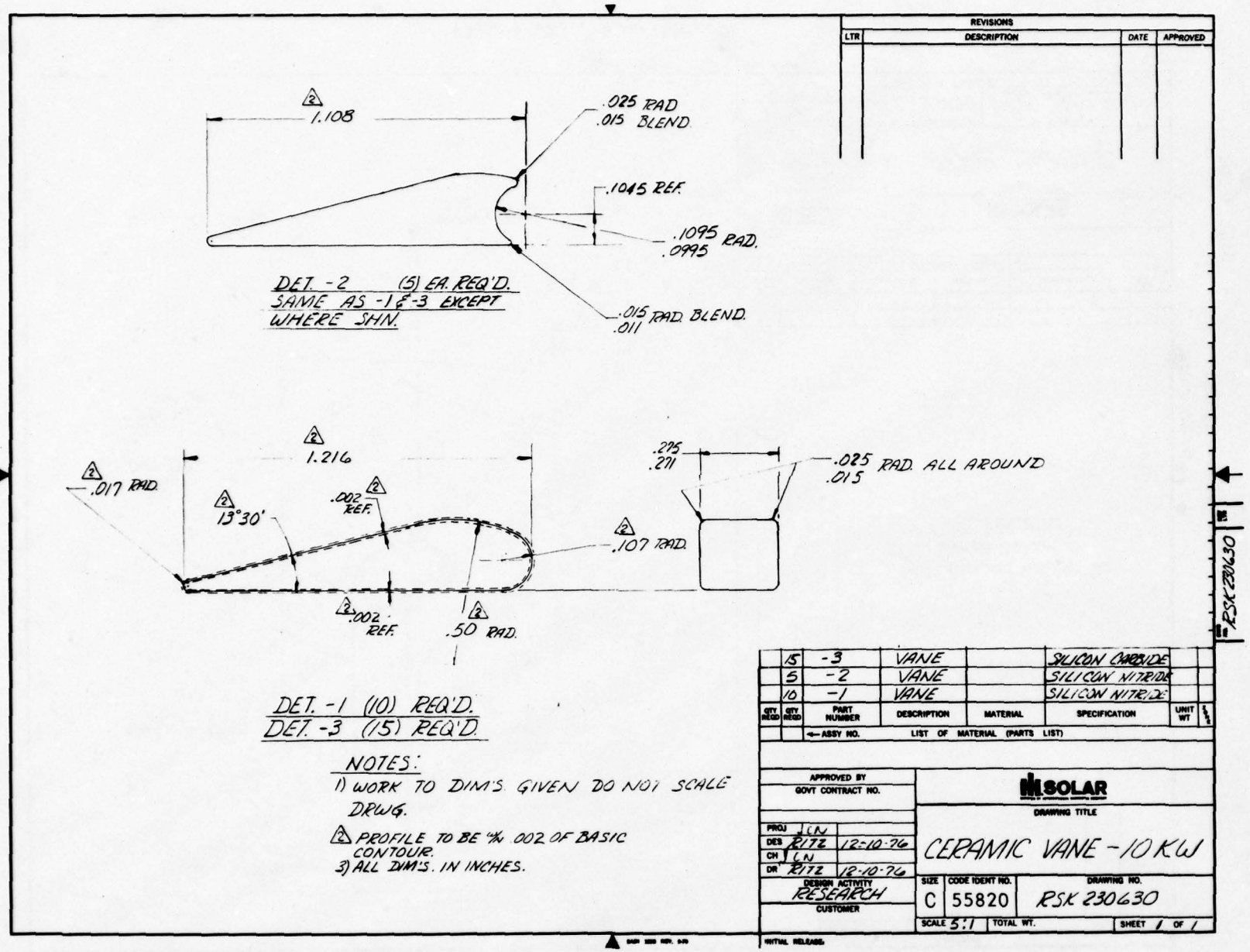

Figure 124. Ceramic Vane - 10 kW

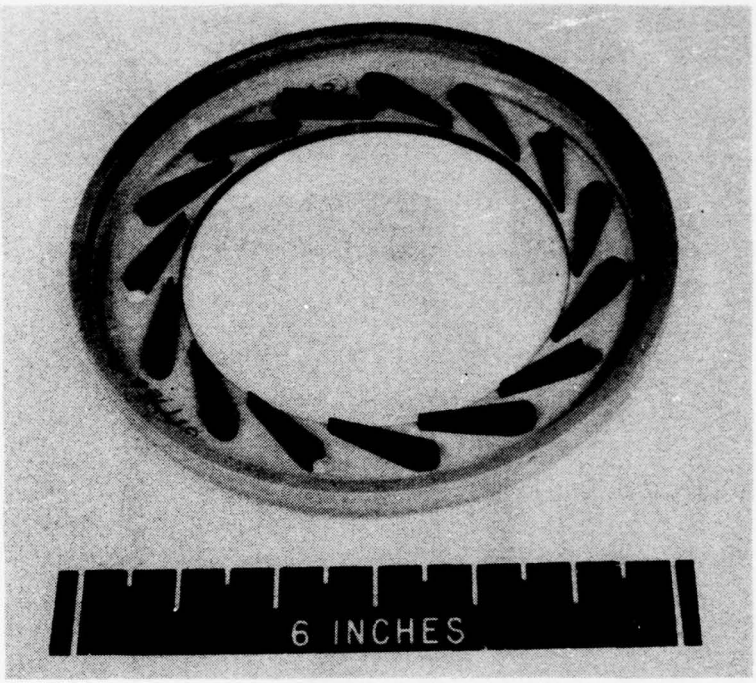

Figure 125. Reaction Bonded Silicon Nitride Forward Shroud With Hot Pressed Silicon Nitride Vanes in Place

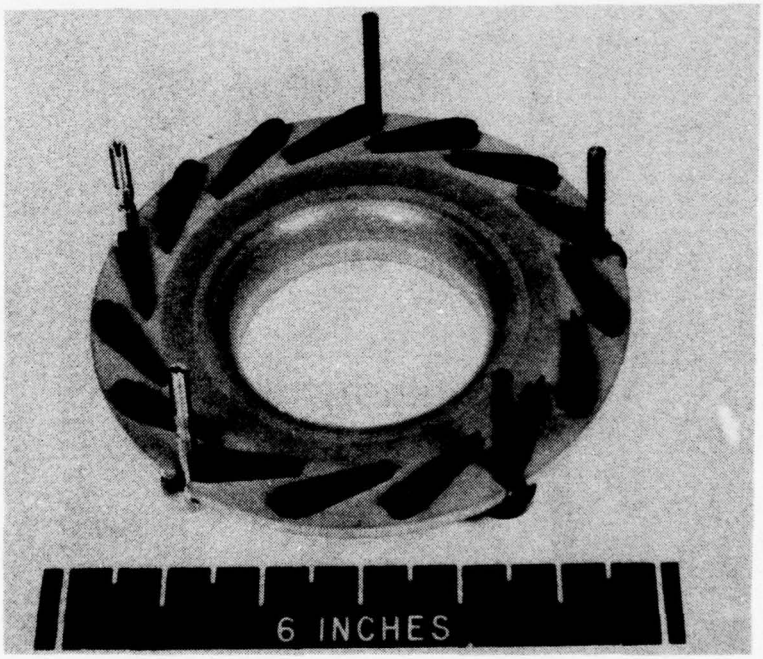

Figure 126. Reaction Bonded Silicon Nitride Rear Shroud With Hot Pressed Silicon Nitride Vanes, Hot Pressed Silicon Nitride Bolts (Concept 2) and Inco 718 Bolts (Concept 1) in Place

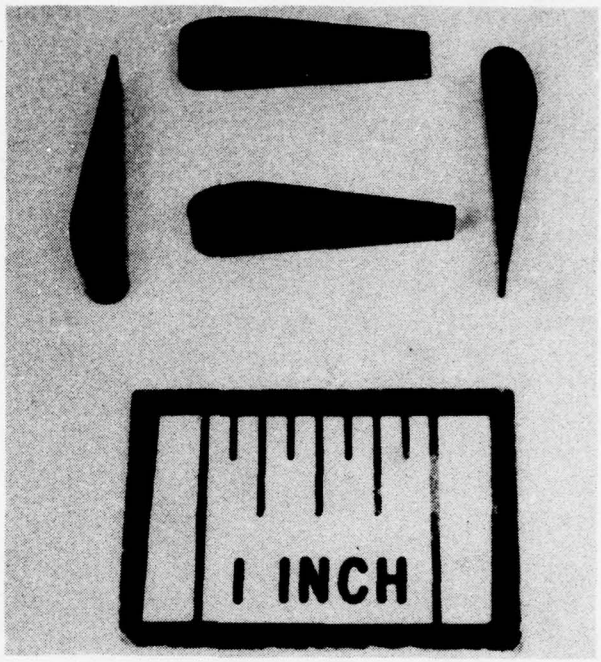

Figure 127. Hot Pressed Silicon Nitride Vanes RSK 230630, Detail 1

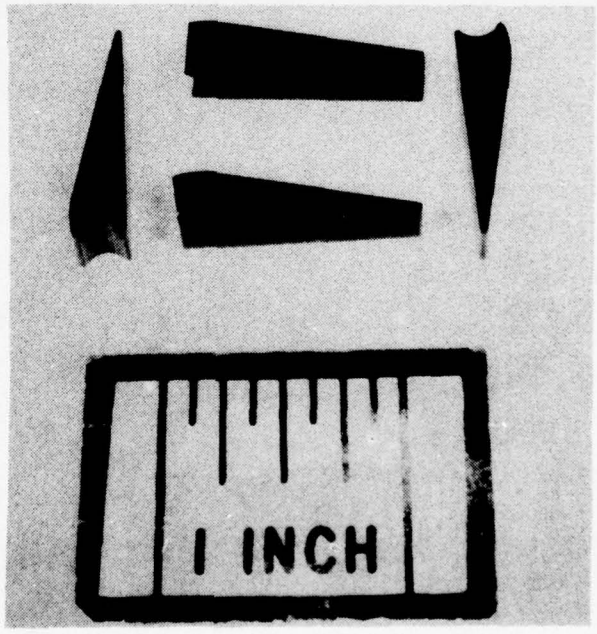

Figure 128. Hot Pressed Silicon Nitride Vanes RSK 230630, Detail 2

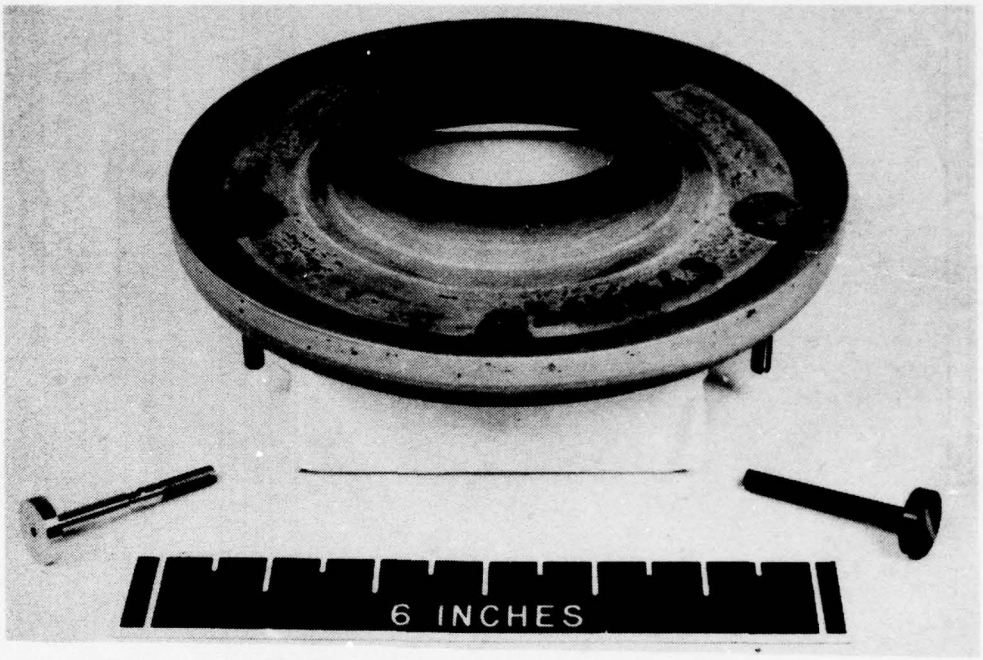

Figure 129. Ceramic Nozzle Shrouds and Bolts From: 718 Superalloy (Design Concept 1) and Hot Pressed Silicon Nitride (Design Concept 2)

3. A groove 0.030 inch deep was machined in this diffusor housing diameter at the region opposite to the position where the spring retaining can (RSK 230773) is attached to the nozzle retaining ring (RSK 230782) with the retaining cap pins (RSK 230781). This measure is to insure that the cap pins will not interfere with the diffusion housing at peak temperature conditions.

4. Five axial slots 0.015 inch wide and 0.5 inch deep were electro discharge machined in the combstor can housing section, which slips over the nozzle retaining ring. The slots have 3/32 inch holes at their termination point and foil spot tacked over these holes. This measure insures that this slip joint will not bind in a thermal downshock condition.

5. A 0.030 inch deep recess was machined into the inlet housing outer diameter face which matches with the combustor can outer diameter flange. The recess is placed such that the combustor can flange fits into it and automatically centers the two assemblies to each other.

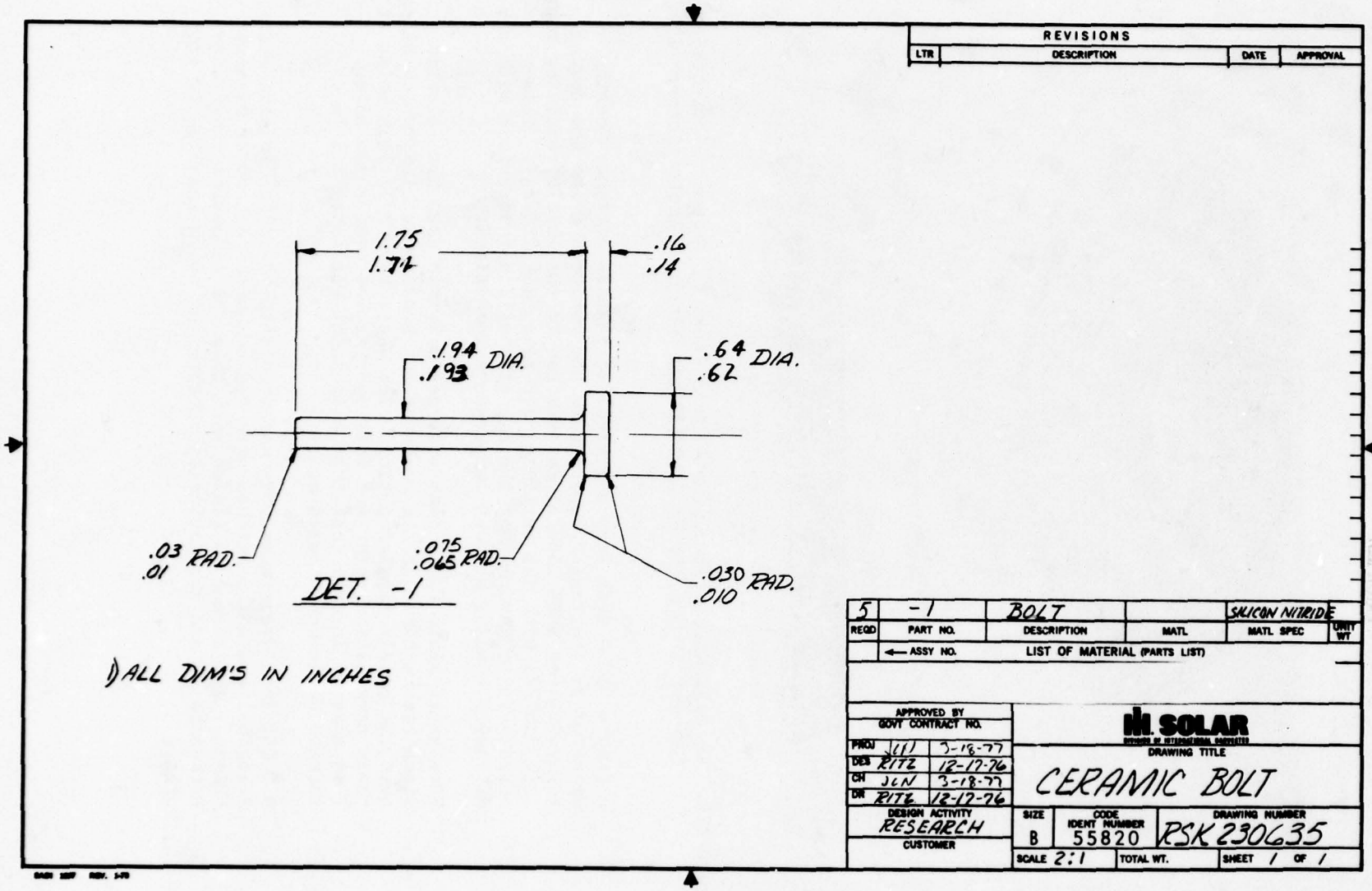

Figure 130. $HPSi_3N_4$ Ceramic Bolt

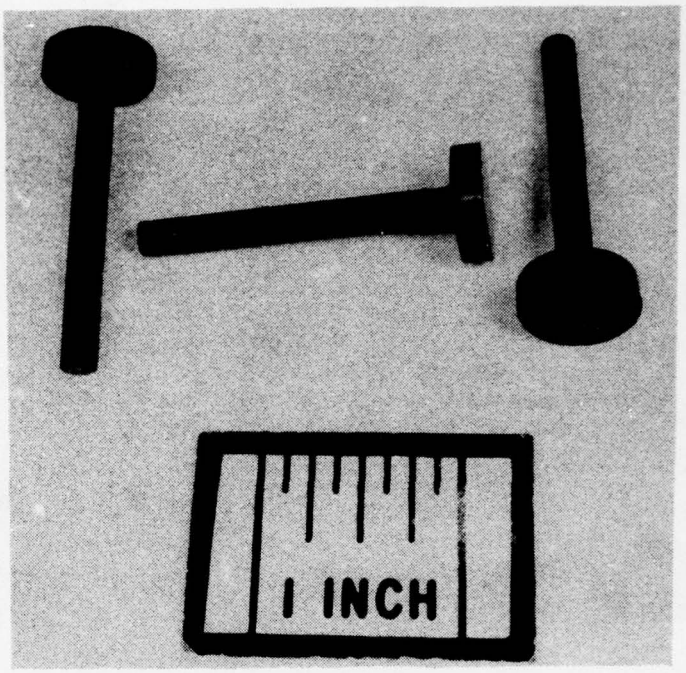

Figure 131. Hot Pressed Silicon Nitride Bolts, RSK 230635

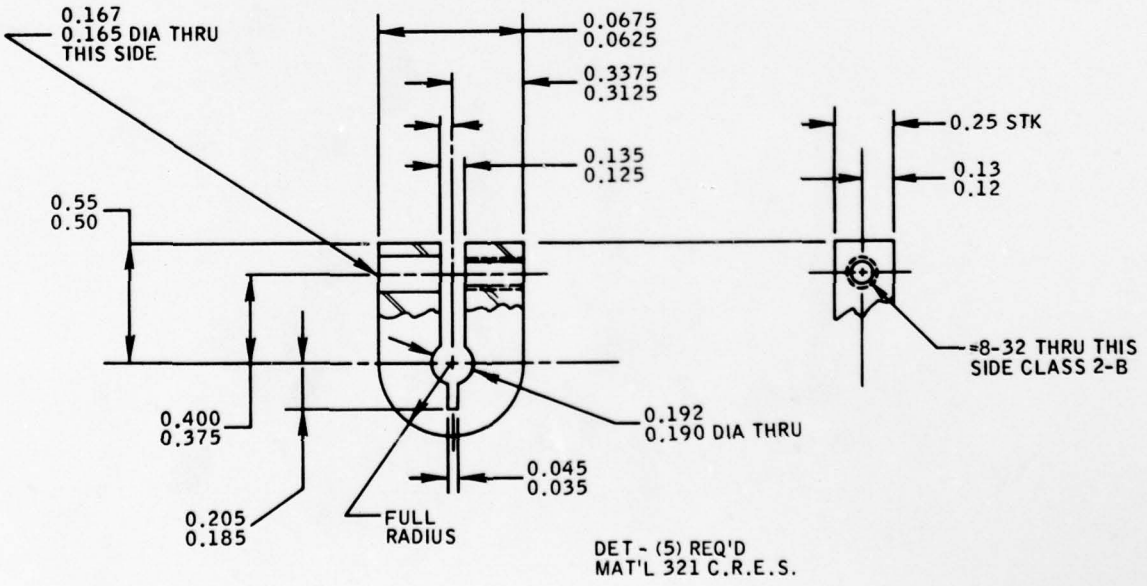

Figure 132. RSK 230786 - Collet Fastener for Ceramic Bolt

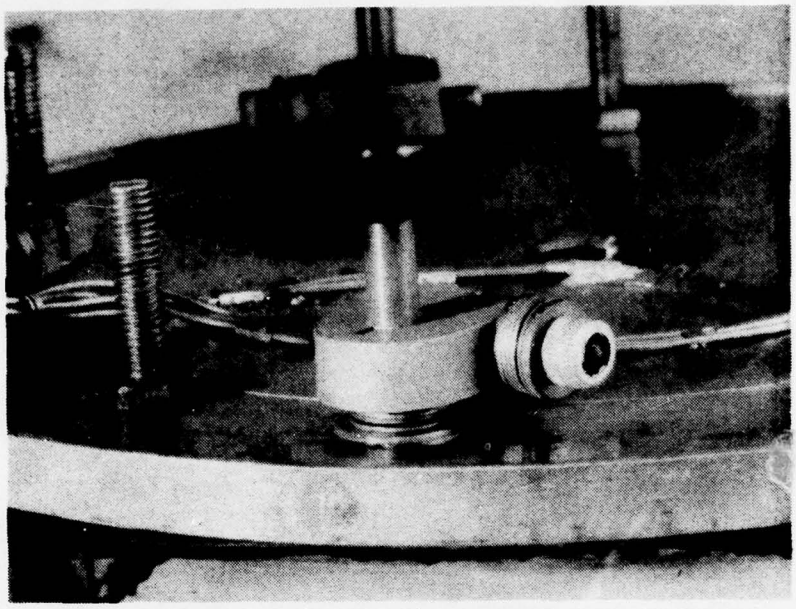

Figure 133. View of Collet Attachment of $HPSi_3N_4$ Ceramic Bolt

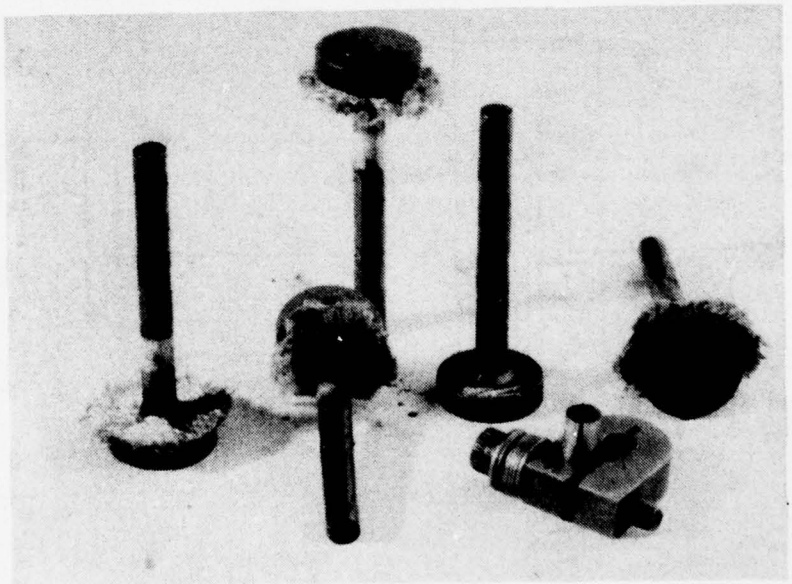

Figure 134. Ceramic Bolts ($HPSi_3N_4$ - NC 430) After 100 Cycle Furnace Rig Test. (Note high temperature Refrecell cloth at bolt head)

Table 15

Steady State Diametrical Growth at Seal Plate Interface for Various Materials (Inch)

Operation Point - Turbine Inlet Temperature °F	Compressor Housing	Seal Plate			Nozzle	
	6061 Al	321 CRAS	Incoloy 903	Invar	$RBSi_3N_4$	RCSiC
No Load						
950	0.0226	0.0227	0.0101	0.0047	0.0060	0.0090
1226	0.226	0.02701	0.0117	0.0071	0.0076	0.0115
1419	0.0271	0.3323	0.0138	0.0155	0.0091	0.0140
1900	0.0412	0.0605	0.0326	0.0364	0.0196	0.0249

Table 16

Steady State Diametrical Growth at Bolt Circle (Inch)

Operation Point - Turbine Inlet Temperature °F	Compressor Housing	Nozzle	
	6061 Al	$RBSi_3N_4$	RCSiC
No Load			
950	0.0259	0.0069	0.0103
1126	0.0259	0.00870	0.0132
1419	0.0317	0.0104	0.0160
1900	0.046	0.0224	0.0285

Table 17

Steady State Diametrical Growth at Downstream Turbine Wheel Diameter (Nozzle ID) (Inch)

Operation Point - Turbine Inlet Temperature	Turbine Wheel	Shroud	
	713LC Superalloy	$RBSi_3N_4$	RCSiC
No Load			
950	0.0109	0.0022	0.0034
1226	0.0146	0.0028	0.0044
1419	0.0189	0.0038	0.0058
1900	0.0318	0.0066	0.00953

Table 18

Emergency Shutdown Thermal Sizes (Inch)

Location	Compressor Housing	Seal Plate	Nozzle Shroud		Turbine Wheel
	6061 Al	Incoloy 903	Si_3N_4	SiC	713LC Superalloy
Bolt Circle Diameter	0.0126	--	0.0009	0.0018	--
Seal Plate Diameter	0.011	0.004	0.0008	0.0016	--
Downstream Turbine Wheel Diameter	--	--	0.0004	0.0009	0.003

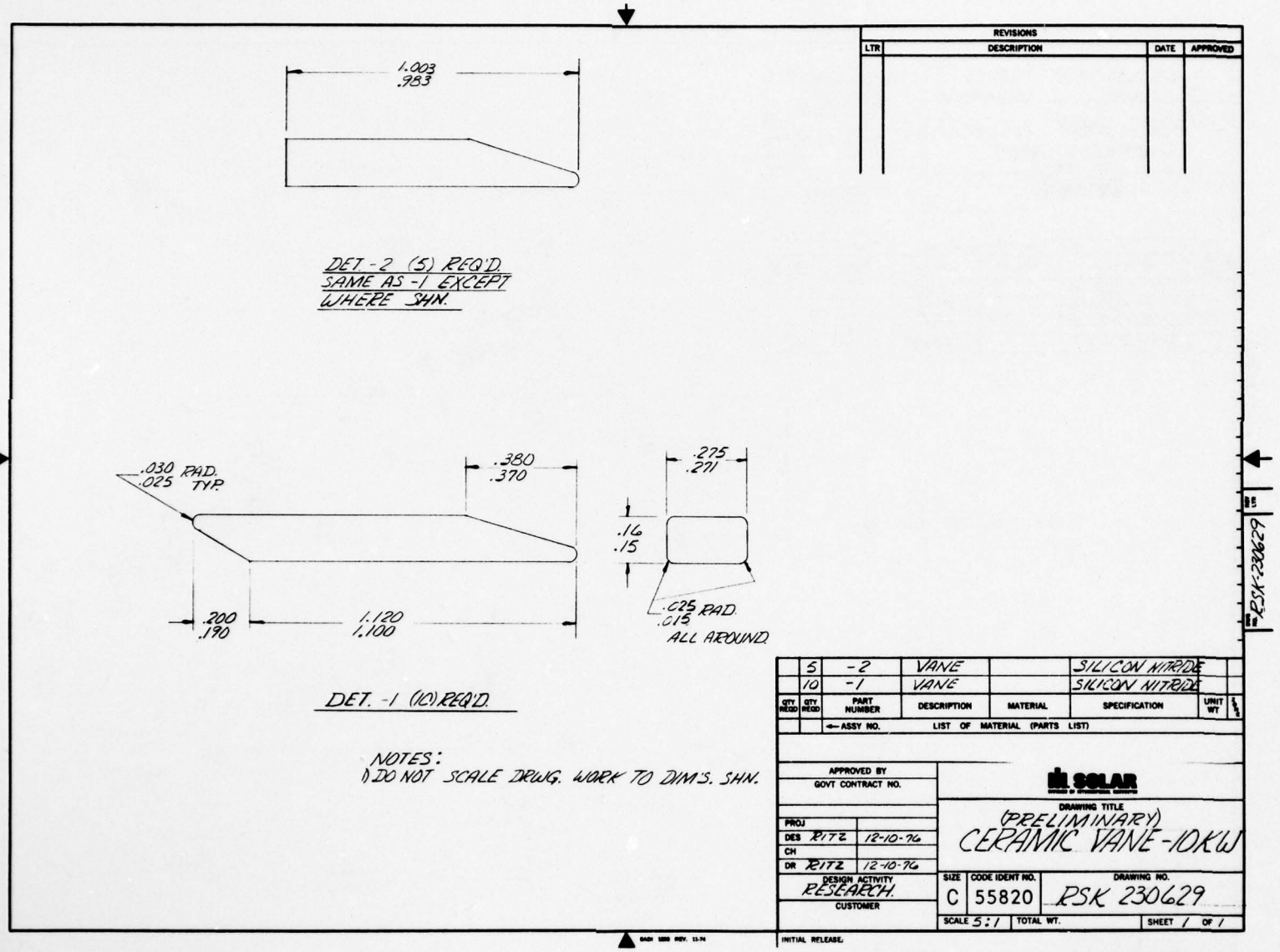

Figure 135. First Ceramic Vane Design Alternative for All-Ceramic Nozzle

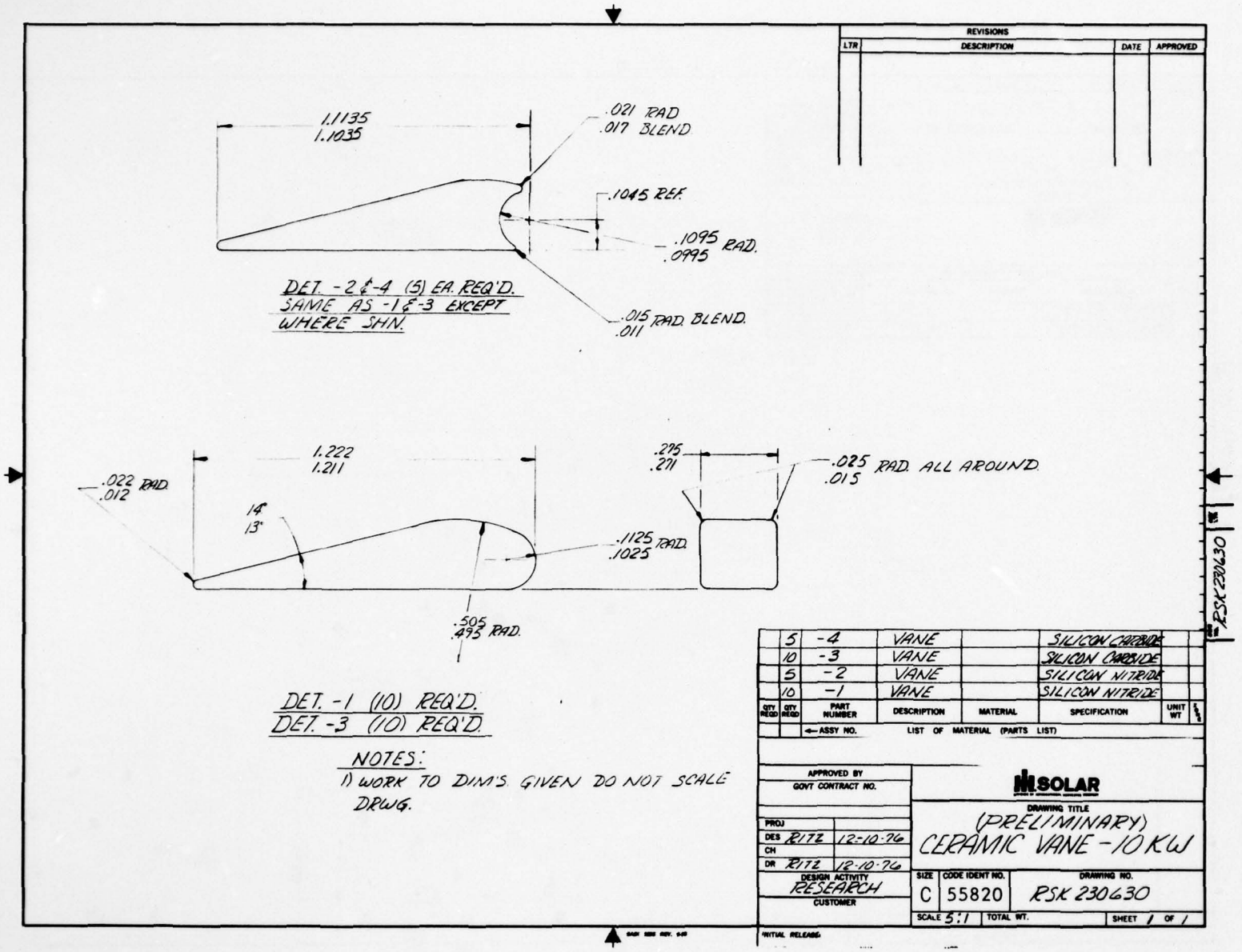

Figure 136. Second Ceramic Vane Design Alternative for All-Ceramic Nozzle

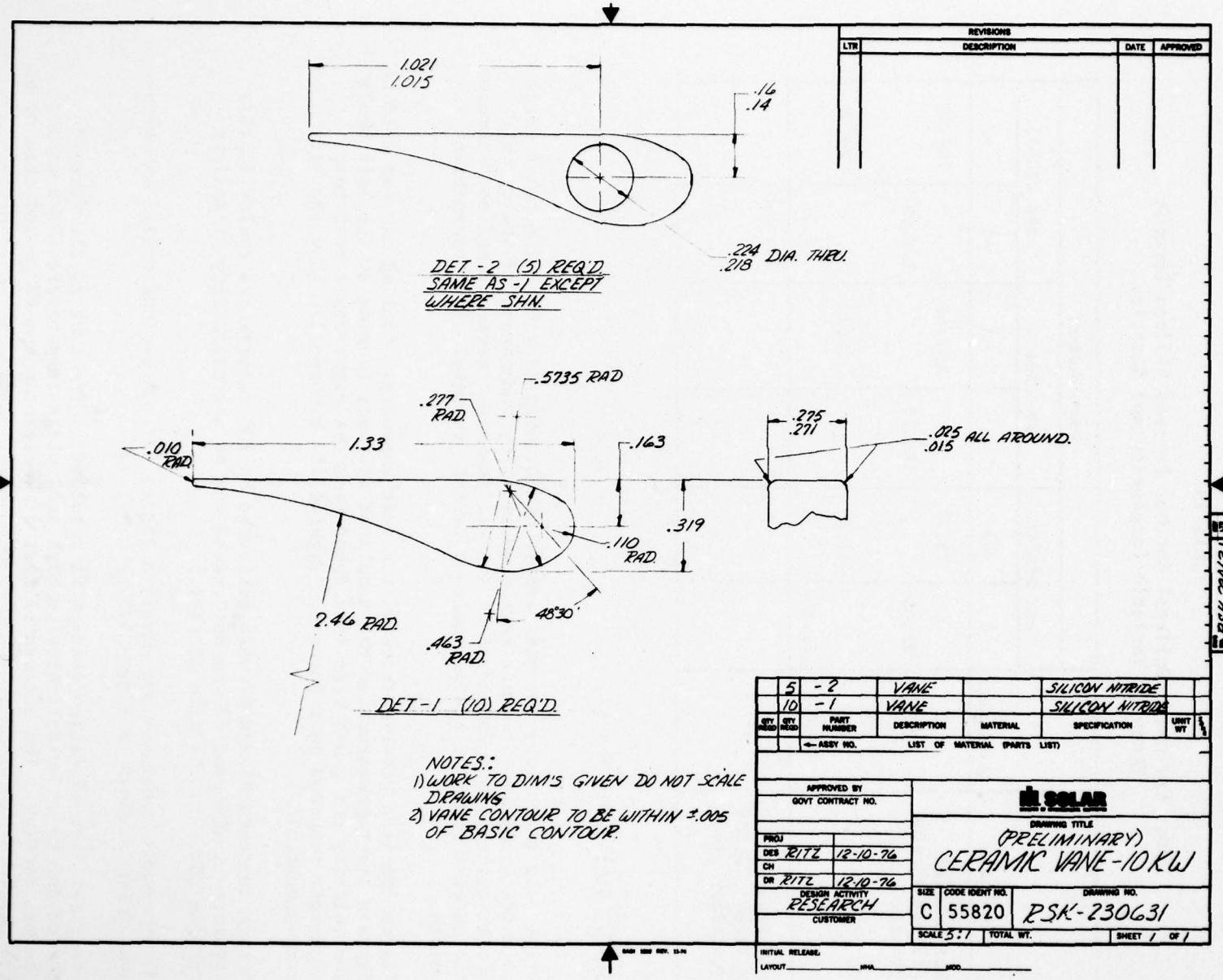

Figure 137. Third Ceramic Vane Design Alternative for All-Ceramic Nozzle

Table 19

Cost Estimate (Dollars) for Hot Pressed Silicon Ceramic Vanes of Variable Complexity and Quantity

Material	Quantity	Part Number					
		RSK 230629		RSK 230630		RSK 230631	
		-1	-2	-1	-2	-1	-2
Hot Pressed Silicon Nitride (Ceralloy 147)	11		73.79		137.68		194.93
	22	78.05		106.16		123.59	
	33						
	500		48.67		59.33		49.51
	1000	51.96				64.51	
Hot Pressed Silicon Carbide (Ceralloy 146A)	1500					58.82	

3.4.6 *Static Rig Tests*

Static rig tests were for the purpose of investigating the effects of large relative growths of ceramic versus metal alloy components on the ceramic nozzle assemblies independent of thermal transient stresses and to determine the effectiveness of static seals at ceramic to metal alloy transition points.

Figure 166 is a cross-section of the test assembly. Cooling air was used to depress the temperature of the simulated diffusor housing at the left while low velocity hot gases were introduced from the right via a coil heat exchanger immersed in a furnace. Figures 167 through 170 show the test arrangement.

Design concepts #1 and #2 were subjected to 100 temperature cycles in this apparatus. (Concept #3 was not tested due to unavailability of silicon carbide parts at the time of test.)

Thermocouple locations are given in Figure 171. A typical cyclic temperture excursion is shown in Figure 172.

The first test of design concept #1 resulted in fracture of the forward shroud due to an unrealistically high seal plate temperature which caused thermal binding. The successful test of design concept #2 proved this to be the case.

Table 20

Procurement Schedule for Ceramic Components

Design Concept	Component	Material	Quantity
1	Forward Shroud RSK 230632	$RBSi_3N_4$ NC-350	3
	Rear Shroud RSK 230633	$RBSi_3N_4$ NC-350	3
	Vane-Long RSK 230630-1	$HPSi_3N_4$ NC-132	11
	Vane - Short RSK 230630-2	$HPSi_3N_4$ NC-132	6
2	Forward Shroud RSK 230632	$RBSi_3N_4$ NC-350	3
	Forward Shroud RSK 230633	$RBSi_3N_4$ NC-350	3
	Vane - Long RSK 230630-1	$HPSi_3N_4$ NC-132	10
	Vane - Short RSK 230630-2	$HPSi_3N_4$ NC-132	5
	Bolt RSK 230635	$HPSi_3N_4$ NC-132	7
3	Forward Shroud RSK 230636	RCSiC NC-430	3
	Rear Shroud RSK 230637	RCSiC NC-430	3
	Vane RSK 230630-3	HPSiC NC-203	31
Bond one nozzle assembly including one RSK 230636, fifteen RSK 230630-3 and one RSK 230637.			

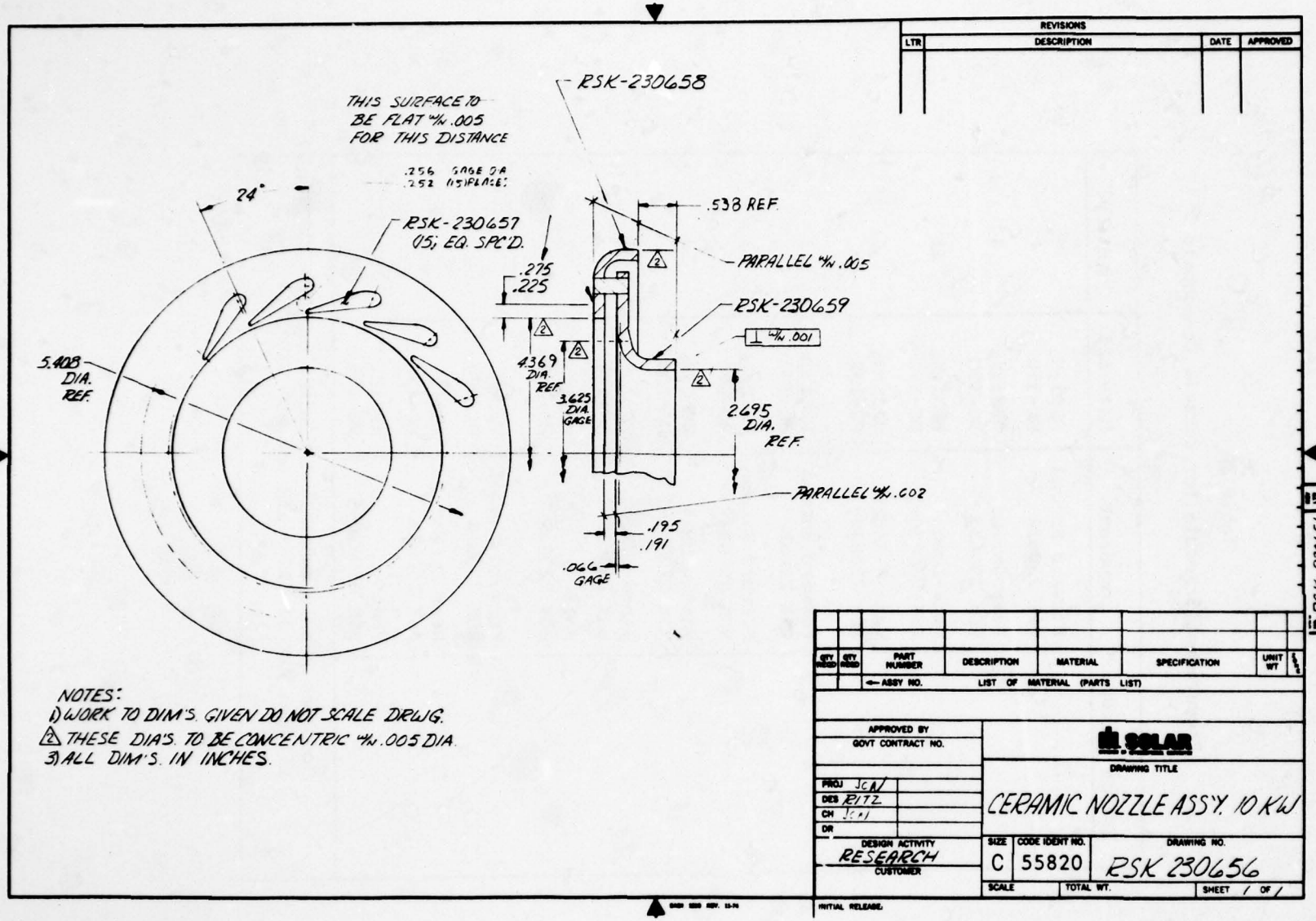

Figure 138. Ceramic Nozzle Assembly 10 kW

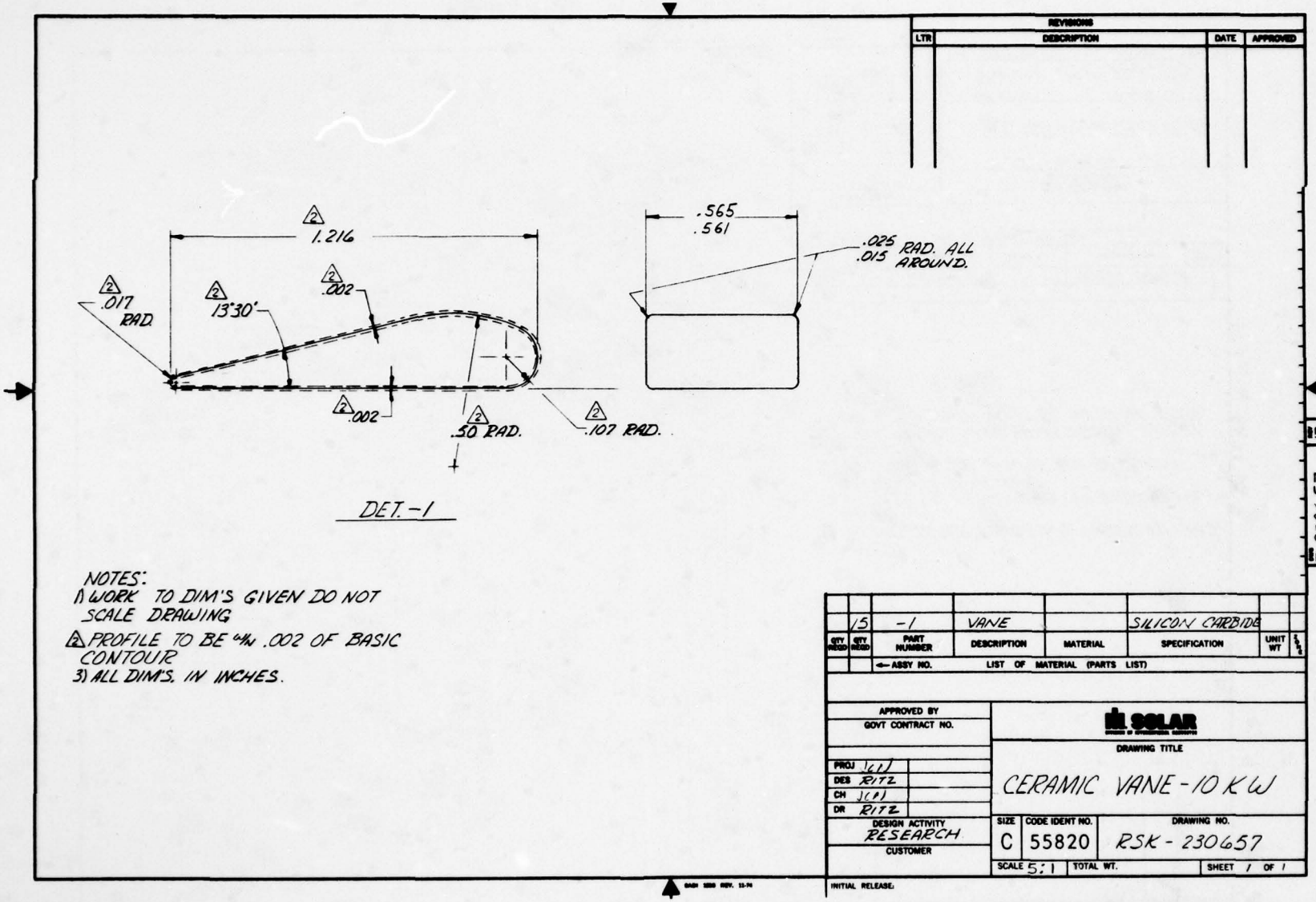

Figure 139. Ceramic Vane - 10 kW

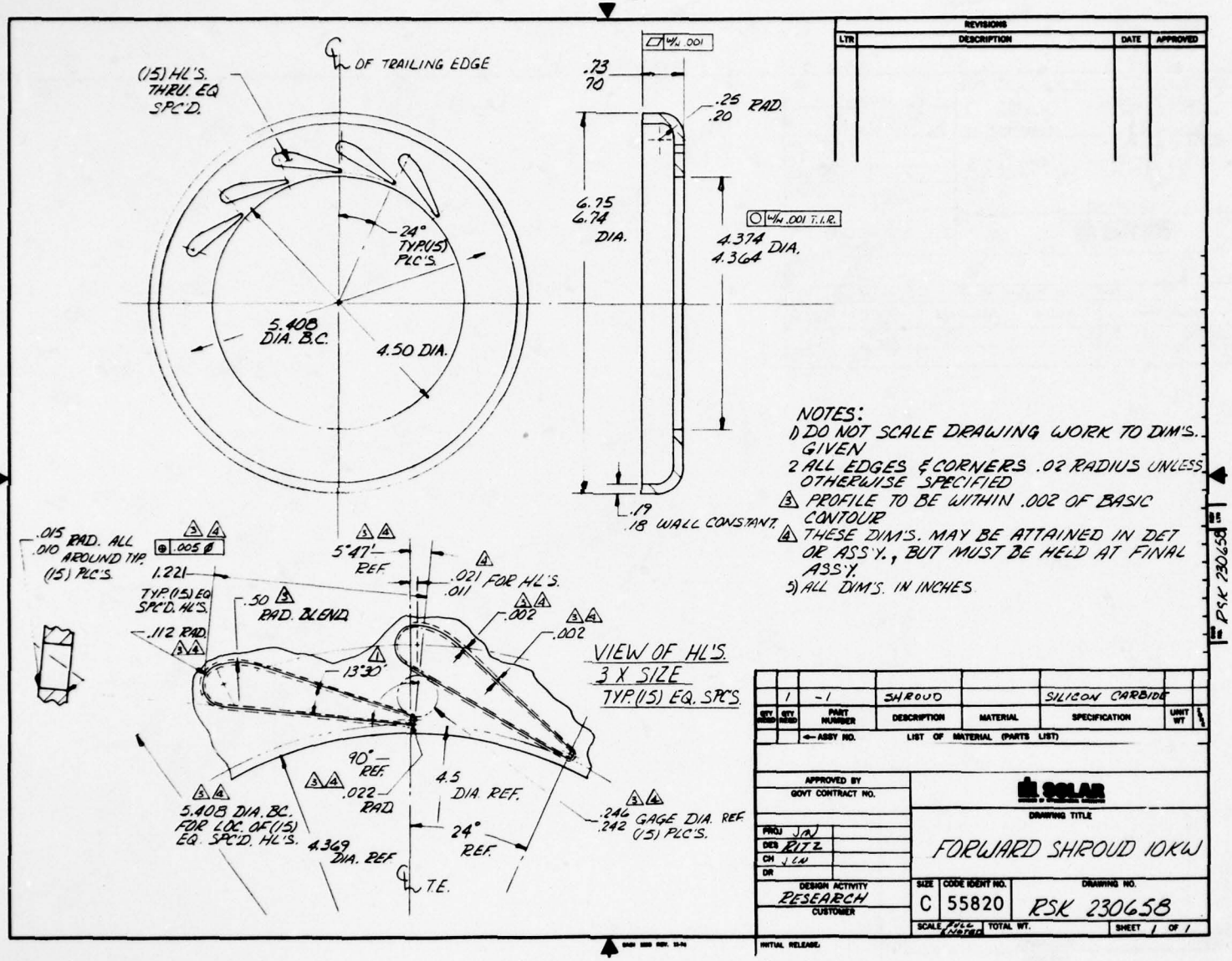

Figure 140. Forward Shroud - 10 kW

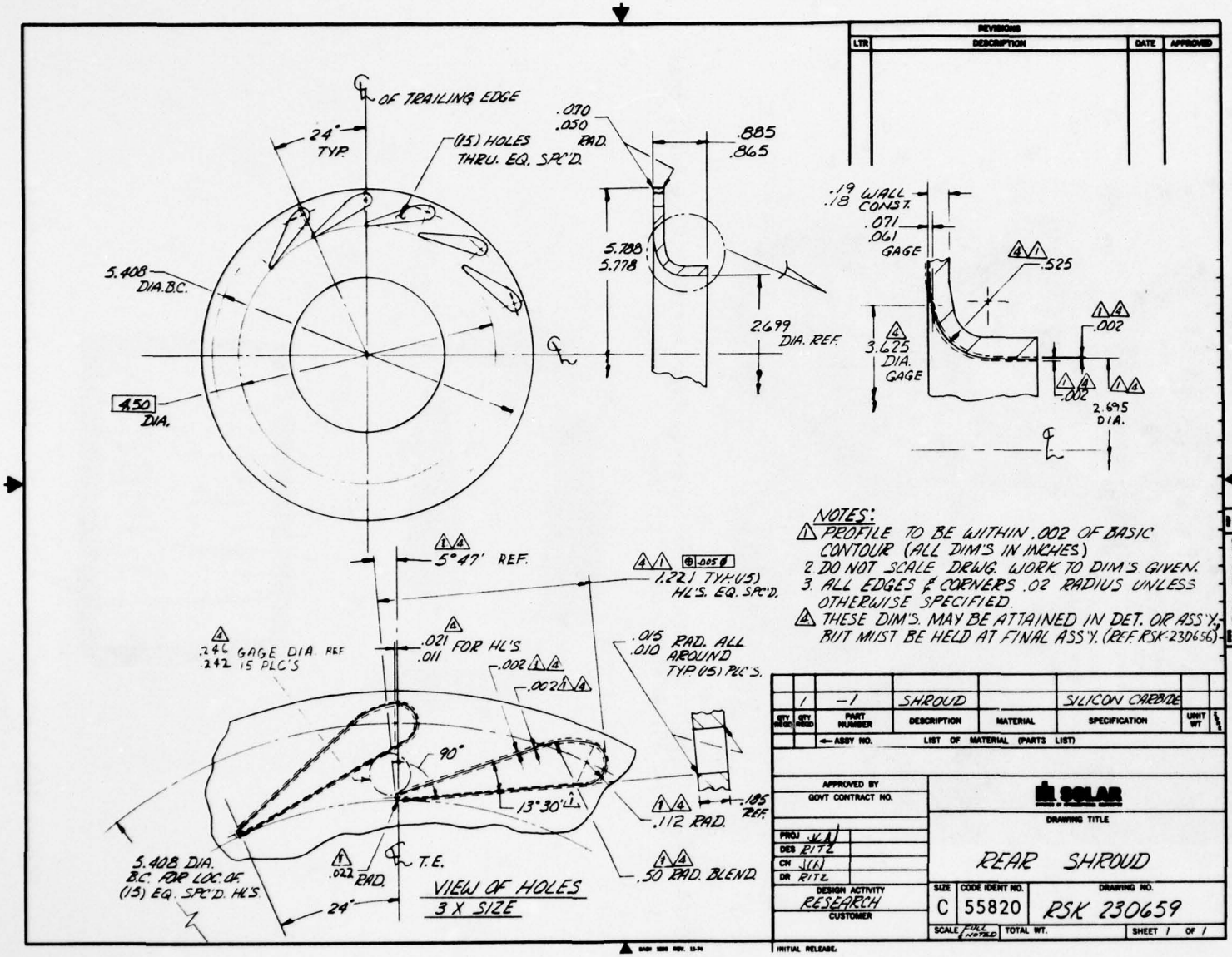

Figure 141. Rear Shroud

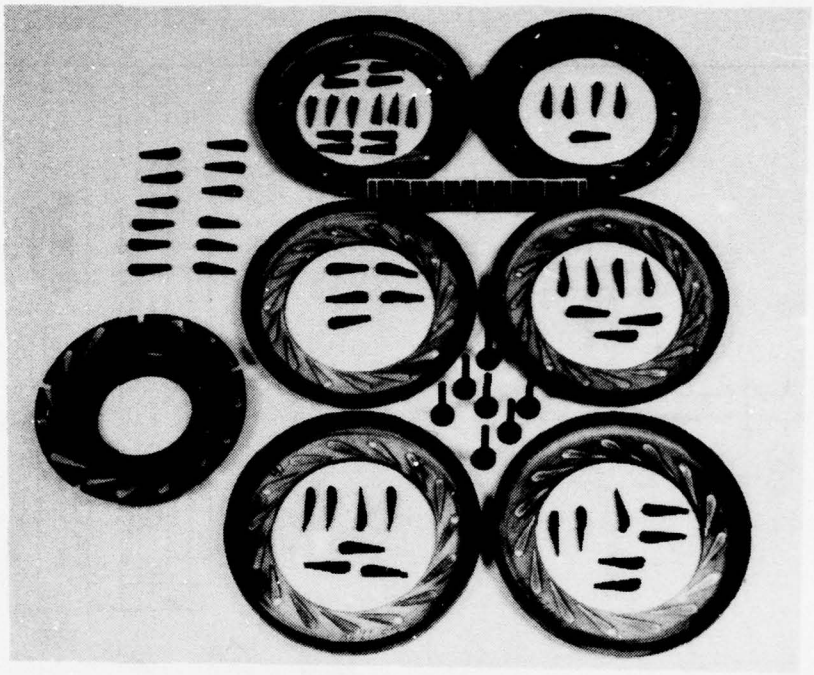

Figure 142. Ceramic Components As-Received From Norton. Five Additional NC 350 Rear Shrouds Not Shown

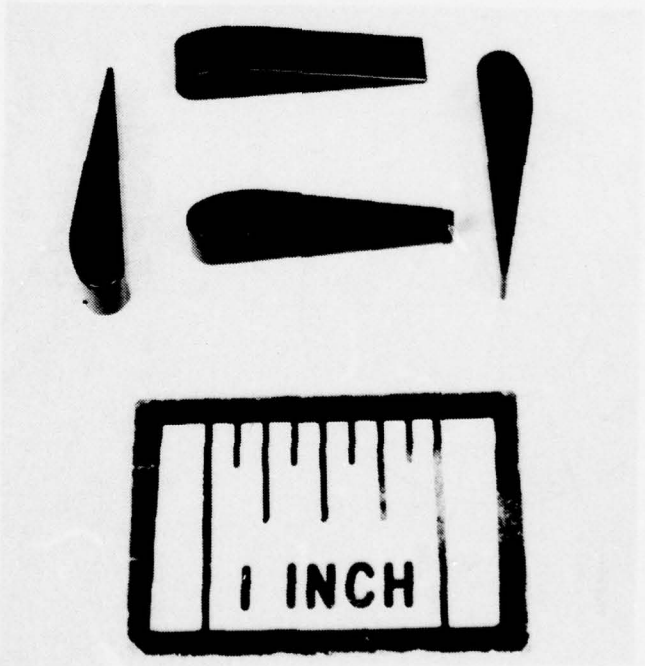

Figure 143. Hot Pressed Silicon Nitride Vanes RSK 230630, Detail 1

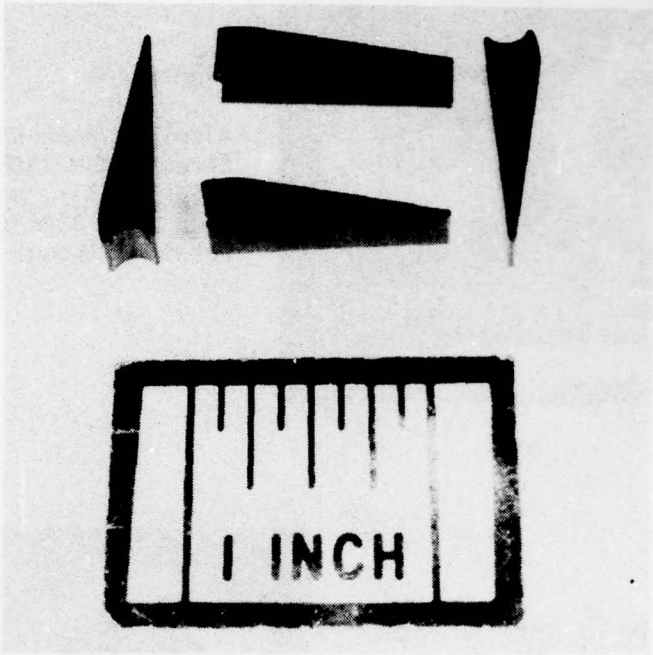

Figure 144. Hot Pressed Silicon Nitride Vanes RSK 230630, Detail 2

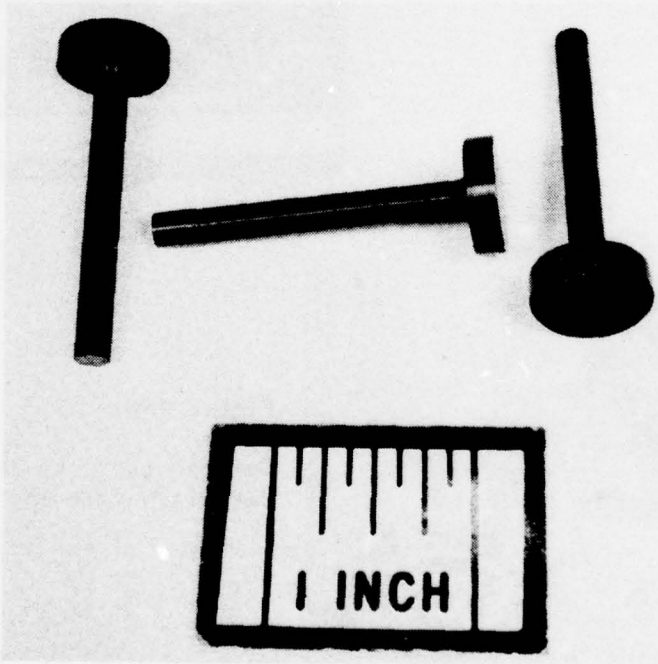

Figure 145. Hot Pressed Silicon Nitride Bolts, RSK 230635

AD-A081 184 SOLAR TURBINES INTERNATIONAL SAN DIEGO CA F/G 21/5
APPLICATION OF CERAMIC NOZZLES TO 10 KW ENGINE.(U)
DEC 78 J C NAPIER, A G METCALFE, T E DUFFY DAAK02-75-C-0138
UNCLASSIFIED SR80-R-4375-43 NL

3 OF 3
AD-
A081184

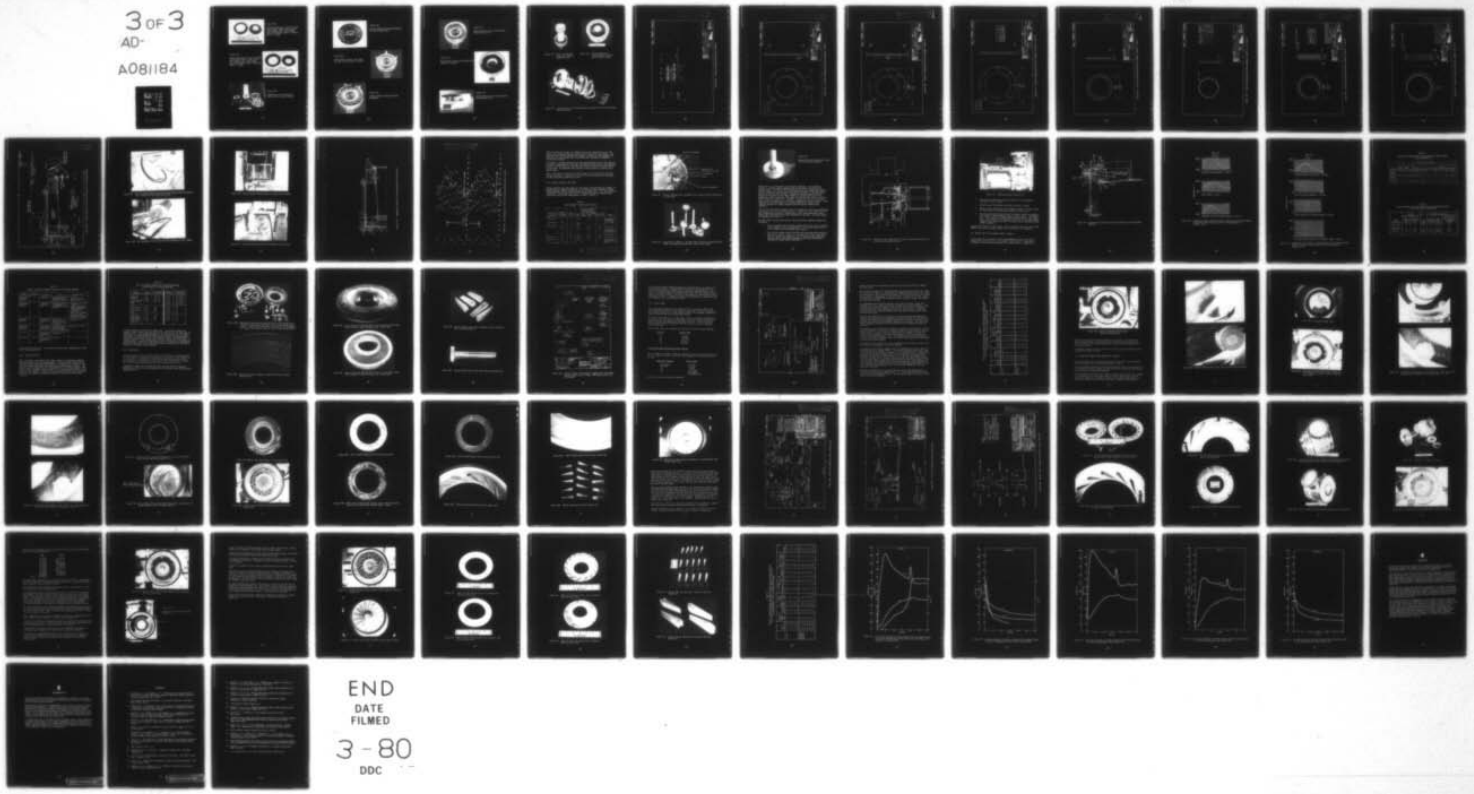

END
DATE
FILMED
3-80
DDC

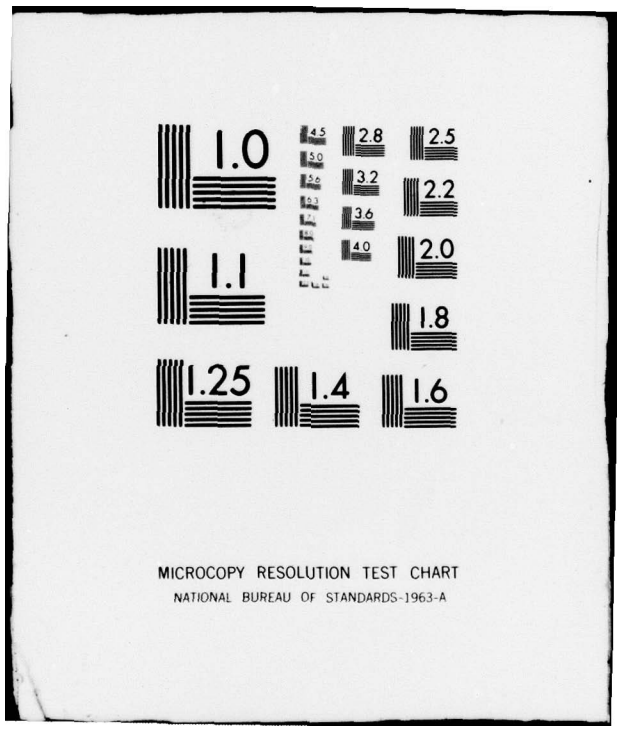
1.0
1.1
1.25
1.4
1.6
1.8
2.0
2.2
2.5
2.8
3.2
3.6
4.0
4.5
5.0
5.6
6.3
MICROCOPY RESOLUTION TEST CHART
NATIONAL BUREAU OF STANDARDS-1963-A

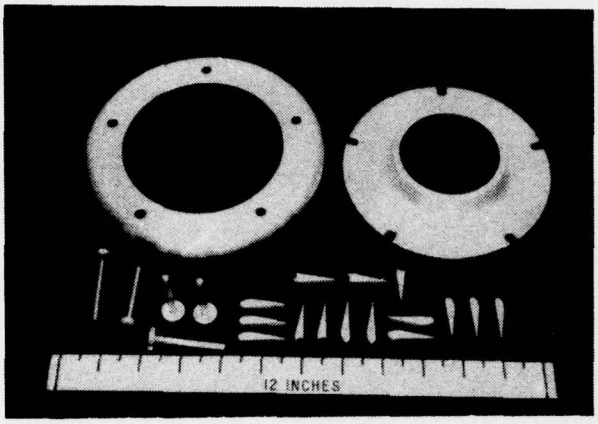

Figure 146.

Aluminum Mock-Up of Ceramic Forward Shroud (RSK 230632), Rear Shroud (RSK 230633), Bolt (RSK 230635), Vane (RSK 230630), Detail 2 (Short), Detail 1 (Long)

Figure 147.

Aluminum Mock-Up of Ceramic Forward Shroud (RSK 230632), Rear Shroud (RSK 230633), Bolt (RSK 230635, Vane (RSK 230630), Detail 2 (Short), Detail 1 (Long).

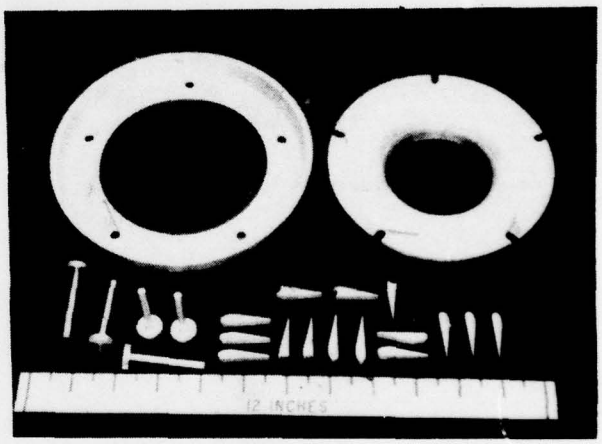

Figure 148.

Components to be Included in Ceramic Nozzle Engine Assembly

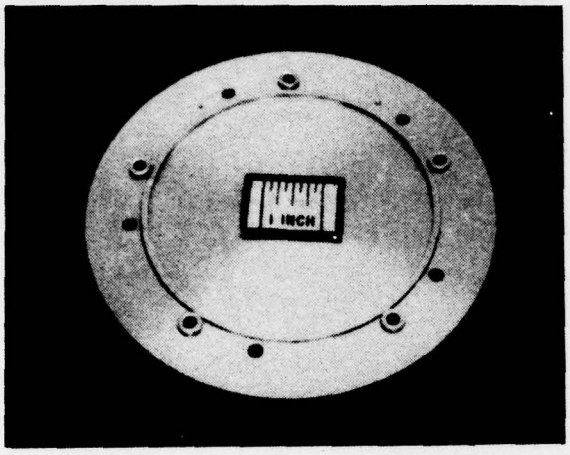

Figure 149.

Fixture Simulating Diffuser Housing for Rig Furnace Tests

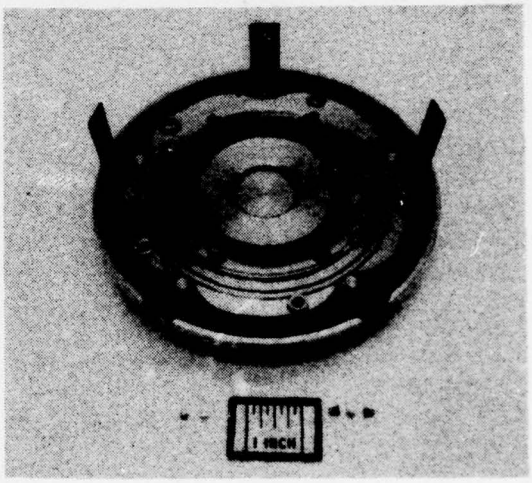

Figure 150.

Spring Retaining Can, Seal Plate and Seal Plate Diaphram Installed

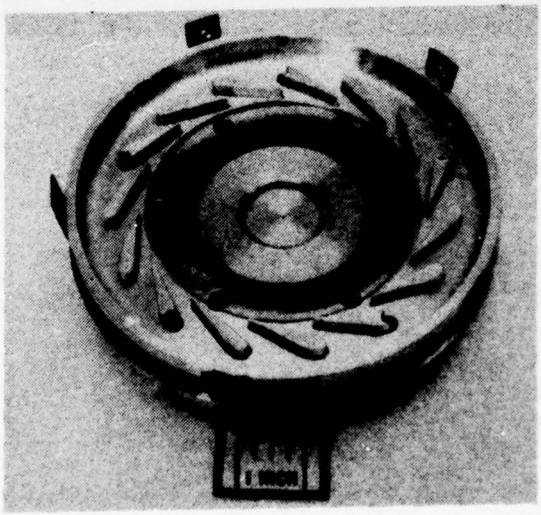

Figure 151.

Forward (Outer) Shroud and Vanes Installed

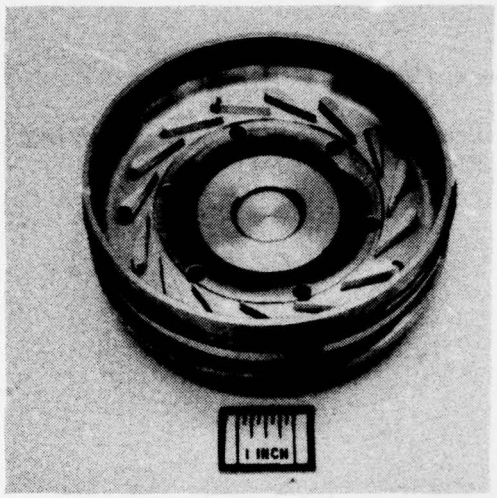

Figure 152.

Nozzle Retainer Ring Installed With Retaining Cap Pins

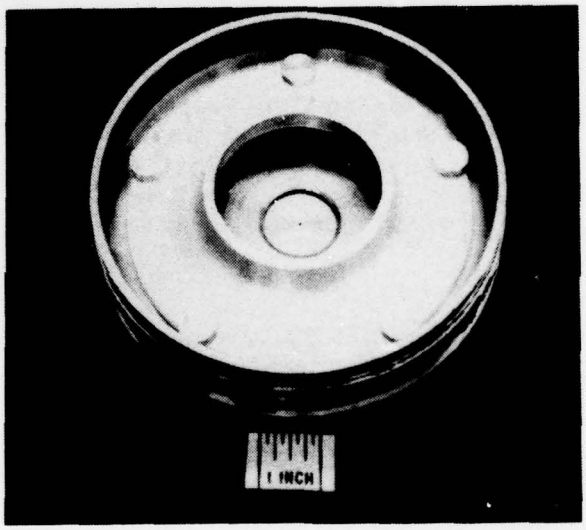

Figure 153.

Rear (Inner) Shroud and Through Bolts (Ceramic) Installed

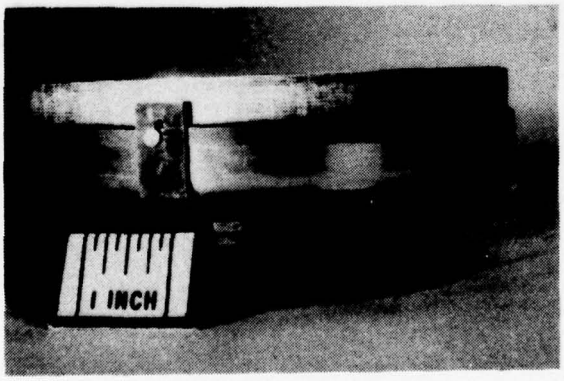

Figure 154.

Nozzle Retainer Ring Installed With Retaining Cap Pins

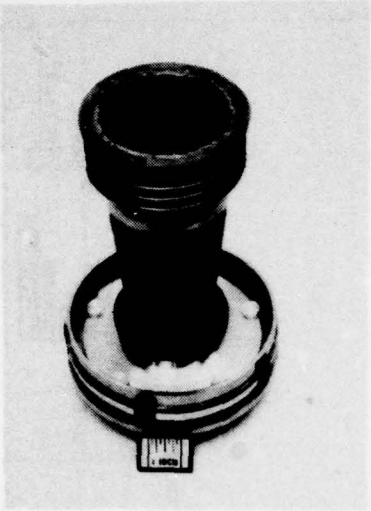

Figure 155. Scroll and Bellows Positioned (Without Combustor Case)

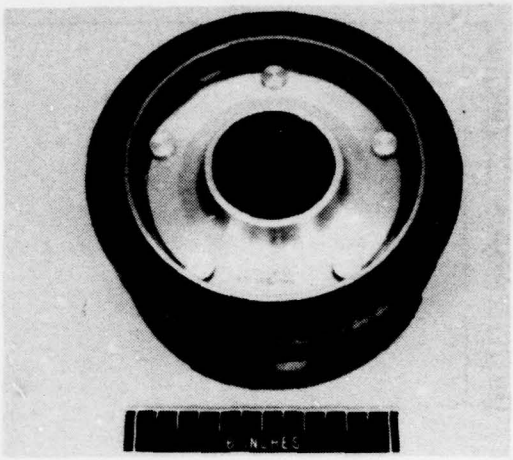

Figure 156. Aluminum Mock-Up of Ceramic Nozzle in 10 kW Inlet-Diffuser Housing

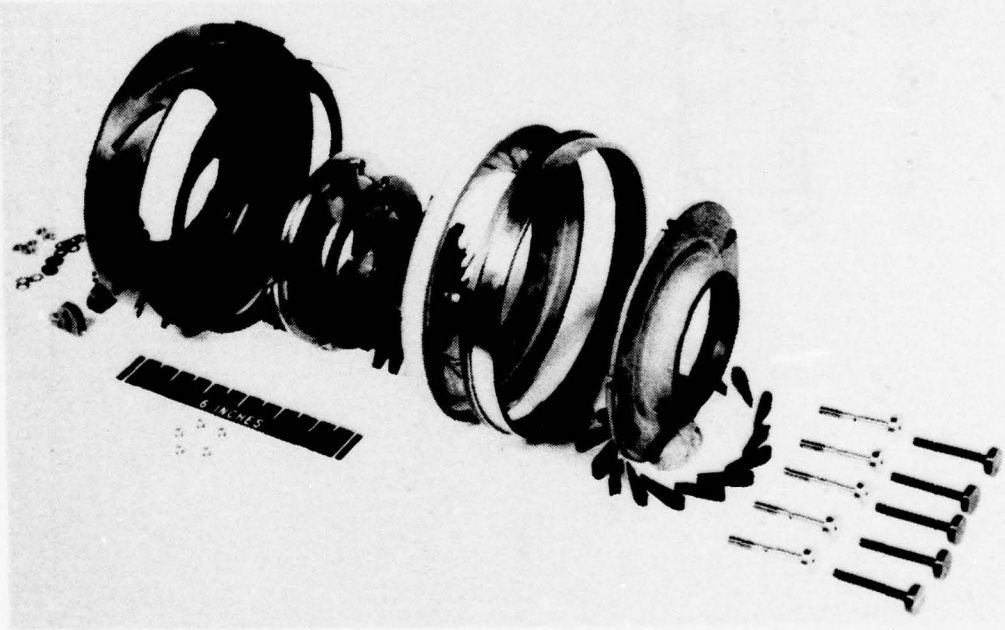

Figure 157. Exploded View of All-Ceramic Nozzle Components With Si_3N_4 Shrouds, Vanes and Bolts

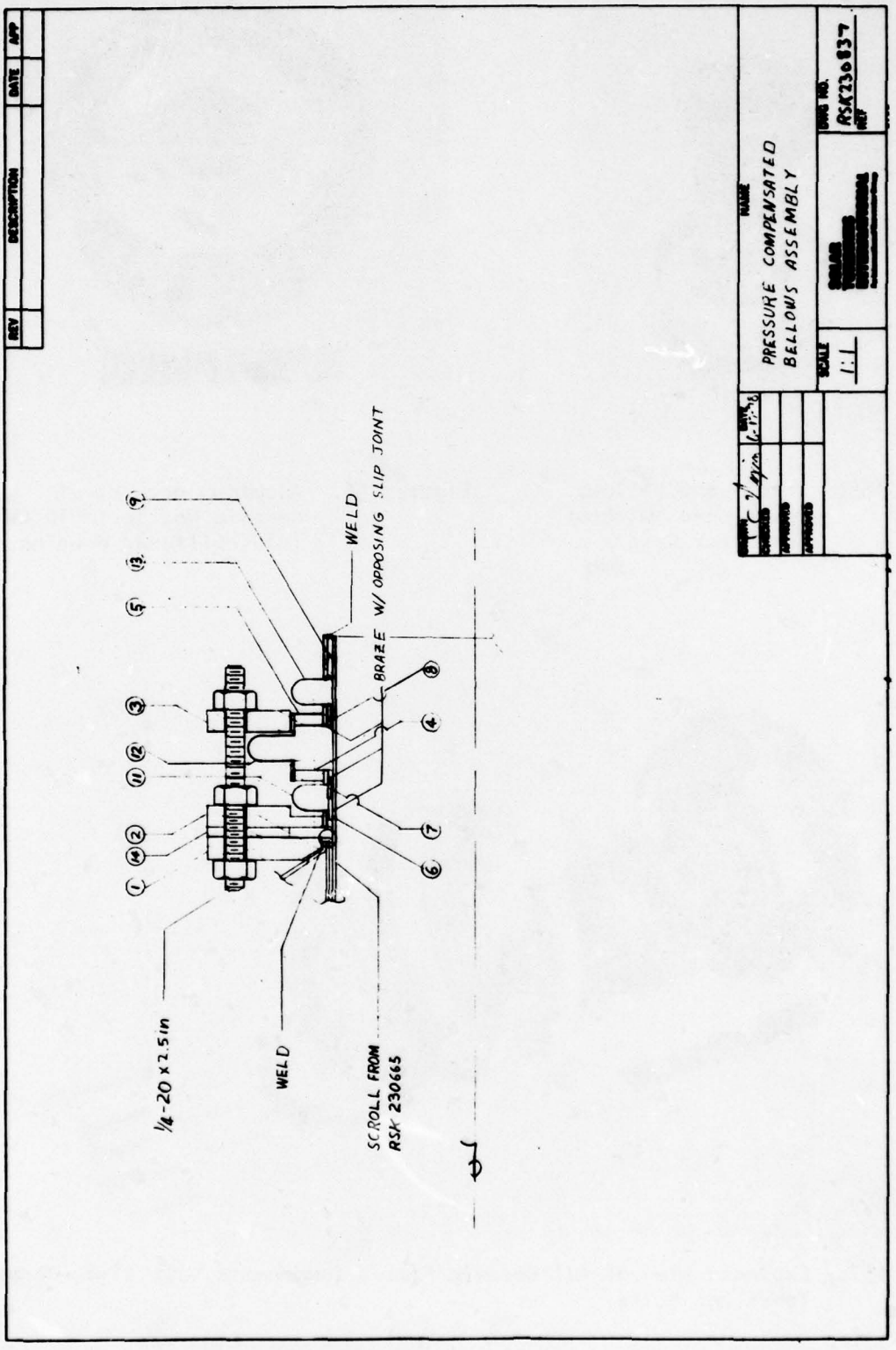

Figure 158. Pressure Compensated Bellows Assembly

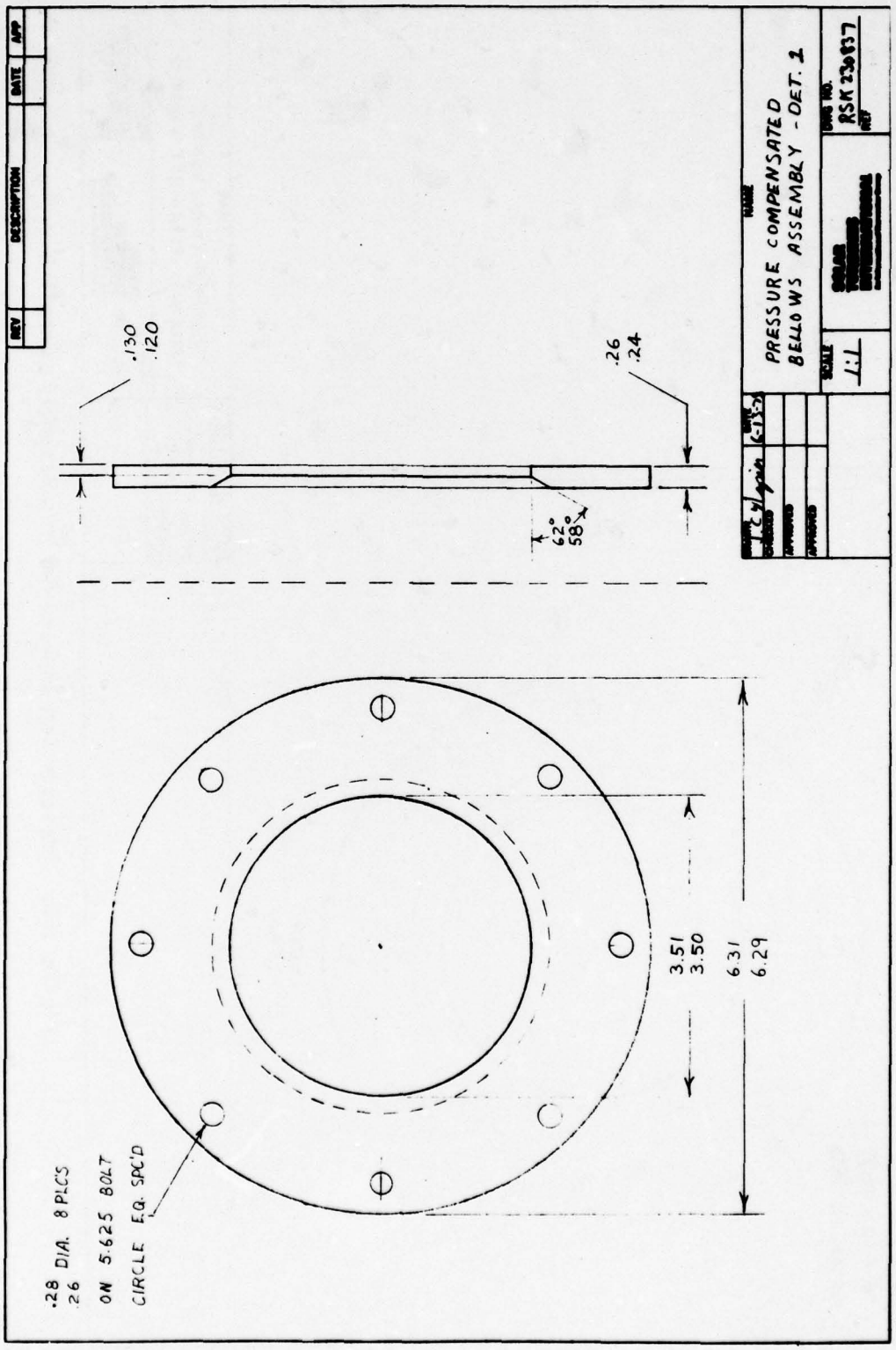

Figure 159. Pressure Compensated Bellows Assembly, Detail 1

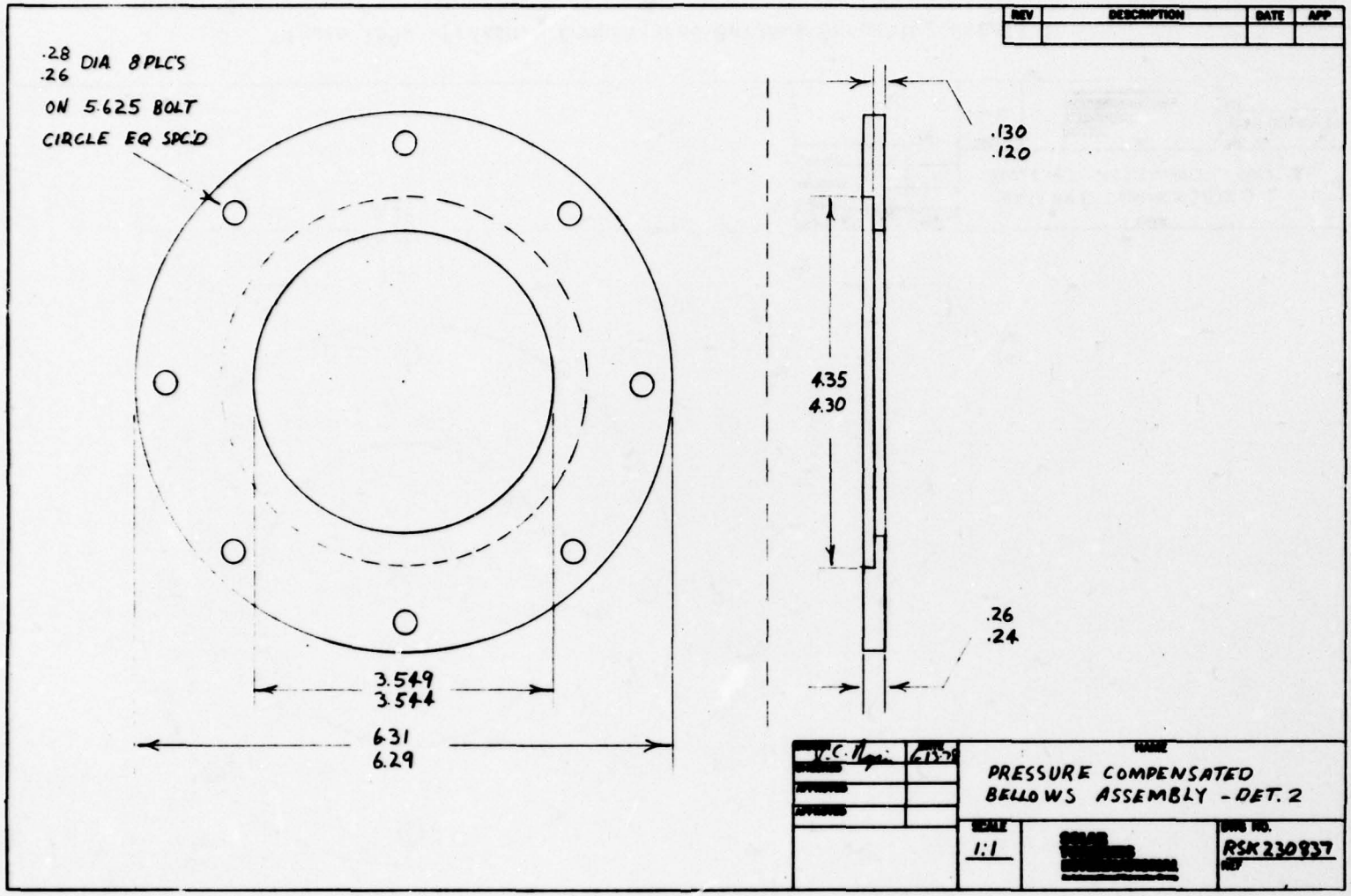

Figure 160. Pressure Compensated Bellows Assembly, Detail 2

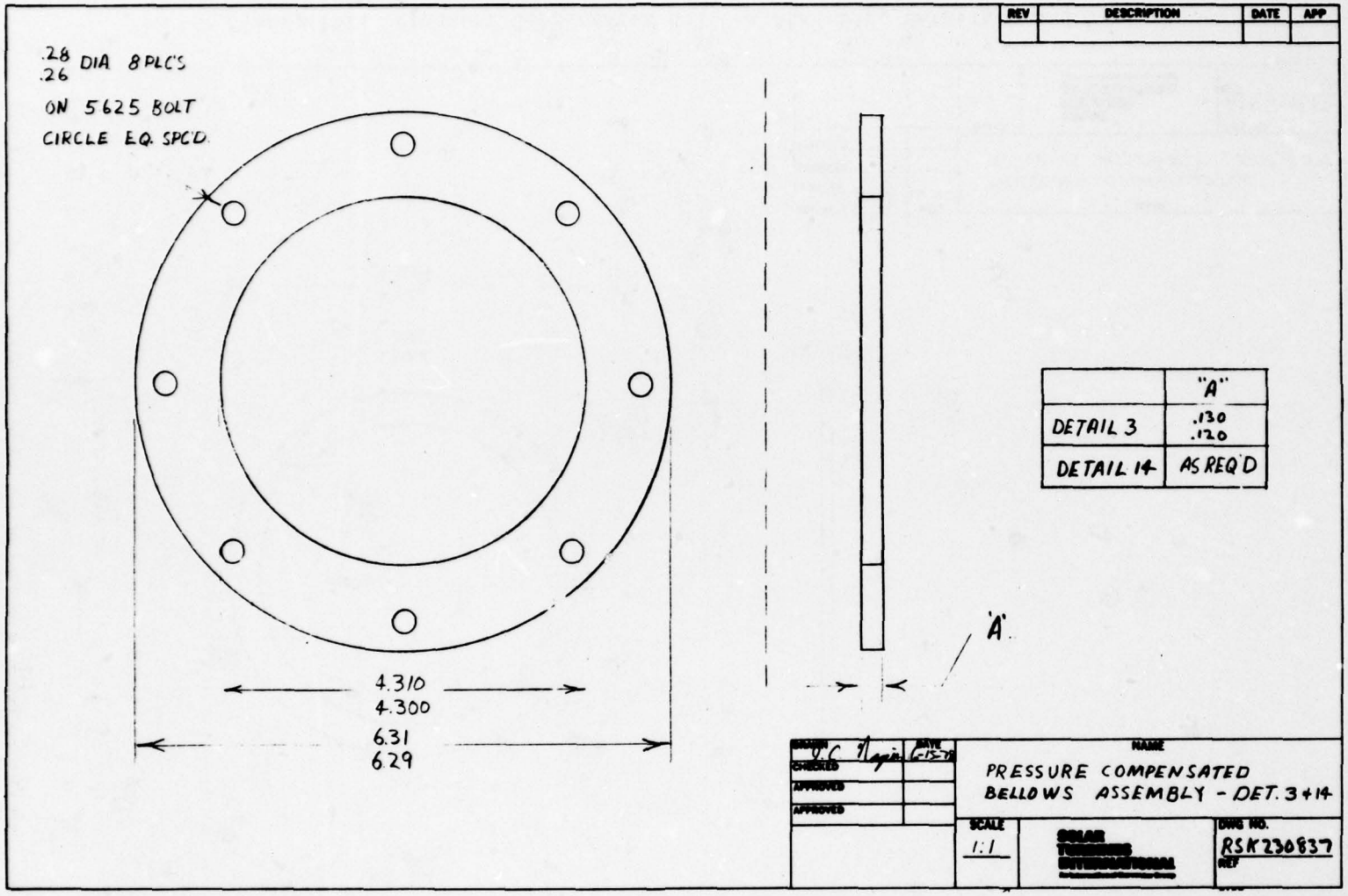

Figure 161. Pressure Compensated Bellows Assembly, Details 3 and 14

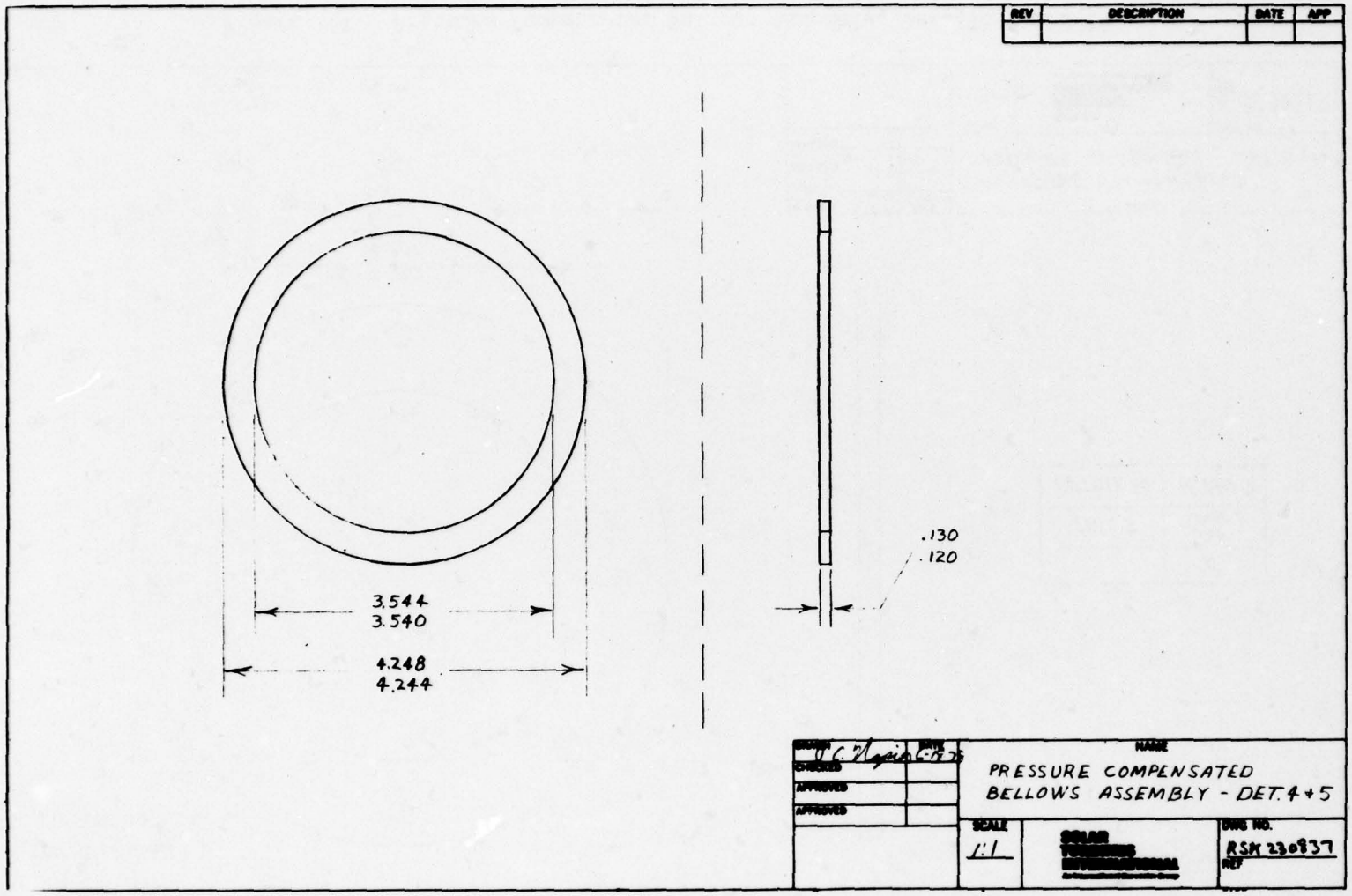

Figure 162. Pressure Compensated Bellows Assembly, Details 4 and 5

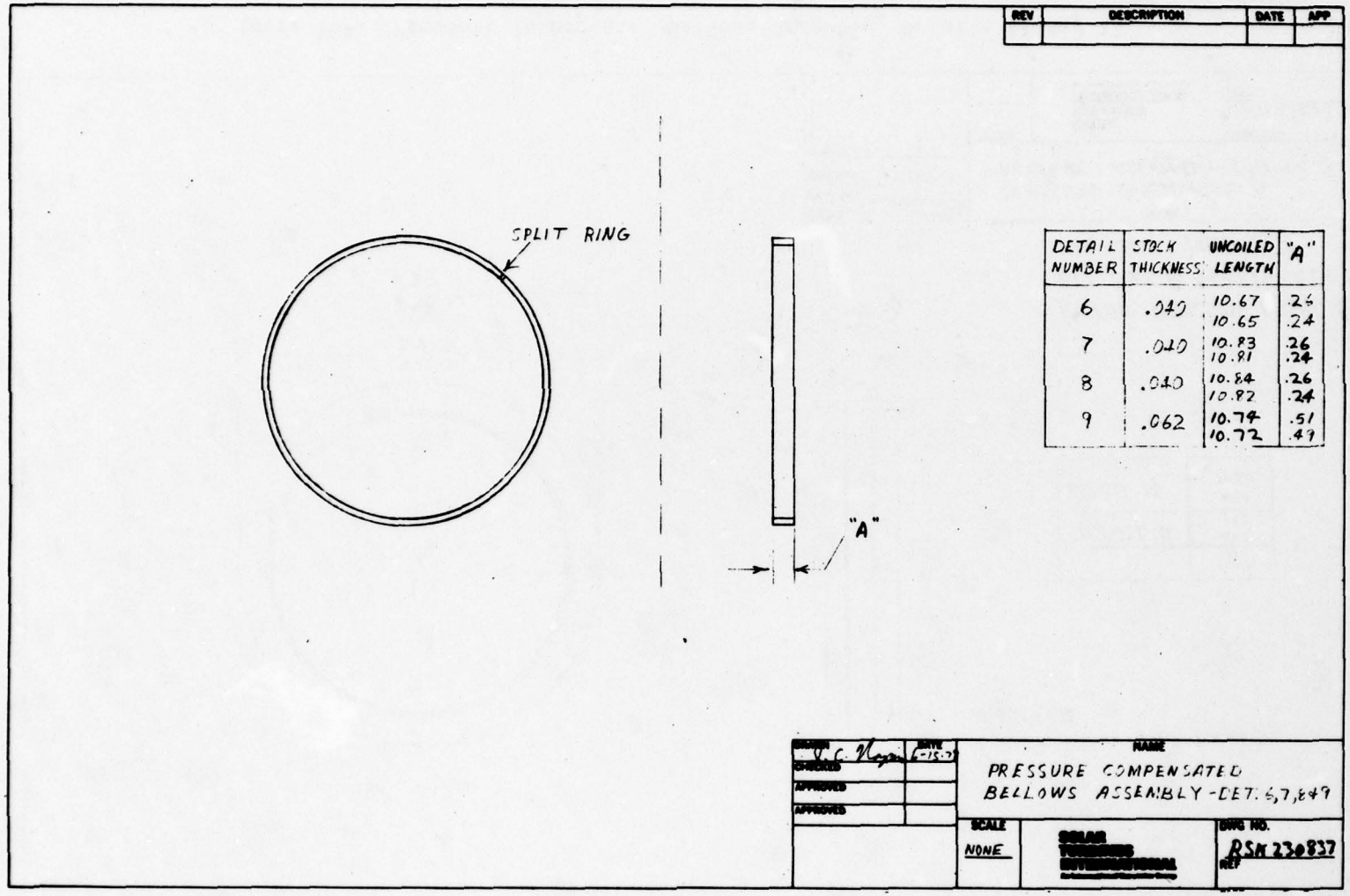

Figure 163. Pressure Compensated Bellows Assembly, Details 6, 7, 8 and 9

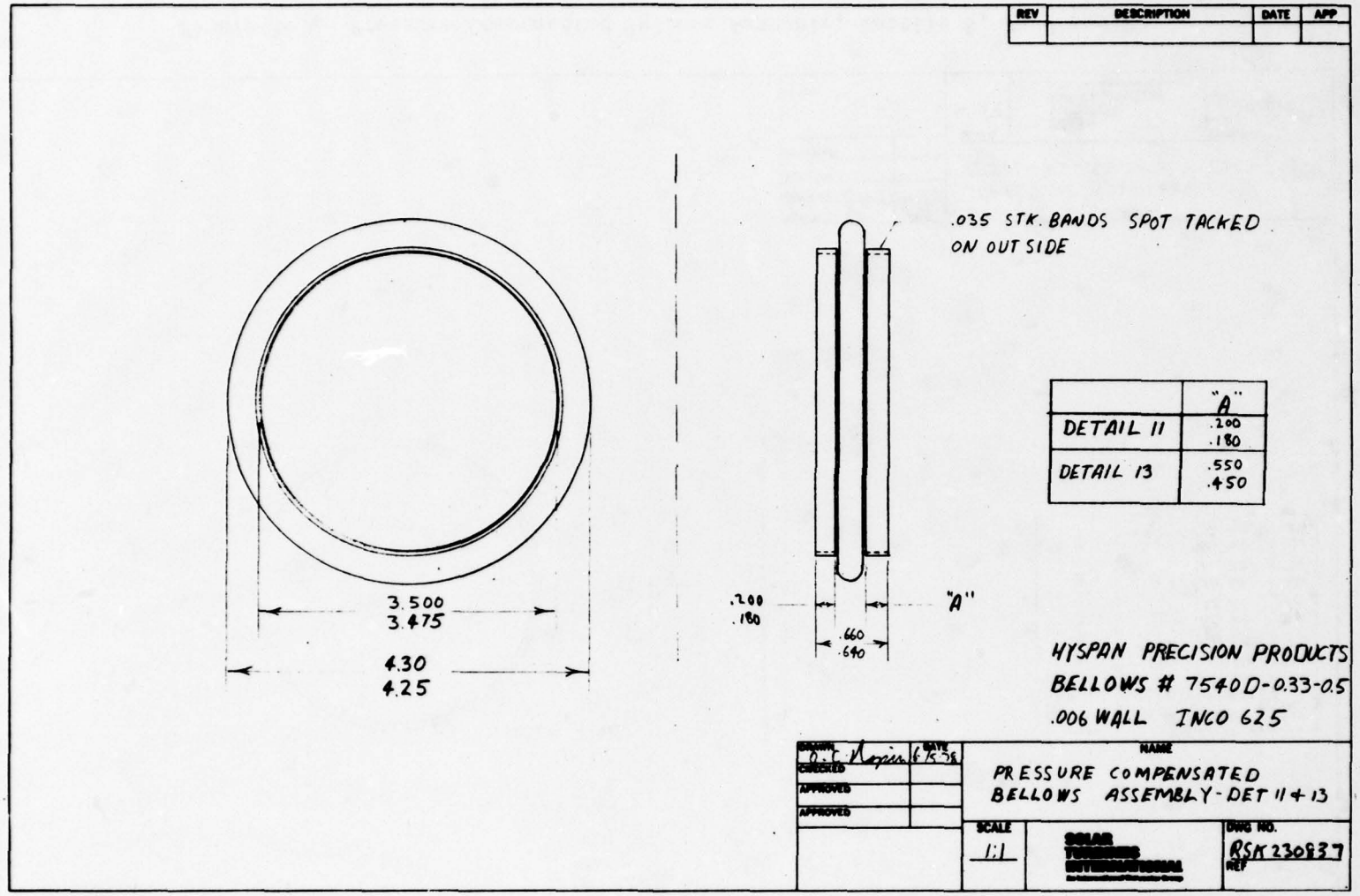

Figure 164. Pressure Compensated Bellows Assembly, Details 11 and 13

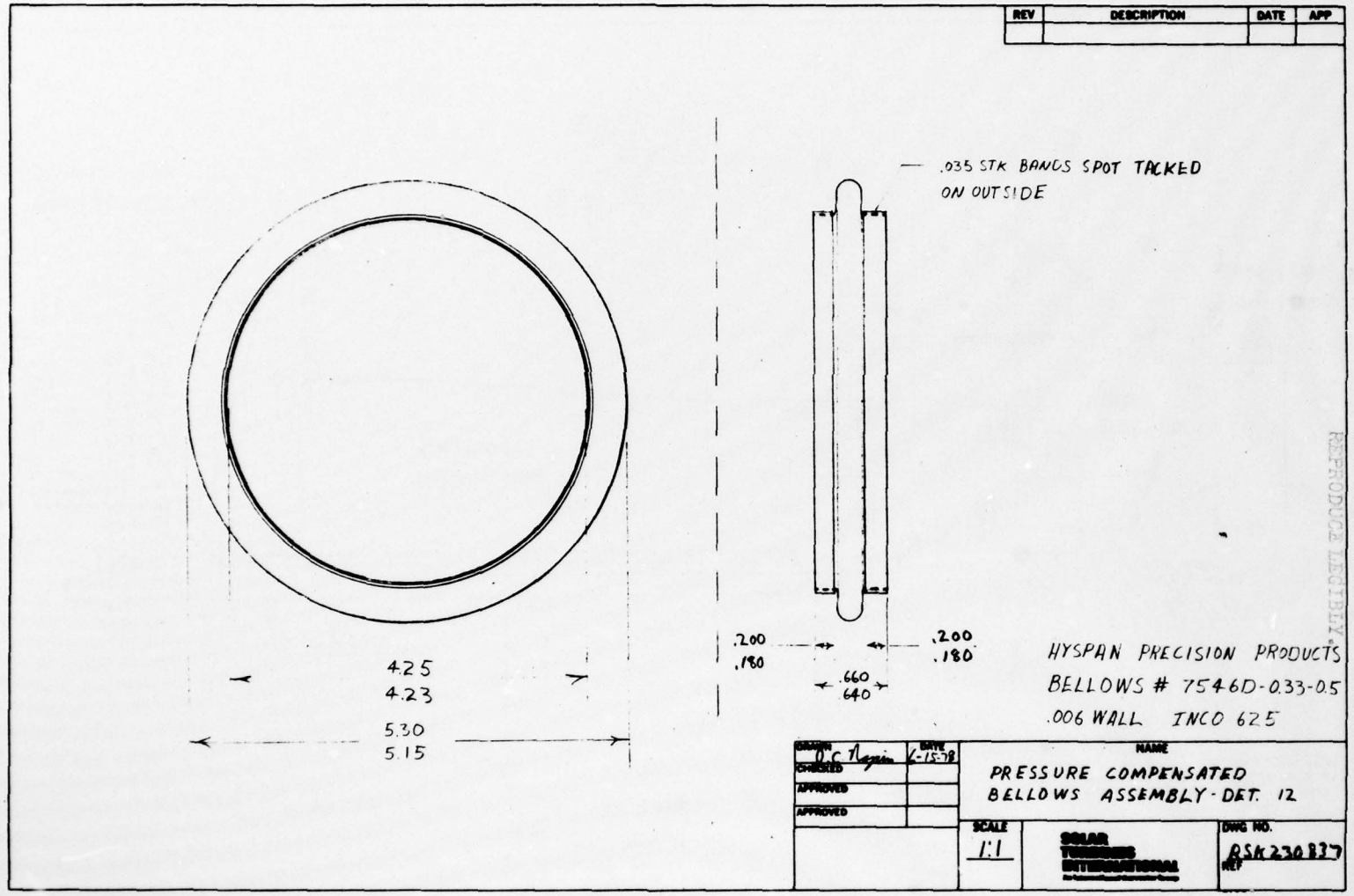

Figure 165. Pressure Compensated Bellows Assembly, Detail 12

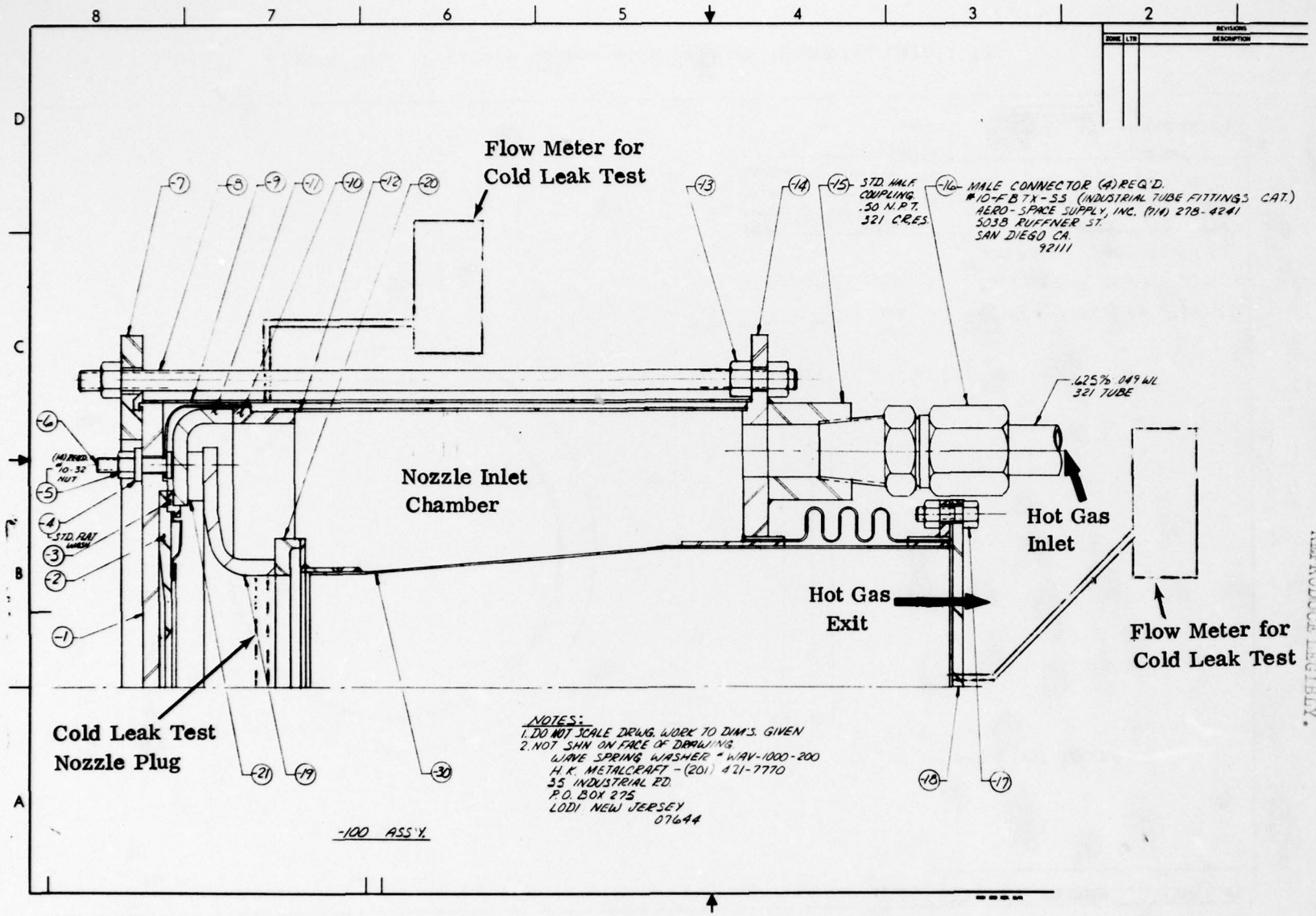

Figure 166. Furnace Thermal Cycline Test Fixture for All-Ceramic Nozzle

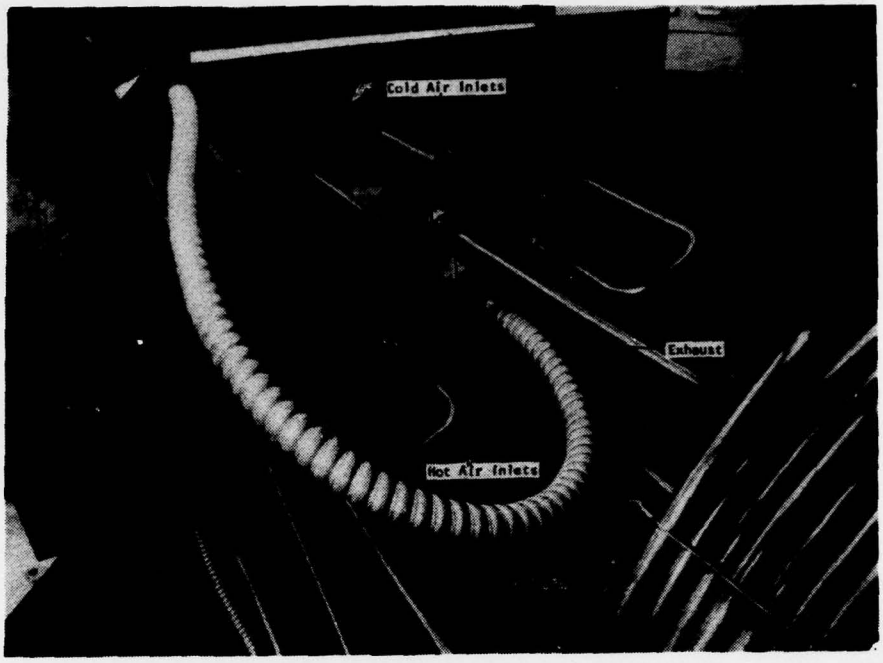

Figure 167. View of Furnace Thermal Cycling Test Rig Showing Case Corresponding to Combustion Can Downstream Section

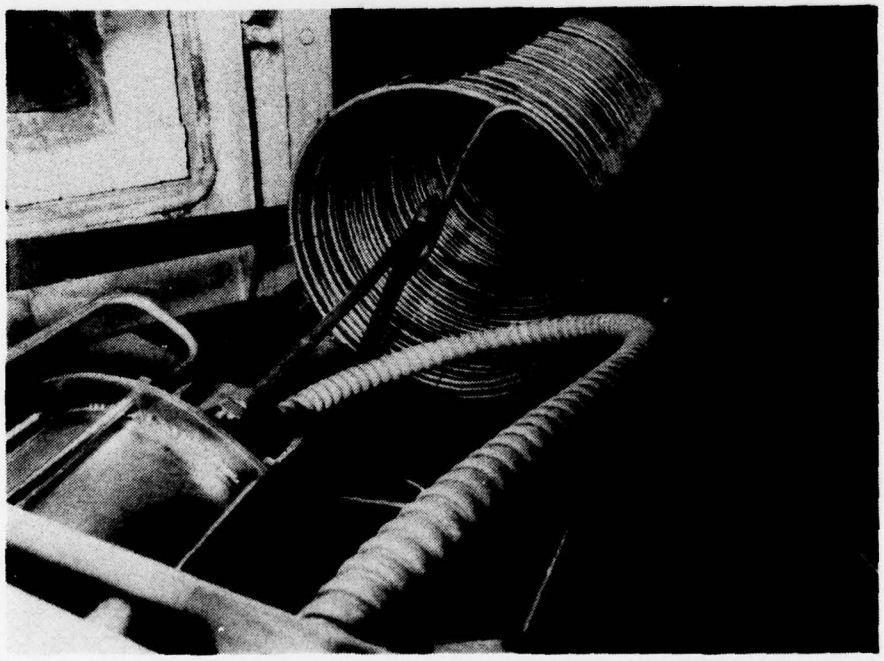

Figure 168. Heat Exchanger Coils to Heat Air Flow Upstream to Test Chamber

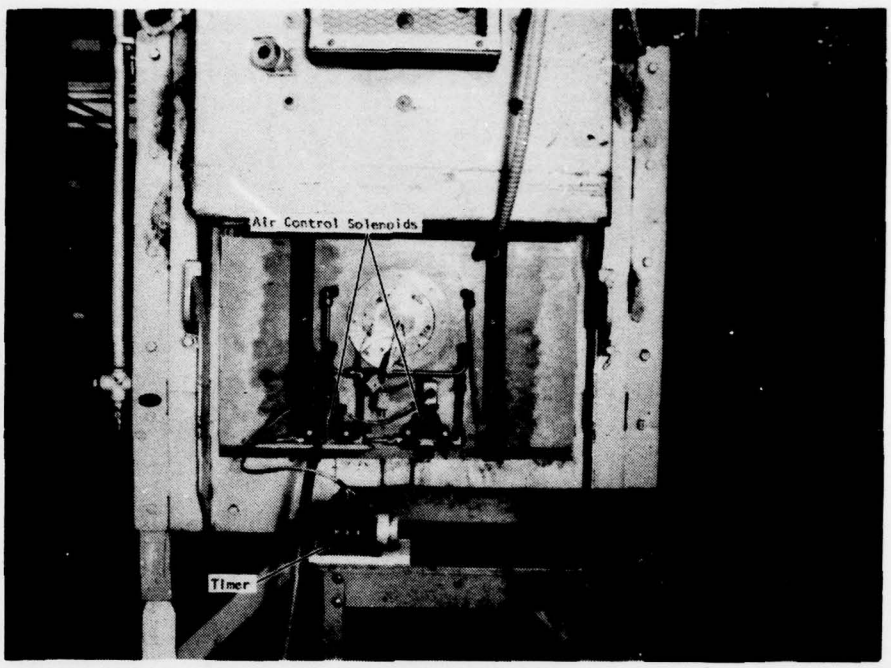

Figure 169. Furance Thermal Cycling Test Rig Installed in Furnace

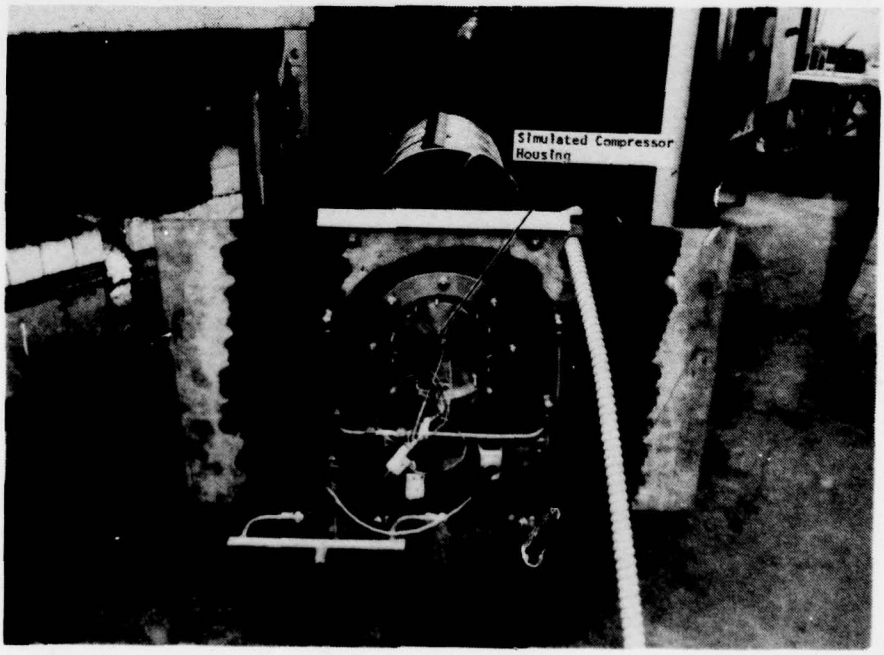

Figure 170. Furnace Thermal Cycling Test Rig Removed From Furnace

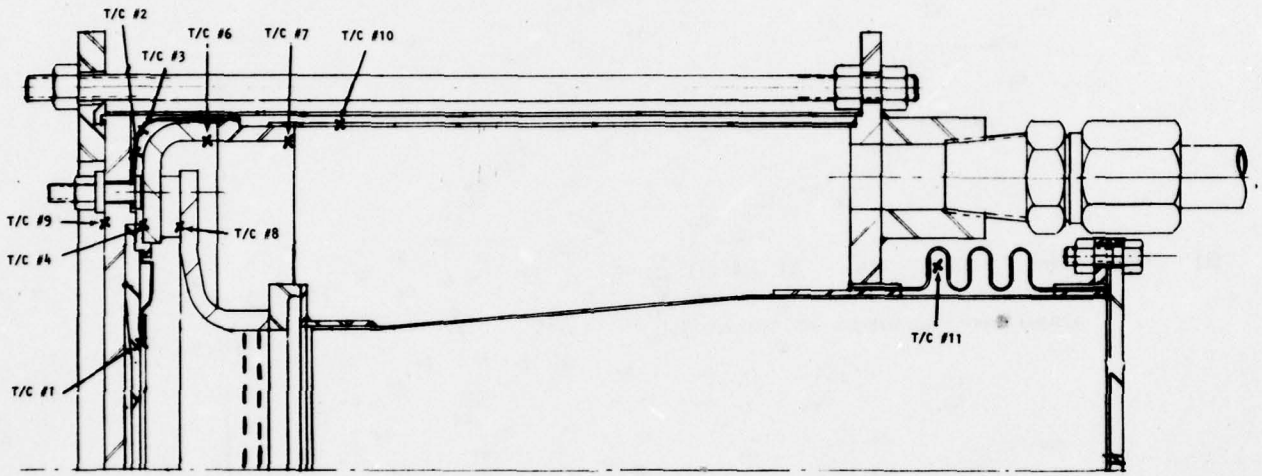

Figure 171. Thermocouple Code for Furnace Thermal Cycling Test Rig

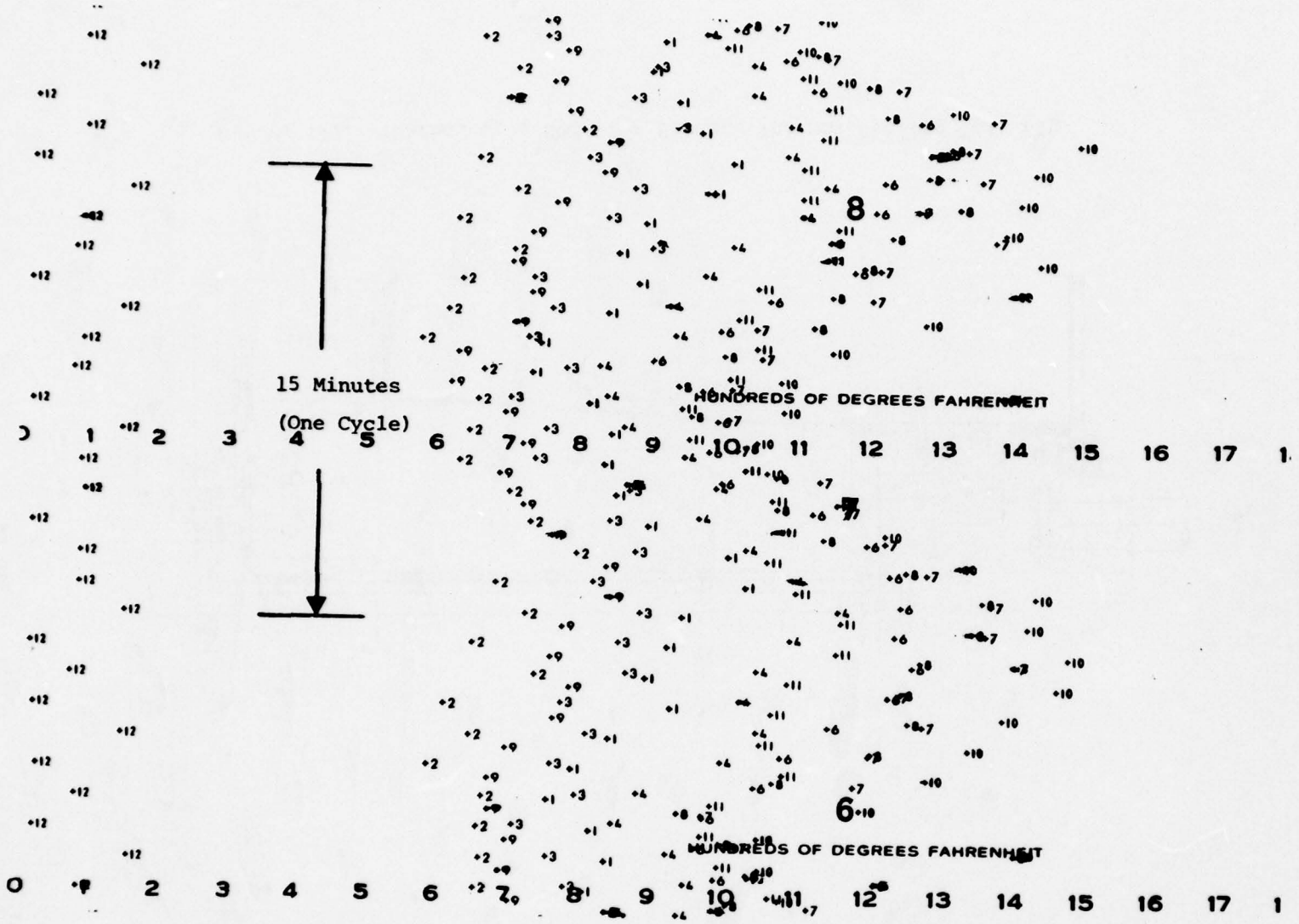

Figure 172. Time Temperature Trace for Furnace Thermal Cycle Rig Test

Table 21 shows the results of leakage tests of the combustor can to outer shroud seal system and the rear shroud to exhaust scroll seal system. The results in the column indicated as "leakage - percent of total engine flow" show that the seal systems were functioning well assuming no component failure had occurred.

An attempt to improve sealing of the rear shroud exhaust scroll face seal by applying a glass adhesive (40% B402, 40% GN19 and 30% Cr_2O_3) to the interface resulted in bonding at the interface and caused fracture of the rear shroud on cool-down. No adhesives were applied at static seals in further rig or engine tests.

Test of the design concept #2 included ceramic nozzle bolts which survived without difficulty. Figures 173, 174 and 175 show the method of attachment for the bolt and the bolts after test.

3.4.7 Engine Simulator Rig Tests

Engine simulator rig tests were for the purpose of duplicating as closely as possible actual engine environment at the nozzle section such that ceramic nozzle behavior could be studied prior to an engine test. The test sequence consisted of a four hour run at 927°C (1700°F) TIT and 500 thermal shock cycles with peak shroud temperatures of 1066°C (1950°F).

Table 21

Seal Leakage in Furnace Cycling Test

Design Concept and Seal Location	Combustor Presurization ΔP (psig)	Air Temperature (°F)	Leakage scfm	Equivalent Leakage in Engine at 1900°F TIT 3.5:1 Pressure Ratio ΔP ≈ 18 psi on Exhaust Scroll; 2 psi on Outer Shroud (scfm)	% of Total Engine Flow	Comments
#1 Exhaust Seal	1.64	70	0.196	0.732	0.21	At conclusion of 100 cycle test Out of furnace
Outer Shroud	1.64	70	Off Scale	--	--	Out of furnace
#2 Outer Shroud	1.26	70	0.489	0.695	0.20	Prior to test
	1.14	500	0.445	0.494	0.14	At conclusion of 100 cycle test: cold flow cycle
	0.228	1800	0.133	0.215	0.06	Hot flow cycle
Outer Shroud	1.64	70	0.498	0.620	0.18	Out of furnace
Exhaust Seal	1.64	70	0.489	1.83	0.5	Out of furnace Fracture at seal surface

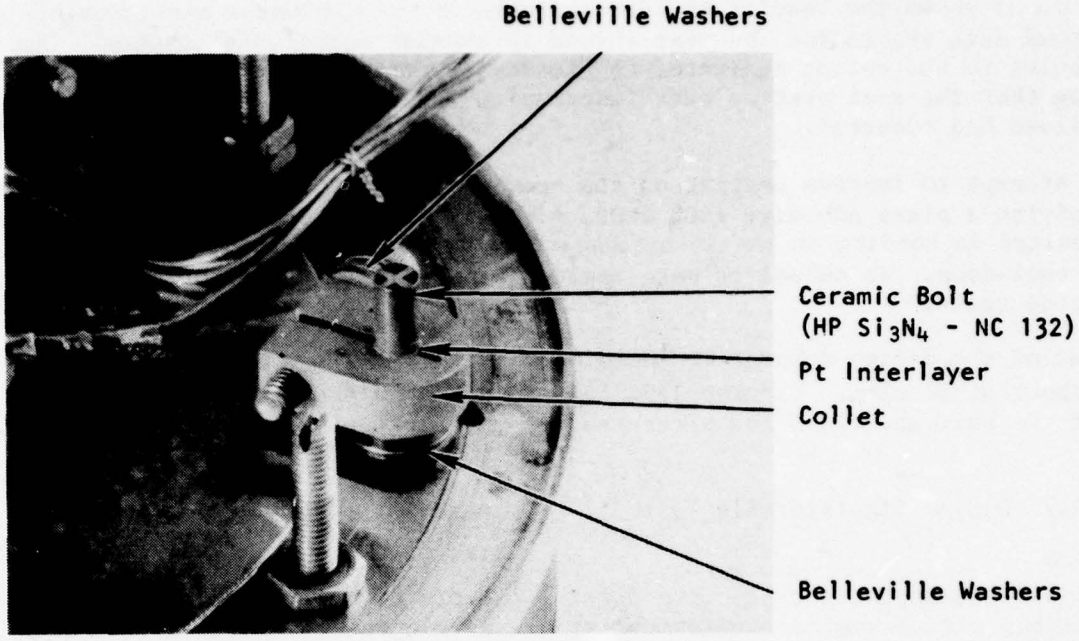

Figure 173. Ceramic ($HPSi_3N_4$) Bolt Assembled Into Furnace Rig With Collet and Pt Interlayer

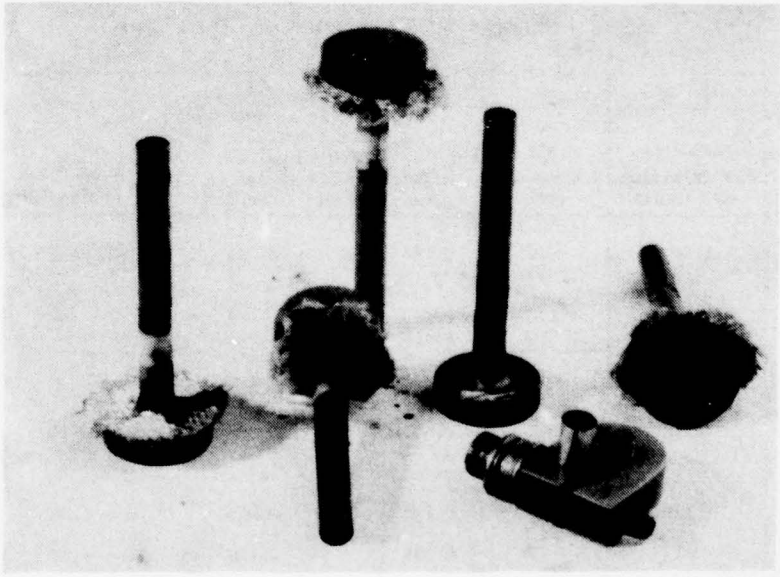

Figure 174. Ceramic Bolts ($HPSi_3N_4$ - NC 430) After 100 Cycle Furnace Rig Test. (Note high temperature Refrecell cloth at bolt head)

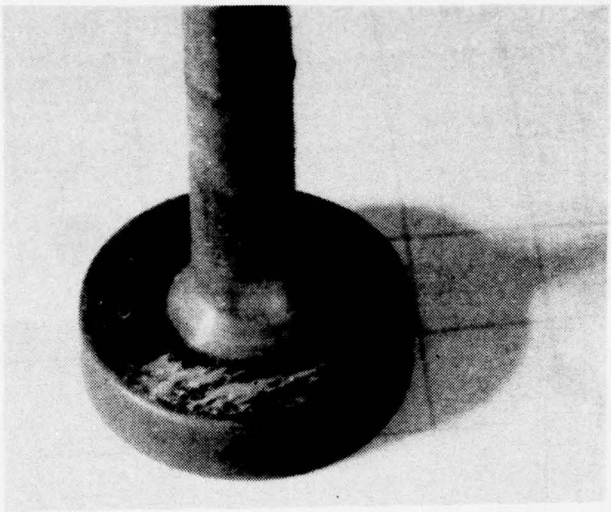

Figure 175.

Close-Up View of Ceramic Bolt After 100 Cycle Furnace Rig Test

Figure 176 is a cross-section of the engine simulator. The simulator includes a complete engine assembly with the exception of vanes on the turbine wheel. Portions of the vanes were left at the turbine wheel inlet and exit sections to measure axial and radial clearance to the rear shroud while the simulator was running. A gaging system which used the roller bearing at the center of the engine shaft as a pivot point was used to measure the radial clearance. The shaft was attached such that it could be moved axially to measure axial clearance. Figure 177 shows the simulator after it had been modified to its final configuration in this project. (This modification included passing of the high pressure air supply to the combustor through the engine compressor section before entering the combustor.)

Each of the three design concepts were run a minimum of once in the specified rig sequence or until a failure occurred. Figures 178, 179, Tables 22 and 23 give thermocouple locations, thermal shock cycle time-temperature traces, steady state temperatures and flow conditions of the test. The test results are summarized in Table 24.

The test which included six separate nozzle build-test sequences showed the following:

1. Silicon carbide nozzle shrouds (concept #3) did not fail in either of two complete test runs consisting of four hours steady state at 927°C (1700°F) and 500 thermal shock cycles.

2. Rear shroud turbine contour location and centering was accurate as measured for design concept #1. (See Table 25.) (This measurement was not possible for concepts #2 and #3 since turbine wheel vane sections used to determine clearance deteriorated during high temperature thermal shock excursions.)

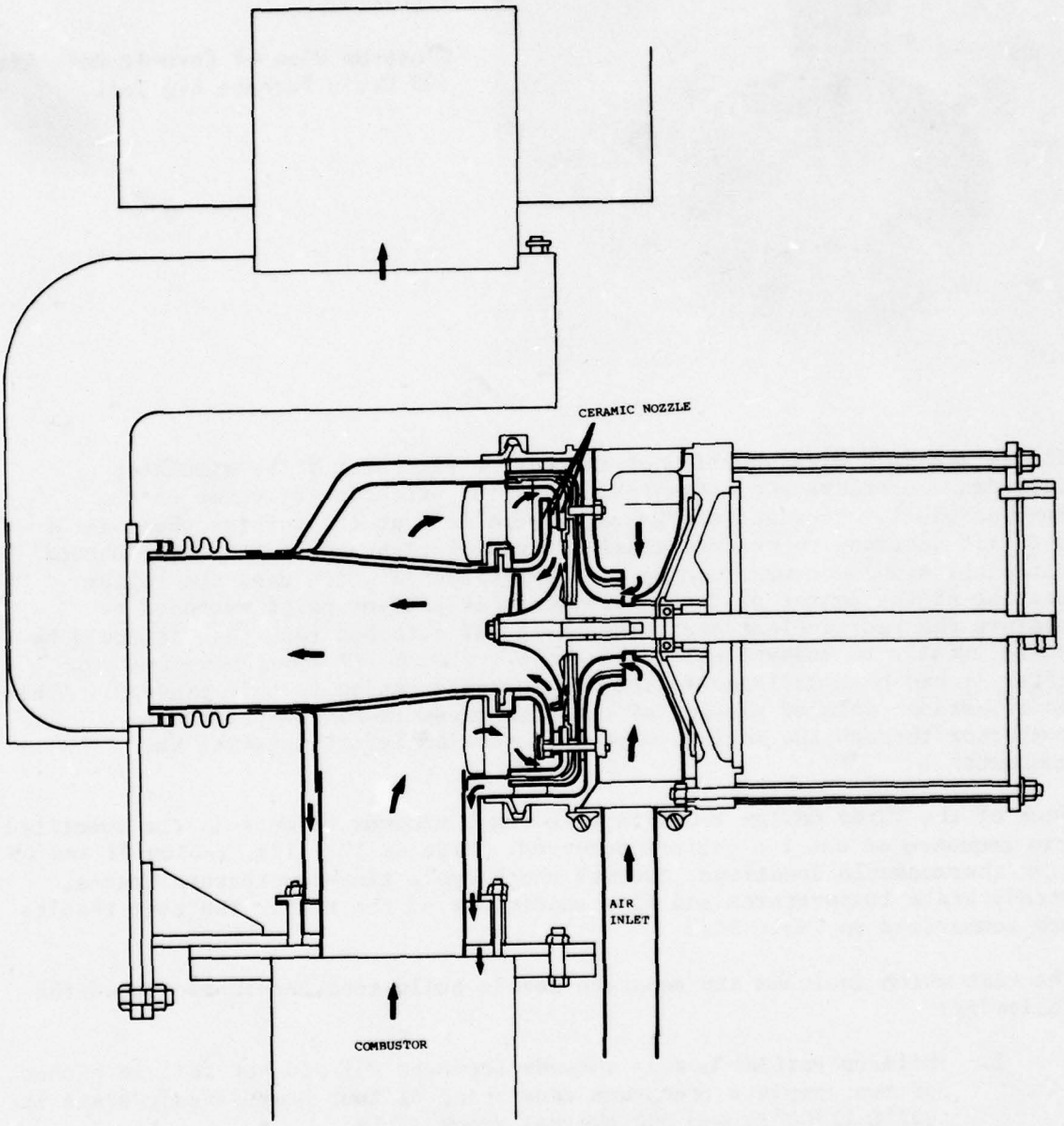

Figure 176. Thermal Rig Test Apparatus for Engine Simulator Testing of All-Ceramic Nozzle Design Concepts

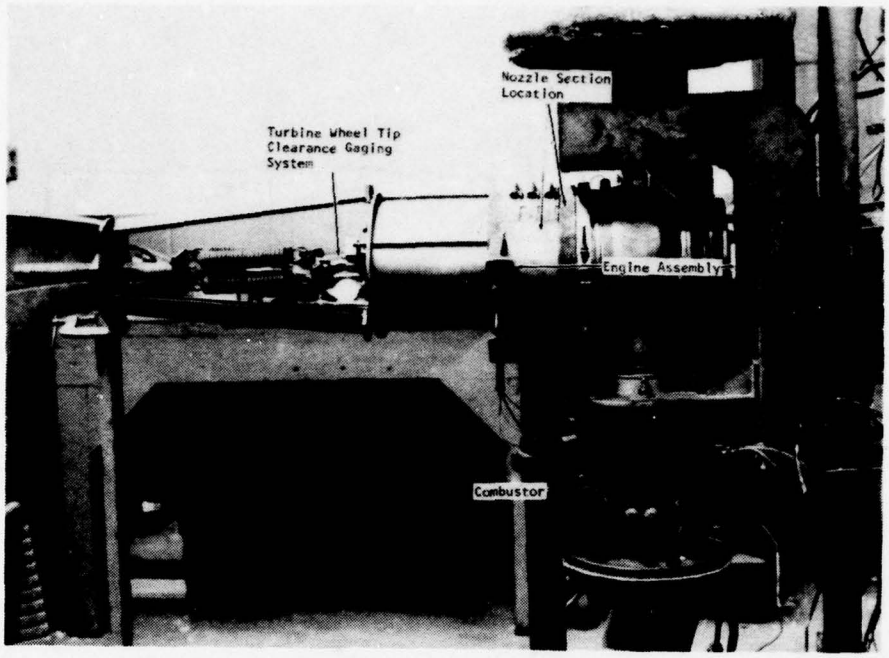

Figure 177. Modified Engine Simulator Rig

3. The silicon nitride rear shroud survived all test sequences (concept #1 and #2 tests).

4. Ceramic vanes from HPSi$_3$N$_4$ and HPSiC survived all tests.

5. HPSi$_3$N$_4$ bolts survived the test sequence applied to design concept #2 even though the forward shroud failed in this test.

6. The silicon nitride foward shroud consistently failed in simulator tests despite design measures taken to avoid failure. The final test of the concept #1 forward shroud produced only a sub-critical flaw. The location and propagation direction of this flaw highly suggests that failure was due to internal thermal stresses in this ceramic component.

Figures 180 through 184 show ceramic nozzle components after four hour 927°F (1700°C) TIT plus 500 thermal shock cycle test runs in the simulator.

3.5 ENGINE TEST OF ALL-CERAMIC NOZZLE - PHASE IV

At this point in the program a joint Solar/MERADCOM decision was made to proceed with engine test of an all-ceramic nozzle section. Based upon information and technologies generated in program Phase I through III, a

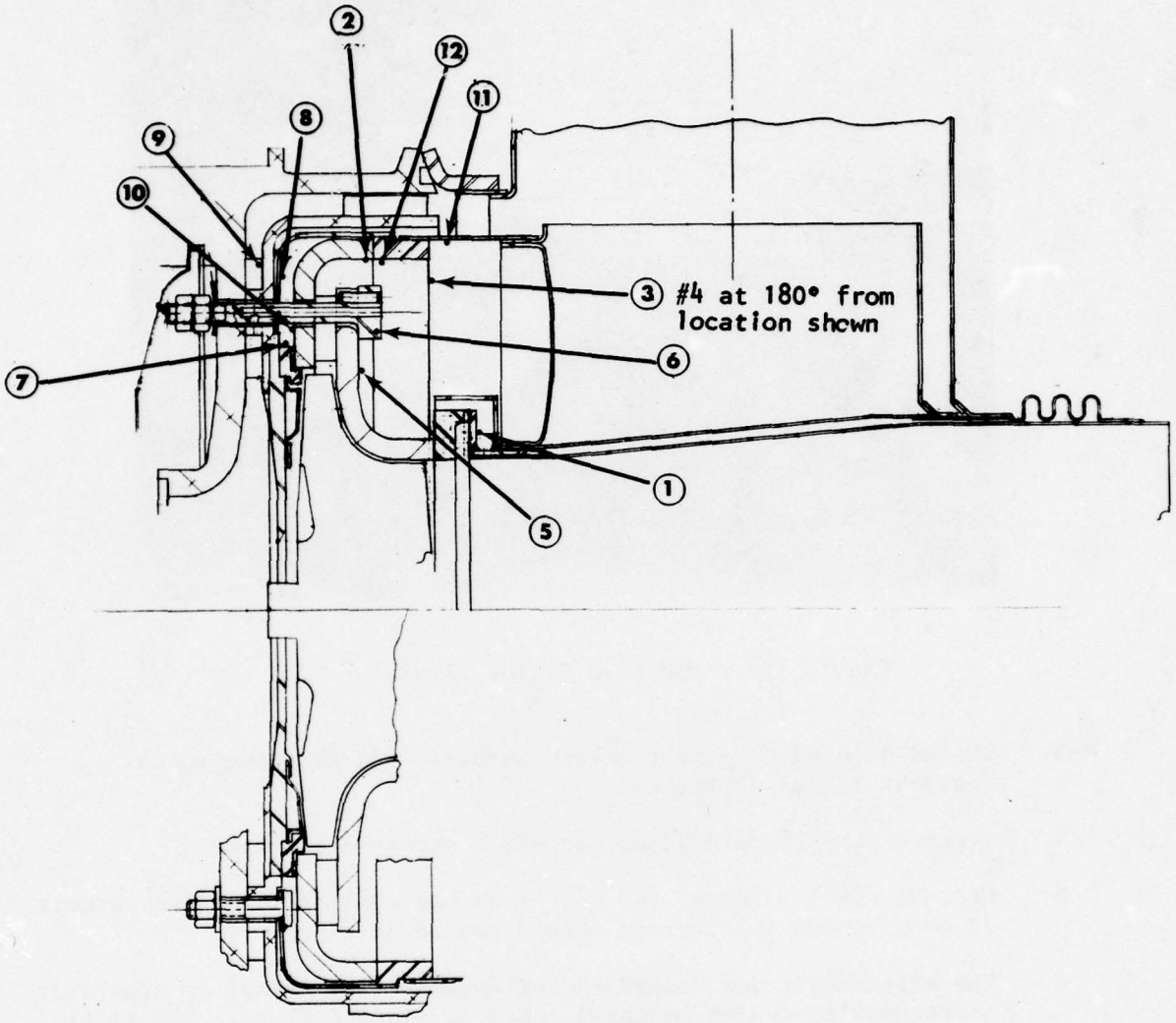

Figure 178. Thermocouple Locations for Engine Simulator Test of Ceramic Nozzles

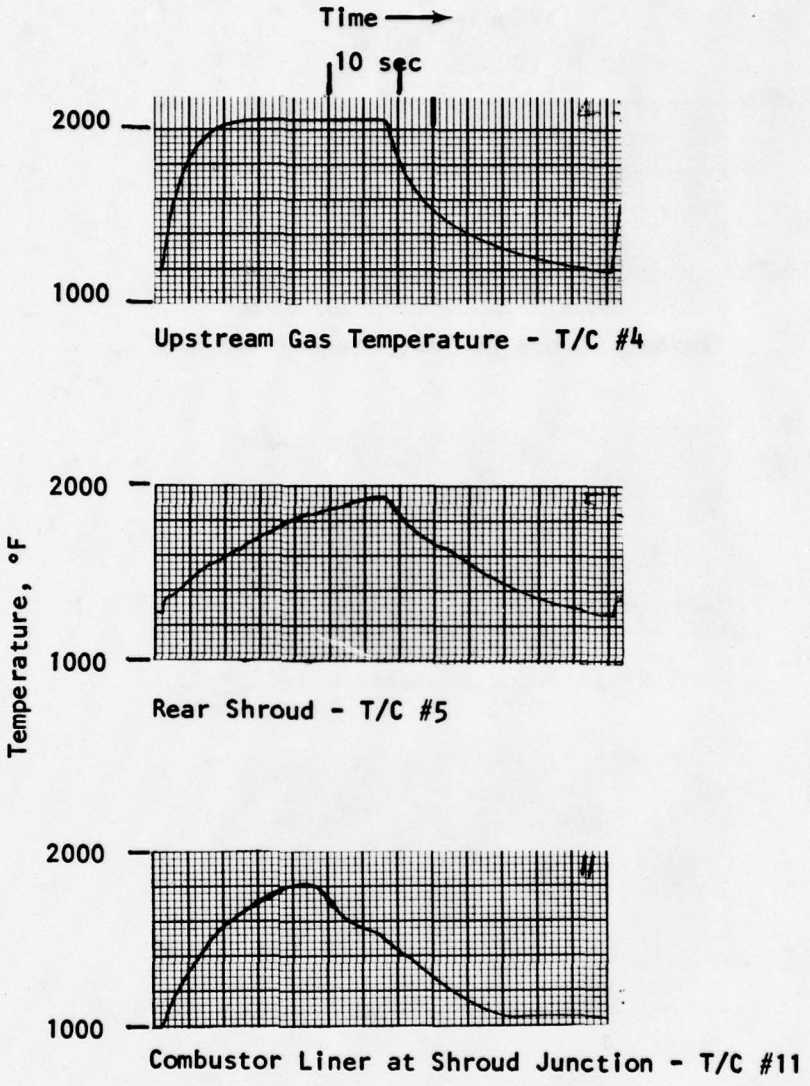

Figure 179. Temperature Time Traces for Thermal Shock Cycle of Ceramic Nozzle in Engine Simulator (See Fig. 173 for T/C Locations) (Sheet 1 of 2)

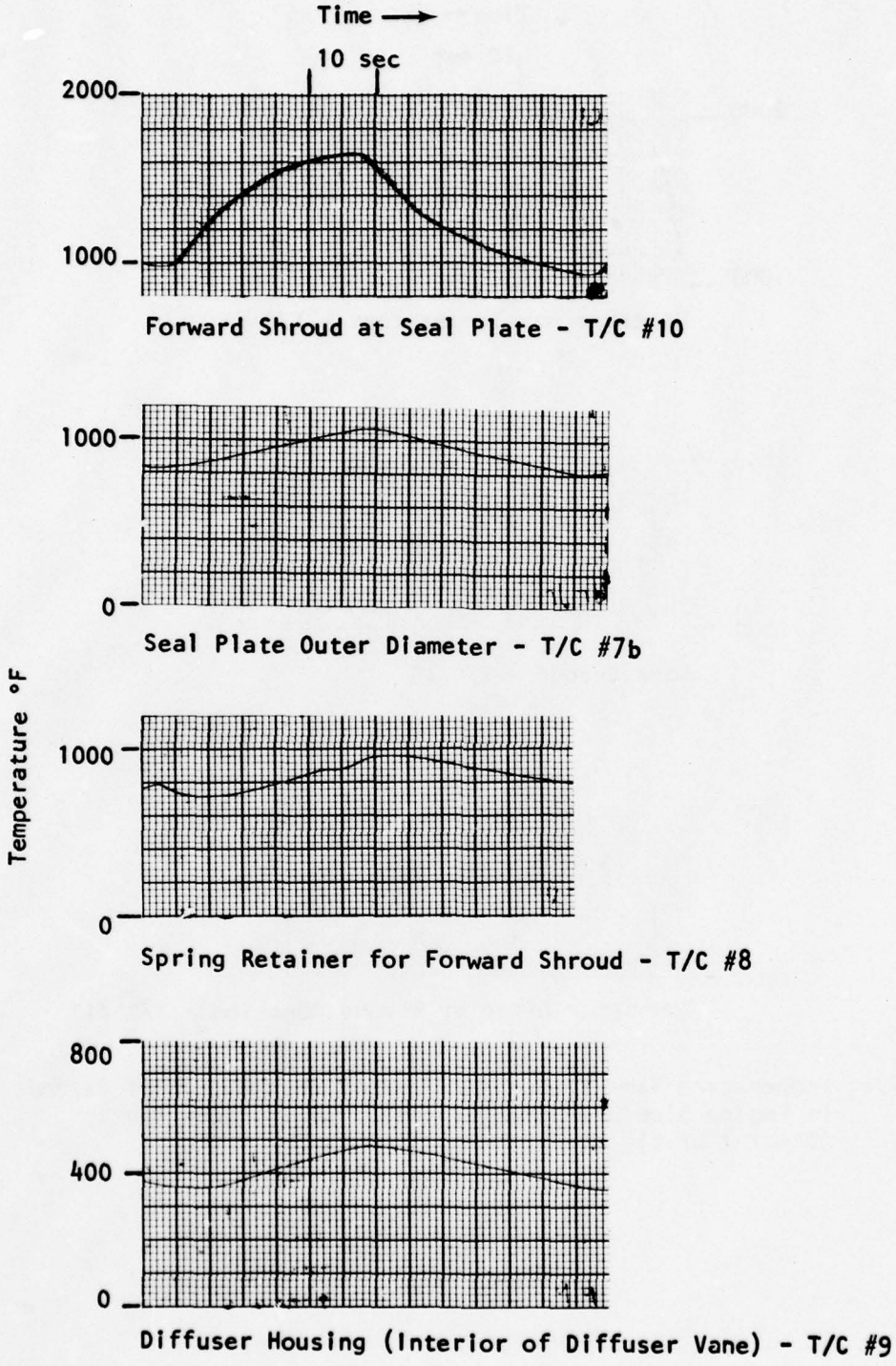

Figure 179. Temperature Time Traces for Thermal Shock Cycle of Ceramic Nozzle in Engine Simulator (See Figure 173 for T/C Locations) (Sheet 2 of 2)

Table 22

Steady State Temperatures (°F) for Nominal 1700°F Turbine Inlet Temperature

	Thermocouple Number and Location											
	1	2	3	4	5	6	7	8	9	10	11	12
Nozzle Designation	Exhaust Scroll Face Seal	Forward Shroud OD	Gas	Gas at 180°	Rear Shroud	Bolt	Seal Plate	Retaining Can	Diffuser Housing	Forward Shroud ID	Combustor Liner	Retaining Ring
Concept #1 Nozzle #1 After 30 min.	1680	1390	1700	1700	1590	1700	625	--	445	1170	1240	1320
Concept #1 Nozzle #2 After 50 min.	1600	1690	1700	1710	1600	1630	--	1060	385	1145	1180	1060
After 1 hour 50 minutes	1600	1700	1700	1700	1610	1630	900	1060	410	1180	1210	1320

Table 23

Engine Simulator Rig Flow Conditions With All-Ceramic Nozzle Designed for Engine Installation

	Nozzle Upstream Conditions		Nozzle Throat Conditions			
Test Conditions	Total Pressure (psia)	Total Gas Temperature (°F)	Mach Number	Gas Velocity (ft/sec)	Gas Density (lb/ft^3)	Total Mass Flow ÷ Nozzle Coefficient of Discharge (lb/sec)
Steady State	24.7	1700	0.894	1907	0.02133	0.206
Thermal Shock:						
High Fire	20.0	2060	0.678	1610	0.01721	0.141
Low Fire	18.7	1180	0.597	1154	0.02597	0.152

Table 24

Summary of Engine Simulator Testing of All-Ceramic Nozzles

Nozzle Configuration	Nozzle Identification	Test Sequence	Results	Design Modifications
Design Concept #1 $RBSi_3N_4$ Shrouds $HPSi_3N_4$ Vanes 718 Bolts	1-A	2 hours steady state at 1700°F TIT	Forward shroud fractured due to inadvertent sea salt ingestion and corrosion interference on seal plate	- Rig cleaned - Seal plate 4.356/4.353 diameter reduced to 4.341/ 4.338
Design Concept #1 $RBSi_3N_4$ Shrouds $HPSi_3N_4$ Vanes 718 Bolts	1-B	4 hours steady state at 1700°F TIT 167 thermal shock cycles	Forward shroud fractured due to overtemperature of diffuser housing in T.S. test and subsequent assembly interference	- Radiation heat shield placed at nozzle OD - Simulator air supply path modified to prevent hot gas leakage to diffuser housing and to better simulate engine operation - Additional groove in diffusion housing for more clearance - Provide better radial registration at inlet housing/ combustor section interface
Design Concept #3 RBSiC Shrouds HPSiC Vanes	3-A	4 hours steady state at 1700°F TIT and 500 thermal shock cycles	Successful run. One nozzle vane partially escaped recess on cool-down due to scroll spring overtemperature	Provide thermal isolation for spring.
Design Concept #2 $RBSi_3N_4$ Shrouds $HPSi_3N_4$ Vanes $HPSi_3N_4$ Bolts	2-C	4 hours steady state at 1700°F TIT and flameout without cold air supply shut off	Forward shroud fracture due to thermal binding at combustor can to outer nozzle shroud retainer ring joint and/or thermal stress	Provide additional clearance at joint
Design Concept #1	1-D	4 hours steady state at 1700°F TIT and 500 thermal shock cycles	Sub-critical crack due to thermal stress	
Design Concept #3	3-D	4 hours steady state at 1700°F TIT and 500 thermal shock cycles	Successful run.	

design selection was made. This design was fabricated, assembled and tested in a 45 hour engine run.

3.5.1 Design Selection

Engine simulator tests showed that design concept #1 performed acceptably with the exception of the forward shroud. The rear shroud, vanes and all anciliary design components performed well. Centering and location of the rear shroud which must match the turbine wheel contour was also good. The ceramic bolts of design concept #2 performed well in testing, however, this design concept assembly was not exposed to the thermal shock portion of the simulator test sequence. Finally, the all-silicon carbide nozzle performed well, but uncertainties remained concerning the accuracy of rear shroud location.

Table 26

Axial and Radial Turbine Tip Clearances Measured During 1700°F TIT Steady State Run

Nozzle Designation	Axial Clearance	Angle From 0° Reference	Radial Clearance	Angle From 0° Reference
Design #1 Nozzle #2 at 1.0 to 1.5 hours running time	0.010	60° (2)	0.014	330 (2-90)
	0.0065	180° (4)	0.013	90 (4-90)
	0.0075	300° (6)	0.004	210 (6-90)
			0.0068	270 (1-90)
Same test at 3.0 to 3.5 hours running time	0.010	60°	0.011	330
	0.007	180°	0.0124	90
	0.009	300°	0.0035	210
Same test cold measurement after 4 hours steady-state run	0.009	60°	0.024	330
	0.011	180°	0.020	90
	0.0095	300	0.023	210

A hybrid design was selected for engine test. The design selected was concept #1 with a direct substitution of SiC (NC-430) for the Si_3N_4 (NC-350) forward shroud. This design incorporates the best features of the three considered. Additional benefits beyond those evidence by engine simulator tests include a potentially low cost injection molded rear shroud which requires accuracy of the turbine wheel contour surface, and a slip cast SiC forward shroud. Since the forward shroud runs at temperatures considerably cooler than the rear shroud, the higher expansion properties of SiC make a thermally coordinated nozzle assembly.

3.5.2 Fabrication

In order to use a silicon carbide (NC-430) forward shroud in design concept #1 (RSK 230632) the forward shroud type used in concept #3 (RSK 230636) had to be modified to include five 0.240/0.230 through holes at vane leading edge position to accommodate the five nozzle bolts (RSK 230795) of concept #1. This was easily accomplished by Electro Discharge Machining.

Assembly for engine test followed the same procedure used for simulator experiments. Figure 185 lists clearances at the turbine wheel contour gaged during build-up.

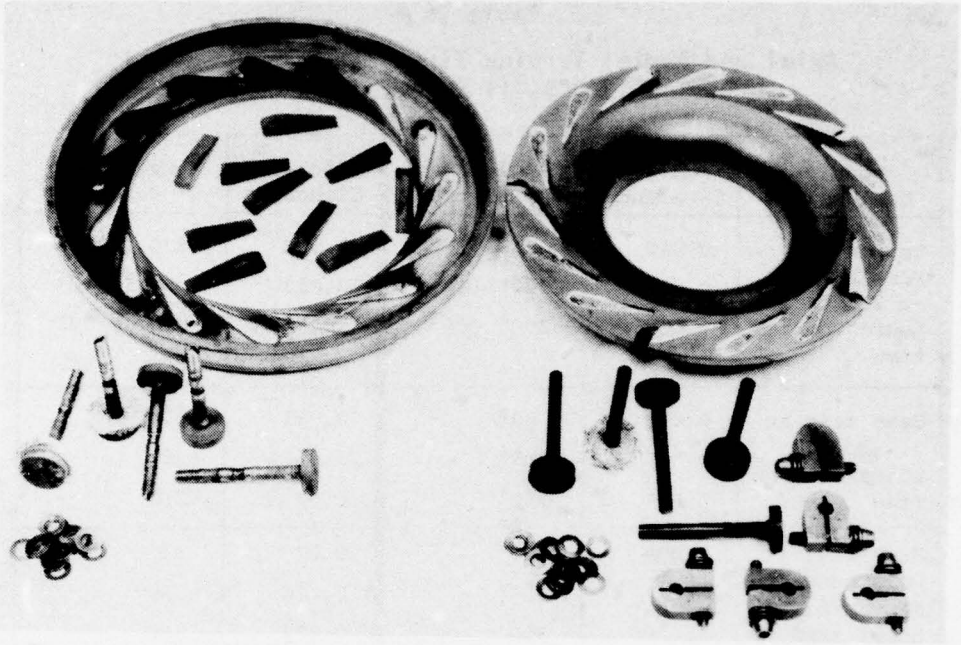

Figure 180a. Components From Design Concept #1 After Engine Simulator Test (Four hours steady state at 1700°F TIT and 500 thermal shock cycles.) (Ceramic bolt assemblies from Concept #2 successfully run through the simulator test are shown at the bottom right.)

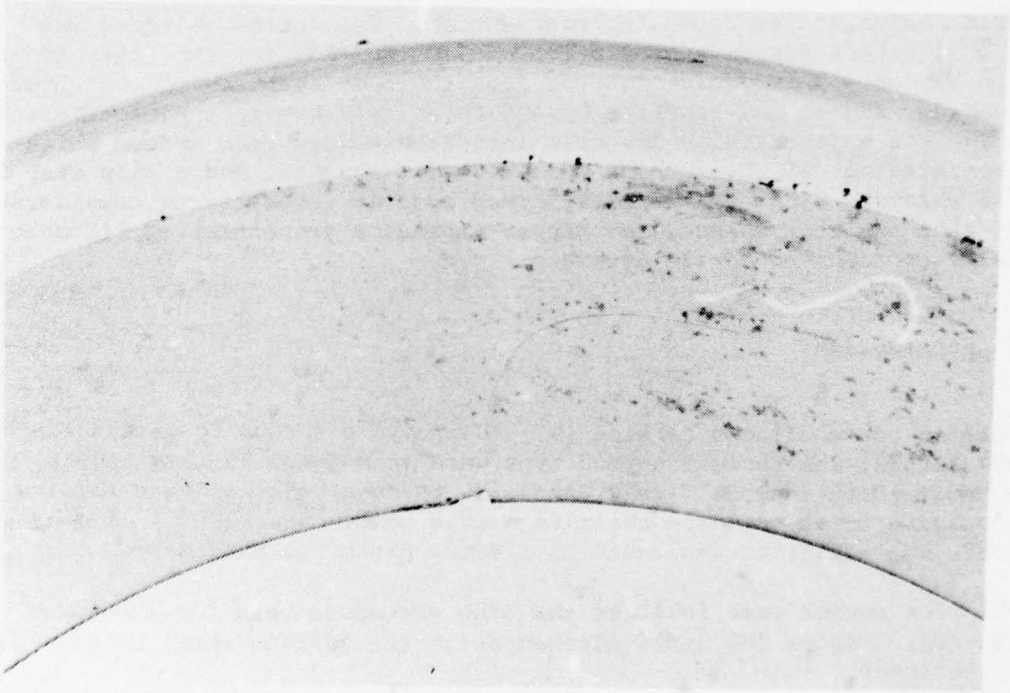

Figure 180b. Subcritical Crack in RBSi$_3$N$_4$ Forward Shroud After Engine Simulator Test

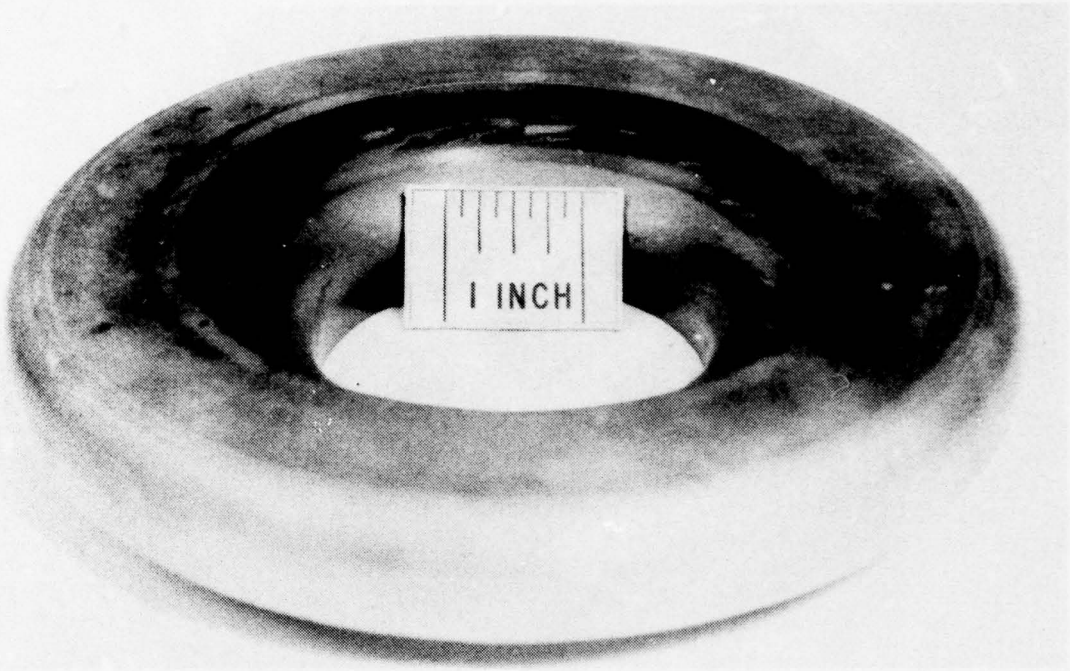

Figure 181. Design Concept #3 (NC-430) RBSiC Shrouds, (NC-203) HPSiC Vanes After Successful Engine Simulator Run. Nozzle #3-B

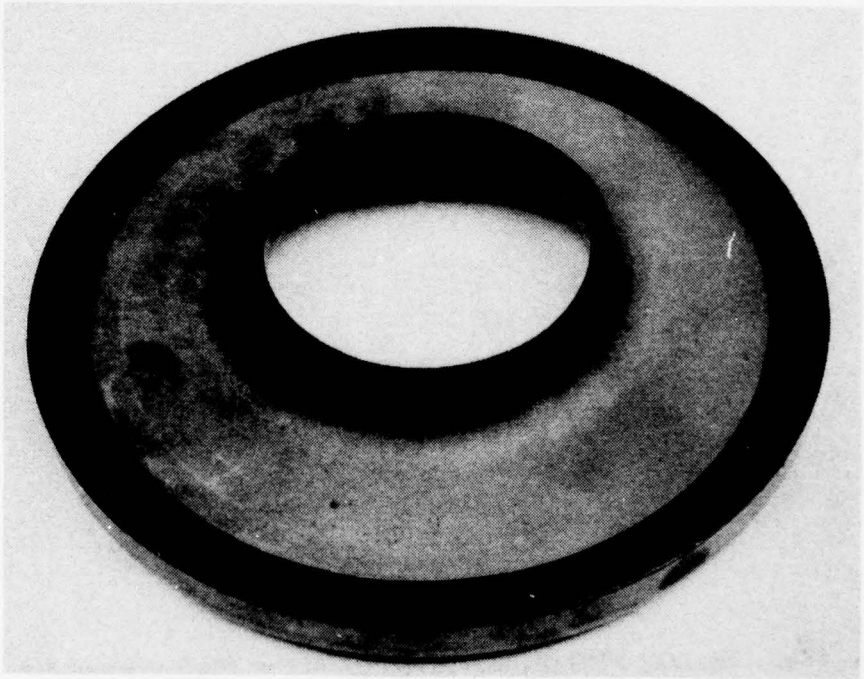

Figure 182. Design Concept #3 (NC-430) RBSiC Shrouds, NC 203 HPSiC Vanes After Successful Engine Simulator Run. Nozzle #3-B

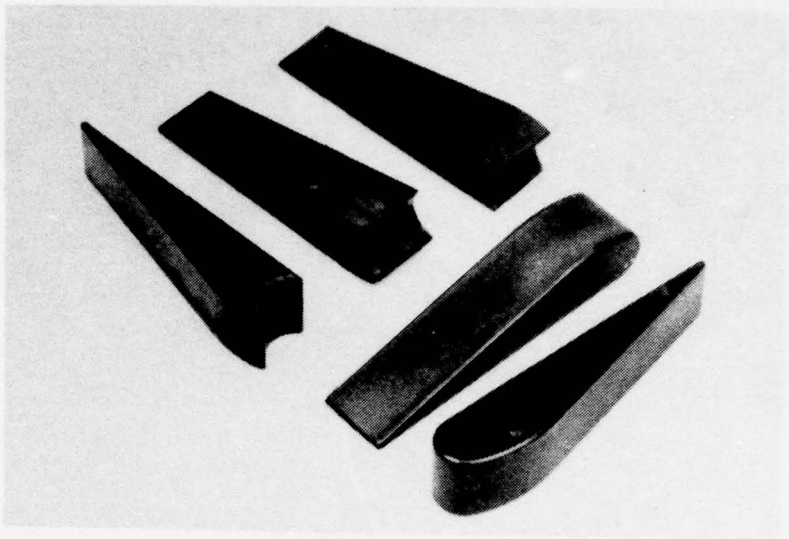

Figure 183. Typical HPSi$_3$N$_4$ Vanes After Successful Engine Simulator Run in Design Concept #1

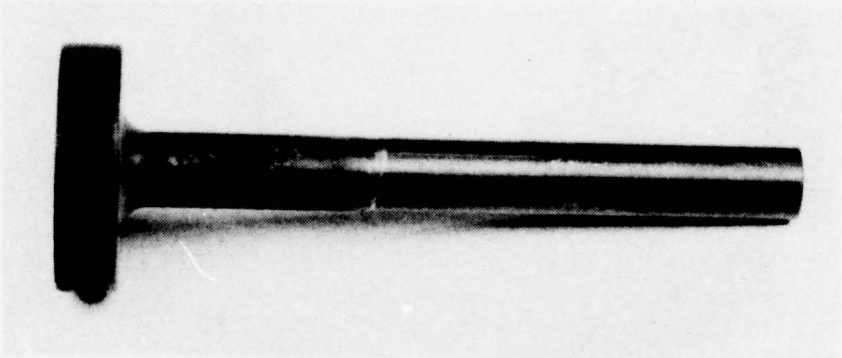

Figure 184. Typical HPSi$_3$N$_4$ Bolts (2-C) After Engine Simulator Run

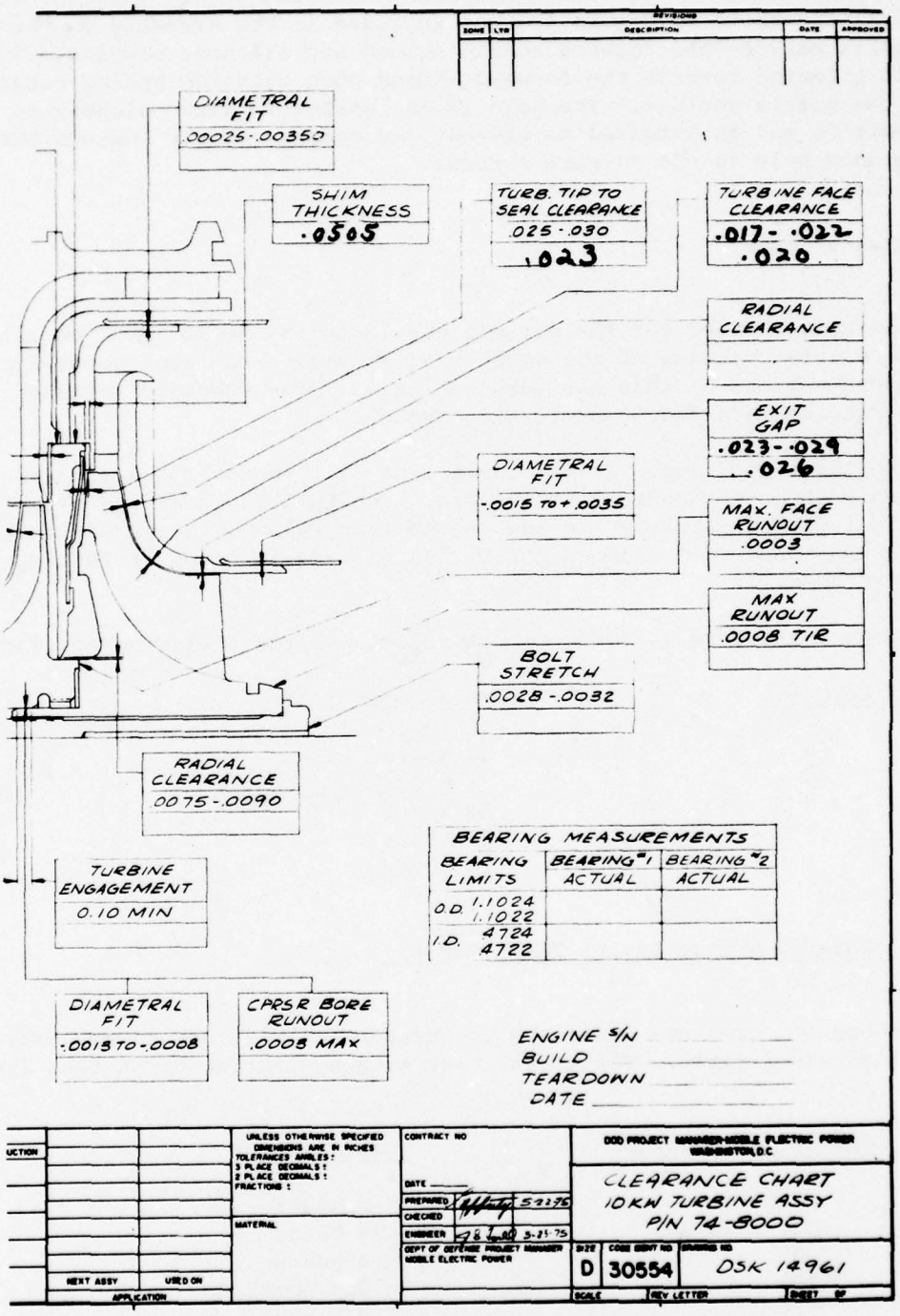

Figure 185. Clearance Chart 10 kW Turbine Assembly With All-Ceramic Nozzle - Engine Test #3 (Sept. 1978 Engine Serial #1) P/N 74-8000

One additional design change was made prior to engine test. A washer with a location spring shown in Figure 186 was included in the assembly on the nozzle bolts between the forward nozzle shroud and diffusor housing. The washer is oriented towards the forward shroud such that the spring retains it against the nozzle surface. The hole in the washer is sized closely to the nozzle bolt OD and is intended to prevent any compressor air leakage through the clearance hole in the forward shroud.

3.5.3 Engine Tests

The engine test planned for the ceramic nozzle in the Gemini GTED DC set was an abreviated version of the 6,000 hour endurance run used to qualify the standard version of this gas turbine engine. The schedule included 200 hours of running time and 50 start/stop cycles.

Two engine tests were run. In the first (run #3), the hybrid design nozzle was run only 50 hours due to difficulties. The full 200 hour run plus 50 start/stop test was completed in the second (run #4). This run was with nozzle design concept #1 using SiC (NC 430) shrouds in place of $RBSi_3N_4$ (NC 350) shrouds.

The 200 hour test cycle includes two iterations of the following sequence.

Load (%)	Time at Load
50	24 hours
0	4 hours
100	24 hours
25	24 hours
75	24 hours

First All-Ceramic Nozzle Engine Test (Run #3)

Due to combustion problems caused by compressor surge in the first test, time at full load was limited. The actual test sequence in the first test (run #3) was:

Operating Condition	Time at Load
Calibration	5 hours
50% load	24 hours
0	4 hours
100	10.5 hours
75	6.5 hours
	50 hours total

Ninteen start/stop cycles were completed.

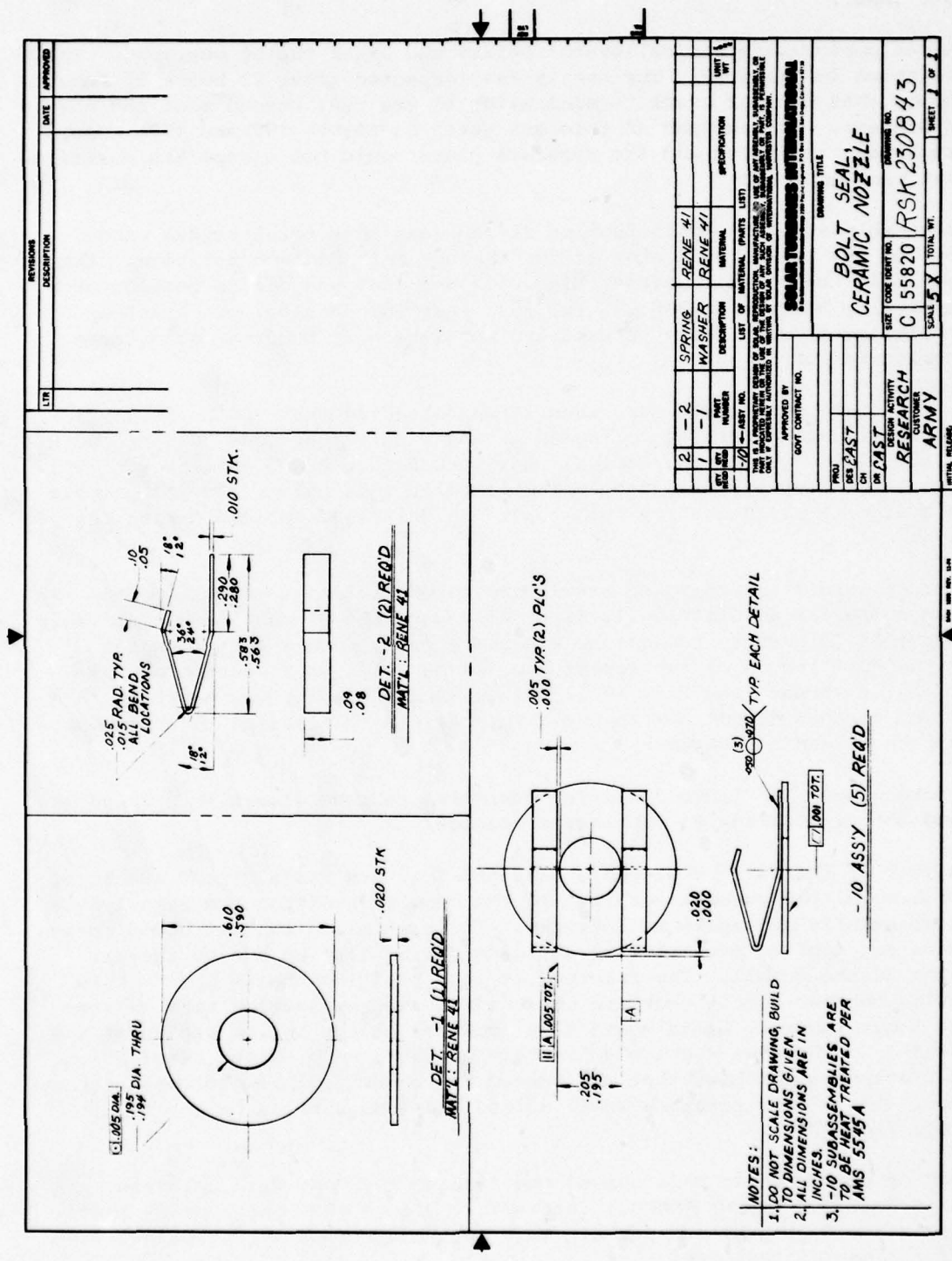

Figure 186. Bolt Seal, Ceramic Nozzle

Maximum turbine inlet temperature (TIT) during this test was 904°C (1660°F) (at full load).

The engine performance was calibrated before and after the 50 hour run. This data is shown in Table 26. The nozzle was inspected after 33 hours of running and showed that a minor crack termininating at the rear shroud slot and nozzle OD was present. Photographs of this are given in Figure 187 and 188. Since the crack was terminated and the separate piece could not escape its position, the test was continued.

On disassembly after 50 hours running it was seen that metal oxides were attached to the rear shroud slot at the through bolt contact position. This suggests that the first fracture (Figs. 187 and 188) was due to bonding of 718 superalloy bolts with $RBSi_3N_4$ (NC 350) rear shroud slot. On start-up both positions grow radially outward and metal-ceramic bonding would cause bonding and failure.

The test was stopped at 50 hours when it was observed that the Hastelloy X exhaust scroll had partially collapsed during high temperature running and a fracture was observed in the $RBSi_3N_4$ rear shroud (see Figs. 189 through 191). Nineteen start/stop cycles had been completed at this point. One stop cycle was an emergency shutdown from full load with full load applied during the shutdown.

The exhaust scroll collapse was attributed to possible hot streaking from the side can combustor as its flow is directed toward the exhaust scroll section. A heat shield is present around the exhaust scroll, however, it does not extend the full length of the scroll and leaves a 1/4 inch section of the scroll in the stream (see Fig. 192). This attachment point was modified to a a position further downstream in the all-ceramic nozzle design to accommodate the face seal loading system.

The fracture seen in Figure 191 were considered serious enough to suspend the test and not risk damage to the engine package.

An analysis of the failure suggests that the fracture was a direct result of the buckling of the exhaust scroll. In the buckled position the scroll does not slide axially as easily as intended. It is surmized that it bound during operation and applied excessive axial loads during heat up due to thermal expansion of the scroll. The fracture is in a position that supports this conclusion because scroll buckling occurred at the top section thus shortening its length there. Loads would have occurred at the bottom region of the rear shroud in the area where the fracture was observed. Close examination of the fracture also shows that the shroud had been displaced forward at the face seal side of the fracture as if a load had been applied on the face seal (see Fig. 191C).

Analysis of fractures in this shroud was done at the Army Materials and Mechanics Research Center (AMMRC) (Ref. 27). Figure 191E shows crack initiation points and propagation paths. This analysis supports conclusions given above for cause of failures.

Table 26

Test #3 - Calibration Data for Gemini Engine With All-Ceramic Nozzle
(Corrected to Standard 59°F and 14.7 psia Ambient Conditions
(Linear Loading - No Cycle Convertor Losses)

	Data Point No.	Load	Cummulative Engine Running Time (hours)	Corrected Fuel Flow (pph)	Shaft Power Output (kW)	Corrected Shaft Specific Fuel Consumption lb JP-4 kW-hr	Corrected		Measured Gas Exhaust Temperature (°F)	Turbine Inlet Temp. Calc. From EGT (°F)	Actual Compressor Inlet Temperature (°F)	Actual Fuel Flow
							Exhaust Gas Temperature (°F)	Turbine Inlet Temperature (°F)				
Pre-Test	1	0%	start of run	15.7	--	--	745	1064	795	1115	76	18.5
	2	25%	SOR	20.2	2.27	8.92	827	1169	876	1221	75	22.4
	3	50%	SOR	24.7	6.33	3.90	879	1240	928	1294	75	25.5
	4	75%	SOR	29.6	9.52	3.11	963	1345	1031	1427	82	30.6
	36	100%	31	29.6	12.6	2.35	1068	1479	1116	1537	74	30.2
After given run time	28	50%	18	23.3	6.44	3.61	877	1234	965	1340	91	27.2
	35	0%	31	15.9	--	--	745	1068	786	1107	72	18.7
	39	100%	32	28.4	12.6	2.25	1070	1490	1127	1559	77	29.1
	59	75%	49	31.5	9.52	3.31	1015	1408	1049	1446	69	32.0

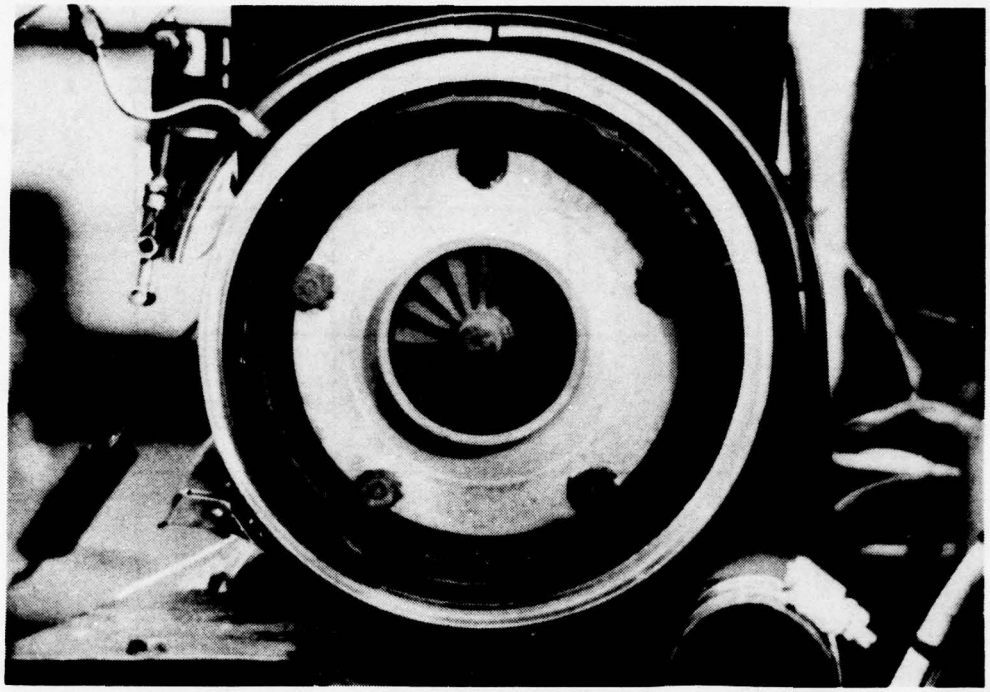

Figure 187. Hybrid All-Ceramic Nozzle After 33 Hours Engine Running

Figures 193 through 196 show disassembly of the nozzle. It reveals that other components with the exception of one vane (which fractured due to misfit of the forward shroud receses) were in good condition after the 50 hour engine test.

In addition, Figure 197 shows that the rear shroud was well centered to the turbine wheel after the test.

3.6 SECOND ALL-CERAMIC NOZZLE ENGINE TEST (RUN #4)

The two hundred (200) hour all-ceramic nozzle engine test run including 50 start/stop cycles was successfully completed in run #4.

To avoid problems occurring in the first all-ceramic nozzle test (engine run #3) a materials change to RBSiC (NC 430) for the rear shroud was made as well as modifications to metallic components.

The redesigned turbine hot end is given in Figures 198, 199 and 200. Changes include addition of a heat shield exterior to the exhust scroll, thicker gage scroll material, a diameter increase of the center bellows section of the PCD activated ceramic to metal face seal, a ceramic shroud material

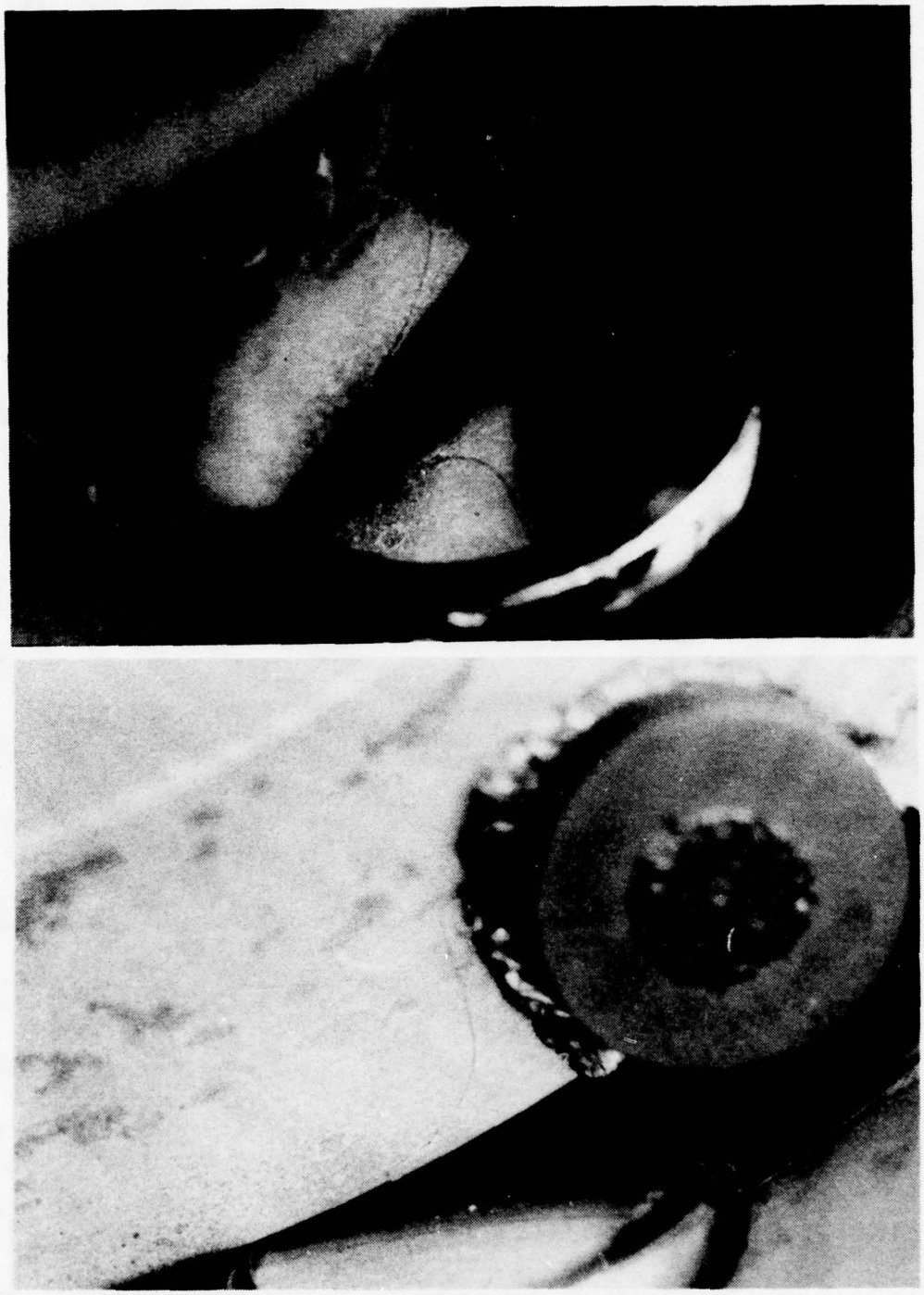

Figure 188. Crack in RBSi$_3$N$_4$ Rear Shroud After 33 Hours Engine Running

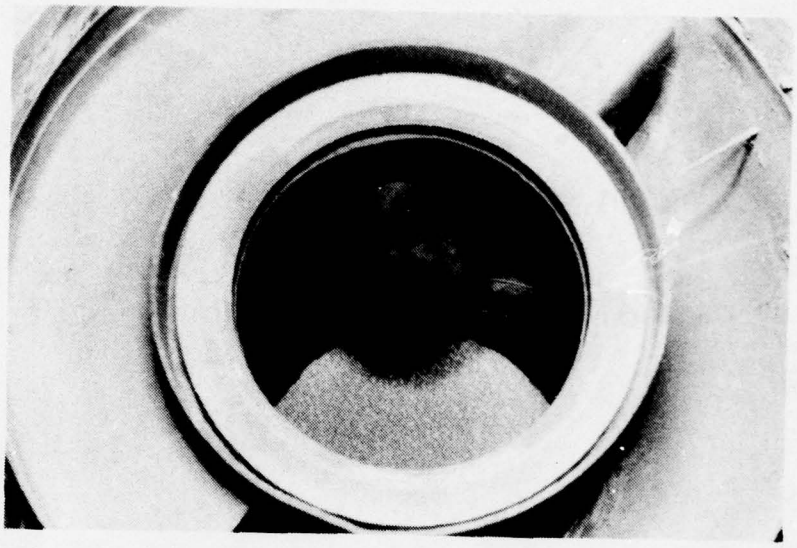

Figure 189. Collapsed Exhaust Scroll

Figure 190. All-Ceramic Nozzle After 50 Hour Engine Run (Note fracture at bottom section of RBSi$_3$N$_4$ rear shroud)

A

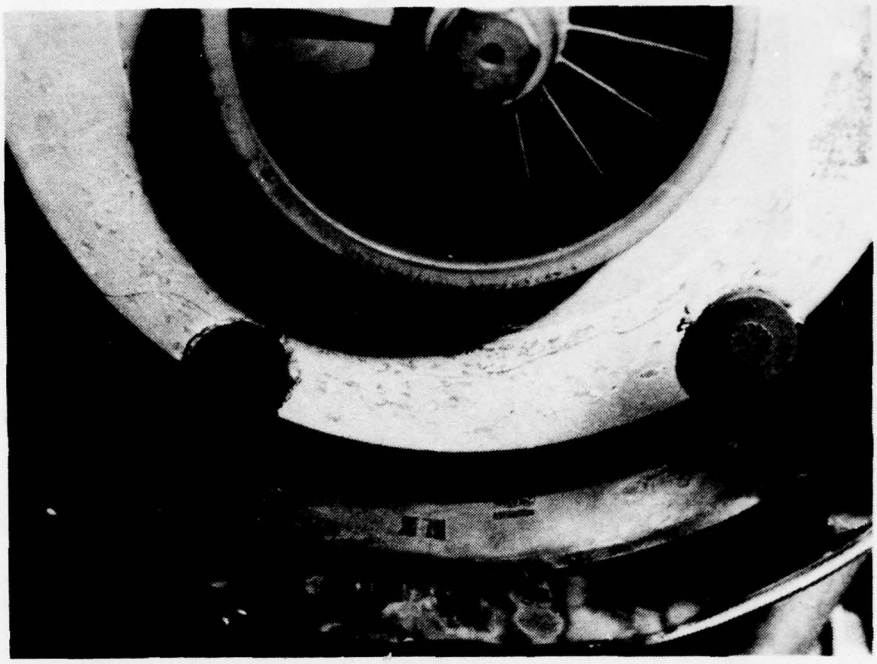

B

Figure 191. All-Ceramic Nozzle After 50 Hour Engine Run (Note fracture at bottom section of $RBSi_3N_4$ rear shroud) (Sheet 1 of 3)

C

D

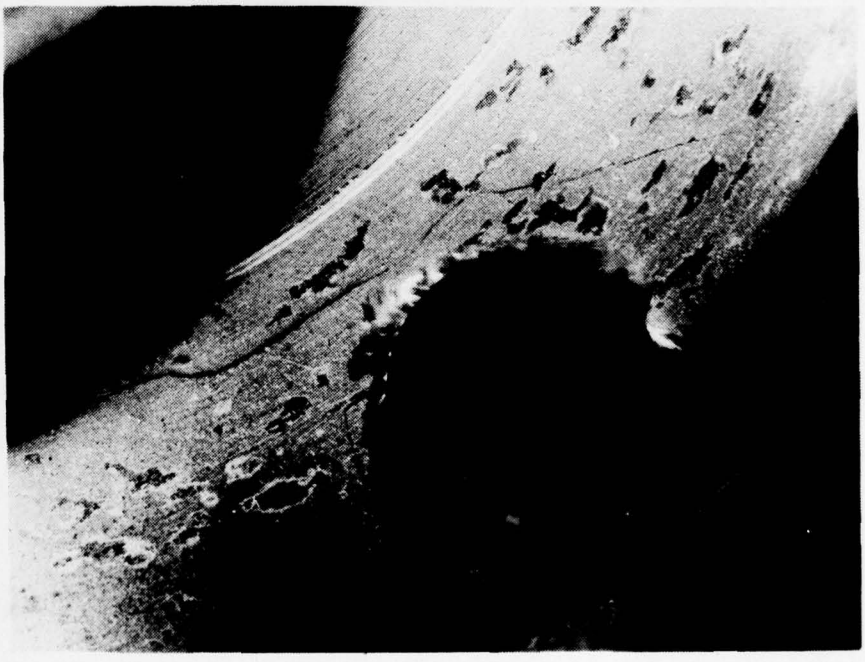

Figure 191. All-Ceramic Nozzle After 50 Hour Engine Run (Note fracture at bottom section of $RBSi_3N_4$ rear shroud) (Sheet 2 of 3)

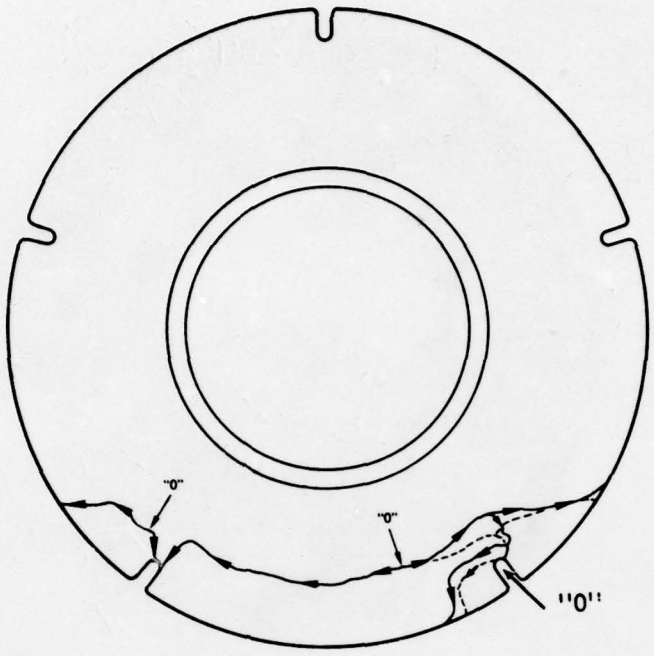

Figure 191. Failure Origins and Crack Propagation in All-Ceramic Nozzle After 50 Hour Engine Run (Sheet 3 of 3)

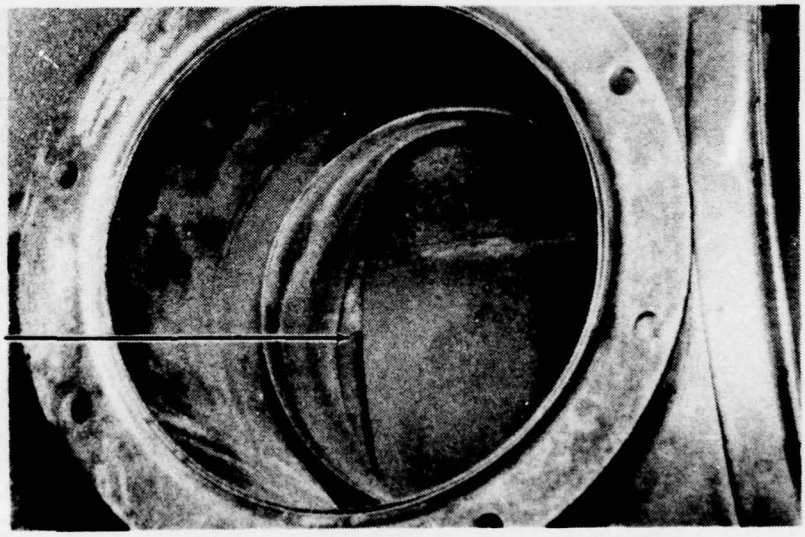

Figure 192. Gap in Exhaust Scroll Heat Shield Below Side Can Combustor for an Above Exhaust Scroll Collapsed Section

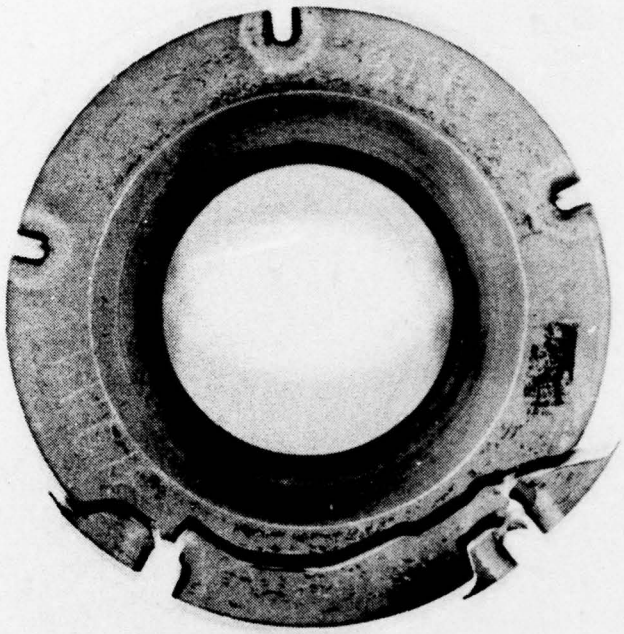

Figure 193. RBSi$_3$N$_4$ Rear Shroud After 50 Hour Engine Test

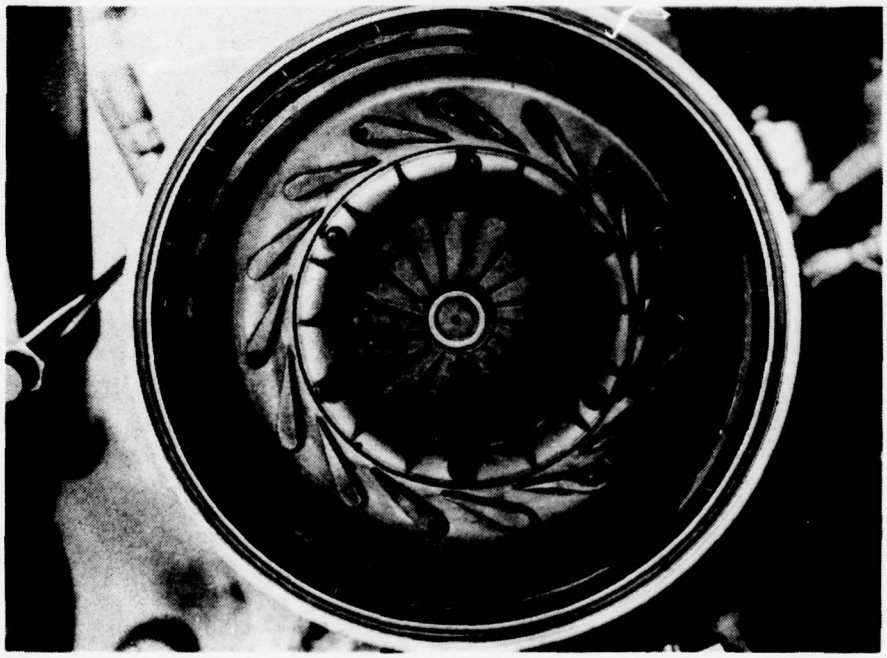

Figure 194. HPSi$_3$N$_4$ Vanes and RCSiC Forward Shroud After 50 Hour Engine Test

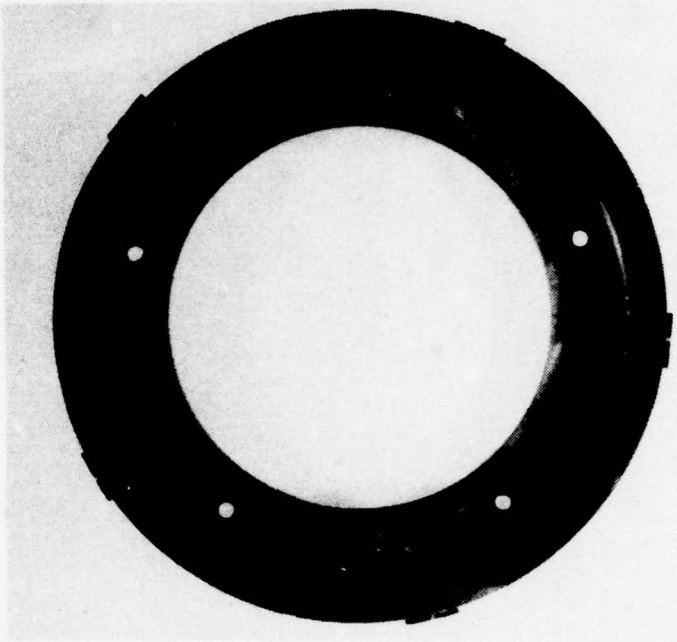

Figure 195a. RCSiC Forward Shroud After 50 Hours Engine Test

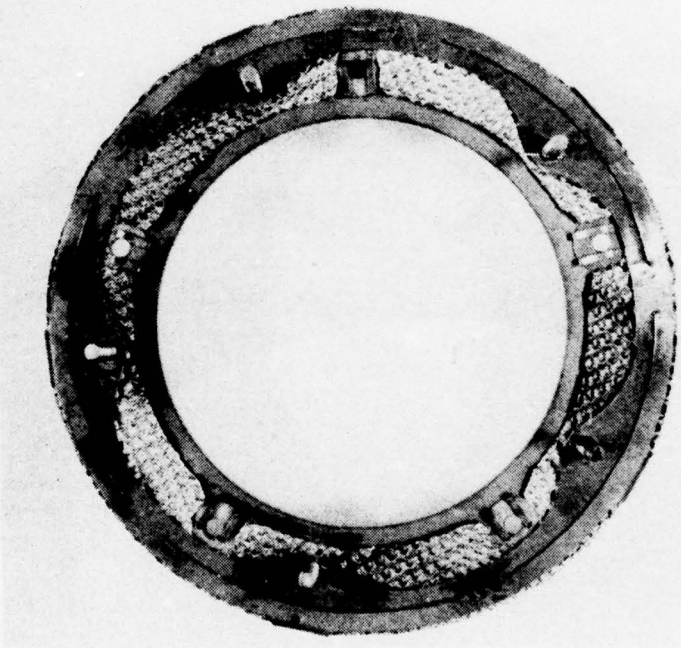

Figure 195b. RCSiC Forward Shroud After 50 Hour Engine Test With Spring Retainer Can, Heat Shield and Bolt Seals in Place

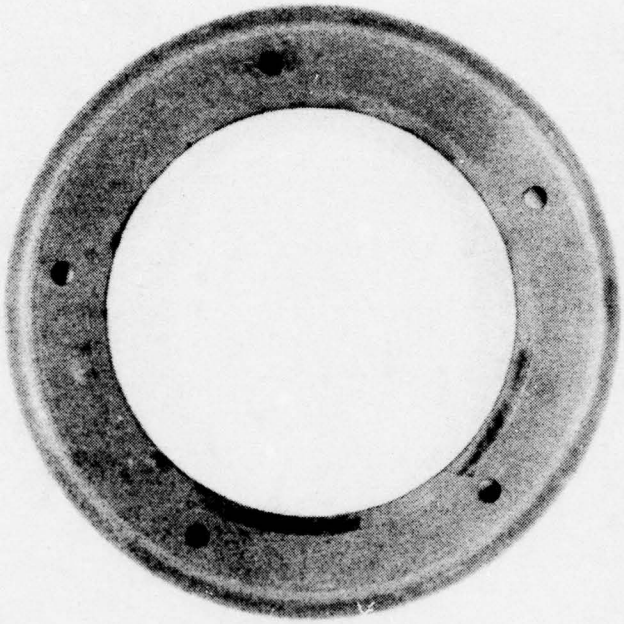

Figure 195c. RCSIC Forward Shroud After 50 Hours Engine Test

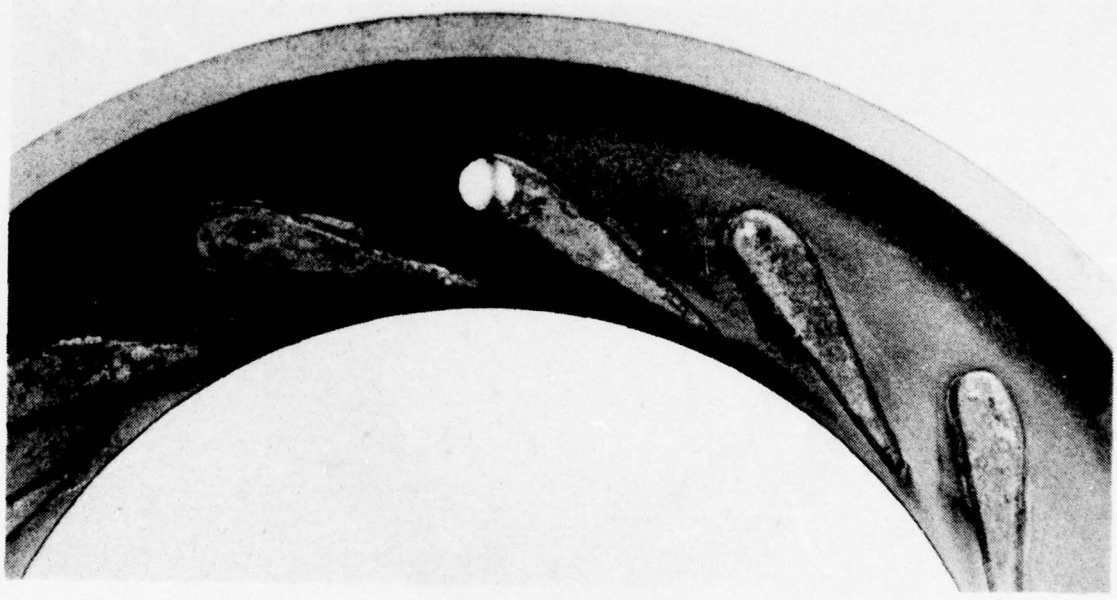

Figure 195d. RCSIC Forward Shroud After 50 Hour Engine Test

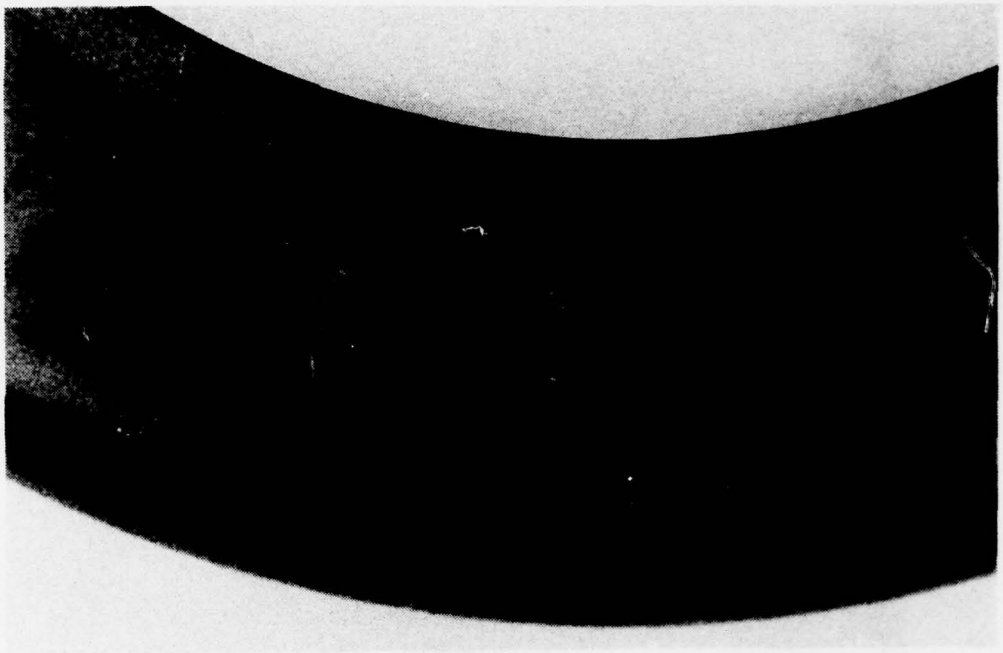

Figure 195e. RCSIC Forward Shroud After 50 Hour Engine Test

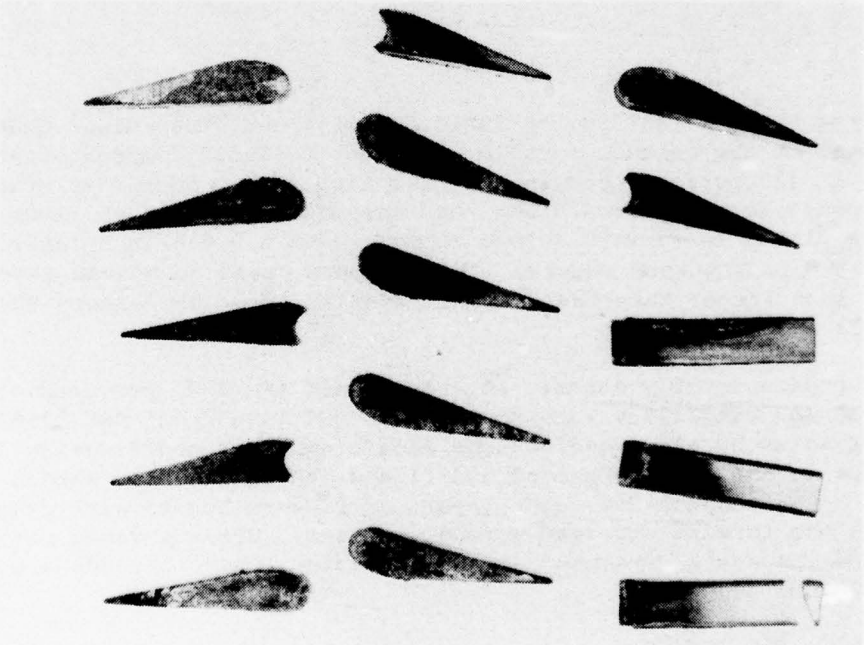

Figure 196. HPSi$_3$N$_4$ Vanes After 50 Hour Engine Test

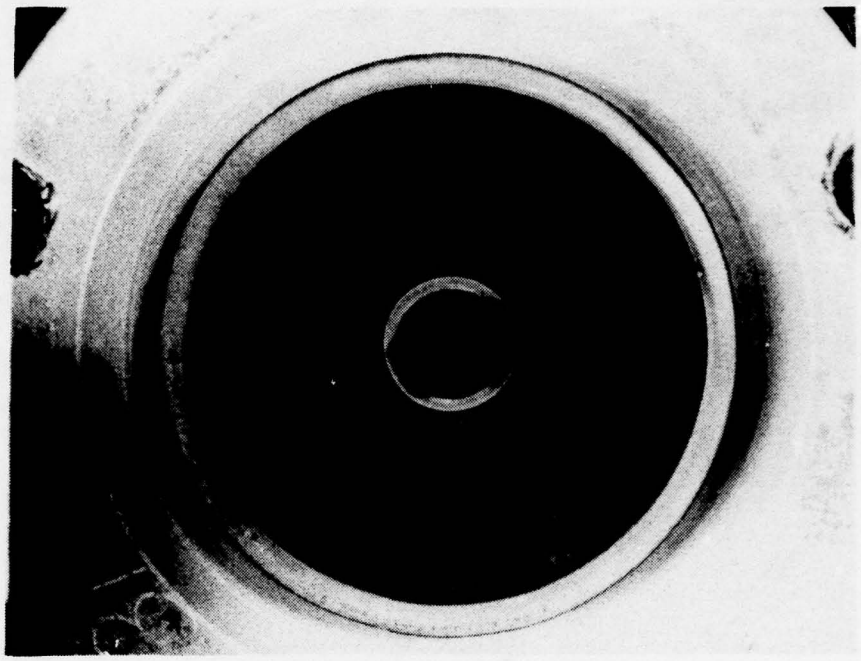

Figure 197. Centering of Rear Shroud From $RBSi_3N_4$ to Turbine Wheel After 50 Hour Engine Test

change from $RBSi_3N_4$ (NC 350) to RBSiC (NC 430) and other minor changes to sheet metal on the exhaust scroll. In order to avoid compressor surge which occurred at 100 percent load in the last test due to out-of-tolerance overdeep recesses in both forward and rear shrouds, a 0.005 inch layer of platinum was placed in forward shroud recesses and a 0.010 inch layer of Pt was added in the rear shroud recess. This measure opens up nozzle throat height to 0.005 inch larger than the nominal resulting from components RSK 230632, RSK 230633 and RSK 230630.

Prior to engine asembly ceramic shrouds of SiC (NC 430) per drawing numbers RSK 230636 and RSK 230637 were modified to RSK 230632 and RSK 230633 respectively at Solar by electro-discharge machining. This modification involves five holes in the forward shroud and five slots in the rear shroud as seen in Figures 201 through 204. The layers of Pt were bonded with cynoacrylate cement in the forward and rear shroud recesses. $HPSi_3N_4$ vanes per RSK 230630, Det. 1 and 2 were used in the assembly. These shrouds are shown in Figures 201 through 204.

Figure 205 is a view of the pressure activated bellows assembly for loading the rear-shroud to exhaust scroll face seal given in Figure 206.

Separate components of the combustor can are shown in Figure 207 and the ceramic nozzle as assembled into the engine is shown in Figure 208.

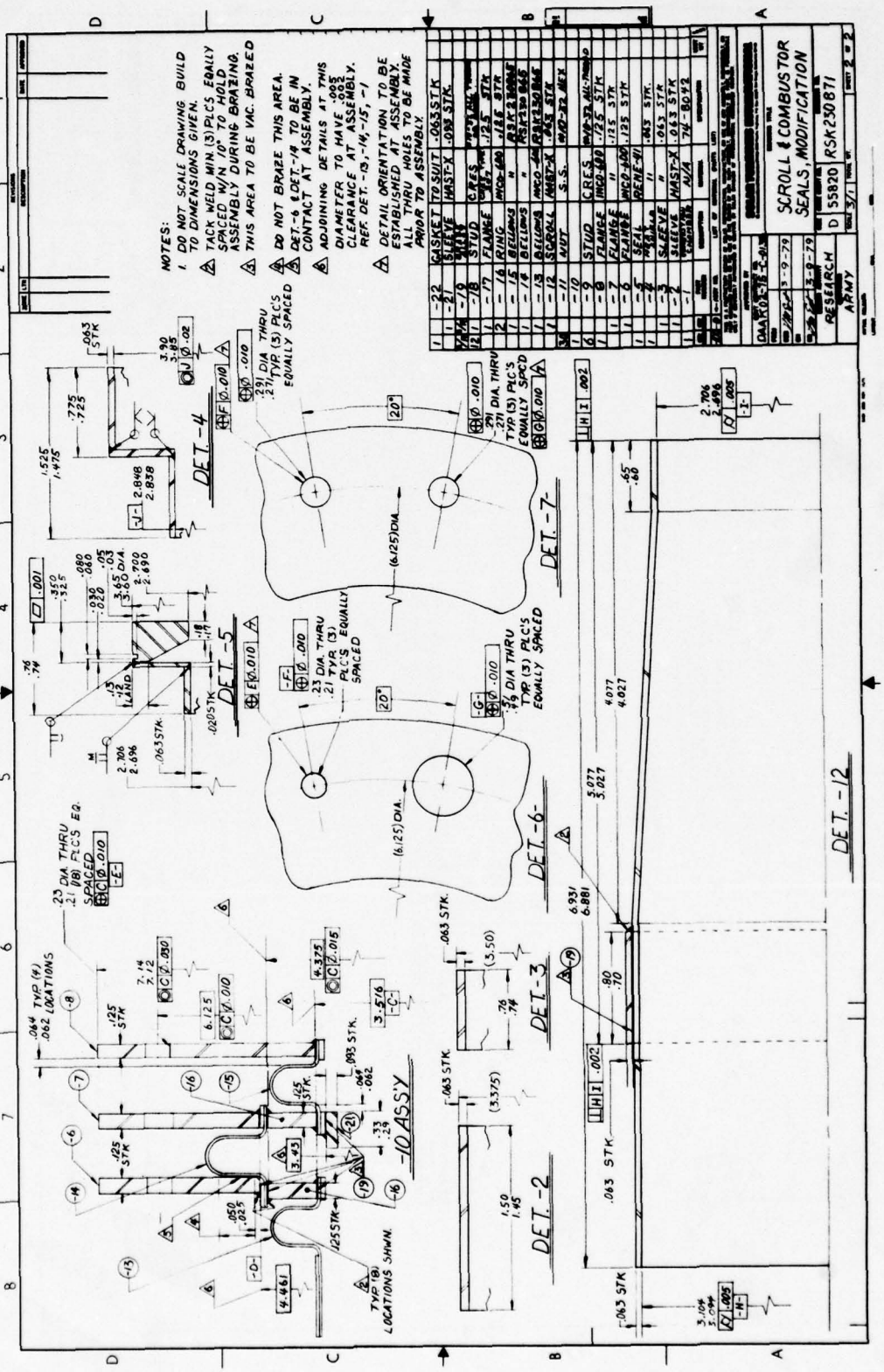

Figure 198. Scroll and Combustor Seals, Modification

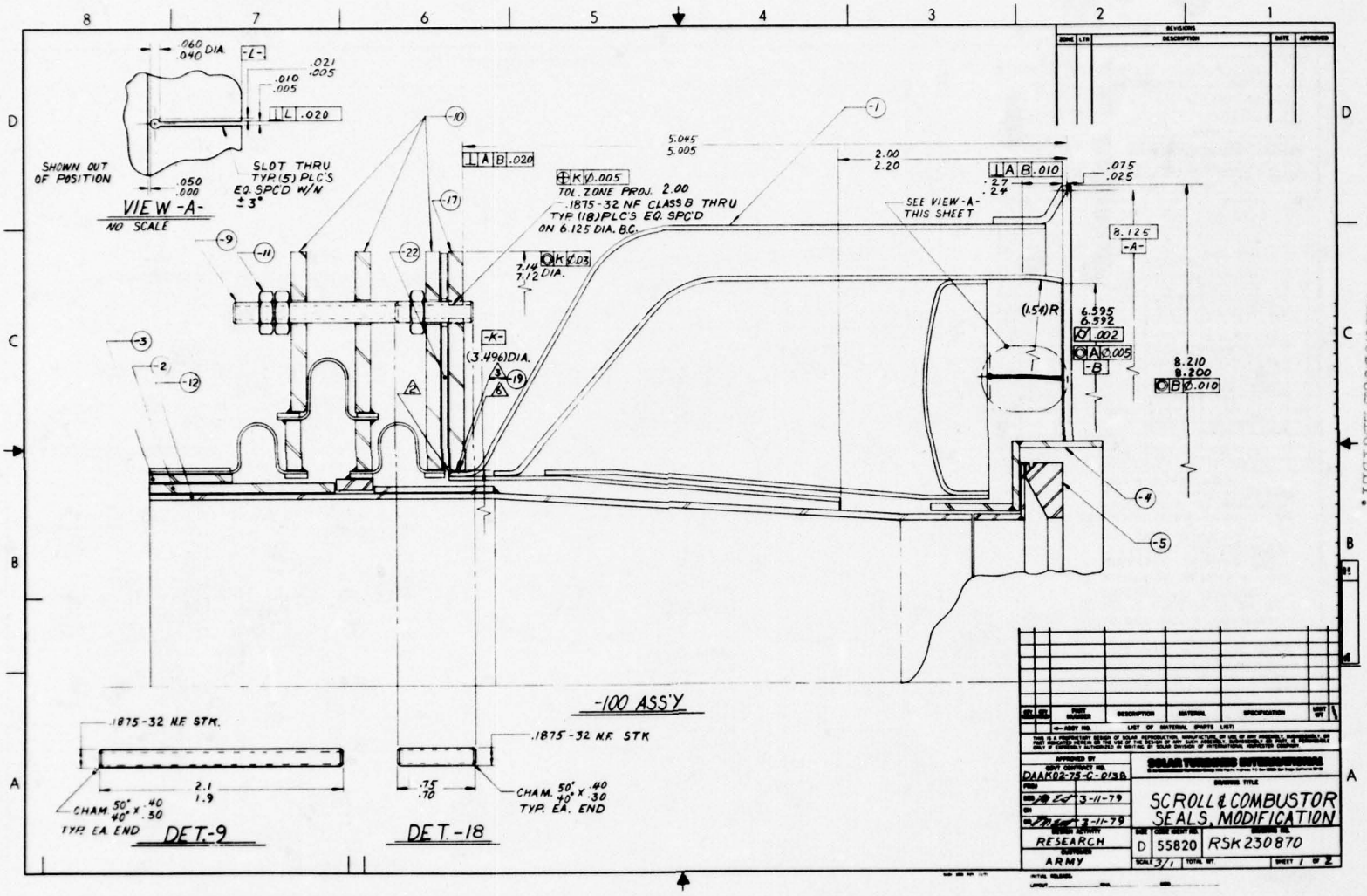

Figure 199. Scroll and Combustor Seals, Modification

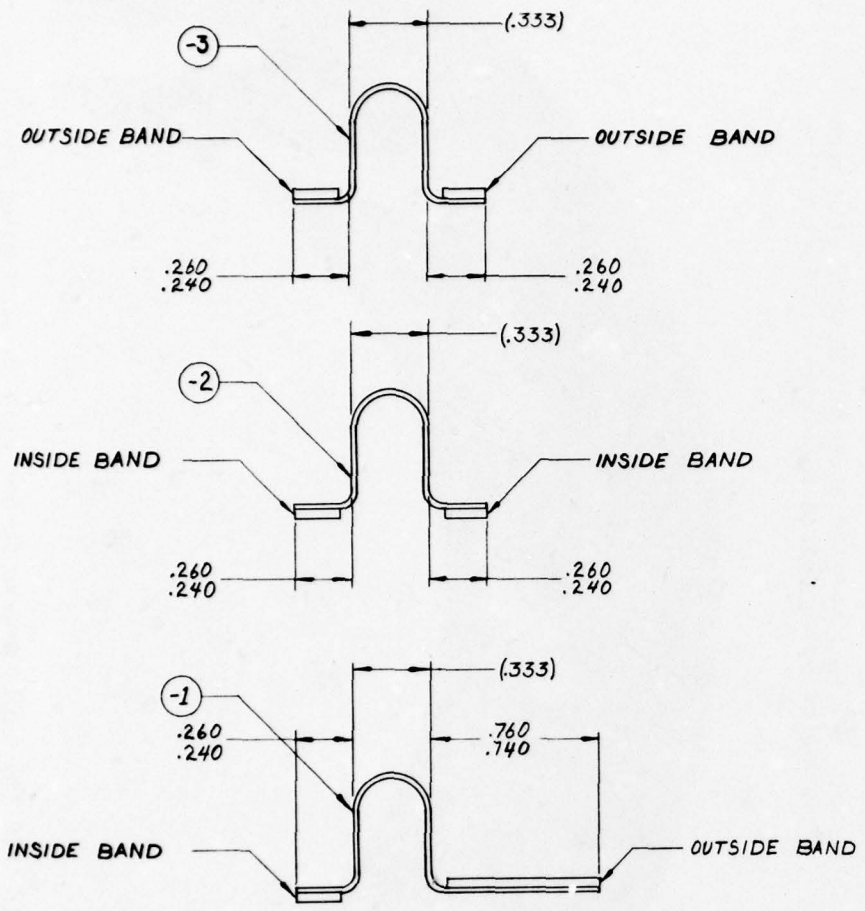

NOTES:

1. DO NOT SCALE DRAWING. BUILD TO DIMENSIONS GIVEN.
2. DRAWING IS TO SPECIFY NECK TRIM ONLY
3. CONVOLUTION DIMENSIONS AND TOLERANCES ARE PER MANUFACTURER'S SPECIFICATIONS AND REQUIREMENTS.

PER HYSPAN #

QTY REQD	QTY REQD	PART NUMBER	DESCRIPTION	MATERIAL	SPECIFICATION	UNIT WT
	1	-3	BELLOWS	INCO 600	#7547G-(33)-.25	
	1	-2	BELLOWS	INCO 600	#7540G-(33)-.25	
	1	-1	BELLOWS	INCO 600	#7540G-(33)-.25/.75	
	-00	← ASSY NO.	LIST OF MATERIAL (PARTS LIST)			

APPROVED BY
GOVT CONTRACT NO. DAAK02-75-C-0138
PROJ 3-1-79
DES 2-28-79
CH
DR 2-28-79
DESIGN ACTIVITY RESEARCH
CUSTOMER ARMY

SOLAR TURBINES INTERNATIONAL

DRAWING TITLE
BELLOWS, SEAL, EXHAUST, ALL CERAMIC TURBINE NOZZLE

SIZE	CODE IDENT NO.	DRAWING NO.
C	55820	RSk 230865

SCALE 3/1 | TOTAL WT. | SHEET 2 OF 2

Figure 200. Bellows, Seal, Exhaust All-Ceramic Turbine, Modified

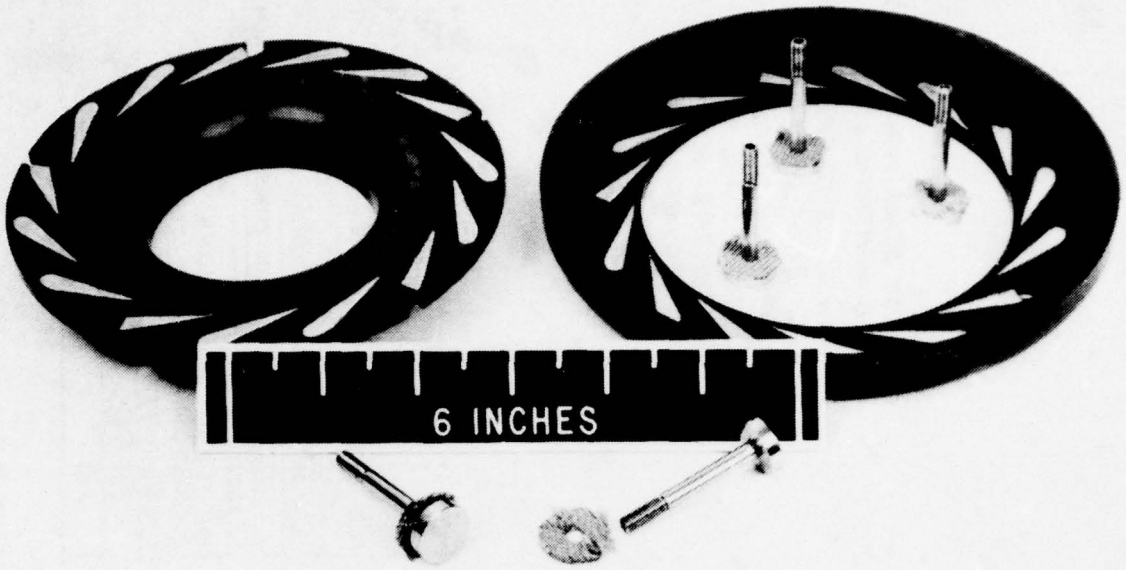

Figure 201. SiC (NC 430) Forward and Rear Shrouds With Rene 41 Mounting Bolts Before Assembly into Test Engine

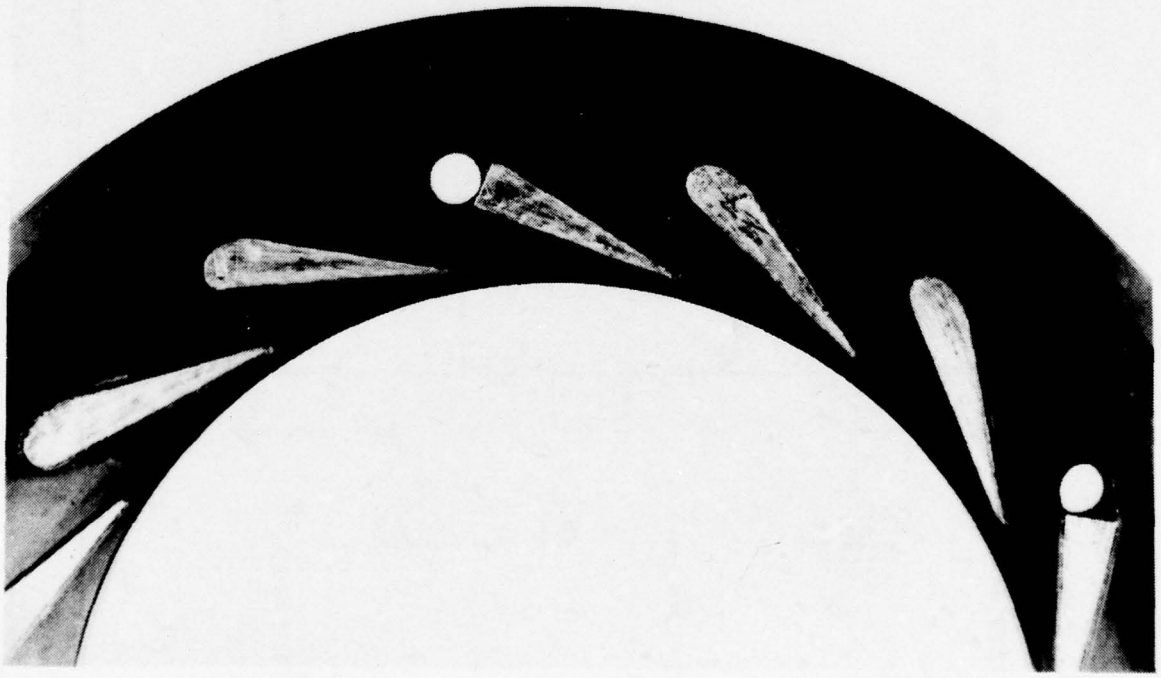

Figure 202. SiC (NC 430) Forward Shroud With Through Holes Added and Pt Layer in Vane Recesses

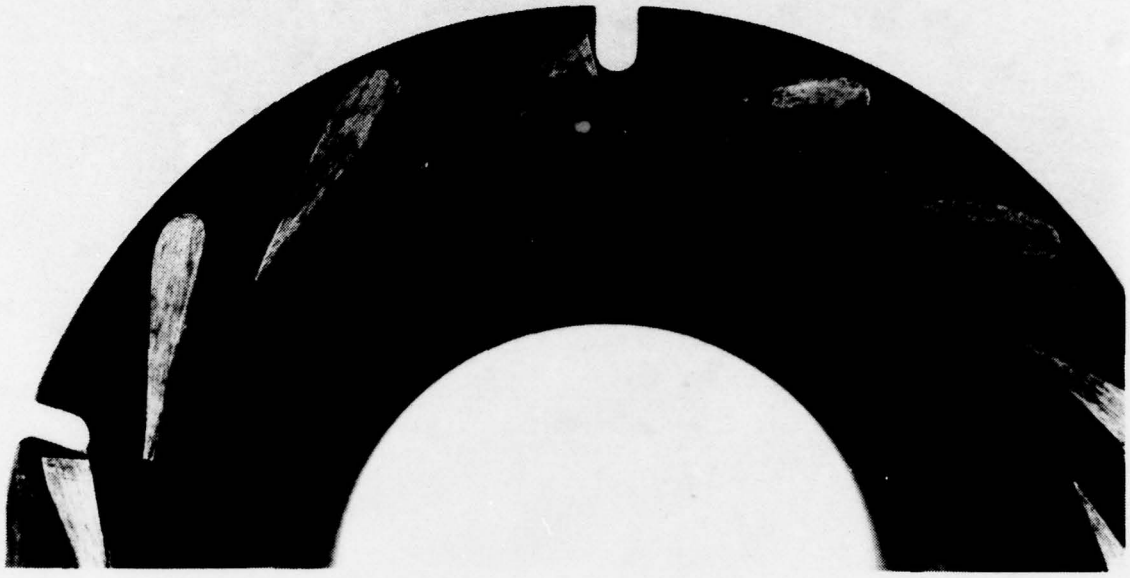

Figure 203. SiC (NC 430) Rear Shroud With Slots Added and Pt Layer in Vane Recesses

Figure 204. SiC (NC 430) Rear Shroud Before Engine Test

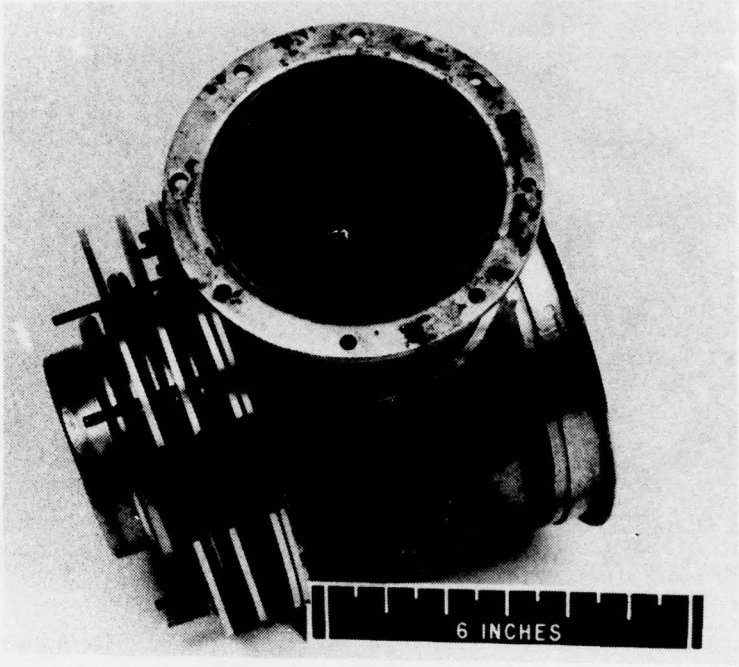

Figure 205. Combustor Housing With Pressure activated Bellows Assembly for Loading Rear Shroud to Exhaust Scroll Face Seal

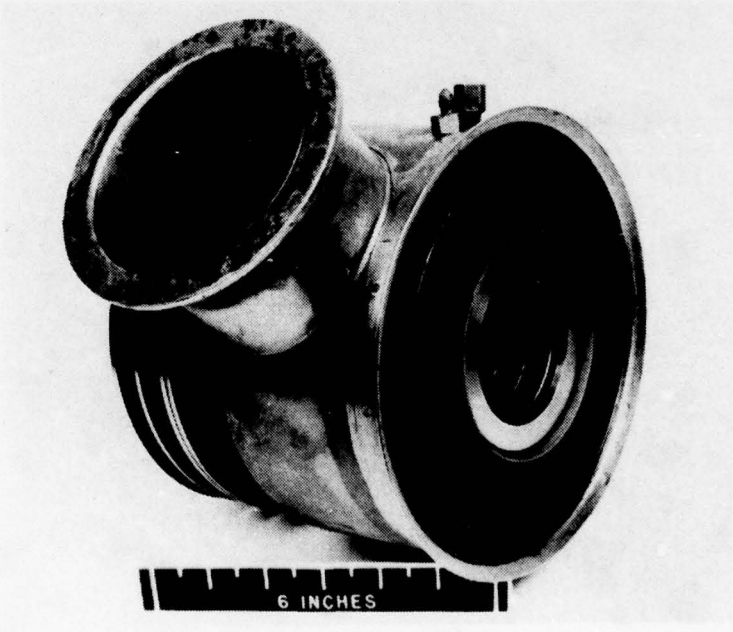

Figure 206. View of Combustor Housing Showing Exhaust Scroll Face Seal

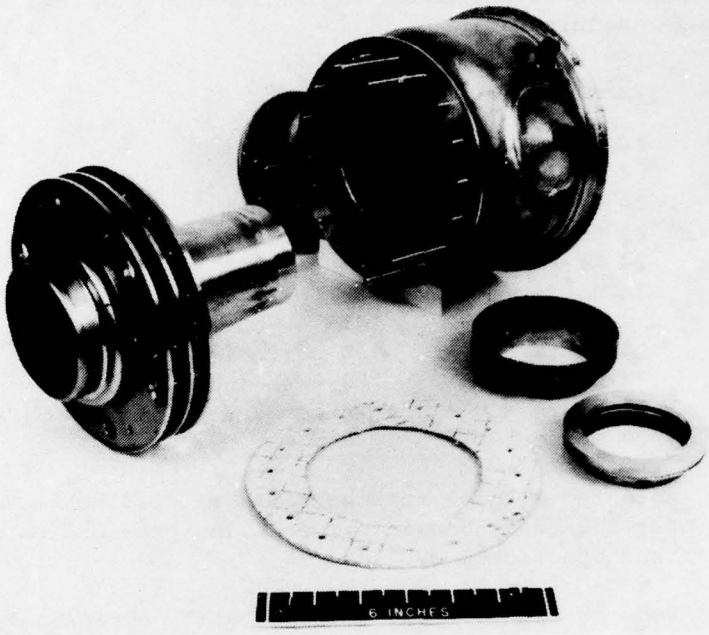

Figure 207. Components of Combustor Housing

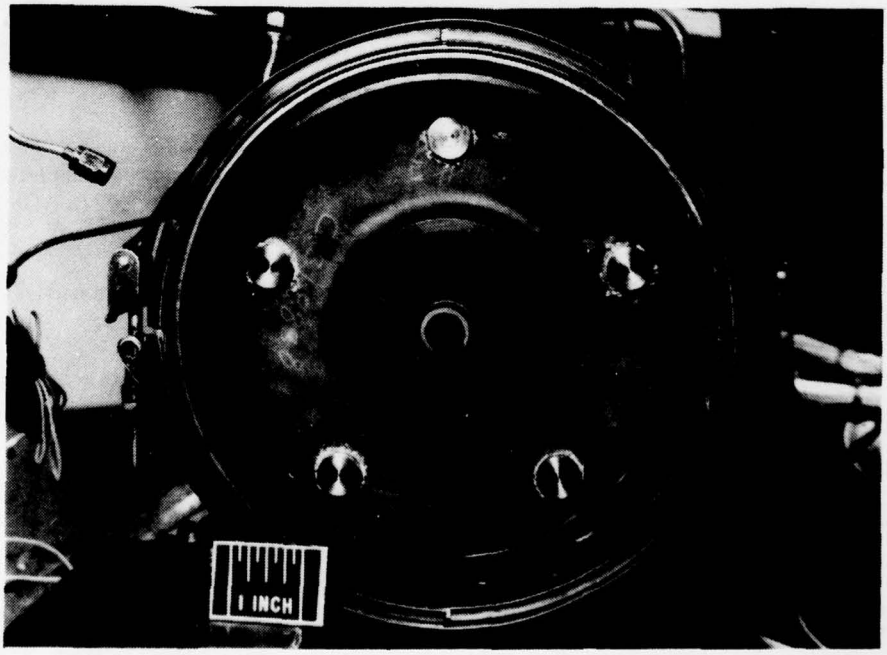

Figure 208. SiC (NC 430) Ceramic Nozzle Before Engine Test Run #4

The test cycle consisted of 200 hours engine running time and 50 start/stop cycles. The load schedule was:

	Time	Load
	24 hours	50 percent
	4 hours	Idle
	24 hours	100 percent
	24 hours	25 percent
	24 hours	75 percent
	24 hours	50 percent
	4 hours	Idle
	24 hours	100 percent
	24 hours	25 percent
	24 hours	75 percent
Total	200 hours	

The Hobbs meter indicated a total running time of 210.9 hours. The balance of running time over 200 hours was incurred during pre- and post-test performance calibration and start/stop cycling.

Three flame-outs from 50 percent load occurred after approximately 15 hours of running due to fuel system problems.

An unscheduled shutdown occurred after 121 hours of running. The shutdown was believed to be due to sizing of the starter one-way clutch, but disassembly of the gear box section showed the existing clutch to be in working order. It was replaced, however, as a precautionary measure. The shutdown most likely resulted from air in the fuel delivery time. The combustor housing was removed at this time for inspection of the ceramic nozzle. All ceramics visible in this partial disassembly showed no apparent flaws.

The axial turbine tip to rear shroud clearances were measured at 121 hours to be in the range of 0.0180 to 0.020 inch which is within the specified limits of 0.0175 to 0.022 inch. These clearances were approximately 0.019 to 0.021 inch at the start of the test.

After inspection at 121 hours the combustor housing was re-assembled and the test continued until completion of the 200 hour endurance run.

A total of 41 start/stop cycles were incurred in completing the 200 hours of endurance running time. An additional nine starts and stops were made at the end of endurance running to bring the total to 50 starts.

Disassembly of the engine showed ceramic nozzle components consisting of forward and rear shrouds and 15 vanes to be in excellent condition.

The engine was disasembled after the 200 hour endurance run. Figure 209 shows the rear ceramic (NC 430, RBSiC) nozzle shroud with the combustor housing (shown in Figure 210) removed after completion of the 200 hour endurance run.

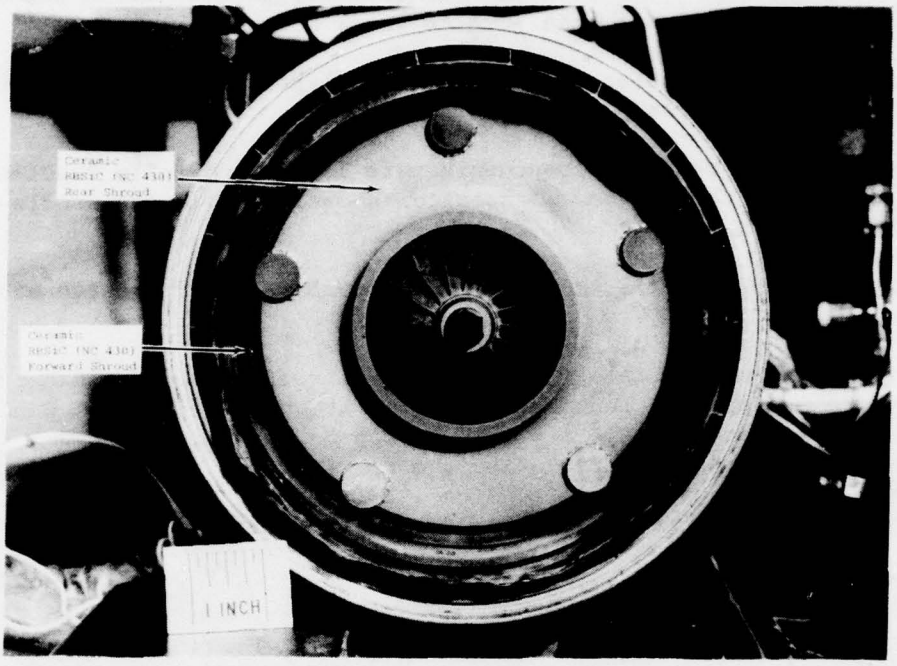

Figure 209. Gemini Radial Ceramic Turbine Nozzle After Successful 200 Hour Engine Test

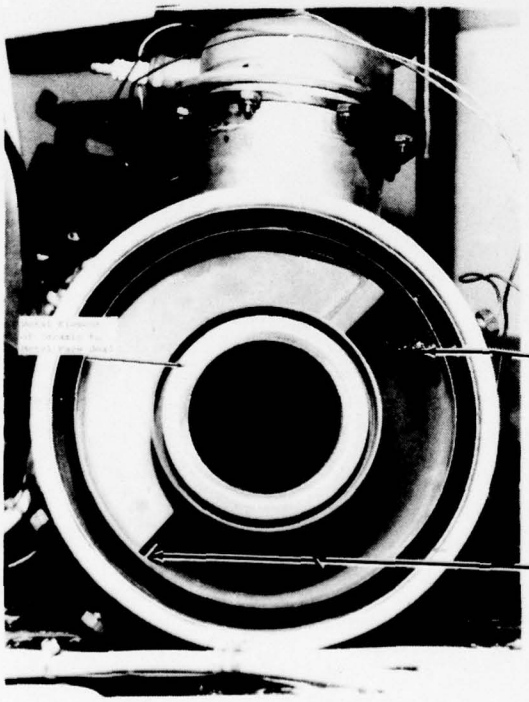

Figure 210.

Combustor Housing After 200 Hour Engine Test

Figure 211 shows the forward ceramic (NC 430, RBSiC) nozzle shroud, ceramic vanes (NC 132, $HPSi_3N_4$), the turbine wheel and seal plate.

Figure 212 is a close-up view of the radial turbine wheel exducer and ceramic rear shroud illustrating good radial centering control.

All-ceramic and metallic components were intact and fully functional upon disassembly of the engine. Inspection showed no evidence of flaws or cracks in the ceramics.

Figures 213 through 218 show ceramic components after the 200 hour engine test.

The face seal at the interface between the rear shroud and exhaust scroll showed no evidence of leakage or deterioration. Evidence of bonding of face seal Rene 41 ring and SiC rear shroud can be seen in Figure 212 in the form of small metal pieces attached to the rear shroud. This did not affect the performance of the seal since no radial streaking as might occur with leakage was present on the seal faces.

An engine performance calibration was made at the start of the test and at completion of the endurance run. These results, seen in Table 27, show that performance improved slightly during the run. This may have resulted from better nozzle recess seating with running time, however, the improvement is not statistically significant enough to draw definite conclusions.

Figures 219 through 223 show thermocouple temperature readouts for typical engine start and stop cycles. Thermocouple locations are shown in Figure 210.

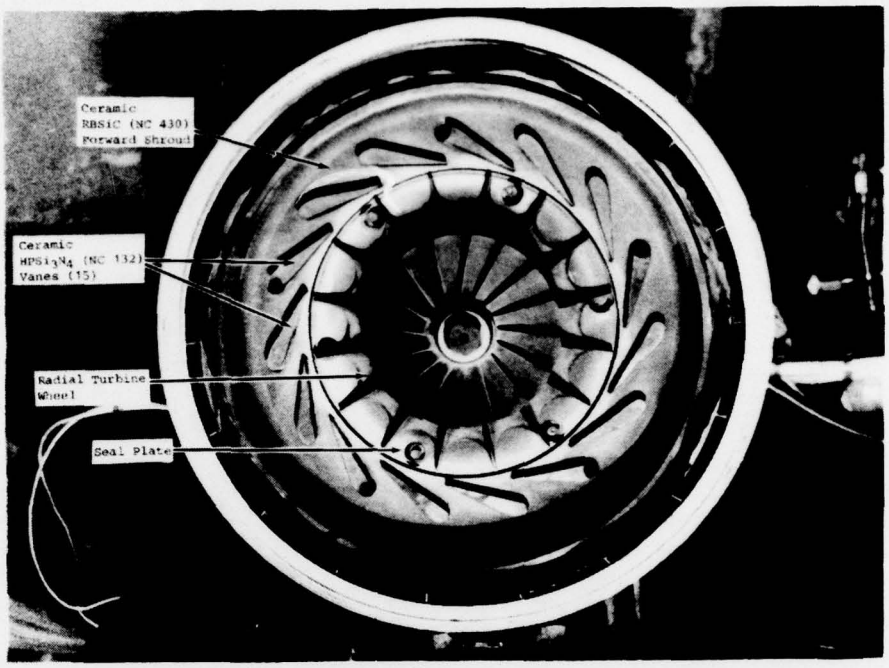

Figure 211. Ceramic Forward Shroud and Vanes After Successful 200 Hour Engine Test

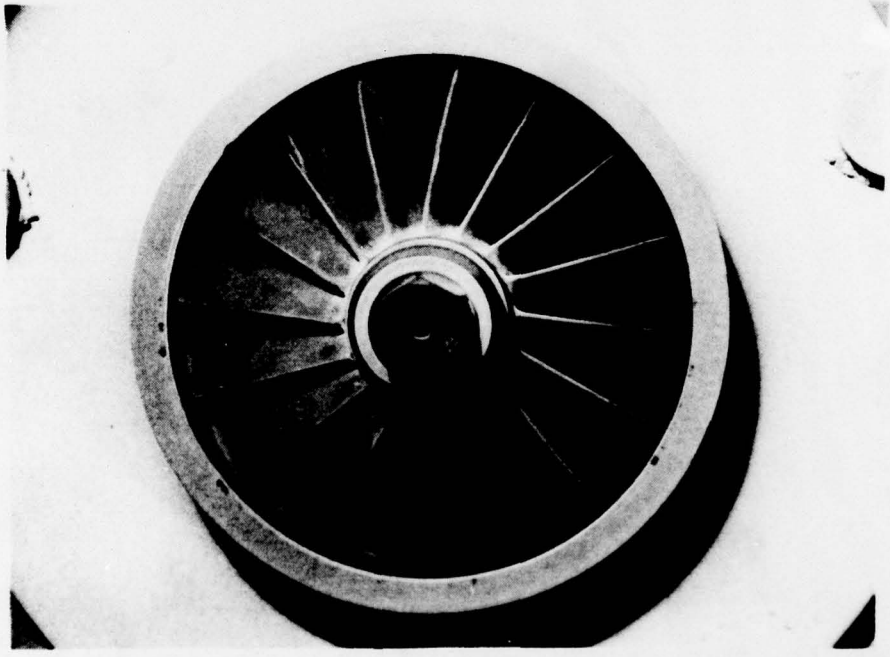

Figure 212. Ceramic Rear Shroud and Radial Turbine Wheel Exducer

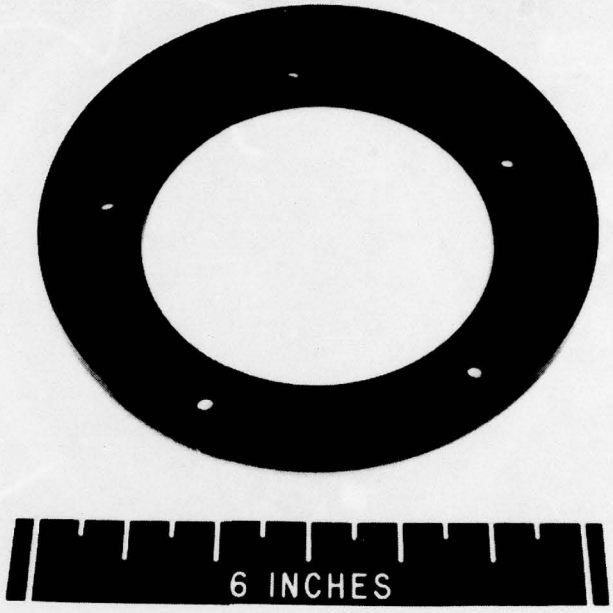

Figure 213. RBSiC (NC 430) Forward Shroud After Successful 200 Hour Engine Test

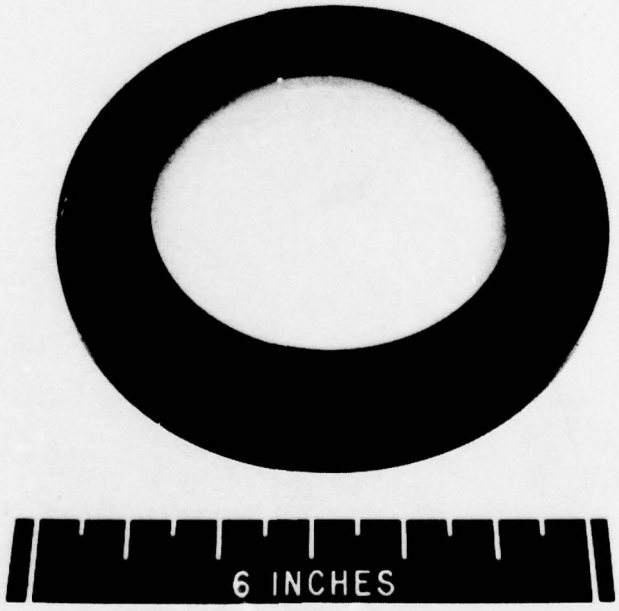

Figure 214. RBSiC (NC430) Forward Shroud After Successful 200 200 Hour Engine Test

Figure 215. RBSiC (NC 430) Rear Shroud After Successful 200 Hour Engine Test

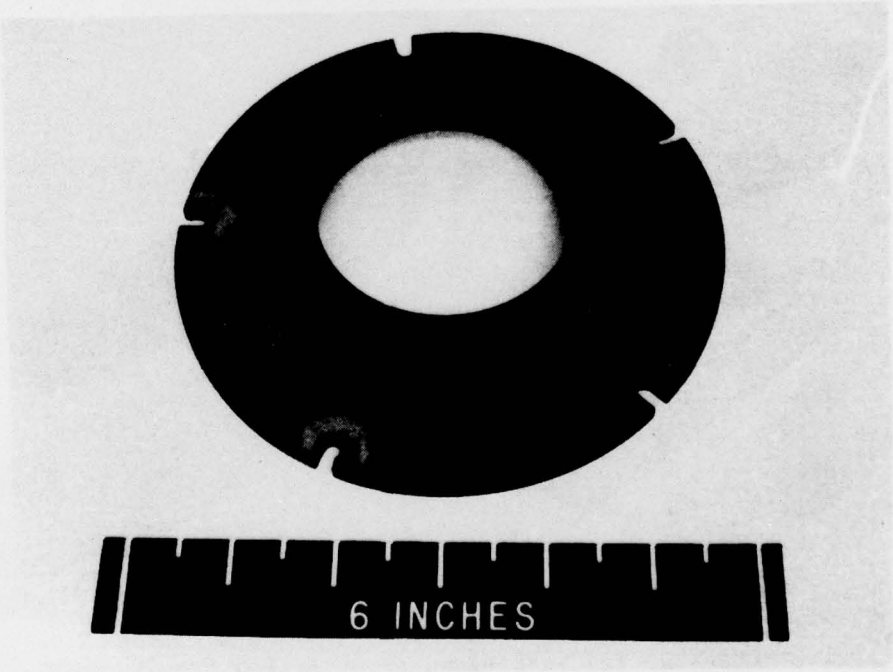

Figure 216. RBSiC (NC 240) Rear Shroud After Successful 200 Hour Engine Test

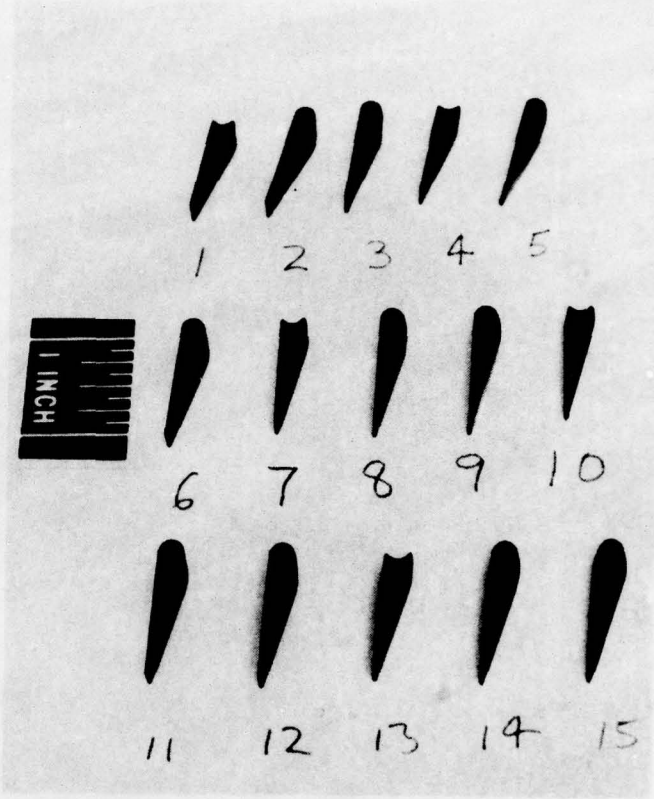

Figure 217. $HPSi_3N_4$ (NC 132) Vanes After Successful 200 Hour Engine Test

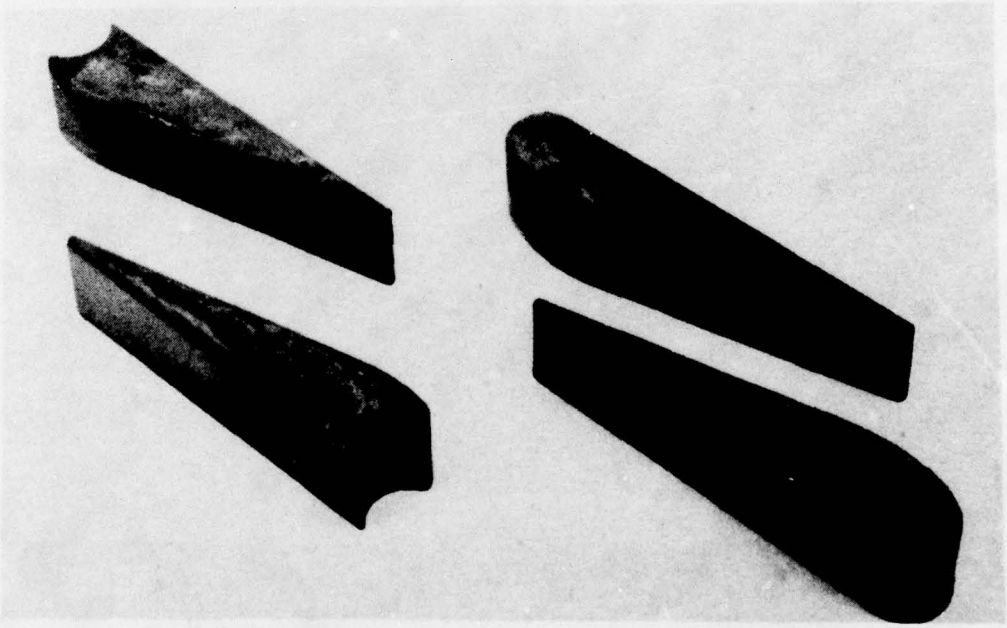

Figure 218. $HPSi_3N_4$ (NC 132) Vanes After Successful 200 Hour Engine Test

Table 27

Test #4 - Calibration Data for Gemini Engine With All-Ceramic Nozzle (Corrected to Standard 59°F and 14.7 psia Ambient Conditions) (Linear Loading - No cyclo Convertor Losses)

	Data Point No.	Load	Cummulative Engine Running Time (hours)	Corrected Fuel Flow (pph)	Shaft Power Output (kW)	Shaft Specific Fuel Consumption lb JP-4 kW-hr	Corrected		Measured Exhaust Gas Temperature (°F)	Turbine Inlet Temp. Calc. From EGT (°F)	Actual Compressor Inlet Temperature (°F)	Actual Fuel Flow
							Exhaust Gas Temperature (°F)	Turbine Inlet Temperature (°F)				
Pre-Test	65	0%	33	13.8	--	--	732	1042	767	1098	78	14.7
	81	25%	60	17.6	3.25	5.42	800	1124	881	1217	89	18.9
	24	50%	70	21.7	6.17	3.51	903	1255	981	1349	87	22.8
	124	75%	97	22.6	9.38	2.40	986	1366	1060	1456	84	23.4
	78	100%	42	26.0	12.4	2.10	1081	1491	1110	1527	68	26.3
After 200 hour run and 50 start/ stop cycles	285	0%	209	15.7	--	--	742	1058	812	1132	84	16.9
	286	25%	209	18.1	3.33	5.45	814	1154	893	1242	87	19.3
	287	50%	209	19.7	6.23	3.16	870	1222	973	1343	96	21.1
	283	75%	208	23.4	9.72	2.40	998	1384	1090	1496	90	24.4
	288	75%	210	22.4	9.25	2.42	971	1349	1051	1445	86	23.3
	289	100%	210	25.6	12.45	2.05	1064	1481	1147	1584	86	26.45

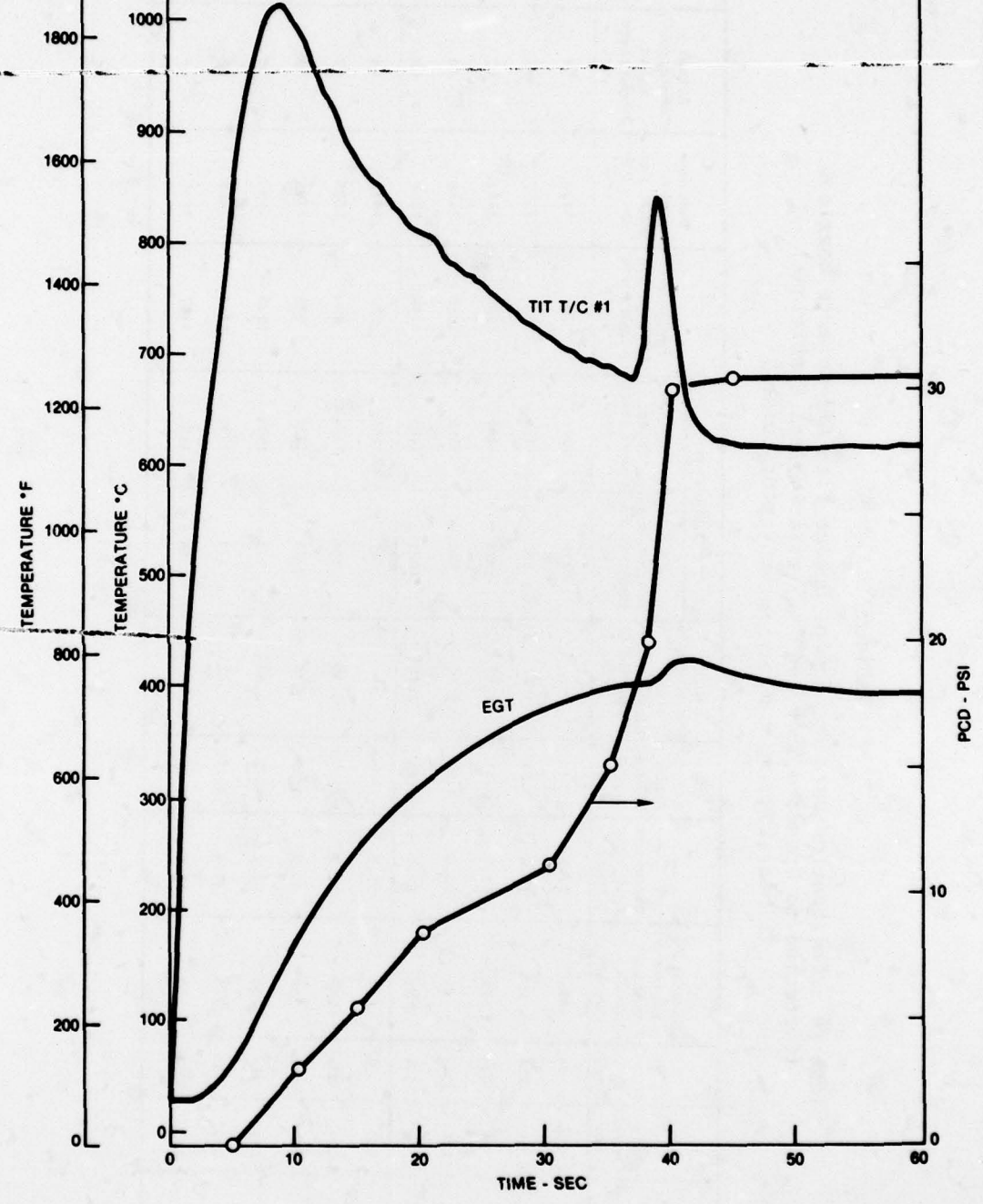

Figure 219. Cold Start Transient for Gemini Engine With All-Ceramic Nozzle TIT and EGT Thermocouple Traces Versus Time and Pressure at Compressor Discharge (PCD)

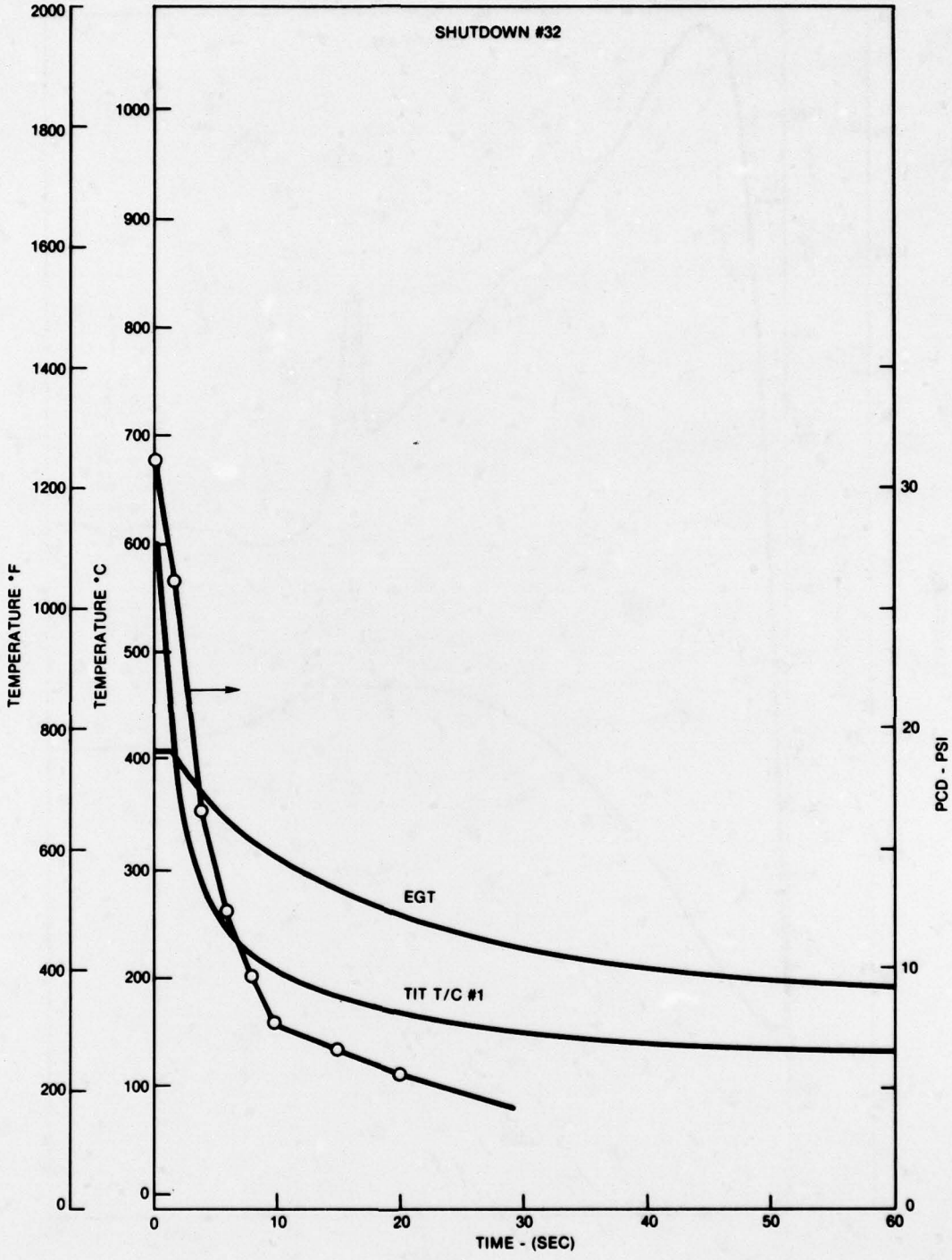

Figure 220. Shutdown Transient for Gemini Engine With All-Ceramic Nozzle TIT and EGT Thermocouple Traces Versus Time and PCD

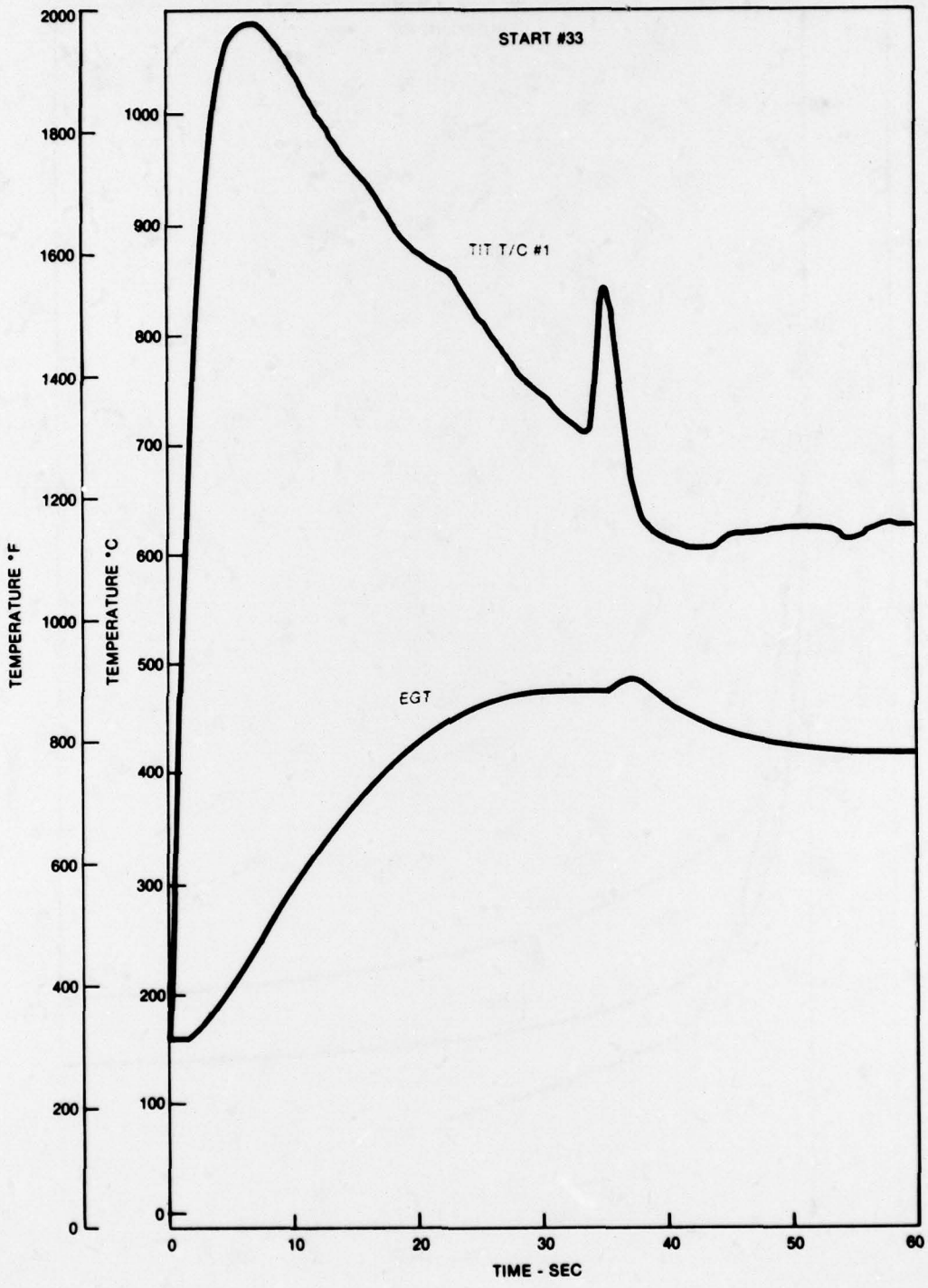

Figure 221. Hot Start Transient for Gemini Engine With All-Ceramic Nozzle TIT and EGT Thermocouple Traces Versus Time

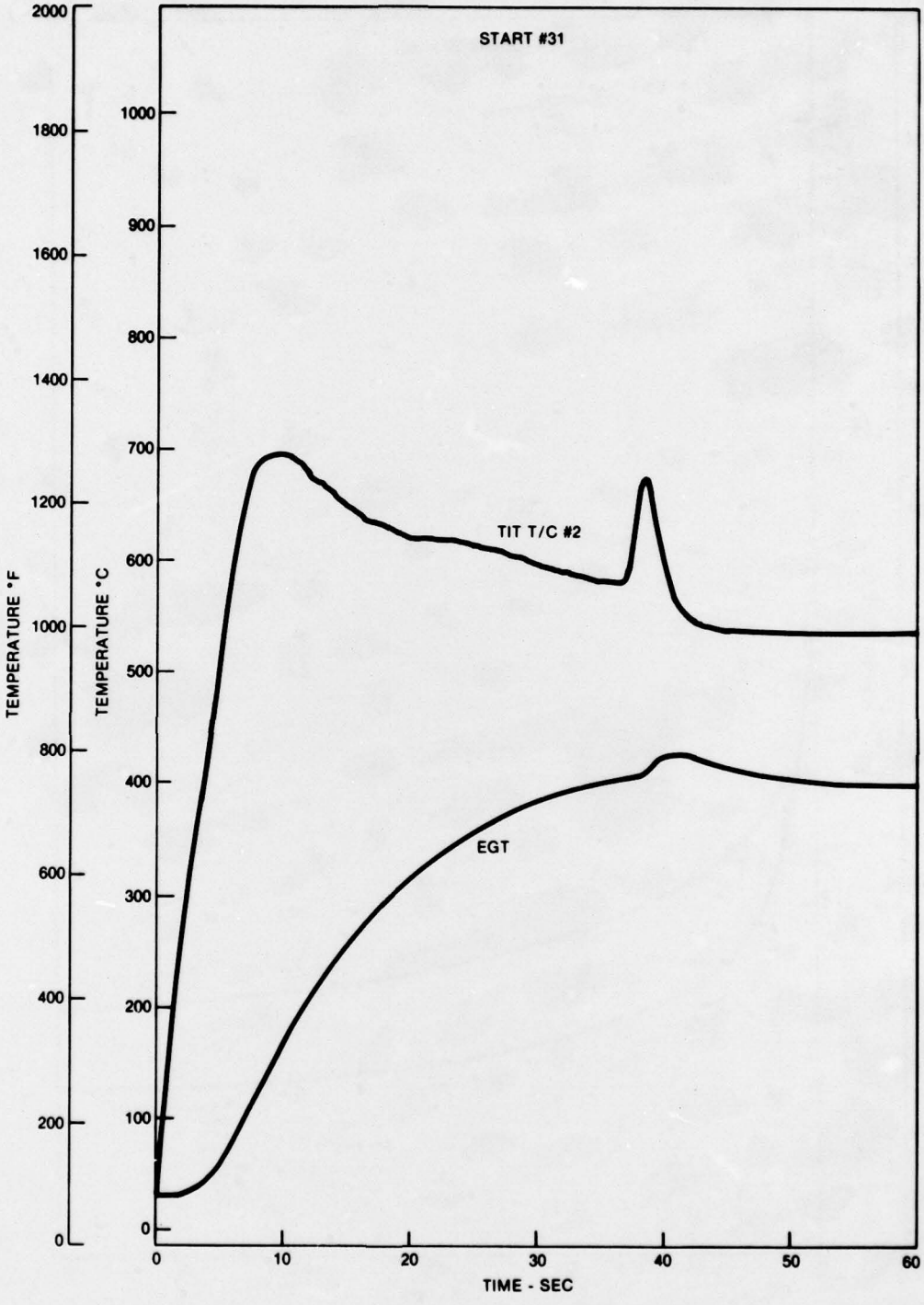

Figure 223. Cold Start Transient for Gemini Engine With All-Ceramic Nozzle TIT and EGT Thermocouple Traces Versus Time

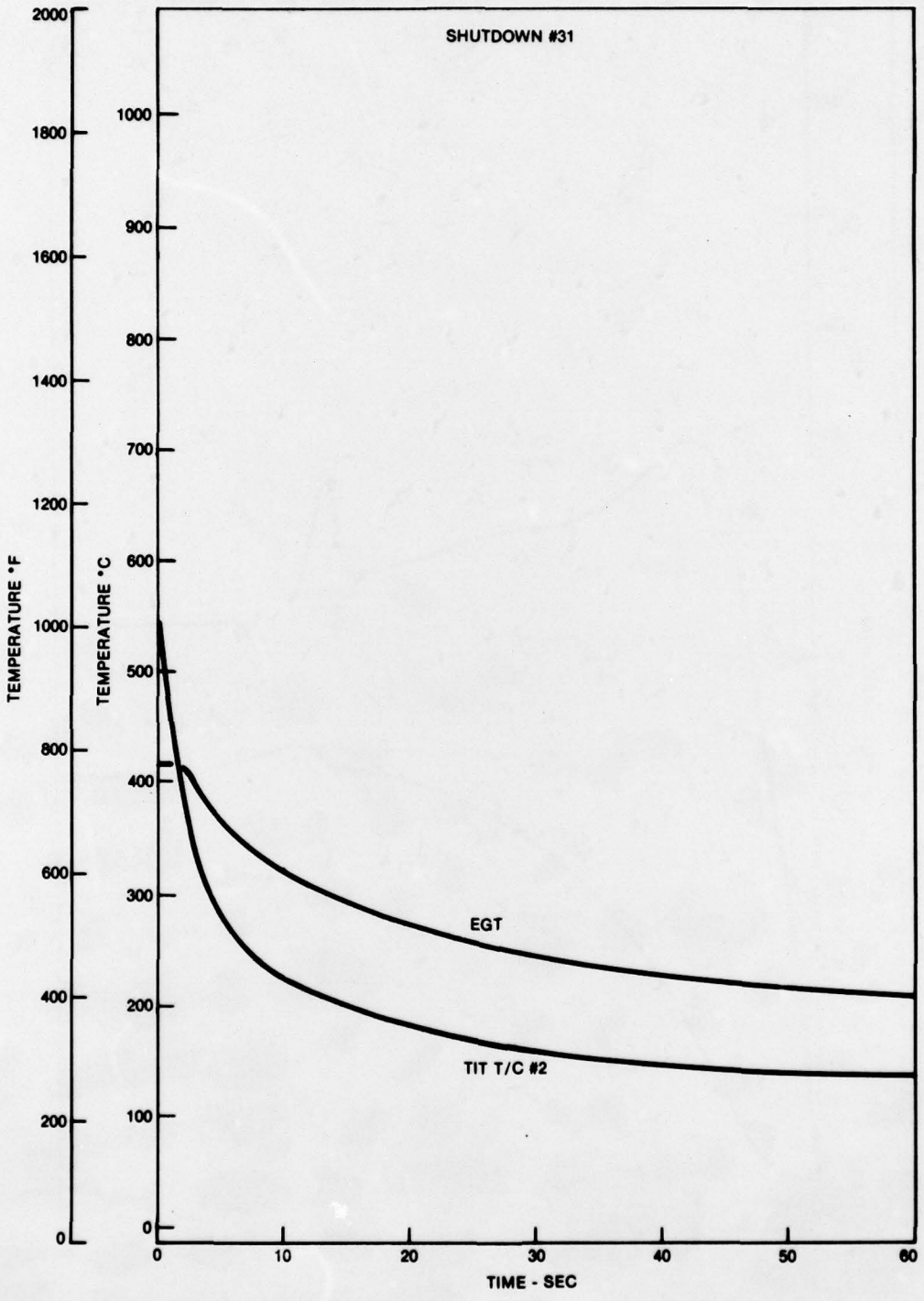

Figure 222. Shutdown Transient for Gemini Engine With All-Ceramic Nozzle TIT and EGT Thermocouple Traces Versus Time

4

CONCLUSIONS

Engine testing has shown feasibility of operating the Gemini gas turbine engine with ceramic vane inserts for high erosion resistance and with an all-ceramic nozzle for up-rating turbine inlet temperature.

The first goal of this project which was to engine demonstrate ceramic nozzle vane inserts was met in a 25 hour engine run which included an additional 50 start/stop cycles. This was a re-run of the initial run of the same test in which disassembly revealed trailing edge fractures in one-third of the fifteen vanes. Design changes in supporting metallic components and addition of a relaxing glass adhesive to ceramic metal interface produced the successful engine run.

Engine simulator experiments performed in preparation for these engine tests showed that this nozzle has erosion resistance one to two orders of magnitude greater than the standard superalloy nozzle. Sea salt corrosion and thermal shock tests showed the $HPSi_3N_4$ vane inserts to perform with considerably less corrosive attack than the surrounding superalloy assembly pieces and to have good thermal shock properties.

An all-ceramic nozzle is considered to be the critical element to up-rating the uncooled turbine inlet temperature of this engine to 1066°C (1950°F). A 200 hour engine test showed the feasibility of operating an all-ceramic nozzle in the 10 kW. At the conclusion of this test no deterioration of ceramic nozzle components or engine performance was observed. The engine test results have allowed the conclusion to be drawn that an all-ceramic nozzle can be integrated withmetallic components in a small radial turbine and successfully perform the critical function of a nozzle which includes: providing good transition seals from metallic to ceramic components, and an accurate turbine tip seal location.

5

RECOMMENDATIONS

Areas which should be considered in advancement of ceramics in the Gemini turbine engine include cost reduction and up-rating of other hot end components with further engine testing.

Work has been initiated in a MERADCOM/Solar cost reduction project entitled "Manufacturing Methods for Ceramic Nozzle Section of Gas Turbine Powered APU's" which is initially looking at alternative silicon based ceramic materials and manufacturing methods for ceramic vane inserts for the 10 kW nozzle. It is planned that this effort will ultimately show economic advantages of using ceramics in the turbine nozzle section for improved erosion resistance and lower engine life cycle costs.

To fully up-rate the 10 kW Gemini engine to higher turbine inlet temperature and higher power output, it is further recommended that the combustor and elements of the combustor can including baffles and scrolls be improved for higher temperature operation by redesign of metal components and/or integration of specific ceramics into this assembly.

REFERENCES

1. Shoemaker, H. E. and Shumate, C. P., "Techniques for Reducing Sand and Dust Erosion in Small Gas Turbine Engines", SAE Paper 700706, Society of Automotive Engineers (Sept. 1970).

2. "Gas Turbine Sand and Dust Effects and Protection Methods", SAE Paper 700705 (Sept. 1975).

3. Compton, W. A. and Steward, K. P., "Dust Erosion of Compressor Materials - Experience and Prospects", ASME Paper 68-GT-55, The American Society of Mechanical Engineers (March 1968).

4. Smeltzer, C. E., Gulden, M. E. and Compton, W. A., "Mechanisms of Metal Removal by Impacting Dust Particles," ASME Paper 69-WA/Met-8, The American Society of Mechanical Engineers (1969).

5. Smeltzer, C. E. and Compton, W. A., "Mechanisms of Sand and Dust Erosion in Gas Turbine Engines," Final Report on Contract DAAK02-68-C-0056 (1968).

6. Finnie, I., "Erosion of Surfaces by Solid Particles," Wear, Vol. 3, pp. 87-103 (1960).

7. Consylman, H. M., Shumate, C. P. and Owen, W. M., "Product Support Program", Final Report on Contract N00019-71-C-0311 for the Naval Air Systems Command, Solar Report ER 2429 (Feb. 1973).

8. Jack, K. H., "The Production of High Temperature, High Strength Nitrogen Ceramics," Proceedings of the Second Army Materials Technology, Brook Hill (1974).

9. C&EN, June 14, 1976, p. 8.

10. Baumgartner, H. R., Norton Co., Industrial Ceramics Div., Personal Communication.

11. Campbell, ed. *High Temperature Technology*, New York: John Wiley & Sons, Inc., (1956), p. 460.

12. Beck, R. J., "Evaluation of Ceramics for Small Gas Turbine Engines," SAE 740239 (March 1974).

13. Mumford, S. E. and Booker, C. R., "Testing of Ceramic Stator Vanes to 2500°F (1371°C)," ASME 75-GT-103.

14. Sanders, S. A. and Probst, H. B., "Behavior of Ceramics at 1200°C in a Simulated Gas Turbine Environment", SAE 940240.

15. McLean, A. F., et al., "Brittle Materials Design, High Temperature Gas Turbine," Interim Report, AMMRC CTR 73-9.

16. McLean, A. F., et al., "Brittle Materials Design High Temperature Gas Turbine", Interim Report, AMMRC CTR 73-32.

17. Norton Co., Industrial Ceramics Division, "Ceramics for Engine Components", Product Bulletin.

18. International Nickel Company, Inc.

19. McLean, A. F., et al., "Brittle Materials Design, High Temperature Gas Turbine," Interim Report AMMRC CTR 74-26.

20. Torti, M. L., "Ceramics for Gas Turbines Present and Future", SAE 740242.

21. "Manufacturing Methods for Ceramic Nozzle Section of Gas Turbine Powered APU's", U.S. Army MERADCOM/Solar Turbines International Contract DAAK70-78-C-0156.

22. Lumby, R. J., et al., "The Development of Silicon Nitride to Achieve Higher Inlet Temperatures in Land Based Gas Turbines," SAE 720170.

23. Black, *Machine Design*, McGraw Hill Book Co. (1955).

24 Smeltzer, C. E., Gulden, M. E., McElmury, S. S., and Compton, W. A. "Mechanisms of Sand and Dust Erosion in Gas Turbine Engines," USNAVLABS Technical Report 70-26 (1970).

25. "Manufacturing Methods for Ceramic Nozzle Section of Gas Turbine Powered APU's, MERADCOM/Solar Turbines International, Contract DAAK70-78-C-0156.

26. Sanday, S. C., et al, "Design and Analysis of a Ceramic Stator Vane," ASME 75-GT-100.

27. D. R. Messier and L. Schioler, AMMRC (personal communication)